uOttawa

L'Université canadienne
Canada's university

FACULTÉ DES ÉTUDES SUPÉRIEURES ET POSTOCTORALES

uOttawa

l'Université canadienne
Canada's university

FACULTY OF GRADUATE AND POSDOCTORAL STUDIES

Daniel Eumine Suk
AUTEUR DE LA THÈSE / AUTHOR OF THESIS

Ph.D. (Chemical Engineering)
GRADE / DEGREE

Department of Chemical Engineering
FACULTÉ, ÉCOLE, DÉPARTEMENT / FACULTY, SCHOOL, DEPARTMENT

Development of Surface Modifying Macromolecule Blended Polyethersulfone Membranes for Vacuum Membrane Distillation

TITRE DE LA THÈSE / TITLE OF THESIS

Takeshi Matsuura
DIRECTEUR (DIRECTRICE) DE LA THÈSE / THESIS SUPERVISOR

CO-DIRECTEUR (CO-DIRECTRICE) DE LA THÈSE / THESIS CO-SUPERVISOR

EXAMINATEURS (EXAMINATRICES) DE LA THÈSE / THESIS EXAMINERS

Xudong Cao

Jim Dickson

Boguslaw Kruczek

Christopher Lan

Gary W. Slater
LE DOYEN DE LA FACULTÉ DES ÉTUDES SUPÉRIEURES ET POSTDOCTORALES /
DEAN OF THE FACULTY OF GRADUATE AND POSTDOCORAL STUDIES

DEVELOPMENT OF SURFACE MODIFYING MACROMOLECULE BLENDED POLYETHERSULFONE MEMBRANES FOR VACUUM MEMBRANE DISTILLATION

Daniel Eumine Suk

A thesis submitted to the School of Graduate Studies and Research in partial fulfillment of the requirements for the degree of

DOCTOR OF PHILOSOPHY

in the Department of Chemical Engineering
University of Ottawa

2006

Your file Votre référence
ISBN: 978-0-494-15048-1
Our file Notre référence
ISBN: 978-0-494-15048-1

ABSTRACT

Surface modifying macromolecule (SMM) has been developed aiming at the preparation of membranes with greater surface hydrophobicity and greater chemical resistivity at a lower cost than conventional hydrophobic membranes. Throughout the whole work in this study, the membranes, which contains SMM as an additive and PES as a base polymer, are called 'SMM blended PES membranes' or 'SMM modified PES membranes'. The objective of this study is the preparation of SMM blended membranes to be used for the removal of VOCs from their aqueous solutions by the membrane distillation process.

In the first part of this work, a SMM, "tSMM", was synthesized by a traditional method and the tSMM blended PES membranes were prepared to study the effects of tSMM on PES membranes by different methods; e.g. bubble-point method and gas permeation, pure water permeation (PWP), contact angle measurement, and X-ray photoelectron spectroscopy (XPS). In particular, based on the XPS results, the kinetics of surface migration of tSMM was studied. According to the results of experimental and theoretical studies, it was observed that the tSMM blended membranes prepared had a potential to be used in membrane distillation (MD), however to meet the requirement of MD membrane, relatively long evaporation time (over 10 minutes) and high evaporation temperature (110°C) should be needed during membrane preparations.

In the second part of this work, a novel SMM, "nSMM" was designed and synthesized. Synthesized nSMMs from two different batches (nSMM1 and nSMM2) were characterized by GPC and the weight average molecular weight (M_w) of nSMM2 was about twofold of nSMM1. Furthermore, "nSMM' blended PES membranes were prepared and characterized. According to the results, the nSMM seems to be a better alternative to tSMM for membrane distillation, since a shorter period at room temperature was required for "nSMM" to migrate to the membrane surface. The ultrafiltration (UF) tests also gave the information on the

effects of nSMM on PES membranes. nSMM was fully segregated to the surface of membrane forming a distinctive surface layer and this was observed from optical microscope and scanning electron microscopy (SEM) results. In the end of the second part, the nSMM blended PES membranes were successfully applied in vacuum membrane distillation (VMD) for the removal of ethanol from water.

ACKNOWLEDGMENTS

I wish to express my sincere appreciation and gratitude to Professor Takeshi Matsuura for his invaluable guidance, continued encouragement and constructive criticism throughout the course of this study including the preparation of the thesis.

My sincere thanks are due to Professor J. P. Santerre and his research group including Ms. J. Ho of Department of Biomaterials, University of Toronto, and Professor R. M. Narbaitz and his research group of Civil Engineering, University of Ottawa for their helpful suggestions and help. I wish to acknowledge the technical and financial support provided by Dr. Ho Bum Park and Professor Young Moo Lee and their research group of Department of Chemical Engineering at Hanyang University, Seoul, Korea.

The staff and students of the Industrial Membrane Research Centre, and the staff and students of the Department of Chemical Engineering created a friendly, inspirational, and supportive environment. The financial support of the Materials and Manufacturing Ontario is gratefully acknowledged.

Lastly, I would like to thank my father Dr. Ho Chun Suk, my mother Mi Hae Suk, my brother Eugene Suk, my uncle Dr. Jae Ek Son, my love Ha Young Lim, all other family and friends for their encouragement and support.

"But by the grace of God I am what I am... (Corinthians 15:10)"

List of Publications and Presentations

Publications

- D.E. Suk, G. Chawdhury, R.M. Narbaitz, P. Santerre, G. Pleizier, Y. Deslandes and T. Matsuura, "Study on the Kinetics of Surface Migration of Surface Modifying Macromolecules in Membrane Preparation", ***Macromolecules***, 35, 3017-3021, 2002

- D.E. Suk, G. Pleizier, Y. Deslandes and T. Matsuura, "Effects of Surface Modifying Macromolecule (SMM) on the Properties of Polyethersulfone Membranes", ***Desalination***, 149, 303-307, 2002

- M. Khayet, D.E. Suk, R.M. Narbaitz, J.P. Santerre and T. Matsuura, "Study on surface modification by surface-modifying macromolecules and its applications in membrane-separation process", ***J. Appl. Polym. Sci.***, 89, 2902-2916, 2003

- D.E. Suk, H.B. Park, Y.M. Lee and T. Matsuura, "Synthesis of a New Type of Surface Modifying Macromolecules (nSMM) and Characterization and Testing of nSMM Blended Membranes for Membrane Distillation" ***J. Membr. Sci.***, accepted 2005

- D.E. Suk and T. Matsuura, "Membrane-based Hybrid Processes: A Review", ***Separation Science and Technology***, accepted 2005.

One more paper based on the results data presented in Chapter 7 and 8 is under preparation for publication.

Presentations

- "Synthesis of a New Type of Surface Modifying Macromolecules (nSMM) and Characterization and Testing of nSMM Blended Membranes", ***International Congress on Membranes and Membrane Processes (ICOM)***, August 21-26, 2005 (Poster Presentation)

- "Study on Surface Modifying Macromolecule (SMM) blended Polyethersulfone Membranes", ***Annual Meeting of Korean Membrane Society***, Busan, Korea, November 8-9, 2002 (Oral Presentation)

- "Effects of Surface Modifying Macromolecule (SMM) on the Properties of Polyethersulfone Membranes", ***International Congress on Membranes and Membrane Processes (ICOM)***, Toulouse, France, July 7-12, 2002 (Oral Presentation)

- "Surface Modified Membranes for Environmental Application (II)", ***Materials and Manufacturing Ontario (MMO) Partnerships***, Toronto, Canada, June 15, 2000 (Poster Presentation)

- "Surface Modified Membranes for Environmental Application (I)", ***Materials and Manufacturing Ontario (MMO) Partnerships***, Toronto, Canada, May 27, 1999 (Poster Presentation)

Table of Contents

List of Tables

List of Figures

Nomenclature

List of symbols

a NRTL equation parameter for a binary system, [-]

a' slope of linear regression defined in Equation 3.1, [m kPa^{-1} hr^{-1}]

a_p water permeability of membrane, [m hr^{-1} kPa^{-1}]

a_s Stokes radius, [m], used [cm] in Equation 2.18

A_0 intercept of linear regression on log-normal probability paper, [-]

A_1 slope of linear regression on log-normal probability paper, [-]

b NRTL equation parameter for a binary system, [K]

c_L total molar concentration in the liquid phase, [mol m^{-3}]

c_f solute (TOC) concentration in the feed solution, [ppm]

c_p solute (TOC) concentration in the permeate, [ppm]

c_w TOC concentration in the pure water, [ppm]

C tSMM concentration in the surface layer at t = t > 0 defined in Section 5.1, [mol m^{-3}]

C^* equilibrium tSMM concentration in the surface layer, [mol m^{-3}]

C_b tSMM concentration in the bulk at t = t > 0 defined in Section 5.1, [mol m^{-3}]

$C_b°$ tSMM concentration in the bulk and the surface layer at t = 0 defined in Section 5.1, [mol m^{-3}]

C^∞ tSMM concentration in the surface layer at t = ∞, [mol m^{-3}]

C_f Fluorine content in the surface layer at t = t > 0 defined in Section 5.1, [atomic %]

$C_{bf}°$ Fluorine content in the bulk and the surface layer at t = 0 defined in Section 5.1, [atomic %]

C_f^∞ Fluorine content in the surface layer at t = ∞ defined in Section 5.1, [atomic %]

d_{max} maximum pore diameter, [m]

d_{min} minimum pore diameter, [m]

d_p pore diameter, [m], used [nm] in Equation 2.11

$d_{p,avg}$ average pore size, [m]

d_s solute diameter, [m], used [nm] in Equation 2.9

D_{AB} diffusivity of solute, [$cm^2\ s^{-1}$]

f solute separation, [%]

f_i fraction of pores of diameter d_i, [-]

f_v void fraction, [-]

G parameter defined in Equation 2.33, [-]

h heat-transfer coefficient in the liquid phase, [$W\ m^{-2}\ K^{-1}$]

ΔH molar latent heat of vaporization, [$J\ mol^{-1}$]

J molar flux, [$mol\ m^{-2}\ s^{-1}$]

$\Delta J_{a,i}$ volume flux of air through the pores of radius r_i, [$m^3\ s^{-1}\ m^{-2}$]

$J_{w,i}$ solvent (water) flux through the pores of diameter d_i, [$m^3\ s^{-1}\ m^{-2}$]

J_w total solvent (water) flux, [$m\ s^{-1}$, $m\ hr^{-1}$]

k mass transfer coefficient of tSMM at $t = t > 0$ defined in Equation 5.1, [$m\ s^{-3}$]

$k°$ mass transfer coefficient of tSMM at $t = 0$ defined in Section 5.1, [$m\ s^{-3}$]

k_B Boltzmann constant, $k_B=1.38\times10^{-23}$ [$kg\ m^2\ s^{-2}\ K^{-1}$, $erg\ K^{-1}$]

k_L mass-transfer coefficient in the liquid phase, [$m\ s^{-1}$]

K_m membrane permeability coefficient defined in Equation 2.2, [$s\ mol^{1/2}\ m^{-1}\ kg^{-1/2}$]

L a bulk layer of thickness from which tSMM migrates in Section 5.1, [m]

M molecular weight, [$kg\ mol^{-1}$, $g\ mol^{-1}$]

M_n number average molecular weight, [$kg\ mol^{-1}$, $g\ mol^{-1}$]

M_w weight average molecular weight, [$kg\ mol^{-1}$, $g\ mol^{-1}$]

n_i number of pores of radius r_i (or diameter d_i) per unit area, [m^{-2}]

n total number of pores per unit area, [m^{-2}]

N mass flux, [$kg\ m^{-2}\ s^{-1}$]

N_i molar flux of a permeating species, i, [$mol\ m^{-2}\ s^{-1}$]

p_i partial pressure of species i, [Pa]

Δp partial pressure gradient, [Pa]

P downstream pressure, [Pa]

P' total gas pressure, [Pa]

P_i° vapor pressure of pure component i, [Pa]

ΔP transmembrane pressure, [Pa]

P_I interface pressure, [Pa]

P_2 vacuum side pressure, [Pa]

P°_W water vapor pressure, [Pa]

r pore radius, [m]

r_{max} maximum pore radius, [m]

r_{min} minimum pore radius, [m]

R gas constant, R=8.314 [J mol^{-1} K^{-1}]

S_p surface porosity, [%]

t evaporation time in Section 5.1, [min]

t_{lag} the initial lag time, [min]

t_{min} the minimum evaporation time, [min]

T temperature, [K]

T_b temperature at the feed bulk side, [K]

T_I temperature at the interface, [K]

x_b mole fraction in the liquid bulk, [-]

x_I mole fraction at the interface, [-]

Y_I mole fraction in the vapor phase at the interface, [-]

Y_2 mole fraction in the vapor phase at the vacuum side, [-]

z parameter defined in Equation (2.9), [-]

z_x effective XPS sampling depth defined in Equation 3.2, [nm]

Greek letters

α proportionality constant defined in Equation 5.4, [-]

β parameter defined in Equation 5.10, [t^{-3}]

ε the volume fraction of polymer in a cast solution film in Section 5.1, [-]

ϕ	NRTL equation parameter for a binary system, [-]
δ	a surface layer of thickness into which tSMM migrates in Section 5.1, [m]
δ_p	skin layer thickness, [m]
ψ	tortuosity factor, [-]
η	viscosity, [Pa s, poise]
η_w	water viscosity, [kg m^{-1} s^{-1}]
$[\eta]$	intrinsic viscosity of PEG/PEO, [dL g^{-1}]
γ	surface tension, [N m^{-1}]
θ	contact angle, [radians]
θ_x	take-off angle, [radians]
μ_s	geometric mean solute diameter, [m], used [nm] in Equation 2.9
μ_p	geometric mean pore diameter, [m], used [nm] in Equation 2.11
λ	mean-free path, [m]
λ_x	effective mean path for electrons to escape the surface, [m], used [nm] in Equation 3.2
σ	collision diameter of the diffusing species(gas molecule diameter), [m]
σ_g	geometric standard deviation of solute diameter, [-]
σ_p	geometric standard deviation of pore diameter, [-]
τ	parameter defined in Equation 2.32, [-]

Abbreviations

AGMD	air gap membrane distillation
AFM	atomic force microscopy
AR-XPS	angle-resolved XPS
BAL	Zony BA-L™
BAT	best available technology
CM	confocal microscopy

CPI	chemical process industries
DCMD	direct contact membrane distillation
DEG	diethylene glycol
DMAc	dimethylacetamide
DPS	dihydroxy diphenyl sulfone
DSIMS	dynamic secondary ion mass spectrometry
EPA	Environmental Protection Agency
ESCA	electron spectroscopy for chemical analysis
FRES	forward-recoil spectrometry
FTIR	Fourier transform infrared spectroscopy
GAC	granular activated carbon
MD	membrane distillation
MDI	methylene bisphenyl diisocyanate
NMR	nuclear magnetic resonance
NMP	n-methyl-2-pyrrolidinone (?)
NR	neutron reflectivity
NRC	National Research Council
nSMM	new surface modifying macromolecule
PCL	poly(ε-caprolactone)
PEI	polyetherimide
PEP	poly(ethylenepropylene)
PES	polyethersulfone
PDMS	poly(dimethylsiloxane)
PM	polarized microscopy
PMMA	poly(methylmethacrylate)
PP	polypropylene
PPO	polypropylene diol
PS	polystyrene
PTA	packed tower aeration

PTFE	polytetrafluoroethylene
PU	polyurethane
PUU	polyurethane-urea
PV	pervaporation
PVC	poly(vinylchloride)
PVDF	poly(vinylidene fluoride)
PVME	poly(vinyl methyl ether)
PVP	polyvinylpyrrolidone
PWP	pure water permeation
RO	reverse osmosis
RT	room temperature
SEM	scanning electron microscopy
SFG	sum-frequency generation vibration spectroscopy
SGMD	sweeping gas membrane distillation
SMM	surface modifying macromolecule
THF	tetrahydrofuran
TGA	thermogravimetric analysis
TOA	take-off angle
TOC	total organic carbon
TOF	time of flight
tSMM	traditional surface modifying macromolecule
UF	ultrafiltration
VMD	vacuum membrane distillation
VOC	volatile organic compound
XPS	X-ray photoelectron spectroscopy

1. Introduction

It is well documented that surface chemistry and morphology of the membranes play an important role in the transmembrane transport of penetrants (Matsuura, 1992). In order to enhance the overall performance of the membrane, it is often necessary to modify the membrane surface by changing the membrane material or its structure. Generally, the objective for modification is not only increasing flux and/or selectivity but also improvement of chemical resistance (i.e. solvent resistance, swelling, or fouling resistance), control of pore size and elimination of defects.

One of the membrane modification methods involves annealing of porous membranes by heat-treatment (Pinnau and Freeman, 2000). In the membrane literature, various other techniques were carried out for surface modification of polymeric membranes. Those are physical, chemical or bulk modification (i.e. polymer blends) (Ganbassi et al., 1996). Recently, Pinnau and Freeman (2000) gave a summary of some of the most commonly practiced membrane modification methods such as surface coating, chemical treatment (fluorination, cross-linking, pyrolysis), annealing by heat-treatment and solvent treatment. A less common approach to modifying the properties of a polymer is to introduce additives that can migrate to the film surface and alter the surface chemistry while leaving the bulk properties intact (Ward et al., 1984). Ward et al. (1984) appear to be the first to synthesize a polyurethane block copolymer, to be used as a surface modifying additive for the development of new biomedical polyurethaneurea. They showed that this method is efficient because only a small weight percentage of the additive was required to modify the surface properties while maintaining the bulk properties unaltered.

The surface modification by the above approach is based on the fact that in a polymer blend, thermodynamic incompatibility between polymers usually causes demixing of polymers to occur. If the polymer system is equilibrated in air, the polymer with the lowest surface

energy (hydrophobic polymer) will concentrate at the air interface and reduce the system's interfacial tension as a consequence. The preferential adsorption of a polymer of lower surface tension at the surface was confirmed by a number of researchers for miscible blends of two different polymers (Pan and Prest, 1985; Bhatia et al., 1988; Thomas and O'Malley, 1979; O'Malley et al., 1979; Schmidt et al., 1989).

Based on the above concept, since 1992 a group at the University of Ottawa and University of Toronto has combined their expert areas in membrane technology, environmental engineering, and polymer chemistry, respectively, to conceive, fabricate, and apply novel membranes to separate VOCs from waste streams and contaminated waters (Matsuura et al., 1992). They have been developing surface modifying macromolecule (SMM) to prepare membranes with greater surface hydrophobicity and greater chemical resistivity at a lower cost than those observed in manufacturing conventional hydrophobic membranes. According to this approach, membranes are prepared by casting a solution of a relatively hydrophilic polymer into which a small amount of SMMs is blended. The SMM migrates to the surface of the membrane during the casting step. Since then, many different types of SMM formulations have been synthesized with different combinations and stoichiometries of different reagents, and blended with polyethersulfone (PES). Attempts were made to find out the effects of various types of SMMs and different membrane casting conditions on SMM migration to the top membrane surface. The performance of the SMM modified membranes was tested for use in ultrafiltration, pervaporation and in biomedical applications. The overview of those researches on SMM is well summarized by Khayet et al. (2003).

The objective of this work is the preparation of SMM blended membranes to be used for the removal of VOCs from their aqueous solutions by the membrane distillation process. For this purpose, two different types of SMMs were used. The first type of SMMs is a traditional SMM –SMM10 (Khayet et al., 2003), which has been synthesized and used in the earlier SMM studies, and is called 'tSMM' in this thesis. The second type is a novel

SMM type, which was newly designed and developed for this study, and is called 'nSMM' in this thesis. To meet the objective, the following subordinate studies have been performed:

1. Study on the effects of tSMM blending on PES membranes,
2. Study on the kinetics of surface migration of tSMM in PES membrane preparation (Suk et al., 2002b),
3. Study on the potential of tSMM blended PES membranes for membrane distillation (Suk et al., 2002a),
4. Synthesis of nSMM and study on the surface segregation in blends of nSMM and PES,
5. Study on the effect of nSMM on the performance of PES ultrafiltration membranes,
6. Study on the nSMM blended PES membranes for vacuum membrane distillation.

The above objective and its subordinate studies are set because a) they are of industrial significance; b) the accomplishment of these studies will provide improved understanding in the fundamentals of SMM blended membranes, which is a contribution to membrane science and technology.

2. Literature Survey

2.1 Volatile Organic Compounds (VOCs) and VOC Treatment Technologies

2.1.1 Volatile organic compunds (VOCs)

Volatile organic compounds (VOCs) and their reaction products are increasingly regarded as posing unacceptable risks to public and occupational health, as well as to biological and physical environments (Bloemen and Burn, 1993). VOCs are a class of substances in which organic carbon is bonded to hydrogen or to other elements. As an approximated rule, VOCs may be defined as organic liquids or solids whose vapor pressures at room temperature are greater than about 70 Pa (0.01 psia, 0.0007 atm) and whose atmospheric boiling points are up to about 260°C (500°F, 533 K) (Hunter and Oyama, 2000). The U.S Environmental Protection Agency (EPA) defines a VOC as any compound of carbon that participates in atmospheric photochemical reactions; that is, any such organic compounds other than those listed in Table 2.1 which have been excluded because of their negligible photochemical reactivity (Hunter and Oyama, 2000).

In pre-industrial society sources of VOCs such as wood, 'natural' oils, tars and waxes were exploited largely as fuels, primarily on a domestic scale. When the Industrial Revolution gained momentum in the 19th century, emissions of organic compounds increased exponentially. In pre-war Germany the chemical industry manufactured numerous compounds, among them there were novel VOCs. In this emerging industry, still based on coal, VOCs were usually formed after processing the heavier starting material. Nowadays, light oil products, obtained from crude oil directly or after cracking heavy fractions, make up the essential ingredients of modern transportation, energy generation and the petrochemical industries (Bloemen and Burn, 1993). Groundwater contaminated with a low concentration (in the range of parts per million, ppm) of VOCs is the most common type of hazardous water contamination (Brewer, 1991).

VOCs are also common industrial chemicals and their separation from various liquid or gaseous waste streams is important in waste reduction and control (Amy et al., 1987; Levenston, 1991). Table 2.2 shows the common volatile organic chemicals and their sources.

Table 2.1 Substances excluded from the VOC definition† (Hunter and Oyama, 2000)

Methane, ethane	*t*-Butyl acetate
Acetone	Methylene chloride (dichloromethane)
1,1,1-Trichloroethane (methyl chloroform)	Trichlorofluoromethane (CFC-11)
Dichlorodifluoromethane (CFC-12)	Chlorodifluoromethane (CFC-22)
1,1,1-Trichloro-2,2,2-trifluoroethane (CFC-113)	Trifluoromethane (CFC-23)
1,2-Dichloro-1,1,2,2-tetrafluoroethane (CFC-114)	Chloropentafluoroethane (CFC-115)
1,1,1-Trifluoro-2,2-dichloroethane (HCFC-123)	1,1,1,2-Tetrafluoroethane (HFC-134a)
1,1-Dichloro-1-fluoroethane (HCFC-141b)	1-Chloro-1,1-difluoroethane (HCFC-142b)
2-Chloro-1,1,1,2-tetrafluoroethane (CHFC-124)	Pentafluoroethane (HFC-125)
1,1,2,2-Tetrafluoroethane (HFC-134)	1,1,1-Trifluoroethane (HFC-143a)
1,1-Difluoroethane (HFC-152a)	Volatile methyl siloxanes
Parachlorobenzotrifluoride	

†Also excluded are perfluorocarbon compounds that fall into these classes: (1) Cyclic, branched, or linear, completely fluorinated alkanes: (2) Cyclic, branched, or linear, completely fluorinated ethers with no unsaturations; (3) Cyclic, branched, or linear, completely fluorinated tertiary amines with no unsaturations; and (4) Sulfur-containing perfluorocarbons with no unsaturations, with S bonds only to C or F

Table 2.2 Common volatile organic chemicals and their sources (Bloemen and Burn, 1993)

VOCs	Major sources of exposure
Alcohols (ethanol, isopropanol)	Spirits, cleansers
Aromatic hydrocabons (toluene, xylenes, ethylbenzene, trimethylbenzenes)	Paints, adhesives, gasoline, combustion sources
Aliphatic hydrocarbons (octane, decane, undecane)	Paints, adhesives, gasoline, combustion sources
Benzene	Smoking, auto exhaust, passive smoking, driving, pumping gas
Carbon tetrachloride	Fungicides, global background
Chloroform	Showering (10 min average), washing clothes, dishes
p-Dichlorobenzene	Room deodorizers, moth cakes
Formaldehyde	Pressed wood products
Methylene chloride	Paint stripping, solvent use
Styrene	Smoking
Tetrachloroethylene	Wearing or storing dry-cleaned clothes, visiting dry cleaners
Thichloroethylene	Unknown (cosmetics, electronic parts, correction fluid)
Terpenes (limonene, α-pinene)	Scented deodorizers, polishes, fabrics, fabric softeners, cigarettes, food, beverages

The exposure of the environment and living organisms to VOCs has altered the delicate balance of ecosystems and has caused adverse health effects. The relationship between these health effects and exposure to VOCs was first recognized in the chemical industry, where high concentrations of a limited number of compounds existed. Toxicological research revealed that many VOCs have various reversible and irreversible effects on the human body. Short-term health effects (headache, eye irritation) appear to occur in buildings, particularly new or renovated ones. Although VOCs have not been conclusively shown as the major cause, they are thought to be important. Because of the loss of productivity involved in even minor ailments such as headaches, the effects may have a large economic impact. Long-term health effects may include cancer. However, with the exception of benzene, a human carcinogen, most other prevalent VOCs are not known to cause human cancer, and risk estimates are extremely uncertain (Bloemen and Burn, 1993).

2.1.2 VOC treatment techniques

There is a huge need for investment in industry to reduce VOCs emissions and to adapt the existing equipment to regulations. There are two main VOC treatment technique families; VOC destroying techniques and VOC recovering techniques. Former techniques include thermal incineration, catalytic incineration and biological treatment. Adsorption, absorption, condensation, distillation and membrane separation can be categorized in the latter techniques. The techniques mentioned above, except for membrane separation, are briefly described here and membrane separation will be covered more in detail in the subsequent chapter (Hunter and Oyama, 2000).

Incineration is basically the burning of combustible wastes. For many years, incinerators have been considered to be one of the most effective control devices for VOCs. They are relatively easy to operate, not likely to foul, and do not require additional processes to remove the pollutant. Incinerators are ideal candidates for gas streams, which contain a variety of pollutants and from which any solvent that is recovered is not viable for reuse.

Under proper conditions, the design efficiencies are typically in excess of 98 % and depend primarily on the gaseous components combusted, the residence time, the amount of mixing, and the combustion temperature. However, costs associated with incineration processes are higher than those associated with solvent recovery processes and also incineration could have NO_x and CO generation problems.

Biological treatment consists of using microorganisms to biologically degrade contaminants. Microorganisms are grown on a substrate (*biofiltration*) or are suspended in scrubber liquor (*bio-scubbers*). The scrubber liquid or substrate may also serve as an adsorbent for the pollutants so that the microbes have a constant food supply, even if the process is not operating. As in water treatment operations, the microorganisms break down the large organic molecules for energy to sustain the microbial activity. Biopurification is a good alternative for streams that have relatively low concentrations of organic constituents and is most effective for systems containing alcohols, ethers, aldehydes, and ketones. Biofiltration offers excellent VOC removal, even from dilute gas streams with relatively low maintenance and operating costs. Care must be exercised, however, to remove particulates, ensure that adequate moisture is present, avoid gas channeling, and maintain a fairly constant temperature.

Adsorption refers to the trapping of pollutants on a high-surface area material. The process is typically used to remove contaminants in fairly low concentrations from a gas stream. The pollutants are adsorbed onto the surface or interstitial area of a material such as activated carbon or a molecular sieve by physical or chemical attraction. Once the carbon or adsorbent material is saturated, that is, it can no longer adsorb any more pollutant, the material is regenerated, typically by introducing steam to remove the pollutants. The vent stream is condensed, decanted if necessary to separate the aqueous layer from the organic layer, and, in some cases, further treated. Because of the subsequent separation required to reuse the solvents, carbon adsorption is not well suited to streams that have a large number

of VOCs, nor does it work effectively on streams that have constituents that are difficult to separate.

Absorption (or Scrubbing) is a physical process consisting of the dissolution of a pollutant in a liquid. In absorbers (or scrubbers), the vapor stream is introduced into a chamber where it is intimately mixed with the liquid. The amount of pollutant remaining in the gas stream as it leaves the scrubber is governed by Henry's law, which establishes the amounts of a component in equilibrium in the gas and liquid streams for dilute mixtures. With countercurrent gas and water flows, the mass transfer between the vapor and liquid phases is maximized. If the vapor and liquid have adequate contact, the gaseous components that are soluble in the liquid are absorbed, where they may react or be removed by discharge of the liquid. Some additional removal is accomplished by the evaporative cooling that occurs in the scrubber; some components condense out and are removed as the liquid is removed. Absorption, however, is not effective on constituents that are not soluble in the liquid medium. Therefore, it, too, is not well suited to vapor streams that have a large variety of constituents.

Condensation is the liquefaction of condensable contaminants by the use of low temperatures. Specifically, the compounds to be removed from the gaseous phase are cooled to a temperature at which their partial pressure in the gas stream exceeds their dew point so that they transform to liquids. Condensation is most effective for compounds with high boiling points. If a significant portion of the organic material is composed of compounds that solidify at the condenser operating temperature, however, a standard condenser will not be effective, as they will quickly foul the heat transfer area, plugging the condenser. For those cases, a contact condenser in which the hot and cool streams come directly into contact with each other would be more appropriate.

Table 2.3 shows some selection criteria for the VOC removal technologies with VOC concentration, flow rate, recovery, TA-Luft regulation and Robustness.

Table 2.3 Selection criteria, VOC removal technologies (Mukhopadhyay and Moretti, 1993; Strauch, 1995)

	Concentration (ppm)	Flow rate (scfm)	Recovery	TA-Luft†	Robustness
Incineration	20~1k	1~20k	No	Yes	High
Biological treatment	500~2k	1~1,000k	No	Partly	Low
Adsorption	20~20k	300~1,000k	Partly	Yes	Low
Absorption	1k~20k	1k~1,000k	Partly	Partly	Medium
Condensation	5k~10k	1~2k	Yes	Partly	High
Membrane technology	1~1k	1~150	Yes	Partly	High

†Air-pollution control regulation in Germany

2.1.3 VOC removal with membrane technology

Many plant operators in the chemical process industries (CPI) are taking advantage of the benefits of membrane technologies, using them alone or with other treatment techniques to recycle chemicals and solvents and to clean wastewater and polluted air. Currently, such membrane technologies as micro-, ultra-, and nanofiltration, reverse osmosis, electrodialysis, pervaporation and membrane distillation offer interesting possibilities. Specific aspects of pollution control for each technology are shown in Table 2.4. Although none of these methods can, on its own, alter or break down pollutants, each has the ability to separate, fractionate and concentrate contaminants in wastewater. In addition, they (Cartwright, 1994):

- Permit continuous, uninterrupted processing via automatic control.
- Use far less energy than traditional treatment methods.
- Require only minimal temperature changes and no chemical additives.
- Exert no impact on contaminants, and keep them physically separated from the stream.

Are easy to install, either alone or combined with other treatment systems, since they are modular and contain few moving parts.

Table 2.4 Membrane separation technologies for wastewater treatment (Cartwright, 1994)

Feature	Micro-filtration	Ultra-filtration	Nano-filtration	Reverse Osmosis	Electro-dialysis	Per-vaporation	Membrane distillation
Suspended solids removal	Excellent	Impractical	Impractical	Impractical	N/A	N/A	N/A
Dissolved organic removal	N/A	Excellent[1]	Excellent[1]	Excellent[1]	N/A	Good[3]	Good[4]
VOC removal	N/A	Poor	Fair[1]	Fair-good[1]	N/A	Excellent	Good
Dissolved inorganic removal	N/A	N/A	Good (function of salt species)	Very good (90-99% removal)		N/A	Good (liquid-liquid extraction)
Osmotic pressure effects	None	Minor	Significant	High	None	None	None
Concentration capabilities	Up to 5% total solids	Up to 50% organics	Up to 15%[2]	Up to 15%[2]	Up to 20% (ionic con-centration)	N/A	Up to 80% (organics)
Permeate quality	Excellent	Excellent	Good	Excellent	Good	Excellent	Excellent
Energy requirements	20-40 psi	50-100 psi	70-150 psi	225-1,000 psi	Function of ionic concentration	< 25% of distillation	< 60 psi
Capital costs ($/GPD)	0.50-5	0.50-7	0.50-5	0.50-5	0.50-4	7-15	0.50-4
Operating cost ($/1,000 gal feed rate)	0.50-4	0.50-3	0.75-3	1-3	0.50-1	3-5	0.40-4

All technologies are application specific, and testing is required to develop precise data. Estimating specific capital and operating costs is difficult because some waste-streams may require special materials of construction or additional design considerations as a result of high fouling potential

1. Function of molecular weight
2. Function of osmotic pressure
3. Function of vapor pressure
4. Function of vapor pressure and concentration

N/A – not applicable
GPD – gallons per day

Out of the many different membrane processes, pervaporation (PV) and membrane distillation (MD) look the most feasible methods to remove VOC. Schematic diagrams for PV and MD are presented in Figure 2.1.

Pervaporation, PV, whose term derives from the two major integral operations involved in the separation process, namely, permeation and evaporation, is defined as a separation process in which a liquid feed mixture is separated by means of selective diffusion-vaporization through a dense (non-porous) membrane. The PV is usually carried out by placing a liquid stream containing water and VOC in contact with one side of the membrane while a vacuum is applied to the other side (Peng et al., 2003). The PV process is often described by a solution-diffusion model, which consists of the following steps (Peng et al., 2003; Villaluenga et al., 2004, Wijmans and Baker, 1995):

(1) Diffusion through the liquid boundary-layer next to the feed side of the memberane.
(2) Selective partitioning of molecules into the membrane (solution).
(3) Selective transport through the membrane matrix (diffusion).
(4) Desorption into vapor phase on the permeate-side (evaporation).
(5) Diffusion away from the membrane through the vapor boundary-layer on permeate-side of the membrane.

The driving force for PV is the difference in chemical potential of each component across the membrane, and the availability of commercial membranes is one of the most important constraints for the development and application of PV technology.

The term 'membrane distillation' arises from the similarity of the process to conventional distillation. Both MD and conventional distillation rely on vapor-liquid equilibrium as a basis for separation. In MD an aqueous feed is brought into contact with one side of a hydrophobic, porous membrane. The hydrophobic nature of the membrane prevents the penetration of the aqueous solution into the pores, resulting in a vapor-liquid interface at

each pore entrance. Water and VOC evaporate from the interface, diffuse across the pores of the membrane and are removed from the permeate side by applying different removing methods (e.g. vacuum, aqueous solution, etc.). MD will be further reviewed more in detail in Section 2.4.

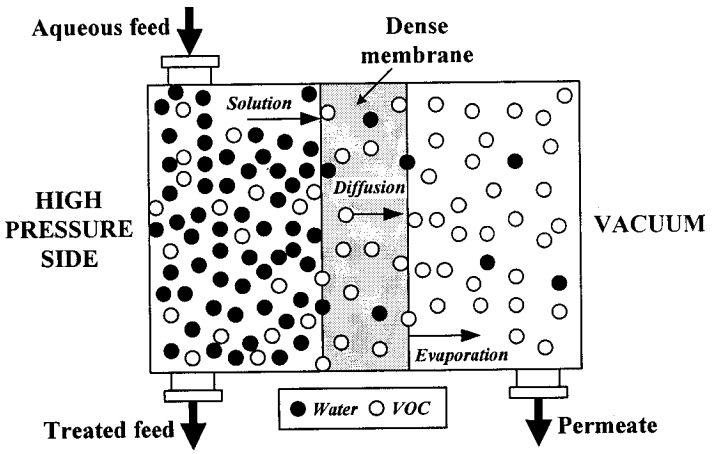

(a) Pervaporation (PV)

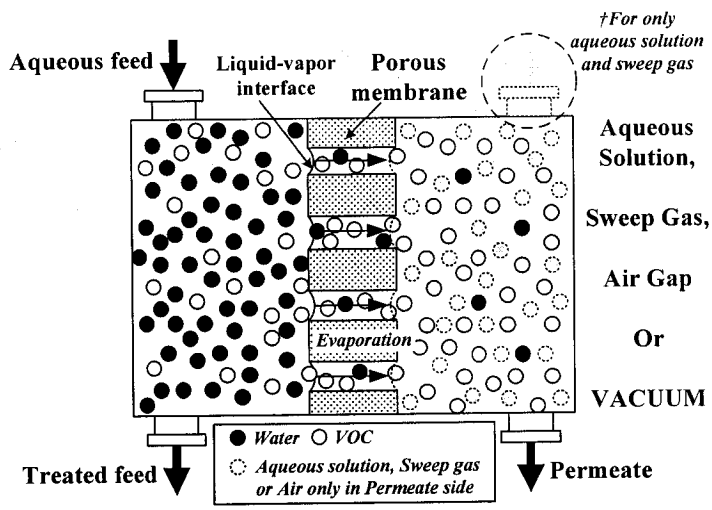

(b) Membrane distillation (MD)

Figure 2.1 Mechanisms of mass transfer in: (a) PV and (b) VMD for VOC removal (Urtiaga et al., 2001; Lawson and Lloyd, 1997)

2.2 Surface Modification and Surface Segregation

2.2.1 Polymer surface modification

Membrane surface plays an important role in the membrane performance. Therefore, the study of the composite membrane has become more and more important in membrane research.

Composite membranes generally comprise two distinctive layers made of two different polymeric materials as shown in Figure 2.2 (Strathmann, 1990; Mulder, 1996). The top layer may be called the surface layer, while the bottom layer may be called the substrate. The surface layer acts as a selective barrier, while the substrate is a porous support. The advantage of a composite membrane is that both the surface layer and the substrate can be adjusted separately to provide membrane performance (Fang, 1997). Many of the possible polymer surface modifications applied to prepare composite membranes are described in Figure 2.3. In Figure 2.3, most of the composite membranes involve two separate steps: formation of a substrate, and formation of a surface layer. But only the composite membrane with a surface-modifying additive differs from the others (Figure 2.3(e)). The latter composite membrane overcomes the complexity of the two-step method and makes it possible to prepare composite membranes in one step.

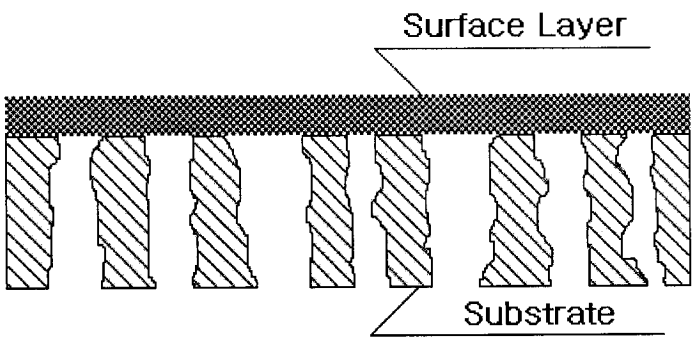

Figure 2.2 Schematic diagram of an asymmetric composite membrane (Strathmann, 1990)

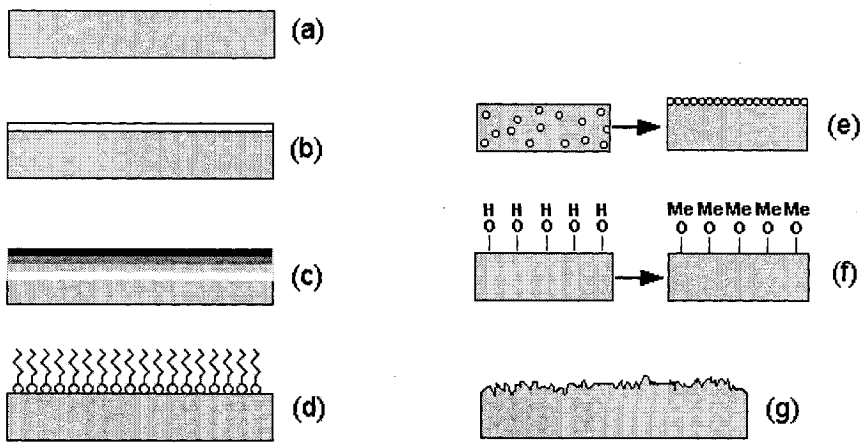

Figure 2.3 A schematic representation of the general morphological features of some surface modifications: (a) Original surface; (b) Overcoat (e.g. solvent coat, radiation graft, plasma graft); (c) Surface gradient graft (e.g. radiation graft); (d) Langmuir-Blodgett overlayer; (e) Surface-modifying additive; (f) Surface reaction; (g) Etching and roughening (surface reaction is also frequently observed)

This phenomenon is usually called 'surface segregation' or 'surface migration'. The study of surface segregation is the study of the effect of the presence of a surface on the rules which control the bulk phase structure. Intuitively, one can expect that the lower surface free energy component will dominate the surface at polymer-air interface, that is, the surface composition will as a result be enriched, with respect to the bulk, in the lower surface free energy component. Surface enrichment, however, means de-mixing, that is the loss of the combinatorial entropy (Garbassi et al., 1996). The thermodynamics of interfacial phenomena and the thermodynamics of polymer blends or mixtures which were involved in surface segregation were well explained by Pham (1995). In addition to these thermodynamic considerations, kinetics also plays an important role: the rate and the degree of attainment of equilibrium, the effect of solvents and crystallinity. These kinetic properties are all important variables which make the study of this problem theoretically and experimentally very demanding (Garbassi et al., 1996).

2.2.2 Studies on surface segregation

There have been many studies on the surface segregation in the field of polymer science. An isotopic blend of polystyrene (PS) and deuterated PS (d-PS) must be one of the most interesting polymer blends for surface segregation studies. The effect of the surface energy on surface segregation was studied with the system of an isotopic blend of polystyrene (PS) and deuterated PS (d-PS). Jones et al. (1989) revealed that the surface of the blend d-PS and PS was enriched with d-PS relative to the bulk using forward-recoil spectrometry (FRES). Zhao et al. (1991) used dynamic secondary ion mass spectrometry (DSIMS) and time of-flight forward recoil spectrometry (TOF-FRES) to measure the surface concentration profiles for a series of d-PS/PS blends and discussed the kinetics of formation and the fine structure of the enriched layer. The effect of molecular weight on the surface enrichment in d-PS:PS blends was studied by Hariharan et al. (1993a) by neutron reflectivity (NR) and DSIMS. They found that surface segregation to air surface was a balance between the isotope effect that partitions the deuterated species to the air surface and the difference in surface tension between the polymer chains of large molecular weights that prefer the partitioning of the segments of the shorter chains to the surface. Hariharan et al. (1993b), as well as Budkowski et al. (1992) also studied surface segregation as a function of film thickness. Geoghegan et al. (1997) studied the kinetics of the formation of a surface-enriched layer of d-PS from a film of a blend with PS based on the data from time-of-flight neutron reflectivity (TOF-NR). Of course, many different blends of polymers have been also used to investigate the surface segregation such as the following examples:

- Poly(ethylenepropylene) (PEP) and deuterated PEP (d-PEP) blend (Norton et al., 1995),
- PS and poly(methylmethacrylate) (PMMA) blend (Kajiyama et al., 1998),
- PS and poly(vinyl methyl ether) (PVME) blend (Pan and Prest, 1985),
- PMMA and poly(vinylchloride) (PVC) blend (Schmidt et al., 1980),
- PVC and poly(ε-caprolactone) (PCL) blend (Clark et al., 1991).

Recently, surface segregation of a small amount of fluorine or silicon-containing polymers in a blend with traditional base polymer has been studied intensively because of their low surface free energy.

Iyengar et al. (1996) synthesized a diblock copolymer of deuterated styrene and isoprene (dPS-IP) incorporated with pendent fluorinated side chains and studied the surface segregation of the block copolymer from a polystyrene (PS) matrix using FRES and contact angle measurement. Affrossman et al. (1996) studied with blends of PS and perfluorohexane end capped PS by Static SIMS, ion scattering spectroscopy (ISS) and X-ray photoelectron spectroscopy (XPS). Their study showed the migration of perfluoro chain ends to the surface and the effect of molecular weight of either backbone (PS) and perfluoro end group. Also a perfluorohexylated-C60 was prepared and its surface activity and mobility in the bulk of a polymer matrix (PS) to the polymer/air interface was studied by Chen and McCarthy (1999) as a function of bulk concentration, annealing temperature, and annealing time using XPS and contact angel measurement. In 2001, the synthesis of fluorocarbon end-capped polyester (F-polyester) and the surface properties of the blend of F-polyester and polyester were researched (Lee et al., 2001) and Fourier Transform InfraRed Spectroscopy (FTIR), Nuclear Magnetic Resonance (NMR), thermogravimetric analysis (TGA) and XPS were used for this study. Their results showed that the surface coverage of fluorocarbon groups increased with increasing the concentration of F-polyester and the length of fluorocarbon end groups.

In the mean time, the silicon-containing polymers also have been one of the important targets for surface segregation studies. In most of the studies, poly(dimethylsiloxane) (PDMS) containing polymers have been used as a silicon-containing polymer. Chen and Gardella (1998) studied the effects of mixed solvents used for casting films of diblock copolymer/homopolymer blends of PDMS-co-PS/PS on the surface of the films using time-of-flight SIMS (ToF SIMS) and XPS. They reported that a complete PDMS segregation process was achieved using a binary solvent mixture of chloroform and cyclohexanone with

2% bulk PDMS. Zhang et al. (1998) did surface studies of PDMS endcapped polyurethane (BS) and phenoxy base polymer (BP) blends by Infrared (IR)-visible sum-frequency generation vibrational spectroscopy (SFG), atomic force microscopy (AFM) and contact angle goniometry. According to their study, there was a strong tendency for BS to segregate to the surface and the BS surface content reached a full coverage at over 1.7 wt% BS bulk concentration. Lee and Archer (2001) also studied with PDMS endcapped PS block copolymer additives (PS-b-PDMS) in a PS host. They investigated the effect of concentration and preparation method on migration and also the effect of polystyrene matrix molecular weight using dynamic contact angle analysis (DCA) and attenuated total reflection Fourier transform infrared (ATR-FTIR). For all cases in their study, selective dimethyl siloxane (DMS) enrichment of the air/polymer interface was observed and near saturation levels of DMS surface coverage were found in PS/PS-b-PDMS blends with bulk copolymer additive compositions as low as 2 wt%.

The surface which was dealt with in the above reviews on the surface segregation meant the very top layer at air-polymer interface, and a component with lower surface energy concentrated on top of the other component with higher surface energy. However, there was a surface segregation study which used the term, surface as a water-polymer interface by Hester and Mayes (2002). They synthesized hydrophilic comb polymers having a methacrylate backbone and poly(ethylene oxide) side chains and made the comb polymer blended poly(vinylidene fluoride) (PVDF) membranes. XPS analysis showed substantial surface segregation of the comb polymer during coagulation in water.

2.3 Review of Previous Works on SMM

As mentioned in the Introduction, various studies on SMM have been conducted since 1992 in University of Ottawa and University of Toronto. At the University of Ottawa, the studies

of SMM have been mainly focused on membrane preparation and applications while the focus was on biomedical applications in University of Toronto. In this chapter, the reviews will be limited to the works regarding on membrane preparation and applications.

2.3.1 Synthesis of surface modifying macromolecules

Pham (1995), Ho (1997) and Mandeep (2001) synthesized a number of novel SMMs that are miscible in a membrane casting solution containing PES with/without PVP. In Table 2.5., a list of the SMMs together with the reactants used and the reaction molar ratio of the diisocyanate:polyol:fluoroalcohol (distilled fraction of the fluoroalcohol) are summarized. These SMMs consisted of three components, a diisocyanate, a polyol, a fluoroalcohol. All SMMs were synthesized by them with methylene bisphenyl diisocyanate (MDI) as a diisocyanate. The polyols employed were polypropylene diol (PPO), polycaprolactone diol (PCL), diethylene glycol (DEG) and dihydroxy diphenyl sulfone (DPS). The oligomeric fluoroalcohols used are commercial products of Zonyl (BA-L) and Zonyl (FSO-100) obtained from DuPont Chemical (Rockville, MD) and designated in Table 2.5 as B and F, respectively.

The SMMs were synthesized using a two step solution polymerization method. The initial step involved the reaction of a diisocyanate with a polyol in a common solvent of dimethylacetamide (DMAc). This mixture formed a urethane prepolymer solution. The reaction was then terminated by the addition of an oligomeric fluoro-alcohol. The resulting polymer was then precipitated with distilled water, washed in 30 vol% of acetone in water to leach out unreacted monomer, and finally dried in an oven at 50°C. The latter step was repeated three times. It must be pointed out that the two polymerization steps were performed in a controlled atmosphere of prepurified nitrogen inside a glove box. Temperature, solvent volume, reactant mole ratio, reactant concentration, and stir rate were important parameters in determining the size distribution of the SMMs.

Table 2.5 Bulk properties of different formations of surface modifying macromolecules (SMMs)

SMM code	SMM formulation and Reaction stoichiometry[a]	M_w $(10^4)^b$	M_n $(10^4)^b$	PD $(M_w/M_n)^b$	F content (wt%)[c]	Reference(s)
S1	MDI:PPO:B(H) = 3:2:2	2.67	1.62	1.65	13.6	Pham, 1995
S2	MDI:PPO:B(H) = 3:2:2 (R)	2.23	1.42	1.57	11.4	Pham, 1995
S3	MDI:PPO:B(H) = 2:1:2	1.63	1.06	1.54	19.8	Pham, 1995
S4	MDI:PPO:B(H) = 2:1:2 (R)	1.8	1.14	1.58	12.1	Pham, 1995
		2.53	1.53	1.65	5.8	Pham, 1995
S5	MDI:PPO:B(L) = 3:2:2	2.52	1.97	1.28	11.4	Ho, 1997
		2.5	2.0	1.3	13.4	Mandeep, 2001
S6	MDI:PPO:B(L) = 3:2:2 (R)	1.93	1.32	1.46	7.9	Pham, 1995
S7	MDI:PPO:B(L) = 2:1:2	1.27	0.92	1.38	17.1	Pham, 1995
S8	MDI:PPO:B(L) = 2:1:2 (R)	1.53	1.02	1.50	11.6	Pham, 1995
S9	MDI:PPO:F(L) = 3:2:2	1.81	1.31	1.38	21.0	Ho, 1997
S10	MDI:PPO:F(I) = 3:2:2	1.81	1.35	1.34	16.3	Ho, 1997
S11	MDI:PPO:F(H) = 3:2:2	1.93	1.53	1.26	14.2	Ho, 1997
S12	MDI:PCL:B(L) = 3:2:2	2.89	2.26	1.28	8.6	Ho, 1997
S13	MDI:PCL:F(L) = 3:2:2	2.05	1.59	1.29	17.2	Ho, 1997
S14	MDI:PCL:F(I) = 3:2:2	2.07	1.63	1.27	16.7	Ho, 1997
S15	MDI:PCL:F(H) = 3:2:2	3.09	2.49	1.24	10.8	Ho, 1997
S16	MDI:DEG:B(L) = 3:2:2	1.4	1.2	1.17	22.0	Mandeep, 2001
S17	MDI:DPS:B(L) = 4:3:2	0.6	0.5	1.20	21.1	Mandeep, 2001

[a] (L), (I), and (H) refer to the low, intermediate, and high fractions of the fluoroalcohols (BA-L designated by B and FSO-100 designated by F). R refers to the reduced prepolymer reactant concentration to 75%.

[b] M_w is the polystyrene equivalent weight-average molecular weight; M_n is the number-average molecular weight; PD is polydispersity.

[c] F is the fluorine in the SMM measured by elemental analysis.

2.3.2 Preparation of SMM blended membranes

The membrane casting solution consisted of a single phase viscous fluid produced by combining a base polymer, SMM and/or polyvinylpyrrolidone (PVP) with a solvent. In most studies which used SMMs in Table 2.5 polyethersulfone (PES) was used as a base polymer, but polyetherimide (PEI) and polyvinylidene fluoride (PVDF) were also used. PES was blended with SMM and/or polyvinylpyrrolidone (PVP), with the solvent dimethylacetamide (DMAc) (Fang et al., 1994; Hamza et al., 1997; Ho, 1997; Pham et al., 1999; Minnery, 2000; Mahmud et al., 2001) or n-methyl-2-pyrrolidinone (NMP) (Zhang et al., 2003; Mosqueda-Jimenez et al., 2004a-b). SMM blended PVDF or PEI membranes with the solvent DMAc were prepared as well (Khayet and Matsuura, 2002; Khayet et al.,

2003). The membrane types in the above studies are listed in Table 2.6 based on the membrane casting solutions used. The bulk of the finished membrane was expected to be PES, as the DMAc was either evaporated or washed out together with PVP in the gelation process. The membrane could thus be referred to as a modified PES membrane.

The phase-inversion method was used to cast the SMM-modified and unmodified membranes. Before use, a chosen base polymer was dried in an air-circulating oven to remove absorbed moisture. Polymer solutions were, then, prepared by dissolving predetermined amounts of a chosen base polymer and/or PVP in DMAc or NMP as solvent. For preparation of the SMM blended membranes, different amounts of SMMs, all less than 5 wt% of the solution, were added to the casting solutions. After dissolution of the polymers, the solutions were filtered and cast on smooth glass plates to a predetermined thickness. The cast films together with the glass plates were either immersed immediately into distilled water or placed in an oven with forced air circulation at over 90°C for solvent evaporation during a predetermined period of time followed by immersion into water. After completing the gelation, the membranes were dried.

Table 2.6 Components of surface modifying macromolecule (SMM) blended membranes

Modified Membrane Type	Membrane casting solution				Reference(s)
	Base polymer	PVP[a]	SMM code(s)[b]	Solvent	
M1	PES	+	S1~S8	DMAc	Pham et al., 1999
M2	PES	+	S5~S8	DMAc	Hamza et al., 1997
M3	PES	+	S5	DMAc	Fang et al., 1994 Mahmud et al., 2001 Minnery, 2000
M4	PES	+	S5, S10~S15	DMAc	Ho, 1997
M5	PES	+	S5	NMP	Zhang et al., 2003
M6	PVDF	–	S16,S17	DMAc	Khayet and Matsuura, 2002
M7	PEI	–	S16,S17	DMAc	Khayet et al., 2003
M8	PES	+/–	S5,S16,S17	NMP	Mosqueda-J et al., 2004a
M9	PES	–	S5,S16,S17	NMP	Mosqueda-J et al., 2004b

[a] +/– means 'with/without PVP' in membrane casting solution.
[b] SMMs listed in Table 2.5.

There are certain advantages for using PES as a membrane material. PES is known as a hydrophilic, amorphous glassy rigid polymer and as a high performance thermoplastic with generally high chemical and heat resistivity. PES is dissolved by esters, ketones, polar aromatic solvents, and methylene chloride, but it has good resistance to inorganic chemicals, oils, greases, aliphatic hydrocarbons, and gasoline. On an arbitrary scale of increasing average chemical resistance of 0 to 10, PES was ranked 9 for acids, 9 for alkali, 6 for oxidizing agents, 8 for oils, greases, petroleum, and fuels, and 6 for hydrocarbons. PES is often used as a sublayer for structural integrity in multilayered membranes. The pores of a PES membrane are unique in type and their distribution. As PES membrane is glassy the pores are non-accommodating, meaning that transport across the membrane is limited to compounds smaller than the average pore size (Minnery, 2000). PVP was initially added to increase the viscosity to facilitate casting and to control pore formation. It is also suggested that PVP plays a role as a compatibilizer to improve the miscibility between PES and the SMM (Pham, 1995).

2.3.3 Characterization of SMM blended membranes

Hamza et al. (1997), Pham et al. (1999), Khayet and Matsuura (2002) and Khayet et al. (2003) reported values of the advancing and receding contact angles of unmodified PES membrane and they are listed in Table 2.7. According to their results of contact angle measurement, it was found that the incorporation of SMMs (Table 2.5) in the PES, PVDF, PEI solutions resulted in producing more hydrophobic film surfaces in any membranes produced in their studies. This was reflected in the increased contact angle values.

Table 2.7 Water contact angles of base polymer membranes

Base polymer	water contact angle		Reference(s)
	Advancing (°)	Receding (°)	
PES	77	49	Pham et al., 1999
PES	67.2	26.0	Ho, 1997
PVDF	85.9	69.3	Khayet and Matsuura, 2002
PEI	59.7	29.7	Khayet et al., 2003

In general, the contact angles increased with increasing the concentration of SMM until a plateau value was reached. This was attributed to the presence of SMM at the surface of the membranes and more directly to the hydrophobic nature of the SMM fluorine tails. In other words, the SMM migrated to the surface of the polymer mixture, yielding a new hydrophobic surface. Based on a simple model reported by Ward et al. (1984) to calculate the amount of additive required to saturate the surface, Fang (1997) and Minnery (2000) estimated that a very small amount, not more than a few percent of SMM, is required to cover the membrane surface completely. However, the model assumed a complete migration of SMMs to the surface and negligible roughness.

Based on the contact angle results discussed earlier, it was anticipated that the incorporation of the SMMs would result in the surface migration and concentration of SMMs. Pham et al. (1999), Fang (1997) and Ho et al. (2000) confirmed this result by studying both the chemical and the elemental group compositions at the surfaces using X-ray photoelectron spectroscopy (XPS). This method is widely used to provide quantitative and qualitative chemical information of the top 1-20 nm of surface (Pan, 1985). Generally, the samples are analyzed at a series of take-off angles (measured from the surface sample to the X-ray lens) to determine whether a compositional gradient exists near the surface. The XPS results showed that SMM migrated to the surface where it dominated the surface properties of the membrane and also that the orientation of the SMM was such that the fluorine tails were present at the surface. According to Khayet et al. (2003), by adding different types of SMMs to PEI membranes, they concluded that the SMM migration rate could be altered.

Differential scanning calorimetry (DSC) was also used to characterize the thermal transition of SMM modified and unmodified membranes and subsequently to assess the occurrence of microphase separation. It was found that the midpoint T_g values of the SMM modified PES membranes were those of PES rich phase. They were slightly lower than that of the pure PES which was recorded as 220°C. In addition, no difference in the behaviour of the SMM modified membranes was found for different concentrations of SMMs. These

results suggested that the macromolecules were not evenly distributed throughout the bulk material, but rather had migrated to the surface of the polymer and had little impact on the bulk phase microstructure (Pham, 1995; Pham et al., 1999; Ho, 1997; Ho et al., 2000). Pham (1995) and Pham et al. (1999) observed that the SMM modified PES membranes had higher heterogeneity than the pure PES material as the T_g widths were almost double. Pham (1995) reported that the microheterogeneity of the materials containing low SMM concentration was seen to be reduced by the presence of PVP in the casting solutions, although the effect of PVP on T_g width was lost at SMM concentrations greater than 2 wt%. It is well known that miscible polymer pairs are usually optically transparent and show only one intermediate T_g for all compositions. Hence, the miscibility of polymer systems can be detected by measuring their T_g values as a function of composition. Since only one T_g was observed for the SMM modified membranes, one might conclude that the SMMs were relatively miscible in the PES material. However, as will be shown later, polarized microscopy analysis of SMM modified PES membranes revealed the presence of phase separated structures in the form of spherical microdomains. In fact, the single observable T_g may have resulted from the low concentration of SMMs ($\leq$5 wt%) in the bulk material as reported by Theocaris and Kefala (1991) and therefore a T_g for the SMM phase was not detected.

Various microscopy techniques such as polarized microscopy (PM), confocal microscopy (CM), scanning electron microscopy (SEM) and atomic force microscopy (AFM) were used to examine the morphology and the structural characteristics of the SMM modified and unmodified membranes. Ho et al. (2000) stated that polarized microscopy technique provided the clearest evidence of the heterogeneous nature resulting from SMM addition to PES. The PM pictures of the unmodified PES membranes were clear and transparent, and no microstructures could be observed. However, microdomains appeared within the SMM modified PES membranes and their size depended on the type of SMM used and on their chemical compositions. Based on the confocal microscopy pictures taken in reflectance mode, Ho (1997) observed a gradual depletion of the number of the microdomain structures

throughout the bulk of the membrane material from the top membrane surface down to a depth of 6 μm. This observation supports the XPS data which suggested a selective migration of SMMs to the air-surface interface. Based on the AFM images, the SMM modified PES membranes were found to be rougher than the unmodified PES membrane and the obtained size of the microdomains was similar to that measured by confocal microscopy (Minnery, 2000). Khayet et al. (2003) analyzed AFM pictures for modified and unmodified PEI membranes and concluded that the nodule sizes, the pore densities and the surface porosities were larger for the SMM modified membranes as well as the membrane surfaces were smoother. Morphological analysis was also performed using SEM. Minnery (2000) observed that the SMM modified PES membranes underwent phase dispersion, and the size and number of dispersed phase elements increased as the solvent evaporation time increased. Minnery (2000) also reported that the SEM did not provide any information about the composition of the top surface, which was shown by Ho et al. (2000) using confocal spectroscopy to be populated by circular (or spherical) SMM-rich domains embedded in a matrix of PES.

Through these microscopy studies, it can be confirmed that surface modification was achieved by the migration of SMM concentrated microdomains to the air-membrane interface and the diameter of the dispersed phase observed by Ho (1997) ranged from 0.1 to 3 μm. Based on the microscopy results, Ho (1997) suggested a simplified model showing the hypothesized organization of SMMs in PES membrane (dry surfaces), which are illustrated in Figure 2.4 and mentioned that the ring structure was based on micellar formations analogous to that of surfactants, and at the surface, it was hypothesized that there was a reorganization of some SMM molecules in which the fluorine tails were exposed at the surface. This hypothesis was based on their XPS studies which showed high elemental fluorine content at the surface and revealed a low concentration of elemental nitrogen at the membrane surfaces, with an increase going deeper into the material.

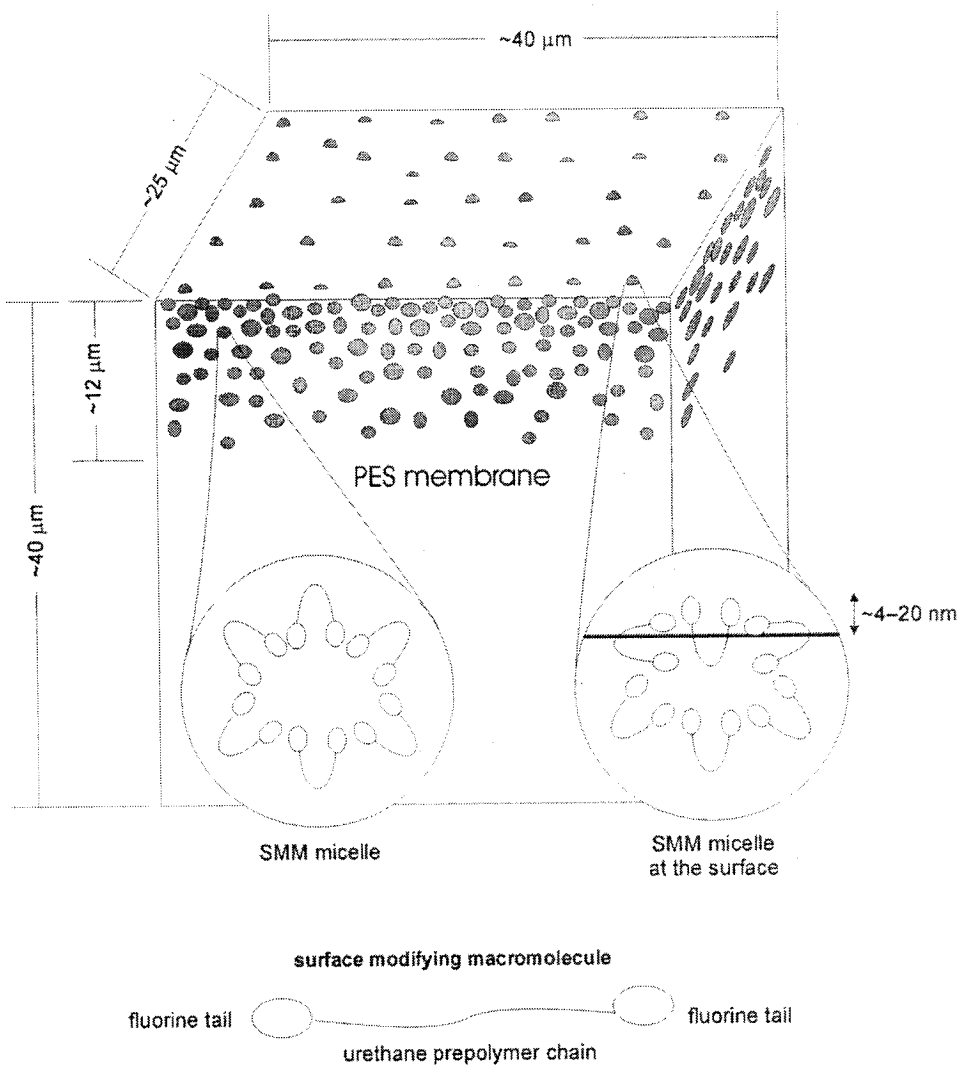

Figure 2.4 Schematic of a flat sheet SMM modified PES membrane (Ho, 1997)

2.3.4 Applications of SMM blended membranes

SMM modified and unmodified membranes were tested for the effect of SMM on permeation rate, separation factor and fouling during ultrafiltration (UF). Hamza et al. (1997) studied the performance of the PES membranes prepared from PES (22 wt% and 17 wt%), PVP (7%) and SMM (S5, S6, S7 and S8) (0 to 1.35 wt%), in a common solvent of

DMAc. Cutting oil (Texaco Soluble Oil)/water emulsion (10 vol% oil), was used as feed. It was found that PES UF membranes modified by SMM generally had lower pure water permeation rates and that the PES membranes modified by SMM were less susceptible to fouling by oil/water emulsions, as reflected in their consistent ability in having higher product rates than unmodified membranes. The oil gel layer resistance of the membranes resulted to be decreased with an increase in the SMM. Zhang et al. (2003) also studied on the SMM (S5) blended PES UF membranes. A series of UF membranes prepared with and without SMM were characterized by the solute transport method and it was concluded that the presence of SMM in PES UF membrane casting solution reduced the mean pore size of the membrane. This was confirmed by Mosqueda-Jimenez et al. (2004a) and they also showed that the presence of SMM (S5) decreased the size of pores and increased the number of pores per unit area. However, Khayet et al. (2003) observed an increase of the mean pore size when SMMs (S16 and S17) were added in PEI UF membranes. Membrane fouling tests with humic acid as the foulant indicated that the permeate flux reduction of the SMM (S5) modified membranes was much less than that of the unmodified ones. Therefore, fouling was more severe for the unmodified membranes (Zhang et al., 2003). Membrane fouling study with SMM (S5, S16 and S17) modified PES membranes were performed again using Ottawa River water, the source water for the city of Ottawa, Canada, by Mosqueda-Jimenez et al. (2004b). They found that although the impact of surface modification with hydrophobic SMMs was not as high as expected, the performances of those membranes were good in terms of NOM (Natural Organic Matter) removal and their permeate flux within the range of tight commercial membranes.

The pervaporation performance of PES membranes prepared with and without incorporating SMM was evaluated via experiments with chloroform/water mixtures (Pham, 1995; Fang, 1997; Fang et al., 1994; Mahmud et al., 2001) and alcohol/water mixtures (i.e. ethanol and methanol) (Minnery, 2000). The pervaporative performance of the SMM modified and unmodified PES membranes was studied by examining the effect of solvent evaporation time, SMM and PVP content in the casting solution, feed concentration, feed

temperature and permeate pressure. Fang et al. (1994) studied the effect of solvent evaporation period (i.e. from 2 to 16 min) on the pervaporative performance of the unmodified PES membranes prepared from casting solutions containing 25 wt% PES, 6 wt% PVP (M_w=4×10^4) in the solvent DMAC. It was found that PES membranes prepared with an evaporation time less than 7 min were water-selective while those having a longer evaporation time were chloroform selective, and the total permeation rate decreased with evaporation time. Fang et al. (1994) studied the effect of SMM concentration on the pervaporative performance of the PES membranes prepared with different amounts of SMM (S5), from 0 to 3.3 wt%. The evaporation time was 7 min and the concentration of chloroform in the feed solution was 1000 ppm. The separation factor increased with an increase in the amount of SMM until an optimal value at 1 wt% SMM, after which the enrichment factor decreased. They found that the addition of 1 wt% of fluorinated SMM in the casting solution enhanced the enrichment of chloroform in the permeate by more than 50 % and the flux kept increasing with an increase in SMM concentration. It would be of interest to identify the SMM molecular characteristics that could be related to the changes in membrane performance, and particularly how this change happens. Unfortunately, the data in the literature are still insufficient to answer these questions. An attempt was made by Pham (1995) to study the relationship between the pervaporation data and the characteristics of the SMM modified PES membranes. Pham (1995) found that the selectivity of membranes toward chloroform was clearly enhanced by the addition of SMM in the casting solution (i.e. S1, S3, S6 and S7). As stated by Fang (1997), Pham also observed an optimum in the enrichment factor, and the concentration at which the maximum occurred was characteristic of the type of SMM under identical membrane preparation conditions. Minnery (2000) studied the effect of SMM on the pervaporative performance of PES membranes using three feed mixtures, ethanol, distilled water and a ternary mixture of 65 wt% water, 30 wt% ethanol and 5 wt% methanol. The membranes were prepared with a 7 min solvent evaporation time from casting solution containing 25 wt% PES, 6 wt% PVP (M_w= 10^4) and SMM (S6) in DMAC. The concentration of SMM was either 0 or 1 wt%. In his study, Minnery (2000) measured the pervaporation flux in

modified and unmodified membranes as a function of the downstream pressure using two types of feed, water and ethanol. Both membranes exhibited a similar trend. The permeated flux decreased gradually approaching a minimum plateau as the downstream pressure increased, and a minimum was attained when the downstream pressure was equal to, or greater than, the vapor pressure of the liquid feed (2.6 kPa at 22°C for water and 6.6 kPa at 22°C for ethanol). The pore flow model provided a good fit for permeation of water and ethanol as a function of pressure (Okada and Matsuura, 1992). The effect of the feed concentration on the performance of the membranes synthesized with and without SMM modification was investigated by Minnery (2000) using aqueous ethanol solutions (from 0 to 100 % ethanol). It was observed that both membranes showed almost similar performances. The modified membrane exhibited a slightly higher mean permeated flux than the unmodified membrane and the mean water selectivity of the unmodified membrane was slightly greater than that of the modified membrane.

2.4 Membrane Distillation

2.4.1 Membrane distillation versus conventional VOC treatment methods

An estimated 1.6 to 5.0 million tons of VOCs enters the environment each year (Shen and Sewell, 1988), which causes significant pollution burden. The conventional treatment methods for removal and recovery of VOCs are incineration, biological treatment, adsorption, absorption, condensation, distillation and membrane separation. These processes are however effective only at specific VOC concentration levels; for example air stripping for low and distillation for high concentration levels. Some of these techniques also result in release of gaseous VOC emissions thereby only transferring the contaminants to another phase (Brewer, 1991).

Among conventional techniques, packed tower aeration (PTA) is the most economical and hence the most widely used process for removal of VOCs from water. It is considered the

best available technology (BAT) for removal of VOCs from drinking water by the US Environmental Protection Agency (USEPA, 1990). However, the contaminants are simply transferred from the water to the air phase during the stripping process and the exhaust air requires further treatment before release to the atmosphere. Gas phase granular activated carbon adsorption (GAC) is currently employed in conjunction with air stripping to control the gas phase emissions from PTA. GAC adsorption has several limitations such as: 1) the contaminants transfer only from the gas to the solid phase; 2) the reduction of effective adsorption capacity due to the presence of competition of moisture in exhaust stripper air and VOCs for adsorption site; and 3) the cost increasing because of the regeneration or disposal problem of the contaminated carbon (Kosuko et al., 1988; McGregor et al., 1988).

Attempts have been made to develop a closed loop air stripping process (CLASP) which couples the packed tower air stripping process with UV photooxidation of the exhaust air (Bhowmick, 1992). In this process, the PTA process uses a much higher air to water ratio during the stripping process than that membrane air stripping (Zander et al., 1989) and a large quantity of byproducts/intermediates is produced (Bhowmick, 1992).

Aerobic biological processes are also gaining importance for removal of organics from contaminated water, however a part of the VOCs is air stripped during the biodegradation process. In summary, existing conventional processes even with modifications still suffer from: 1) Transfer of contaminants from one phase to another creating yet another removal/ disposal problem; 2) Generation of undesirable byproducts/intermediates which only compound the problem; and 3) Processes are specific for contaminant concentration levels. These limitations of existing or modified conventional processes have led to a search for alternative VOC removal methods capable of avoiding these problems.

Separation of VOCs from liquid streams by membrane distillation is being considered as an alternative that may help overcome the shortfalls of PTA. Membrane distillation (MD) can be used over a wide range of VOC concentration levels. Water selective (hydrophilic)

membranes could be used for higher VOC concentrations and organo selective (hydrophobic) membranes for lower VOC concentrations. In this report, only hydrophobic membranes are considered. MD could be usefully applied for water pollution reduction, ground water cleanup and for organic recovery and reuse from industrial and petroleum waste streams. And a few industrial organizations have made hollow-fiber modules commercially available. Membrane devices having other configurations, e.g., spiral wound, are not yet available.

2.4.2 Introduction to Membrane distillation

MD is a relatively new process that is being investigated worldwide as a low cost, energy saving alternative to conventional separation processes such as distillation and reverse osmosis (RO). There are several benefits and limitations to use MD process, as Lawson and Lloyd (1997) reviewed in detail. The benefits of MD compared to other more popular separation processes stem from: (1) 100% (theoretical) rejection of ions, macromolecules, colloids, cells, and other non-volatiles. (2) lower operating pressures than conventional pressure-driven membrane separation processes, (3) reduced chemical interaction between membrane and process solutions, (4) less demanding membrane mechanical property requirements, and (5) reduced vapor spaces compared to conventional distillation processes. MD also has several limitations, which have resulted in a lack of general interest in the process. The primary limitation arises from the defining phenomenon itself: the process solutions must be aqueous and sufficiently dilute to prevent wetting of the hydrophobic microporous membrane. This limits MD to application such as desalination (currently dominated by RO), removal of trace volatile organic compounds from waste water, and concentration of ionic, colloid, or other relatively non-volatile aqueous solutions

Smolders and Franken (1989) compiled 'Terminology for Membrane Distillation' into a journal. According to the journal, the name 'membrane distillation' should be applied for membrane operations having the following characteristics:

- The membrane should be porous.
- The membrane should not be wetted by the process liquids.
- No capillary condensation should take place inside the pores of the membrane.
- The membrane must not alter the vapor-liquid equilibrium of the different components in the process liquids.
- At least one side of the membrane should be in direct contact with the process liquid.
- For each component the driving force of this membrane operation is a partial pressure gradient in the vapor phase.

A wide variety of membranes matching these qualifications are commercially available in flat sheet or tubular form, and they are typically fabricated from polytetrafluoroethylene (PTFE), polypropylene (PP), or polyvinylidenedifluoride (PVDF). Hydrophilic membranes that have been treated to make their surfaces hydrophobic have also been applied successfully to MD (Wu et al., 1992; Larbot et al., 2004). These include a cellulose acetate membrane modified via graft polymerization of styrene onto the surface, and a cellulose nitrate membrane modified via plasma polymerization of both vinyltrimethylsilicon/carbon tetrafluoride and octafluoro-cyclobutane onto the surface. Cheng and Wiersma (1982) received a patent for composite MD membranes that consist of a hydrophobic layer and a hydrophilic layer or a hydrophobic layer sandwiched between two hydrophilic layers.

The defining phenomenon of MD is relatively simple. A heated, aqueous feed solution is brought into contact with one side (feed side) of a hydrophobic, microporous membrane. The hydrophobic nature of the membrane prevents penetration of the aqueous solution into the pores, resulting in a vapor-liquid interface at each pore entrance. Figure 2.5 shows a cross sectional view of a hydrophobic membrane with straight cylindrical pores in contact with an aqueous solution to illustrate how the vapor-liquid interfaces are supported at the pore openings.

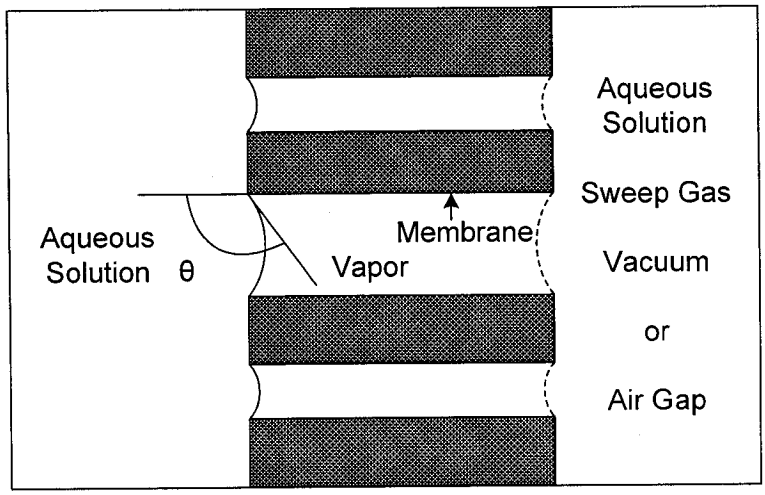

Figure 2.5 Vapor-liquid interfaces in membrane distillation

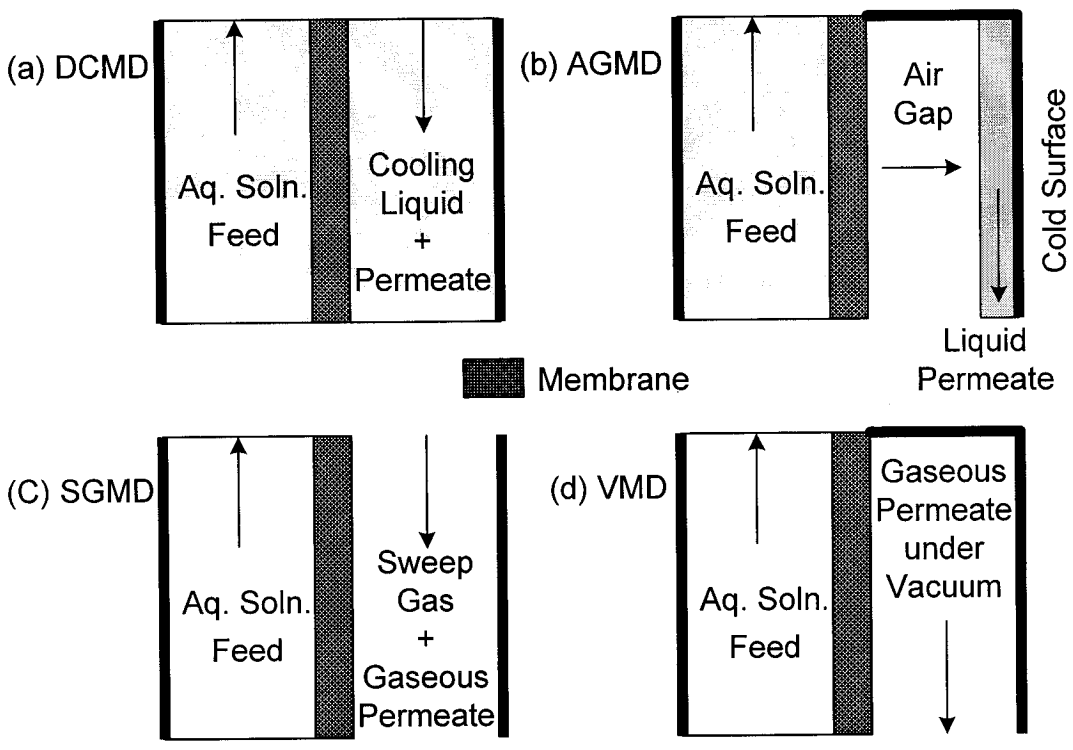

Figure 2.6 Common configurations of the MD process

A variety of methods may be employed to impose a vapor pressure difference across the membrane to drive flux. Figure 2.6 illustrates several common configurations of the MD process that may be utilized to establish the required driving force. The permeate side of the membrane may consist of a condensing fluid in Direct Contact with the membrane (DCMD), a condensing surface separated from the membrane by an Air Gap (AGMD), a Sweeping gas (SGMD), or a Vacuum (VMD). The type of MD process employed is dependent upon the permeate composition, flux, and volatility. The DCMD configuration, which requires the least equipment and is simplest to operate, is best suited for applications such as desalination or the concentration of aqueous solutions (orange juice), in which water is the major permeate component. Either S GMD or VMD should be used when a volatile organic or a dissolved gas is being removed from an aqueous solution; and AGMD, which is the most versatile MD configuration, can be applied to almost any application. In this thesis, only VMD will be focused and discussed.

2.4.3 Vacuum membrane distillation

The VMD process is similar to and is often confused with pervaporation (PV). The fundamental difference between VMD and PV is the role that the membrane plays in the separation. VMD employs a microporous membrane that acts only as a support for a vapor-liquid interface. While the VMD membrane may impart some selectivity based on individual Knudsen diffusivities of diffusing species, the largest degree of the separation is determined by vapor-liquid equilibrium conditions at the membrane-solution interface. On the other hand, pervaporation uses a dense membrane and the separation of each component in the membrane material. Because of these differences, V MD typically achieves fluxes that are several orders of magnitude higher than pervaporation fluxes (Lawson and Lloyd, 1997). The mechanisms for both VMD and PV processes were already shown in Figure 2.1 and their parallelism and differences were studied both theoretically and experimentally by Khayet and Matsuura (2004) and Urtiaga et al. (2001).

The effects of downstream pressure, feed temperature, flow rate, and solute concentration in VMD have been studied intensively by many researchers (Bandini et al., 1997; Lawson and Lloyd, 1996; Schofield et al., 1987; Izquierdo-Gil and Jonsson, 2003; Mengual et al., 2004; Urtiaga et al., 2000; Couffin et al., 1998). Two typical experimental results are shown in Figures 2.7 and 2.8. Figure 2.7 adapted from Sarti et al. (1993) illustrates the effect of permeate pressure on both overall flux and the flux of a volatile contaminant (1000 ppm benzene feed solution) in VMD. At low permeate pressure the overall flux is high relative to the benzene flux, resulting in a relatively poor separation, however at permeate pressures that are higher than the vapor pressure of water, the overall flux is similar to that of benzene, resulting in a highly concentrated benzene permeate. Mengual et al. (2004) found that the MD flux increased with the feed circulation rate and with the water inlet temperature (Figure 2.8). The dependence of the MD flux on the circulation rate confirms the presence of mass transfer boundary layer in the feed side.

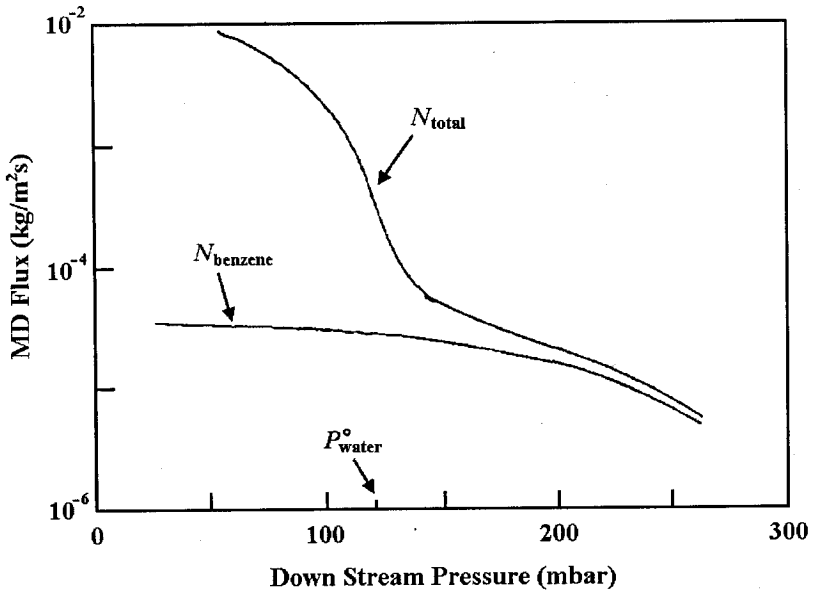

Figure 2.7 VMD flux versus absolute vacuum pressure; with 1000 ppm benzene in water and T_f = 50°C (Sarti et al., 1993)

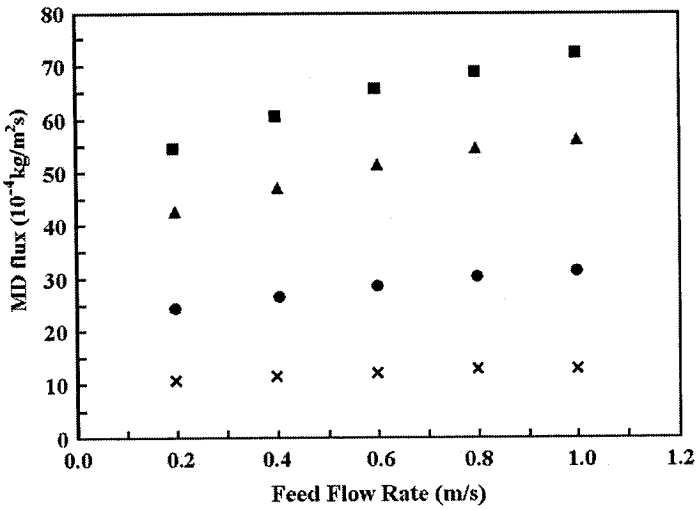

Figure 2.8 VMD flux as function of the water circulation rate for different water inlet temperatures (T_f): (×) for T_f = 40°C; (●) for T_f = 50°C; (▲) for T_f = 60°C; (■) for T_f = 65°C (Mengual et al., 2004)

VMD process has been proposed for various purposes; the extraction of volatile organic compounds (VOCs) from aqueous streams has been the most widely investigated application. Sarti and coworkers investigated the case of dilute binary aqueous mixtures containing methyl tertiary butyl ether (MTBE) and benzene (Sarti et al., 1993), acetone, isopropanol (IPA), MTBE, methylacetate (MeAc) and ethylacetate (EtAc) (Bandini et al., 1997; Bandini and Sarti, 1999). Izquierdo-Gil et al. (2004) used ethanol, EtAc and benzaldehyde as VOCs. Banat and Simandl (1996) studied the removal of benzene tracers from contaminated water. Urtiaga et al. (2000) and Couffin et al. (1998) also tested the VMD process to remove VOCs, particularly halogenated VOCs (HOVs), like chloroform, trichloroethylene (TCE) and tetrachloroethylene. There have been studies on VMD process for other purposes than VOC removal. It has been proposed for; the continuous removal of ethanol form fermentation broths (Hoffmann et al., 1987; Bandini et al., 1992); desalination for sea water (Cabassud and Wirth, 2003; Li et al., 2003); and the concentration of fruit juice (Bagger-Jørgensen et al., 2004; Bandini and Sarti, 2002).

2.4.4 Theoretical studies on VMD membrane permeability

Theoretical work for the permeation characteristics in VMD have been also conducted and combined with experimental results. In VMD, the membrane is usually hydrophobic and the pores are gas or vapor filled. Any theoretical study of gas permeation through microporous structures begins with a comparison of the mean free path, λ of the gas and the mean pore size of the structure. In a large volume of a pure gas, the mean free path of a molecule, λ, is defined as the average distance the molecule travels between successive collisions. The value of λ can be calculated from kinetic theory (Urtiaga et al., 2000):

$$\lambda = \frac{k_B T}{\sqrt{2}\pi\sigma^2 P'} \tag{2.1}$$

where k_B is the Boltzmann constant and σ is the collision diameter of the molecule. If λ of the gas in the membrane is much less than the pore size, the dominant flux mechanism is viscous or Poiseuille flow. If λ is much greater than the pore size, then Knudsen diffusion is the dominant mechanism. In VMD, the mean free path of water can reach relatively high values, because of the dependence of λ on $1/P'$ (Equation 2.1). Usually under normal VMD operating conditions, molecule-pore wall collision is dominant in membranes and therefore, VMD is Knudsen diffusion controlled for membranes with relatively small pores ($r_{ave} \ll \lambda$, where r_{ave} is the average pore radius). By assuming Knudsen diffusion controlled flow, Bandini et al. (1997, 1992) modeled VMD performance with the equation:

$$J_i = \frac{K_m}{\sqrt{M_i}} \Delta p_i \tag{2.2}$$

where J_i is the molar flux of ith species, K_m is the membrane permeability. M_i is the molecular weight of i, and p_i is the partial pressure of i. The kinetic theory of gases is introduced via the $(M_i)^{-1/2}$ term to account for the type of gas used. Although hydraulic permeability could be theoretically calculated if the pore sizes were known, in the view of a nonuniform pore size distribution and an uncertainty of tortuosity factor in the theoretical equation it is more convenient to measure the K_m directly in simple gas permeation experiments (Bandini et al., 1997).

However, VMD membranes still may have pores that are comparable in size to λ, where the flow falls into the Knudsen-Poiseuille transition resion, and various theoretical models have been developed to predict membrane permeability. Schofield et al. (1990) and Izquierdo-Gil and Jonsson (2003) assumed that all pores in the VMD membrane had one size which made Knudsen-Poiseuille transition flow. Based on that assumption, they developed a mass transfer equation for Knudsen-Poiseuille transition flow in a VMD process. This equation contained a parameter, b, of the extent of Poiseuille flow that is 0 for Knudsen diffusion and 1 for Poiseuille flow and the b value was measured by simple gas permeation experiments. Lawson and Lloyd (1996) and Lawson et al. (1995) also developed a Knudsen-Poiseuille transition equation as a linear addition of Knudsen and Poiseuille permeabilites. Khayet et al. (2004) measured mean pore size, pore size distribution, pore density, surface porosity and so on by tapping mode atomic force microscopy (TM-AFM) and divided the pore size into three regions, i.e. Knudsen dominant, Poiseuille dominant and their transition. Then, they added the fractions of the membrane permeabilities that correspond to the respective flow regions.

2.5 Theoretical Studies Regarding Membrane Characterization and Process

2.5.1 Membrane characterization based on the bubble point related method

The Bubble-point related method (Bubble pressure breakthrough) provides a simple means of characterizing the maximum pore size in a given membrane. This method introduced by Bechold is based on the measurement of the pressure necessary to blow air through a water-filled porous membrane. While the top of the membrane is in contact with water and membrane pores are filled with water, air pressure is applied from the bottom of the membrane. As the air pressure is gradually increased bubbles of air penetrate through the largest pores in the membrane at a certain pressure. In addition, the pore size distributions can be obtained by performing this technique by a stepwise increase of the pressure (Mulder, 1996).

Figure 2.9 indicates how the air flows through both dry and wet membranes. In the dry membrane all pores contribute to the air flow in the whole pressure range. The wet membrane is impervious at low pressures. At a certain minimal pressure (the 'Bubble point') the largest pores become empty and the convective gas flow starts to occur through these pores. A further increment in pressure opens smaller pores, which is described by the 'Cantor equation'. At high pressures the flow curve through the dry membrane is asymptotically reached and all pores become empty and the flow rate should become equal to that of the dry membrane (Mulder, 1996; Reichelt, 1991).

The relationship between pressure and pore radius is given by the Laplace equation:

$$r = \frac{2\gamma}{\Delta P}\cos\theta \tag{2.3}$$

where r is the radius of a capillary shaped pore, ΔP the applied air pressure, γ the surface tension of the air-liquid interface and θ the wetting angle with the solid matrix of the membrane. If the fluid totally wets the membrane, we can assume cos θ = 1 and we reach the Cantor equation (Hernandez et al., 1996):

$$r = \frac{2\gamma}{\Delta P} \tag{2.4}$$

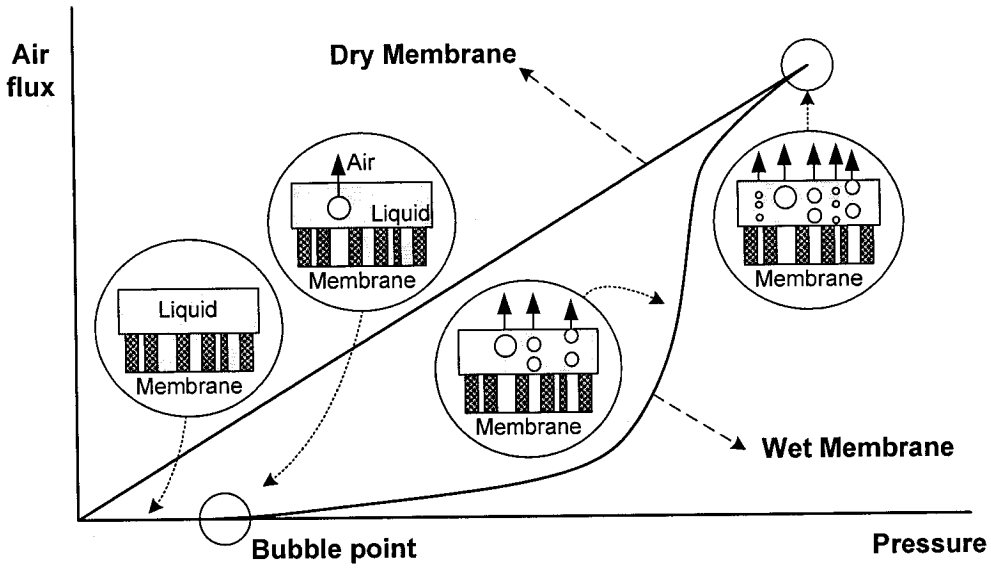

Figure 2.9 Gas flux in the permeation related bubble-point measurement

The following discussion (Kesting, 1985) on the air flux and pressure curve is based on the simplified assumption that a membrane is composed of a film of constant thickness through which parallel circular capillaries penetrate perpendicular to the surface. The radius of the capillaries varies between the maximum value r_{max} and a minimum value $r_{min} > 0$.

Consider first a single capillary with radius r and pore length δ which is filled with water and brought into contact with air (Figure 2.10a). When pressure is between 0 and ΔP (= $2\gamma/r$) the air flux, J_a is zero. When pressure is equal to ΔP the effluent flux becomes ΔJ_a. With a further increase in pressure J_a increases proportionally to the increase in pressure.

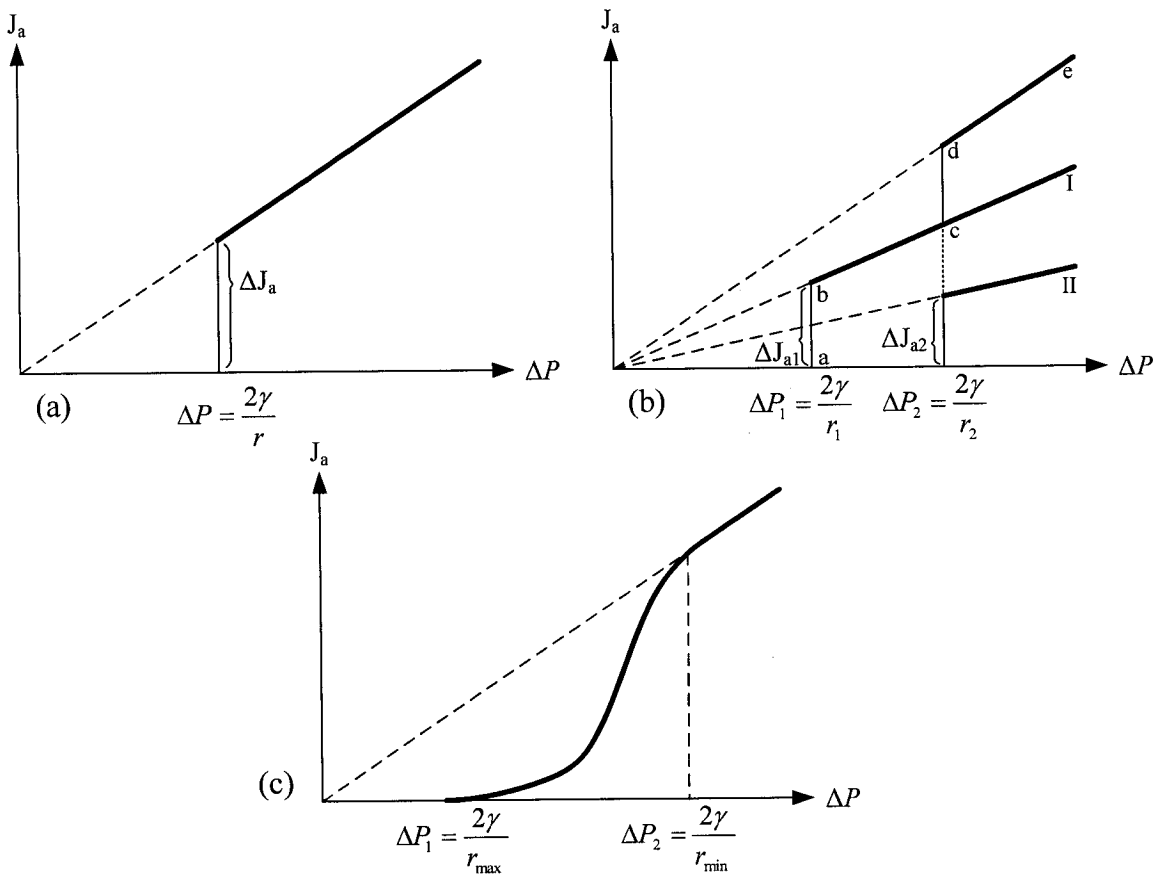

Figure 2.10 Air flux and pressure curve for (a) one or more capillaries of a given radius, (b) a system of two different capillaries and (c) a microfiltration membrane (Kesting, 1985)

Consider next a system consisting of two capillaries of equal length but of different radii, r_1 and r_2 ($r_1 < r_2$) (Figure 2.10b). The air flux through each capillary is not influenced by the presence of the other. Through the capillary with the larger radius r_1, the air flux is $\Delta J_{a,1}$ when $\Delta P = \Delta P_1$. At pressures greater than ΔP_1, the effluent flux increases along line I. Through the second capillary, with the smaller radius, an additional flow begins at $\Delta P_2 = 2\gamma / r_2$, so that the air flux becomes $\Delta J_{a,2}$. With further increases in pressure, air flux increases along line II. Since the fluxes through both capillaries are independent from each another, the total air flux is the sum of those through the two individual capillaries. The line 'abcde' graphically portrays the total air flux.

Let us consider now the example of a porous membrane. Because of the large number of pores of various radii, a continuous curve replaces the step function (Figure 2.10c). The air flux and pressure function for membranes is generally an S-shaped curve, whose maximum slope corresponds to the range of maximum pore density. For graphical evaluation of the air flux and pressure curve experimentally obtained for a porous membrane, the continuous curve (Figure 2.10c) is replaced by a step line (Figure 2.11) in which the abscissa is divided into intervals, for example, AB, and the continuous curve A'B' is replaced by a stepped line A'abB'. In Figure 2.11, the pores really present in the interval AB and those whose radii between r_3 and r_4 are replaced by ΔP_3 and ΔP_4 according to the Cantor equation (equation 2.4) and also the common radius $r_{3,4} = \frac{1}{2}(r_3 + r_4)$ is replaced $\Delta P_{3,4}$ according to the same equation. In the stepped line A'abB', the difference between a and b represents the air flux, $\Delta J_{a,3,4}$ which passes through the pores with the common radius $r_{3,4}$. As shown in Figure 2.11, $\Delta P_{1,2}$, $\Delta P_{2,3}$, $\Delta P_{3,4}$ etc. and $\Delta J_{a,1,2}$, $\Delta J_{a,2,3}$, $\Delta J_{a,3,4}$, etc. can be obtained. Then, each $r_{1,2}$, $r_{2,3}$, $r_{3,4}$ etc. can be calculated from $\Delta P_{1,2}$, $\Delta P_{2,3}$, $\Delta P_{3,4}$ etc. and plotted with $\Delta J_{a,1,2}$, $\Delta J_{a,2,3}$, $\Delta J_{a,3,4}$ etc. (Figure 2.12).

After the air flux-pressure (or pore radius) plot has been determined, it is necessary to convert it into a pore density (number of pores per surface unit)-pore radius plot. This could be done by adopting typical gas flow models; Hagen-Poiseuille and Knudsen model.

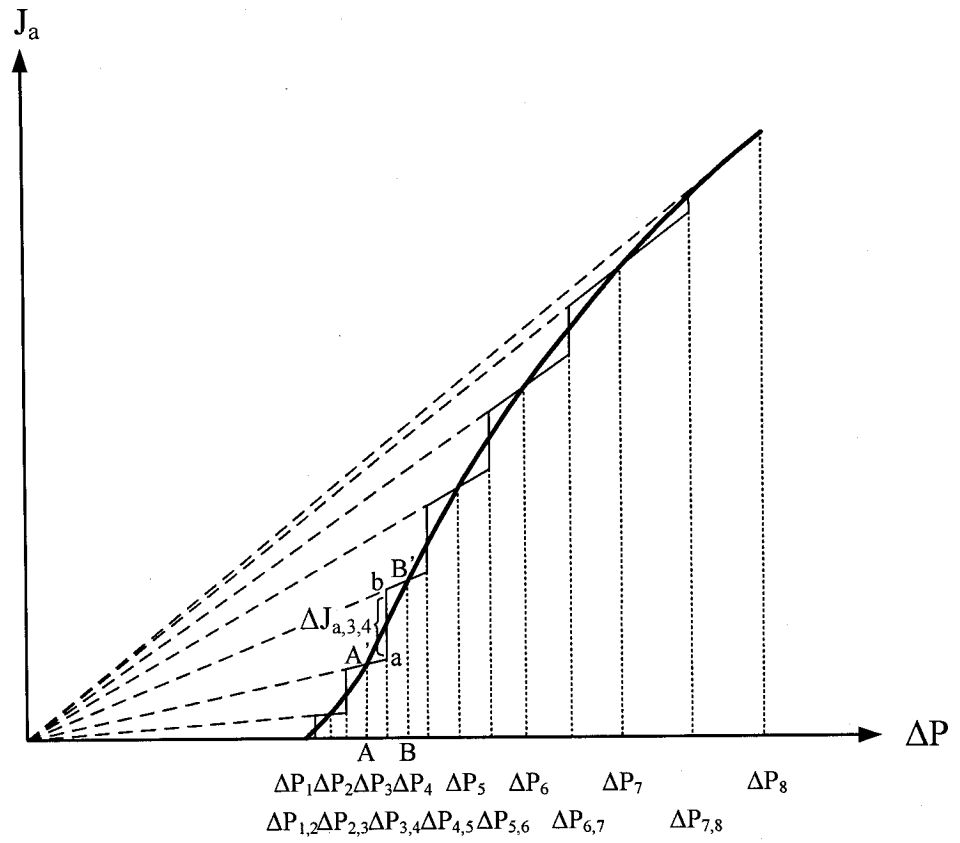

Figure 2.11 Graphical solution of the effluent flux and pressure curve for a porous membrane (Capannelli et al., 1983)

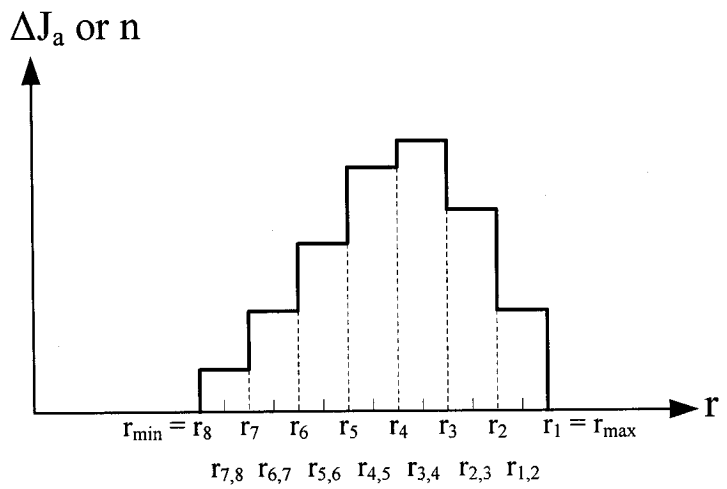

Figure 2.12 Air flux/pore density and pore radius curve for a porous membrane (Kesting, 1985)

As explained in chapter 2.4.4, in Poiseuille flow model, the gas acts as a continuum fluid driven by a pressure gradient, and molecule-molecule collisions dominate over molecule wall collisions, while in Knudsen flow model, the gas density is so low, and /or pore size so small, that collisions between molecules can be ignored compared to collisions of molecules with the walls of the porous media. When the air flows for each pore diameter in the distribution according to the Poiseuille model, the air flux is (Hernandez et al., 1996):

$$\Delta J_{a,i} = n_i \cdot \frac{\pi r_i^4}{8\eta\psi} \cdot \frac{\Delta P_i}{\delta_p} \tag{2.5}$$

where n_i is the density of pores of radius r_i, ψ is a tortuosity factor, η is the gas viscosity and δ_p is the pore length or skin layer thickness. When the air flows according to the Knudsen flow model, then the air flux is (Hernandez et al., 1996):

$$\Delta J_{a,i} = n_i \cdot \frac{2\pi}{3} \cdot \left(\frac{8RT}{\pi M}\right)^{1/2} \cdot \frac{r_i^3}{P\psi} \cdot \frac{\Delta P_i}{\delta} \tag{2.6}$$

where M is the molecular weight of the gas and P is the downstream pressure (1 atm when the downstream is open to the air). Therefore, using the Equations 2.5 or 2.6 for each $r_{1,2}$, $r_{2,3}$, $r_{3,4}$ etc. in Figure 2.12, the number of pores of $n_{1,2}$, $n_{2,3}$, $n_{3,4}$ etc. can be obtained from Figure 2.12.

2.5.2 Membrane characterization by solute transport data (Singh, 1999)

- Mean pore size and pore size distribution

Solute separation, f, in percent is defined as

$$f = \left(1 - \frac{c_p}{c_f}\right) \times 100 \tag{2.7}$$

where c_p and c_f are the solute concentrations in the permeate and in the bulk of the feed solution, respectively. It is to be noted that the effect of concentration polarization on separation is not considered in Equation 2.7. When solute separation (%) of an ultrafiltration membrane is plotted versus the solute diameter on a log-normal probability

paper, a straight line is yielded as reported by Micheals (1980). If solute separation correlates with solute diameter according to the log-normal probability function, then this relationship can be expressed as

$$f = \mathrm{erf}(z) = \frac{1}{\sqrt{2\pi}} \int_{-\infty}^{z} e^{-\frac{u^2}{2}} du \tag{2.8}$$

where

$$z = \frac{\ln d_s - \ln \mu_s}{\ln \sigma_g} \tag{2.9}$$

and d_s is the solute diameter, μ_s is the geometric mean diameter of solute and σ_g is the geometric standard deviation about the mean diameter. According to the Equations 2.8 and 2.9, a straight line in the form of

$$F(f) = A_0 + A_1(\ln d_s) \tag{2.10}$$

will be yielded between f (solute separation in %) and d_s (solute diameter) on a log-normal probability paper. A_0 and A_1 are the intercept and the slope, respectively. From this log-normal plot, mean solute size (μ_s) can be calculated as d_s corresponding to f = 50%. σ_g can be determined from the ratio of d_s at f = 84.13% and at 50%. By ignoring the dependence of solute separation on the steric and hydrodynamic interaction between solute and pore size (Micheals, 1980), the mean pore size (μ_p) and the geometric standard deviation (σ_p) of the membrane can be considered to be the same as solute mean size and solute geometric standard deviation. From μ_p and σ_p, the pore size distribution of a ultrafiltration membrane can be expressed by the following probability density function (Youm and Kim, 1981).

$$\frac{df(d_p)}{dd_p} = \frac{1}{d_p \ln \sigma_p \sqrt{2\pi}} \exp\left[-\frac{(\ln d_p - \ln \mu_p)^2}{2(\ln \sigma_p)^2} \right] \tag{2.11}$$

where d_p is the pore diameter.

- Pore density and the surface porosity

The number of pores per unit area, known as pore density, can be calculated from the permeability data of the membrane using the Hagen-Poiseuille equation. Based on this equation, solvent flux ($J_{w,i}$) through the pores of diameter d_i can be expressed as

$$J_{w,i} = \frac{n_i \pi d_i^4 \Delta P}{128 \eta \delta_p} \tag{2.12}$$

where n_i is the number of pores (per unit area) having diameter of d_i, δ_p is the length of the pores, η is the solvent viscosity and ΔP is the pressure difference across the pores. Total flux J through the membrane can be calculated by adding all the fluxes through the pores of different sizes as

$$J_w = \frac{\pi \Delta P n}{128 \eta \delta_p} \sum_{d_{\min}}^{d_{\max}} f_i d_i^4 \tag{2.13}$$

where n is the total number of pores and f_i is the fraction of the number of pores with diameter d_i. From Equation 2.13, the total number of pores per unit area (n) can be calculated as

$$n = \frac{128 \eta \delta_p J_w}{\pi \Delta P \sum_{d_{\min}}^{d_{\max}} f_i d_i^4} \tag{2.14}$$

Pore length δ_p is considered equivalent to the skin layer thickness of asymmetric ultrafiltration membrane.

Similarly, the expression for surface porosity (S_p), which is defined as the ratio between the area of pores to the total membrane surface area, can be derived as

$$S_p = \left(\frac{N \pi}{4} \sum_{d_{\min}}^{d_{\max}} f_i d_i^2 \right) \times 100 \tag{2.15}$$

- Stokes radius of polyethylene glycol and polyethylene oxide molecules

The Stokes radius of a macromolecule can be obtained from the diffusivity in a solution by using the following Stokes-Einstein equation

$$D_{AB} = \frac{k_B T}{6\pi\eta a_s} \tag{2.16}$$

where D_{AB} is the diffusivity, k_B is Boltzmann constant, η is the solvent viscosity and a_s is the Stokes radius. The diffusivity can also be calculated by the following equation (Hsieh et al., 1979)

$$D_{AB} = \frac{2.5\times10^6 k_B T}{\{\eta(M[\eta])^{1/3}\}} \tag{2.17}$$

where M and $[\eta]$ are the molecular weight and the intrinsic viscosity of the polymer, respectively. By combining the Equations 2.16 and 2.17, at any given temperature and solvent we can obtain

$$a_s = 2.122\times10^{-8}(M[\eta])^{1/3} \tag{2.18}$$

where a_s is in cm, M is in g/mol and $[\eta]$ is in dL/g. Intrinsic viscosity of a polyethylene glycol (PEG) and a polyethylene oxide (PEO) of known molecular weight can be calculated from the following equations

For PEG (Meireles et al., 1995),

$$[\eta] = 4.9\times10^{-4} M^{0.672} \tag{2.19}$$

For PEO (Nabi, 1968)

$$[\eta] = 1.192\times10^{-4} M^{0.76} \tag{2.20}$$

Intrinsic viscosities of PEGs of various molecular weights calculated from the empirical Equation 2.19 are in very good agreement with the values determined experimentally (Hsieh et al., 1979). Intrinsic viscosity for some of the PEG molecules are also given by Bessières et al. (1996), and they are also in very good agreement with the values calculated

from the empirical Equation 2.19. By substituting the expression for $[\eta]$ in Equation 2.18, we obtain;

For PEG

$$a_s = 16.73 \times 10^{-10} M^{0.557} \tag{2.21}$$

For PEO

$$a_s = 10.44 \times 10^{-10} M^{0.587} \tag{2.22}$$

From the above empirical Equations 2.21 and 2.22, Stokes radii, a_s of PEG and PEO molecules can be obtained (in cm) from their molecular weights and the calculated a_s values are same to the solute diameter, d_s in Equation 2.10.

2.5.3 Theoretical study on the transport mechanism of vacuum membrane distillation (VMD) (Bandini et al., 1992)

- Membrane permeability

Membrane permeability to the species i, $K_m\sqrt{M_i}$ was defined according to Equation 2.23,

$$N_i = K_m \sqrt{M_i} \Delta p_i \tag{2.23}$$

where N_i is the mass flux ($kg \cdot m^{-2} \cdot s^{-1}$), Δp_i the partial pressure difference across the membrane (Pa), and M_i the molar mass of the permeating species (kg mol^{-1}), respectively. Subscript i is the ith component (VOC).

Making use of the gas kinetic theory applied to a fluid diffusing inside the pore of a solid medium (Dullien, 1979), the permeability coefficient K_m (s $mol^{1/2}$ m^{-1} $kg^{-1/2}$) can be obtained as follows

$$K_m = \frac{4 f_v d_{p,avg}}{3\psi\delta_p (2\pi RT)^{1/2}} \tag{2.24}$$

Apparently, the permeability coefficient K_m depends upon temperature and on the membrane properties only, in terms of average pore-size $d_{p,avg}$ (m), void fraction f_v, and tortuosity factor ψ. Therefore, it can be calculated independently from the permeating species. However, owing to the nonuniform pore-size distribution of the membrane, it is more convenient and reliable to measure K_m directly. Air permeation experiments at different downstream pressures are the simplest way to obtain the K_m values for different membranes. R is the universal gas constant (J mol^{-1} K^{-1}).

As reported by Bandini et al. (1997), when air flux is plotted versus pressure difference across a membrane at low pressure range (about 0 to 50 kPa), a straight line from the origin is yielded. The linear behavior observed indicates that viscous flow in the pores is negligible compared to Knudsen diffusion. They stated that the K_m coefficient depended on temperature only slightly: according to Equation 2.24 only a 2 % change in K_m occurs due to temperature changes over the temperature range investigated by them, from 20°C to 35°C. They also compared experimentally measured K_m and the kinetic theory value (Equation 2.24), and concluded that the measured and calculated K_m values are remarkably close to each other.

- Heat and mass transfer in vacuum membrane distillation

The model describing vacuum membrane distillation (VMD) has been widely investigated and its ability to represent the separation process has been already well documented as presented in Section 2.4.4. With reference to any membrane module cross-section, the main physical phenomena involved in the VMD are summarized as follows (Sarti et al., 1993):

- heat and mass transfer from the liquid bulk to the membrane surface;

- evaporation of the liquid mixture at the liquid-vapor (L-V) interface immobilized at the pore entrance;
- mass transfer through the membrane.

Due to the rather low pressure in the permeate side, it can be safely assumed that there are no temperature, concentration and pressure differences between the membrane downstream surface and the bulk gaseous phase. A schematic representation of VMD mechanism shows the temperature and concentration polarization in the liquid feed (Figure 2.13).

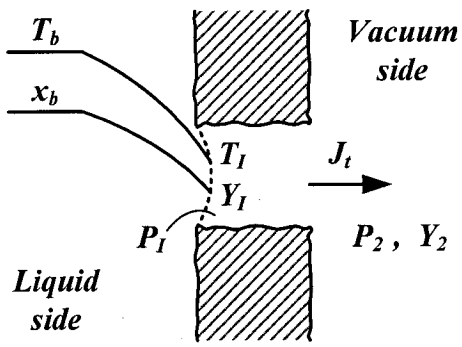

Figure 2.13 A schematic representation of transfer mechanisms in vacuum membrane distillation (Bandini et al., 1997)

The total transmembrane flux which is generated may follow either the Poiseuille or the Knudsen regime or a transition regime, depending upon the pore size compared with the molecular free path as stated earlier. However, since for all the typical operative conditions the membrane pore size is well below the mean free molecular path of the permeating species, in VMD process the Knudsen diffusion is dominant over the Poiseuille diffusion. Therefore, only the Knudsen diffusion was taken into account as the mechanism of mass transport through the membrane.

As a consequence, the molar flux of a permeating species J_i (mol m^{-2} s^{-1}) is linearly related to its partial pressure difference across the membrane

$$J_i = \frac{K_m}{\sqrt{M_i}}(P_1 Y_{i,1} - P_2 Y_{i,2}) \tag{2.25}$$

where K_m is the permeability coefficient defined in Equation 2.23. P_1 and P_2 are the interface and vacuum side pressures, respectively. Y is the mole fraction in the vapor phase at the interface (I) and at the vacuum side (2). By taking the sum over all the components, the total molar flux J_t (mol·m^{-2}s^{-1}) can be easily expressed as

$$J_t = \frac{K_m}{\sqrt{M_t}}(P_1 - P_2) \tag{2.26}$$

where M_t (kg·mol^{-1}) is a suitable average molecular weight in the permeating stream, defined as

$$\sqrt{M} = \sum_i \frac{J_i}{J_t}\sqrt{M_i} \tag{2.27}$$

In addition to the mass transfer through the membrane embodied by Equation 2.26, heat and mass transfer through the liquid stream should be considered; indeed, the temperature and composition prevailing at the vapor-liquid interface differ from the bulk conditions, as shown in Figure 2.13, where the concentration profile has been drawn making reference to a single volatile solute in water.

The heat required for the interfacial evaporation is supplied by the heat flux through the liquid stream; a simple balance across the evaporation surface gives

$$\sum_i J_i \Delta H_i = h(T_b - T_1) \tag{2.28}$$

where h is the heat-transfer coefficient in the liquid phase (W m^{-2} K^{-1}). In writing Equation 2.28 the convective heat transfer within the gaseous phase was not included since its contribution, though nonzero, is indeed negligible. ΔH is the molar latent heat of vaporization (J mol^{-1}), T_b the liquid bulk temperature, and T_1 the temperature at the liquid-vapor interface.

Mass transfer through the liquid phase could be described by the film theory model (Porter, 1972), which assumes that the drops in temperature and concentration are located in a thin layer close to the membrane. For binary mixture, the mole fraction in the liquid bulk $x_{i,b}$ and at the interface $x_{i,I}$ are related to the molar fluxes by the following relationship

$$\frac{J_t}{k_L c_L} = \ln \frac{x_{i,I} - J_i / J_t}{x_{i,b} - J_i / J_t} \tag{2.29}$$

in which k_L is the mass-transfer coefficient in the liquid phase (m s^{-1}), c_L is the total molar concentration in the liquid phase (mol m^{-3}).

Equations 2.25 to 2.29, coupled with the relationships describing the vapor-liquid equilibrium conditions existing at the interface, represent the local mathematical model of VMD processes. Firstly, a set of temperature at the liquid-vapor interface (T_I) is assumed. Using T_I and a chosen experimental data point, both heat- and mass- transfer coefficients within the liquid phase h and k_L are calculated. The calculated h and k_L are used to obtain $Y_{I,2}$, the mole fraction in the vapor phase at the vacuum side, and then compared to the experimental results.

- NRTL (Non Random Two Liquid) model

Partial pressure values are necessary to estimate theoretical fluxes from the Knudsen model (Equation 2.25). In Equation 2.25, $P_I Y_{i,I}$ can be estimated using a model for vapor-liquid equilibrium (VLE) (e.g. NRTL). The partial pressure of species i may be expressed as

$$p_i = \gamma_i x_i P_i^{\circ} \tag{2.30}$$

where P_i° is the vapor pressure of pure component i that may be obtained from the Antoine equation, x_i the mole fraction of component i and γ_i the activity coefficient of component i. There are a number of activity coefficient expressions available for calculating vapor-liquid phase diagrams for binary mixtures of organic chemicals such as the methods of Wilson, Van Laar, UNIFAC, and NRTL. Izquierdo-Gil et al. (2004) reported that for ethanol

solutions, there was a good agreement with NRTL model to reproduce the experimental fluxes, and in this study only NRTL model is considered for the vapor-liquid equilibrium (VLE). The NRTL model equation is (Izquierdo-Gil and Jonsson, 2003):

$$\ln \gamma_i = x_k^2 \left[\tau_{ki}^2 \left(\frac{G_{ki}}{x_i + x_k G_{ki}} \right)^2 + \frac{\tau_{ik} G_{ik}}{(x_k + x_{ik} G_{ik})^2} \right] \tag{2.31}$$

$$\tau_{ik} = a_{ik} + (b_{ik} / T) \tag{2.32}$$

$$G_{ik} = \exp(-\phi \tau_{ik}) \tag{2.33}$$

where x_i is the mole fraction of component i and γ_i the activity coefficient of component i, the parameters value a_{ik}, b_{ik} and ϕ used for ethanol mixtures are given by Izquierdo-Gil et al. (2004).

3. Experimental

Throughout this thesis, a series of experiments were carried out using 'surface modifying macromolecules' (SMMs). Two different types of SMMs were used. The first SMM named 'tSMM' in this thesis was one of traditional SMM, S5, which is specified in Table 2.5. The other SMM was newly designed and developed to meet the purpose of this thesis and was called 'nSMM'. Using these two SMMs, a number of investigations were made in the following sequence;

Part I. Experiments with tSMM

(1) tSMM synthesis
(2) tSMM blended PES membrane preparation
(3) Bubble point tests of the tSMM blended membranes
(4) Tensile strength/elongation tests of the tSMM blended membranes
(5) Tests for studying tSMM migration
(6) Tests for membrane distillation studies

Part II. Experiments with nSMM

(1) nSMM synthesis
(2) nSMM blended PES membrane preparation
(3) Tests for studying nSMM migration
(4) Ultrafiltration
(5) Vacuum Membrane distillation

3.1. Materials

The chemicals were used without any further treatment; unless stated otherwise. The materials or chemicals fell into tree different categories based on their purposes: 1) SMM

synthesis, 2) membrane preparation, and 3) membrane-characterization or -performance testing. The information on materials or chemicals used for the last purpose is given in the section where membrane characterization and performance are described. The chemical structures of all the materials are provided in the Appendix A.

3.1.1 Materials used for SMM synthesis

The chemicals used for tSMM synthesis included methylene bis-*p*-phenyl diisocyanate (MDI) (obtained from Eastman Kodak, Rochester, NY), polypropylene diol of average molecular weight 425 (PPO) (Aldirich Chemical Company, St. Louis, MO), oligomeric fluoroalcohol, Zonyl BA-L^{TM} of average molecular weight 443 (BAL) (Dupont Chemical, distributed by Van Waters & Roger, Montreal, Quebec). N,N-dimethylacetamide (DMAc) (99%) (Aldrich Chemical Company, St. Louis, MO) was used as the solvent. Prior to use, DMAc was distilled at about 25°C under a pressure of 0.133 kPa (1.0 torr). PPO and BAL were degassed for 24 hours under 0.067 kPa (0.5 torr) and MDI was also distilled at 150°C under 0.067 kPa. The distillation was performed to remove both impurities and moisture in the chemicals while degassing removed only moisture. The apparatus used for distillation and degassing of chemical and solvents are shown in Appendix B.

The same MDI and BAL were used for nSMM synthesis. However, in nSMM synthesis α, ω-aminopropyl poly(dimethyl siloxane) (PDMS) of average molecular weight 900 (supplied by Shinetsu Co., Tokyo, Japan) was used instead of PPO. Tetrahydrofuran (THF) of Aldrich 99.9% grade (supplied by Aldrich Chemical Co. Inc., Milwaukee, WI) was also used to dissolve PDMS. N,N-dimethylacetamide (DMAc) of 99% grade was supplied by BDH Inc. (Toronto, Canada). The same pretreatment of MDI, DMAc and BAL as in tSMM synthesis was done. PDMS was also degassed for 24 hours under 0.067 kPa (0.5 torr).

3.1.2 Materials used for membrane preparation

Polyethersulfone (PES, Victrex 4100P) supplied by General Electric and Polyvinyl pyrrolidone (PVP) of molecular 10,000 supplied by Aldrich Chemical Company Inc. (Milwaukee, WI) were dried at 60°C for 24 hours before use. N-methyl pyrrolidone (NMP) was supplied by Aldrich Chemical Co. Inc. (Milwaukee, WI).

3.2 SMM Synthesis

Throughout this thesis, two different kinds of SMMs, tSMM and nSMM, were synthesized and used in membrane preparation. Each SMM has two different batches based on their synthesis location. Some of tSMM was synthesized at the University of Toronto (tSMM1) while the rest was synthesized at University of Ottawa (tSMM2). nSMM was developed at Hanyang University, Seoul, Korea and synthesized at both Hanyang University (nSMM1) and University of Ottawa (nSMM2).

The SMMs were synthesized using a two-step solution polymerization method as illustrated in Figure 3.1 below. The first step was conducted in a proper solution to form a polyurethane (PU) or polyurethane-urea (PUU) as a prepolymer. The prepolymer was then, in the second step, end-capped by the addition of oligomeric fluoro-alcohol, resulting in a solution of SMM.

The apparatus used for tSMM1 synthesis at the University of Toronto is illustrated in Appendix C. To eliminate the effect of moisture, the prepolymerization and end-capping steps were performed in a controlled atmosphere of prepurified nitrogen (grade 4.8, BOC Canada Ltd., Etobicoke) inside a glove box. For the batches tSMM2, nSMM1 and nSMM2, the nitrogen atmosphere was applied by using a much simpler apparatus as presented in Appendix D.

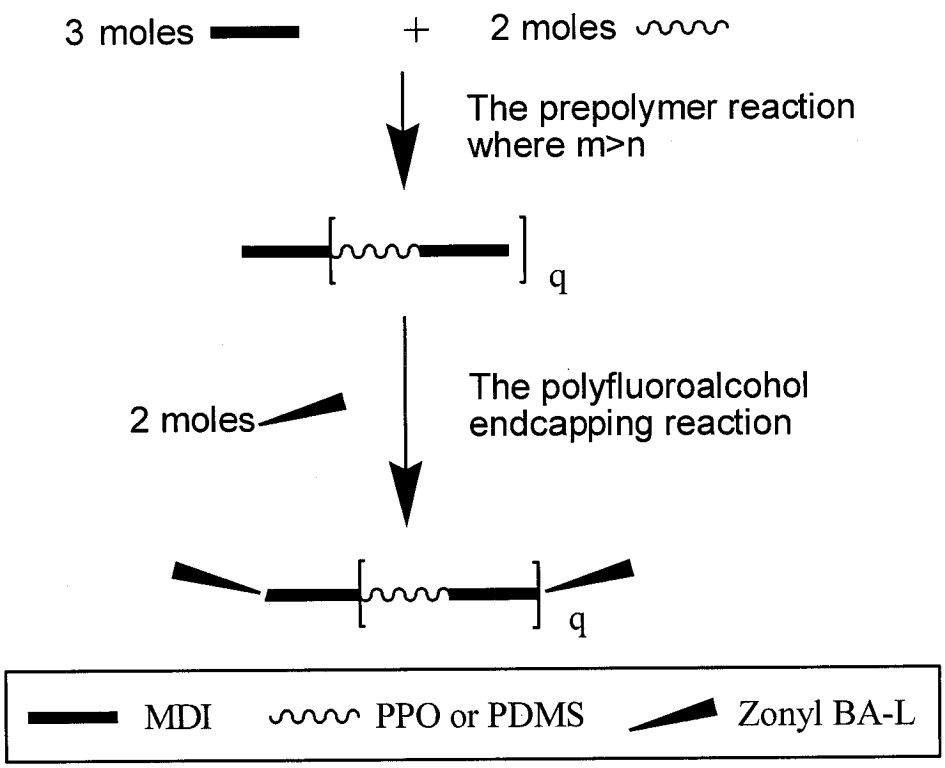

Figure 3.1 The Reaction schematic diagram of SMM synthesis

3.2.1 tSMM synthesis

The synthesis of tSMM is outlined below:

(1) Distillation of MDI,

(2) Degassing PPO for a week,

(3) Degassing BAL for a week,

(4) Distillation of DMAc within 48 h before use,

(5) Reaction overnight,

(6) Precipitation,

(7) Washing and Drying.

The details of distillation and degassing procedure were already given in section 3.1.1. Prior to the reaction, the synthesis apparatus should be assembled as shown in Appendix C or D and the air should be purged from inside the glove box or the glassware setup introducing N_2 gas. The molar ratio of reagents MDI:PPO:BAL was 3:2:2.

8.45 g of PPO and 100 mL of DMAc were poured into the glass reactor (1 L reaction kettle or round-bottom distilling flask). A stirrer controller was turned on, speed being set at 200 rpm. After starting the stirrer, MDI solution (7.5 g of MDI in 50 mL of DMAc) was prepared and added drop-wise to the glass reactor while maintaining the stirring rate set above. The mixture was kept stirred for 3 hours at 50°C until the synthesis of the prepolymer was completed. BAL solution (8.87 g of BAL in 50 mL of DMAc) was then prepared and added to the pre-polymer solution in the glass reactor. The mixture was kept stirred for 24 hours at a temperature of 25°C to complete the synthesis of the surface modifying macromolecule (tSMM).

The tSMM solution was then poured into distilled water in a four liter beaker under vigorous stirring. The tSMM was an elastomeric and coagulated by itself in the water. The conglomerated tSMM was taken out from the water every ten seconds using a metal stick. Those collected tSMM lumps were cut into smaller pieces and washed in distilled water under stirring twice, each time for 24 hours, in order to leach out the residual solvent. The water was changed to 30% acetone in water where the tSMM was kept for another 24 hours period to further remove residual unreacted monomers (specifically BAL). The final polymer was then dried in a circulation oven at 60°C for 5 days. The chemical structure of tSMM is shown in Figure 3.2.

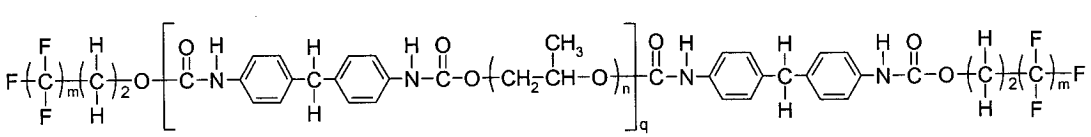

Figure 3.2 The chemical structure of tSMM

3.2.2 nSMM synthesis

Before reaction, MDI was distilled at 150°C under 0.067 kPa (0.5 torr) to remove impurities and water. PDMS and BA-L were both degassed overnight at room temperature under a pressure of 0.133 kPa (1.0 torr).

The air inside the glassware setup should be removed by introducing N_2 gas as was done in tSMM synthesis. PDMS solution (10.8 g of PDMS in 40 g of THF solvent) was loaded to the glass reactor under vigorous stirring (about 200 rpm) and preheated to 50 – 55°C. MDI solution (4.5 g of MDI in 20 g of DMAc) was added to the glass reactor while maintaining the stirring same rate. The mixture was kept stirred for 3 hours at 50°C until the synthesis of the prepolymer was completed. A solution of Zonyl BA-L (5.32 g of Zonyl BA-L in 20 g of DMAc) was prepared and added to the glass reactor. This last step of the reaction was carried out for 24 hours at room temperature. Then the reaction mixture was added drop-wise into distilled water under stirring for the precipitation of the nSMM. The nSMM was more elastomeric than tSMM, which could be caused a longer prepolymer chain of the nSMM than the tSMM. The nSMM also conglomerated by itself in the water. For the nSMM lump collection, the same method as in the tSMM synthesis was used. The collected nSMM lumps were cut into smaller pieces and washed several times with distilled water to leach out the residual solvent and the water-soluble unreacted components, and was further dried in an air-circulated oven at 60°C for 5 days. The chemical structure of nSMM synthesized is illustrated in Figure 3.3.

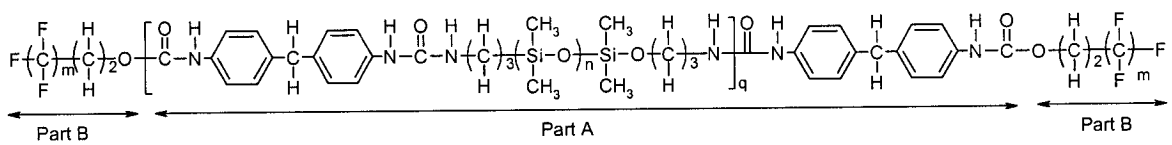

Figure 3.3 The chemical structure of nSMM

3.3 Membrane Preparation Details

The phase inversion method was used. By this method, controlling the initial stage of phase transition enabled us to obtain membranes of different morphology, i.e. porous asymmetric as well as dense homogeneous membranes. For example, immersion precipitation technique was used to make porous asymmetric membranes while solvent evaporation precipitation technique was used to make dense homogeneous membranes.

Different casting solution compositions and casting methods were used, depending on the purpose of the experiment that followed. Details of the membrane preparation methods are described below. The SMMs such as tSMM1, tSMM2, nSMM1 and nSMM2 which were incorporated in membranes for each experiment will be noted in the following subheadings in this Section.

3.3.1 Membrane preparation for the water permeation and bubble-point & gas permeation test (tSMM1)

Membranes, with pores in the range of ultrafiltration membranes, were subjected to the bubble-point test. For this purpose, PES membranes were cast from a casting solution with a composition of PES (10 wt%), PVP (10 wt%) and NMP (80 wt%). tSMM blended PES membranes were cast from a casting solution with a composition of PES (10 wt%), PVP (10 wt%), NMP (78.5 wt%) and tSMM1 (1.5 wt%). The above compositions were similar to that of 10 UD ultrafiltration membranes by which Singh obtained the highest flux (Singh et al., 1998).

Firstly, PES and PVP powder were dried at 150°C and 60°C, respectively, in a convective oven for four hours before use. Secondly, a predetermined amount of PVP was added to a 500 mL glass bottle, followed by the addition of NMP. The PVP was fully dissolved after

approximately three hours of agitation with an orbital shaker at room temperature. Thirdly, SMM was added to the mixture. To fully dissolve the SMM, the solution was agitated for another four hours with the shaker at room temperature. Fourthly, PES in powder form was added. The bottle lid was sealed with Teflon tape on the riveted neck of the bottle and by electric tape around the outside of the lid and the bottle.

To completely mix the solution the bottle was placed on a shaker and allowed to mix for at least 24 hours. After the solution was mixed to a single phase, it was filtered through a filter cloth. The polymer solution was driven through the filter by air or nitrogen gas at a pressure of 241.3-275.8 kPa (35-40 psi). The filtered solution was captured in the same type of bottle from which it was poured. Polymer solution films were cast on a glass plate to a nominal thickness of 0.24 mm by running a glass rod over the electric tapes that were placed at both edges of the plate. The films were immersed to a gelation bath immediately after casting together with the glass plate. The gelation bath contained ice-cold water the temperature of which was about 4°C. The membranes were kept in the gelation bath for an hour before being dried by solvent exchange technique. The solvent exchange technique will be described in Section 3.4.

3.3.2 Membrane preparation for tensile strength/elongation test (tSMM1)

The experiment for tensile strength and elongation was to find out the effect of tSMM on the mechanical strength of membranes. First of all, the membranes with same compositions and preparation conditions to those in Section 3.3.1 were prepared for mechanical tests. As noted in the section, one of the casting solutions had a composition of PES (10 wt%), PVP (10 wt%) and NMP (80 wt%), while the other PES (10 wt%), PVP (10 wt%), NMP (78.5 wt%) and tSMM1 (1.5 wt%). However, those membranes must have very porous structures because of their low polymer (PES) concentrations in the casting solutions and the existence of the pore forming PVP, and they could be too weak to compare each other for

verifying the effect of tSMM. Therefore, dense homogeneous membranes were prepared by the solvent evaporation precipitation technique. The casting solutions for these membranes contained higher PES concentrations and PVP was not added to the casting solutions. The membranes without tSMM were cast from a casting solution with a composition of PES (20 wt%) and NMP (80 wt%). The membranes with tSMM were cast from a casting solution with a composition of PES (20 wt%), tSMM1 (1.5 wt%) and NMP (78.5 wt%). After casting the solution on a glass plate in the same way as for the earlier membranes, the polymer solution film, in this time, was transferred into an oven immediately together with the glass plate and kept in the oven at 110°C for eight minutes. The membrane was further dried in a vacuum oven for 48 hours at room temperature. The completely dried membrane was attached to the glass plate and the membrane film could be peeled off after trimming away the edges of the film by cutting knife.

3.3.3 Membrane preparation for studying tSMM migration (tSMM1)

The casing solution containing PES (20 wt%), tSMM1 (1.5 wt%) and NMP (78.5 wt%) were first prepared. A predetermined amount of tSMM1 was added to a 500 mL glass bottle, followed by the addition of NMP. The glass bottle was shaken with an orbital shaker at room temperature for four hours to fully dissolve the SMM. Then, PES powder was added and the bottle lid was sealed with a Teflon tape on the riveted neck of the bottle and with an electric tape, or parafilm, around the outside of the lid and the bottle. To completely mix the polymer the bottle was placed on the shaker and allowed to be shaken for at least 24 hours. The solution was then filtered through a filter cloth under a pressure of 241.3-275.8 kPa (35-40 psi). The solution was cast on a smooth glass plate to a pre-determined thickness (0.12, 0.18 and 0.24 mm) using a casting bar. The solvent, NMP, was then evaporated by placing the cast film together with the glass plate in an oven with forced air circulation for a pre-determined period. The oven temperature was maintained at 110°C. The solution film was then immersed in water at 4°C for an hour. The membrane was

further dried by the solvent exchange technique to yield a final membrane that was subjected to contact angle measurement and XPS analysis. A PES membrane without tSMM1 was also prepared by exactly the same method except for the absence of tSMM1 in the casting solution.

3.3.4 Membrane preparation for studying tSMM migration (tSMM1, tSMM2)

Casting solutions were prepared in a PES solution (12 wt%) with and without tSMM1 and tSMM2 (2 wt%). In this study, the PES in the casting solution was set to lower concentration while the tSMM concentration was set to higher, because more hydrophobic surface as well as porous structure was expected to be obtained. These features are necessary for membrane distillation. The solution was cast to films with different thicknesses (0.2 to 0.3 mm) on the glass plate. The cast solution film was placed in a temperature-controlled (at 110 °C) oven to evaporate solvent for several different periods (0 to 25 min; 2,000 min to complete evaporation), before being immersed in water for gelation. It is believed that SMM migration took place during the solvent evaporation period.

3.3.5 Membrane preparation for studying nSMM migration (nSMM1)

The casting solutions containing PES (15-18 wt%), nSMM (0-1.5 wt%) and NMP (balance) were prepared. The solution was cast on a smooth glass plate to a thickness of 0.25 mm using a casting bar. The cast film was then kept at room temperature for a predetermined period before being immersed together with the glass plate in water at room temperature for gelation. In other experiments, the cast film was placed together with the glass plate in an oven (oven temperature maintained at 110°C) with forced air circulation for a predetermined period before being immersed in water at 4°C. The membranes in the gelation bath were dried in the air at room temperature for 48 hours to yield final membranes that were subjected to contact angle measurement, X-ray photoelectron

spectroscopy (XPS) and scanning electron microscopy (SEM).

A solution with 10.0 wt% of nSMM in NMP was prepared and cast on a glass plate to a thickness of 0.1 mm. The solvent was then evaporated completely by keeping the cast film together with the glass plate in an oven with forced air-circulation for 24 hours. The dense film of nSMM so prepared was used for the measurement of the contact angle of nSMM.

3.3.6 Membrane preparation for ultrafiltraion (nSMM2)

The casting solutions for ultrafiltraiton (UF) membranes containing PES (15 or 17 wt%), nSMM (0 or 1.5 wt%), PVP (0 or 7 wt%) and NMP (balance) were prepared. The solutions were cast on a smooth glass plate to a thickness of 0.25 mm using a casting bar. Some cast solution films were then immersed immediately together with the glass plates in water at 4°C for an hour while other cast solution films were subjected to solvent evaporation for predetermined periods at room temperature before being transferred into water at 4, 18, or 40°C together with the glass plates. Membranes were stored in distilled water in 'never dried state' until UF experiments.

3.3.7 Membrane preparation for vacuum membrane distillation (nSMM2)

Four casting solutions were prepared with PES (15 or 17 wt%), nSMM2 (1.5 wt%), distilled water (0 or 2 wt%) and NMP (balance). The solutions were cast on a smooth glass plate to a thickness of 0.25 mm using a casting bar. After casting all membranes were kept in the air at room temperature for four minutes, and then immersed into water at 4°C for an hour. The membranes in the gelation bath were dried in the air at room temperature for 48 hours to yield final membranes that were subjected to scanning electron microscopy (SEM), contact angle measurement, pure water permeation (PWP) tests and finally vacuum membrane distillation (VMD) experiments.

3.4 Membrane Drying by Solvent Exchange Technique

Some membranes were dried using the solvent exchange technique (Fang, 1997). In this technique, the water that is present in the membrane after the gelation process was replaced by ethyl alcohol with successive immersions in ethyl alcohol/water solutions of progressively higher alcohol concentrations (overnight for each immersion). Ethyl alcohol contents in the solutions were 25, 50, 75 and 100 vol. %. Then, ethyl alcohol was subsequently air evaporated at room temperature for 24 hours to yield the final dry membranes.

3.5 Pure Water Permeation, Bubble-point & Gas Permeation Test

Pure water permeation test and bubble-point & gas permeation test were carried out with the membranes prepared in Section 3.3.1. Figure 3.4 shows a schematic of the testing setup. The effective area of the membrane was 9.6 cm^2. Water permeation test was carried out prior to bubble-point & gas permeation test.

First, the static testing cell (see Figure 3.4a) was filled with water up to the point just below the neck of the cell. Then, permeation test was started by applying pressure from the air cylinder on water. The fluxes of water were measured at 41.37, 55.16, 68.95, 82.74, 110.32, 137.90 and 165.48 kPa gauge (6, 8, 10, 12, 16, 20 and 24 psig, respectively). At each pressure the water flux was measured three times. The water flux was expected to be proportional to pressure, therefore, the slope a' was obtained by applying the least square method to the following equation:

$$J_w = a' \times \Delta P \tag{3.1}$$

where J_w is the water permeation flux [m hr^{-1}] and ΔP is the transmembrane pressure [kPa]. All membrane pores were assumed to be filled during water permeation experiments.

The equipment was then made ready for bubble-point & gas permeation test by modifying the setup used for water permeation test slightly. (from Figure 3.4a to Figure 3.4b). Water was filled to the height of 3 cm from the membrane in the same cell, the design of which is given in Figure 3.5. The bubble-point & gas permeation test was performed immediately after the water permeation test, which allowed us to assume that all the pores of the membrane was filled with water. This time, however, pressure was applied on air which is in a chamber underneath the membrane. The flux of the air flowing from the bottom to the top of the membrane was measured by bubble flow meter for low pressure range and wet flow meter for high pressure range (Figure 3.4b). The pressure of air was increased with 13.8 kPa (2 psi) interval from 0 to the end region of an S-shape curve such as shown in Figure 2.9. At each pressure air flux was measured three times.

For some membranes, to find out the potential of the membrane to be used for MD, liquid entry pressure of water (LEP_w), which is the pressure that must be applied onto pure water before it penetrates into dried membrane pores, was measured.

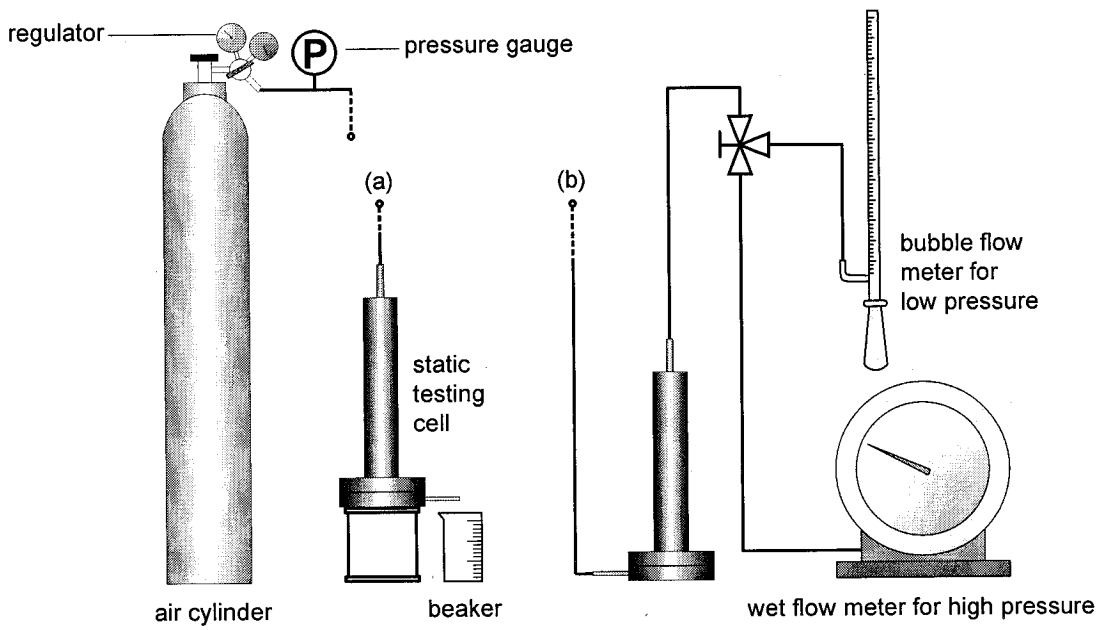

Figure 3.4 Scheme of (a) water permeation setup and (b) bubble-point & gas permeation setup

A schematic of the static testing cell used for the test is shown in Figure 3.5. It should be noticed that the magnetic stirrer of the static reverse osmosis cell was removed, since in this experiment, there was no need to stir the water. However, during bubble-point & gas permeation test, a supporter to prevent membrane lift-up was placed above the membrane. The supporter was perforated with holes of 3 mm diameter. This static cell was a stainless steel pressure chamber consisting of two detachable parts. The membrane was mounted on a stainless steel porous plate embedded in the lower part of the cell. The upper part of the cell would contain water. A filter paper was placed above and below the membrane for protection of membrane surface deformation by pressure. The two parts of the cell were clamped and sealed tight using rubber O-rings. All experiments were carried out at the laboratory temperature (about 21°C).

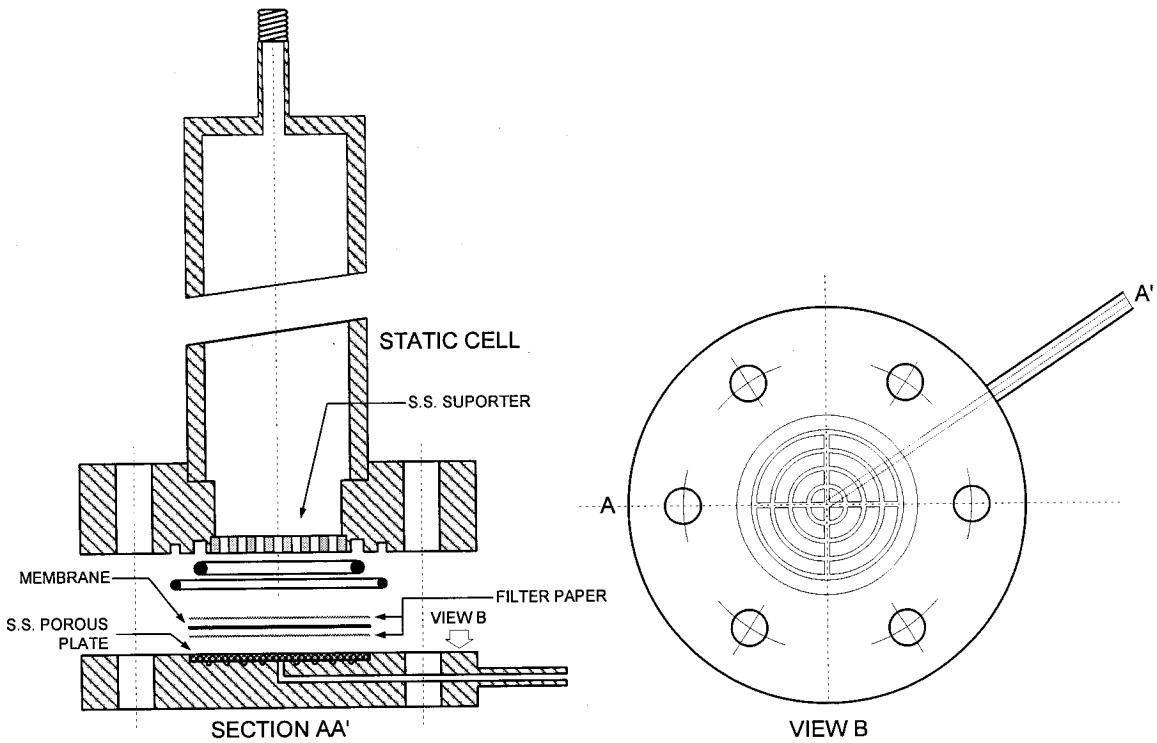

Figure 3.5 Lab scale static testing cell for bubble point tests (Sourirajan and Matsuura, 1985)

3.6 Description of Tensile Strength/Elongation Test

Tensile strength/elongation test that is the most common technique for measuring mechanical properties was performed with an Instron machine at the National Research Council (NRC) in Ottawa, Canada. A schematic diagram of the Instron machine is shown in Figure 3.6.

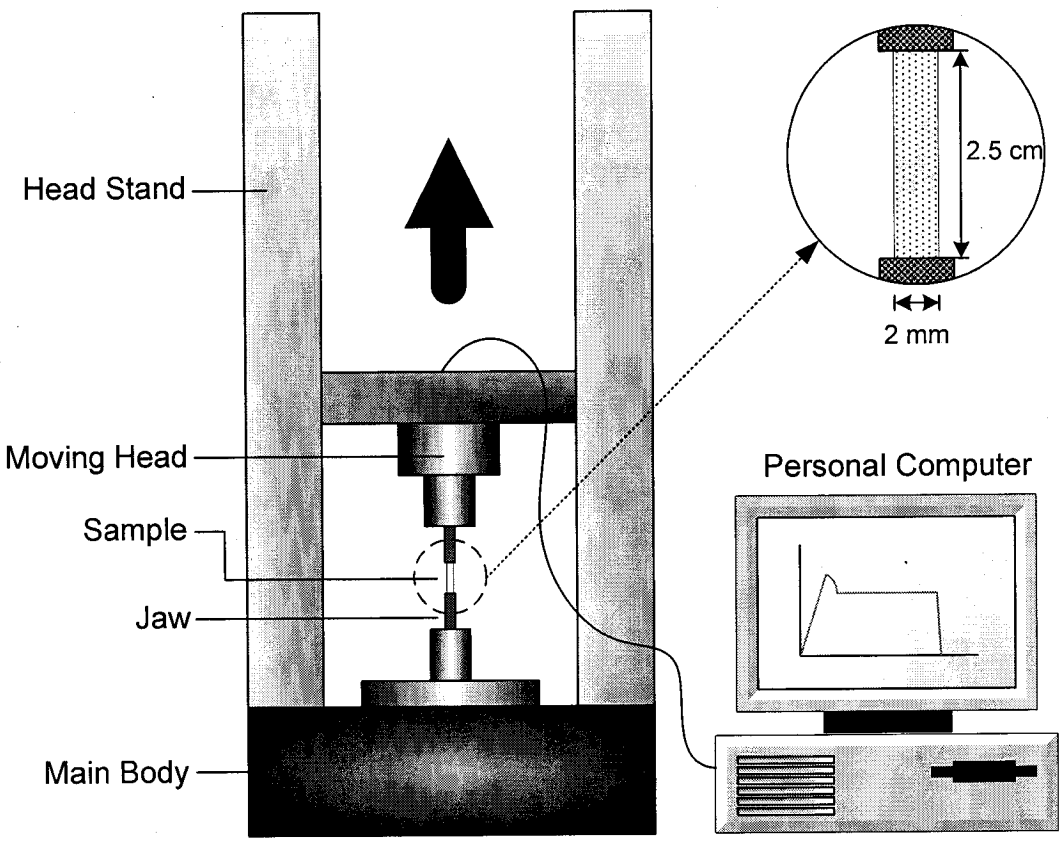

Figure 3.6 Schematic diagram of Instron

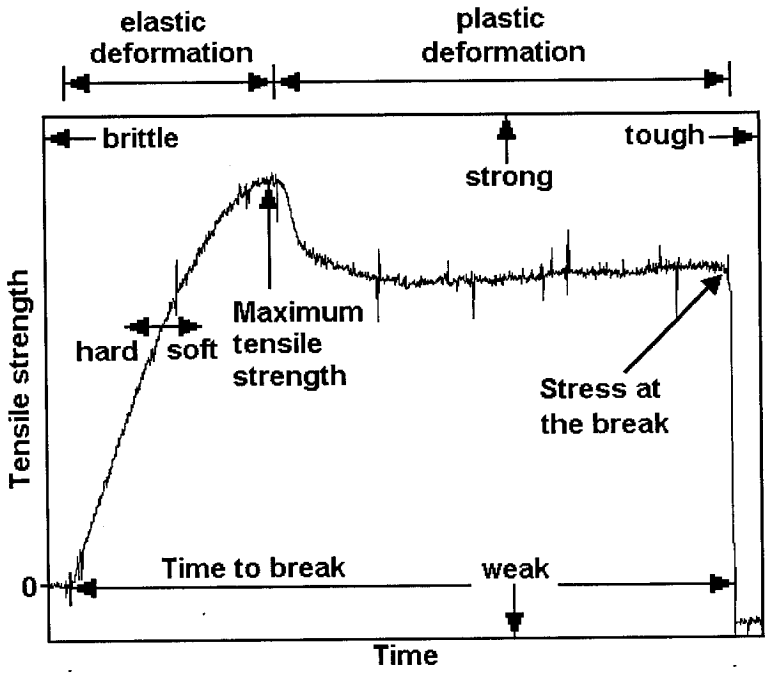

Figure 3.7 Instron data analysis

It was composed of several major parts: 1) main body, 2) moving head stand, 3) moving head, 4) jaws under the moving head and on the body and 5) personal computer. The main body had controllers which controlled the rate of moving head, the zero point adjustment, the working time and the resetting. The moving head contained a sensor to transform the mechanical signal into the electrical signal. The moving head was connected with a personal computer that received, computed the data and then saved and displayed the calculated results. Used samples were prepared by cutting the membranes into pieces with 2 mm width and 4 cm length. Those samples should be carefully cut with special cutting tools. The samples were fitted with the two jaws and before starting the machine the distance from the upper jaw to the lower jaw should be set to 2.5 cm. The membranes which were prepared in Section 3.3.2 were tested with 2 and 5 mm/min moving head rates. Figure 3.7 shows how to analyze the data from the computer. Maximum tensile strength and stress at the break point were depicted from a tensile strength vs. time chart as shown in Figure 3.7.

3.7 Description of Contact Angle Measurement

Contact angles of membranes were measured to determine hydrophobicity/hydrophilicity of SMM blended PES membranes relative to those of the PES membrane using a 14" Horizontal Beam Comparator 22-2000 SERIES (S-T Industries, Inc., St. James, MN, US) whose schematic diagram is given in Figure 3.8.

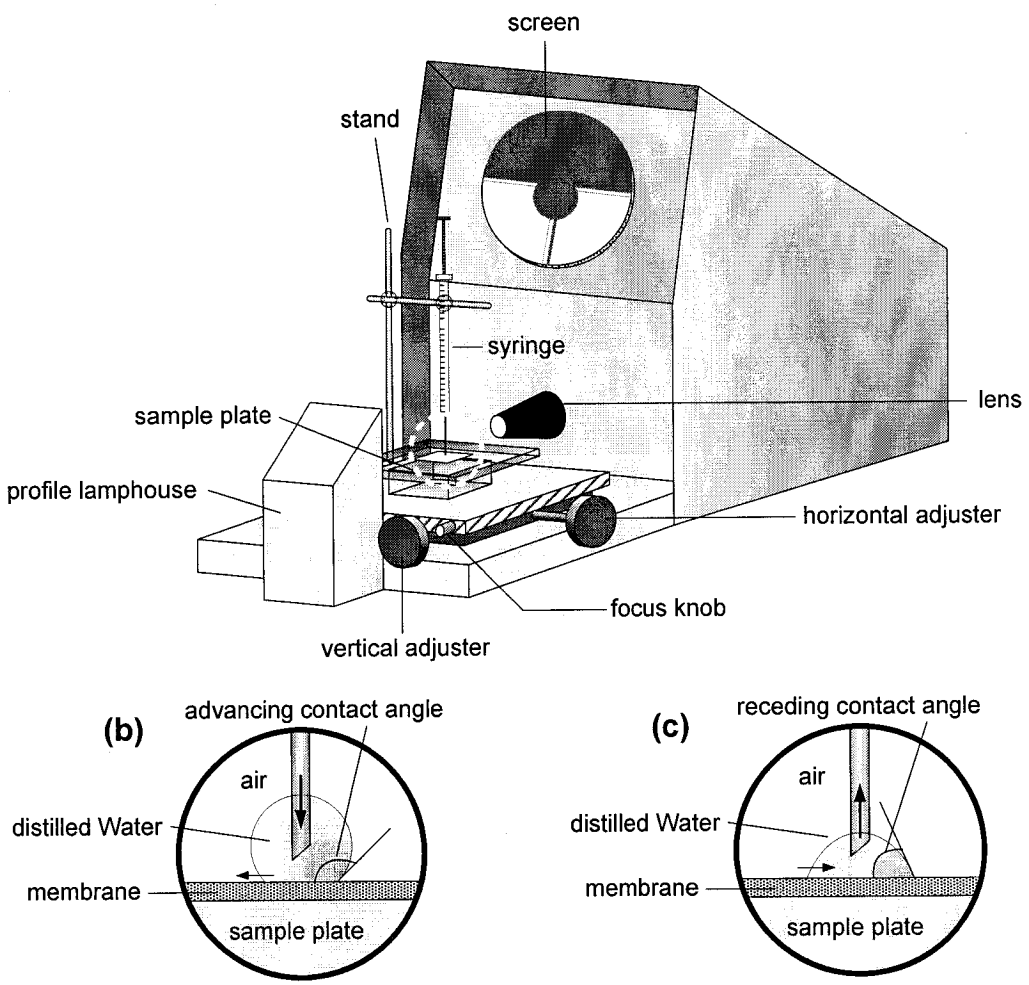

Figure 3.8 A schematic diagrams of (a) 14" Horizontal beam comparator and (b) advancing and (c) receding contact angle measurements

Figure 3.8 also shows the schematic diagrams of techniques for advancing and receding contact angle measurements. In all cases, only the advancing contact angles were measured. Samples were made by cutting the membranes into pieces of 1.5 × 5 cm at random positions. They were placed on the plastic sample plate and fixed with tape. Then a syringe filled with distilled water was installed to stand vertically. The syringe needle should be adjusted 0.5 mm above the membrane surface. 3 μL of water was injected on the membrane surface and the moving bed was adjusted so that water drop was fitted to the scale when projected on the screen. The contact angles were measured at four different spots on each membrane sample.

3.8 X-ray Photoelectron Spectroscopy

The elemental composition at the surface of membrane was determined by X-ray photoelectron Spectroscopy (XPS), also referred to as Electron Spectroscopy for Chemical Analysis (ESCA). The XPS tests were carried out at the National Research Council (NRC) in Ottawa and Hanyang University in Seoul, Korea. Throughout this study, the membranes blended with tSMM were tested at NRC and the membranes with nSMM were tested at Hanyang University.

The tSMM blended membranes prepared in Sections 3.3.3 and 3.3.4 were cut into samples of 1 cm^2 from random positions of the membrane and the samples were sent to the NRC laboratory and analyzed by KRATOS AXIS HS X-ray photoelectron spectrometer (Kratos, Manchester, UK). The size of the analyzed area was about 1 mm^2. Monochromatised Al K_α X-radiation was used for excitation and a 180° hemispherical analyzer with a three channel detector was employed. The X-ray gun was operated at 15 kV and 20 mA. The pressure in the analyzer chamber was 1.33×10^{-4} to 1.33×10^{-5} Pa (10^{-8} to 10^{-9} torr). A schematic diagram of the XPS apparatus is shown in Figure 3.9.

The analytical method was similar to the angle-resolved XPS (AR-XPS) technique described by Deslandes et al. (1998) for probing thinner layers of the surface. A schematic illustration of the AR-XPS is shown in Figure 3.10: the angle (θ_x) between the direction normal to the sample surface and the electron trajectory into the detector is defined as the take-off angle (TOA). At a glancing TOA, only electrons emitted from the near surface region were detected; while at near normal TOA, the surface was sampled more deeply. The samples were analyzed at the TOA of 0° and 60°. At $\theta_x = 0°$, the sample was perpendicular to the detector, leading to maximum sampling depth. The effective sampling depth, z_x, according to Deslandes et al. (1998) is equal to

$$z_x = 3\lambda_x \cos\theta_x \tag{3.2}$$

where λ_x is the effective mean path for electrons to escape the surface. Briggs (1998) provided sampling depths for F1s as a function of TOA. Based on his data, $z_x = 6.3$ nm at $\theta_x = 0°$, and 3.15 nm at $\theta_x = 60°$, which corresponded to an effective mean path, λ_x, of 2.1 nm.

The nSMM were analyzed by using the Multilab ESCA 3000 instrument (Thermo VG Scientific, East Grinstead, U.K.). The spectra were collected using a monochromatized Al K_α X-ray source operating at 14 kV and 300W. The TOA was kept at 0°, which corresponds to the X-ray sampling depth of 6.3 nm. The pressure inside the spectrometer sample chamber was kept under a high vacuum of $6.89\times10^{-4} \sim 6.89\times10^{-5}$ Pa ($10^{-9} \sim 10^{-10}$ psi) during the analysis.

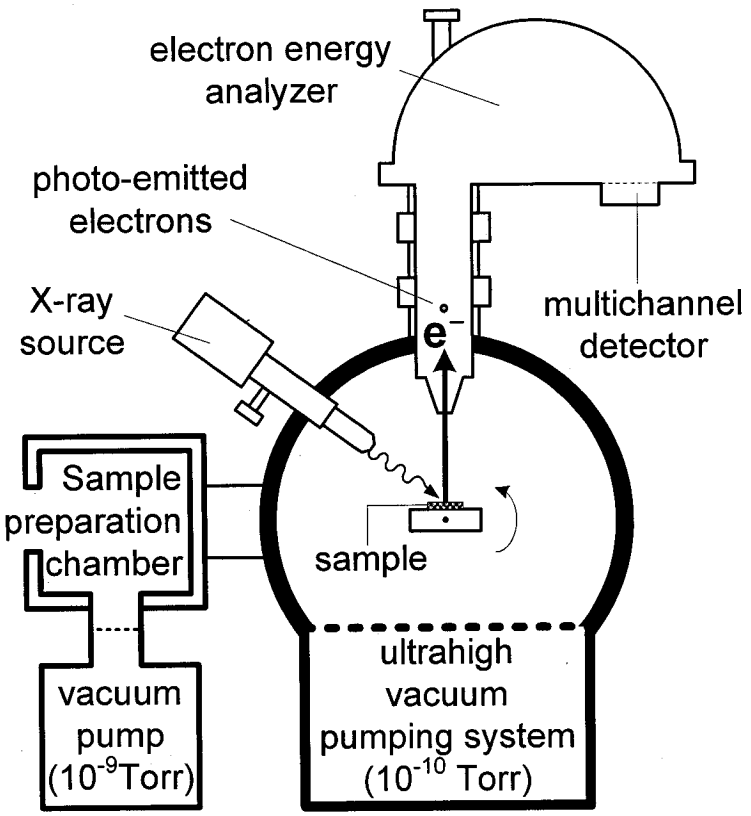

Figure 3.9 The Schematic diagram of the XPS apparatus (Fanelsa et al., 1995)

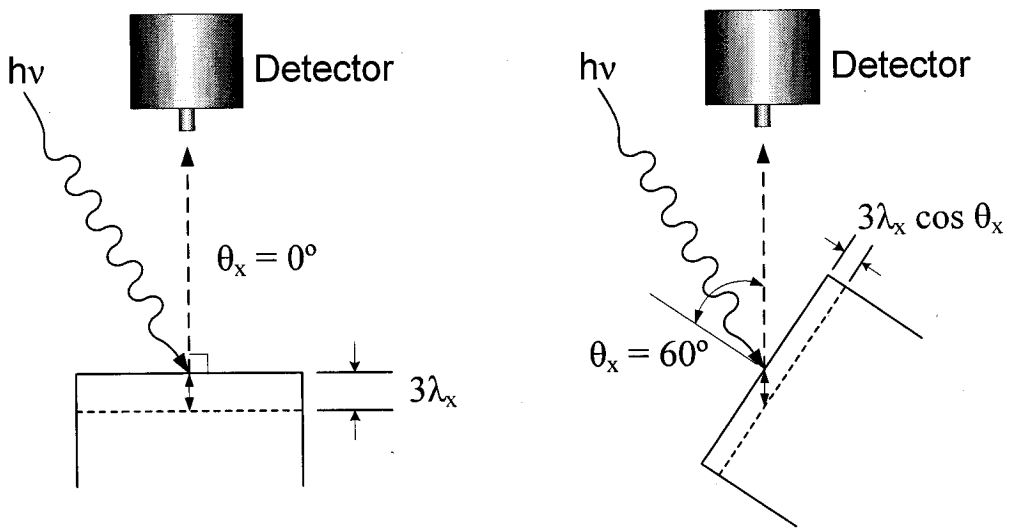

Figure 3.10 A schematic diagram showing the setup of AR-XPS used at different take-off angles (Deslandes et al., 1998, Chang et al., 2000)

3.9 Gel Permeation Chromatography

The molecular weights of the synthesized SMMs (tSMM1, tSMM2, nSMM1 and nSMM2) were measured by gel permeation chromatography (GPC). The GPC tests were carried out at University of Toronto (tSMM1), Hanyang University in Seoul, Korea (tSMM2 and nSMM1) and University of Ottawa (nSMM2).

The GPC (Waters 410 HPLC pump) unit at University of Toronto consists of a series of Waters Styragel™ columns (I.D. HT3, HR2, HR1) and a Waters 410 differential refractometer. The mobile phase was made by dissolving lithium bromide (LiBr) in HPLC grade N,N-dimethylformamide (DMF) to a concentration of 0.05 M. The flow rate was set at 1.0 mL/min and the column temperature set at 80°C. Prior to use, the solution was filtered using vacuum filtration through a 0.45 μm Teflon® membrane (Millipore Corp. Bedford, U.S.). tSMM1 sample was dissolved in the mobile phase at a concentration of 2 mg/mL. The solutions were then filtered through a 0.5 μm Teflon® filter (Millipore Corp., Bedford, U.S.). Polystyrene polymer standards (Tosoh Corp., Tokyo, Japan) with narrow molecular weight distributions were analyzed in the GPC unit.

At Hanyang University, Seoul, Korea, a GPC with HPLC pump, Waters 510, Milford, USA was used for tSMM2 and nSMM1. Three Styragel™ columns (each 30 cm × 7.8 mm I.D. HR-0.5, HR-4, HR-5, all Waters) and a Waters R410 differential refractometeric detector were used. The mobile phase was THF with a flow rate of 1 mL/min. The injection volume was usually 100 μL of stock solutions (0.1-0.5 w/v%). The calibration curve was established by using five standard polystyrenes with molecular weight of 1.28×10^3, 2.96×10^3, 1.13×10^4, 2.85×10^4 and 6.50×10^4 g/mol, respectively (Shodex standard SM-105, Showa Denko, Japan). A Waters Millenium software program was used to prove the data.

The cumulative number- and weight-average molecular weight determination for nSMM2 was performed at University of Ottawa by using a Waters Associates GPC chromatograph

equipped with a Waters 410 refractive index detector. Three Waters UltraStyragel™ packed columns (10^3, 10^4, and 10^6 Å) were installed in series. The THF (HPLC grade, EM Science) was filtered and used as the eluent at a flow rate of 0.3 mL/min at 38°C. The calibration of the instrument was performed using polystyrene (Shodex, Showa Denko, Tokyo, Japan) standards with molecular weight between 1.3×10^3 and 3.15×10^6 g/mol. The standards and samples were prepared in THF (0.2 w/v% solutions) and filtered prior to injection through 0.45-μm filters to remove high molecular weight component. Millenium 32 software (Waters) was used for the data acquisition.

3.10 Elemental Analysis

Synthesized SMMs (tSMM1, tSMM2 and nSMM2) were sent to Galbraith Laboratories, Inc., Knoxvill, TN, U.S.A., for elemental analysis of different atoms in SMMs (e.g. carbon, nitrogen, hydrogen, fluorine and silicone). All samples were dried in vacuum overnight. The results were expressed by weight percent (wt%).

3.11 Scanning Electron Microscopy

The cross sections of the nSMM1 blended membranes were observed and examined by scanning electron microscopy using a model JSF-6340 JEOL field emission scanning electron microscopy (FE-SEM) (Japan Electron Optics Limited, Japan) at Hanyang University, Korea. Selected membranes were cut into pieces with 3 mm width and 10 mm length and, then, immersed into liquid nitrogen reservoir for 5 seconds. Keeping the pieces in the liquid nitrogen, they were broken into two pieces by pulling from both ends. One of the broken pieces was mounted on aluminum mounts with carbon paste and gold-coated prior to use. The cross-sections of the membranes at the broken parts were examined. The cross sections of the nSMM2 blended membranes were observed using a model JSM-6400 JEOL (Japan Electron Optics Limited, Japan) after coating the mounted samples by 60% gold and 40% palladium under vacuum in a sputtering system HUMMER VII.

3.12 Description of Ultrafiltration Experiments

Ultrafiltration (UF) experiments were conducted by using laboratory cross-flow test cells each with an effective area of 13.2 cm^2, the details of which were described elsewhere (Sourirajan and Matsuura, 1985). A sketch of the permeation cell is given in Figure 3.11. Three cells were connected in series as shown in the schematic layout of the UF system (Figure 3.12). Feed solution from the feed tank was pumped by a constant discharge pump to the inlet of the first permeation cell. An accumulator was installed in the pump delivery line to reduce pulsation in the pressure. Since the pump was a constant discharge type, a bypass line was provided to vary feed flow in the system whenever required. As permeation cells were connected in series, the retentate of the first cell became the feed to the second cell and so on. As permeate flow was very small compared to feed flow, the characteristics of the feed solution to all the cells were virtually the same. A pressure regulator was installed at the outlet of the third cell to regulate the pressure in the system. To know inlet and outlet pressures across all three permeation cells, two pressure gauges were installed as shown in Figure 3.12.

All the experiments were conducted at room temperature using an operating pressure of 3.45×10^3 kPa (50 psig) unless specified otherwise. The feed flow rate was 2.2 L/min. Prior to use, each membrane was compressed under a pure water flow at 5.52×10^3 kPa (80 psig) for an hour then at 3.45×10^3 kPa (50 psig) for 5 hours until the permeation rate became steady. The pure water permeation rate was then measured. To characterize the membrane by solute transport method poly(ethylene glycol) (PEG; molecular weight up to 35,000) and poly(ethylene oxide) (PEO; molecular weight of 100,000 and 200,000) were used as the solutes in the feed solutions for the membrane characterization experiments. The feed concentration was 200 ppm. PEG/PEO separation experiments were conducted starting from the lower molecular weight solute. The system was thoroughly flushed with distilled water between the runs with PEG/PEO solutes of different molecular weights.

PEG/PEO contents in the feed and in the permeate side were determined from the total organic carbon (TOC) measured by a TOC analyzer (model DC-190, Rosemount Analytical Inc., Dohrmann Division, Santa Clara, CA). For each sample, solute separation, f, was calculated by

$$f = \left\{1 - \left[\frac{(c_p - c_w)}{(c_f - c_w)}\right]\right\} \times 100 \tag{3.7}$$

where c_p is the permeate TOC concentration in ppm, c_f the feed solution TOC concentration in ppm, and c_w the pure water TOC concentration in ppm. The average values of the separation data so obtained are presented. It is to be noted that the effect of the concentration polarization on separation is not considered by Equation 3.7. The mass transfer coefficient is $> 1.00 \times 10^{-6}$ m/s at the feed flow rate indicating that concentration polarization can be ignored (Sourirajan and Matsuura, 1985).

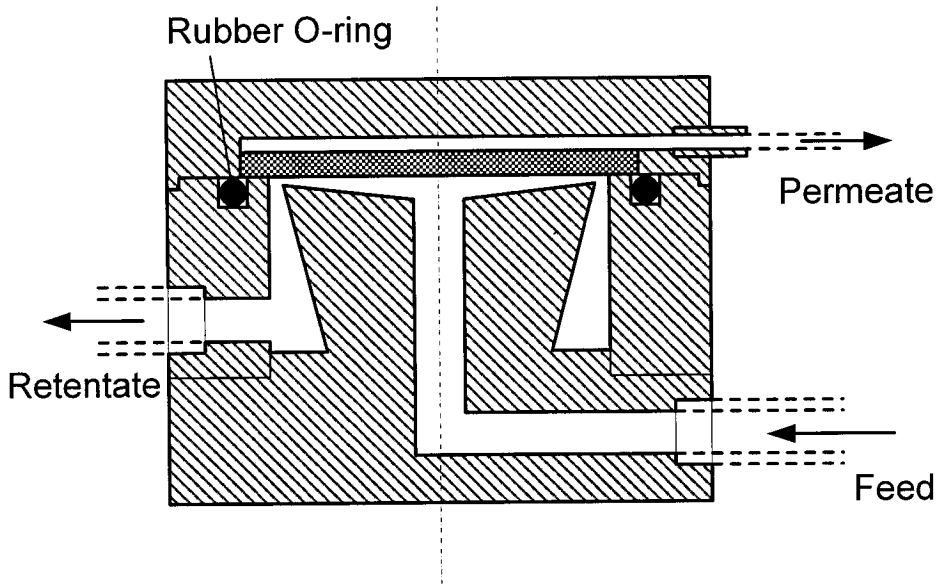

Figure 3.11 Sketch of laboratory cross-flow permeation cell for flat ultrafiltration membrane

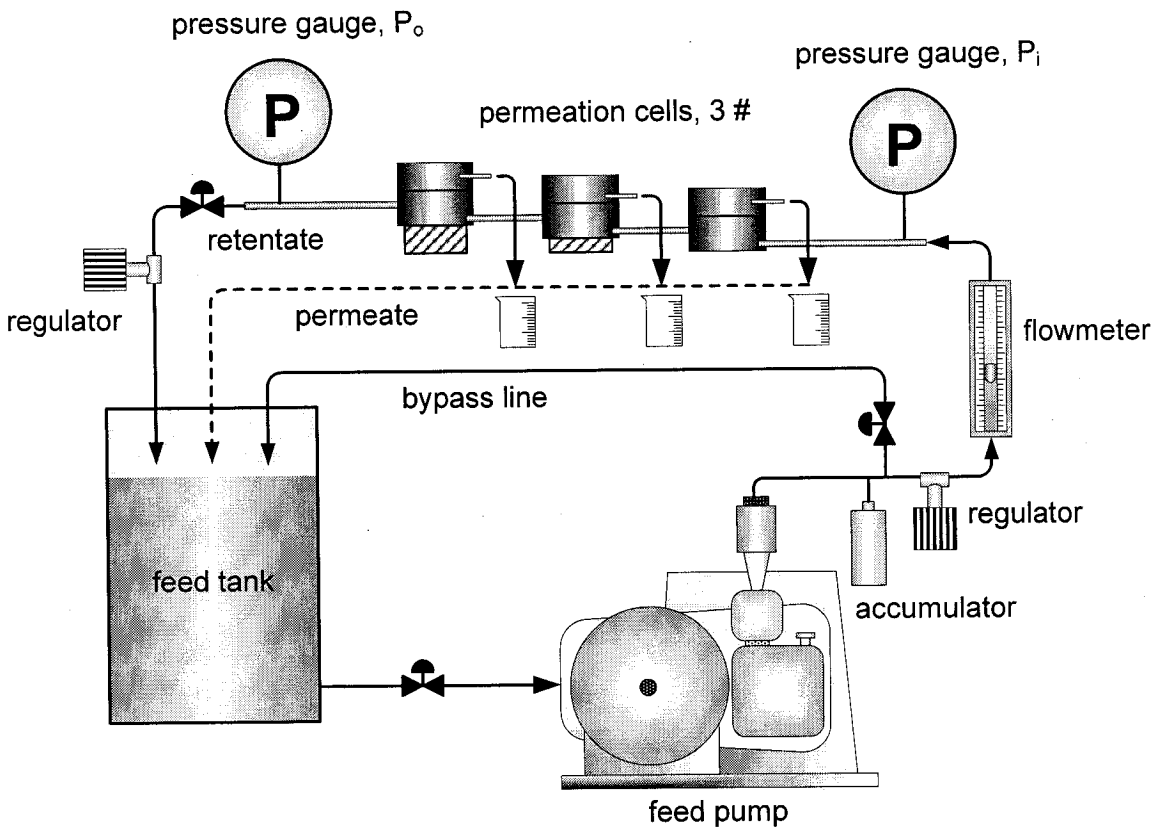

Figure 3.12 Schematic layout of the ultrafiltration system

3.13 Description of Vacuum Membrane Distillation Experiments

Vacuum membrane distillation experiments were conducted using the laboratory system which is shown in Figure 3.13. It consisted of a static stainless cell (Figure 3.14) that could be heated by an electric heating tape. Thus, the temperature of the liquid feed could be controlled. The static cell used for VMD system was similar to the one which was used by Sourirajan and Matsuura (1985) for reverse osmosis and for pervaporation. The effective area of the membrane was 10.2 cm^2. The total volume of the chamber in the upper part of the cell was 381.7 cm^3. The entire chamber space was filled with the feed liquid which was either pure water or water-ethanol mixture. Unlike the static cell (Figure 3.5) which was used for water permeation, bubble point and gas permeation tests in Section 3.5, a magnetic stirrer was fitted about one quarter of an inch above the membrane surface to keep the feed stirred. The temperature was measured by a thermometer through a hole on top of the cell. The upstream side pressure was kept atmospheric. A vacuum pump (Welch Vacuum Tech, Inc, Skokie, Illinois, Welch DuoSeal^{TM} vacuum pump, Model No. 1400), which was associated with a vacuum pressure controller (MKS Instruments Canada, Ltd., Nepean, Ontario, Model 651), was connected to the permeate side of the cell to remove permeating vapor. The downstream pressure was measured by a digital pressure transducer (MKS Instruments Canada, Ltd., Model 122AA-00100AB) with accuracy of ± 2%. Two glass cold traps, filled automatically with liquid nitrogen, were installed to condense and recover the permeate vapor. In all the experiments the temperature was maintained at 26°C and the stirring rate was 54 rps (maximum stirring).

All VMD experiments were performed with the following procedures. At the beginning, the liquid nitrogen flask for the cold trap 1 was filled with liquid nitrogen and the vacuum pump was set to a predetermined pressure, keeping the valves 1 and 2 opened and the other valves closed for about two hours. Then, the valve 4 was slowly opened and kept for an hour without filling the liquid nitrogen flask for the cold trap 2 with liquid nitrogen. By doing this procedure, the moisture in the lines and the cold trap 2 was expected to be

removed. After the moisture removal, the valves 1 and 2 were closed and the valve 3 was opened and kept open for one more hour to reach a steady state. Finally, the valve 7 was opened and the mass flux of the membrane was determined, in every case, from the weight of the condensate collected in the cold trap 2 for a predetermined period of time. The compositions of the feed and permeate were determined using the same TOC analyzer (model DC-190, Rosemount Analytical Inc., Dohrmann Division, Santa Clara, CA) which was used in Section 3.12. The downstream pressure was changed from 400 to 5300 Pa for the pure water feed and from 600 to 2000 Pa for the water-ethanol feed.

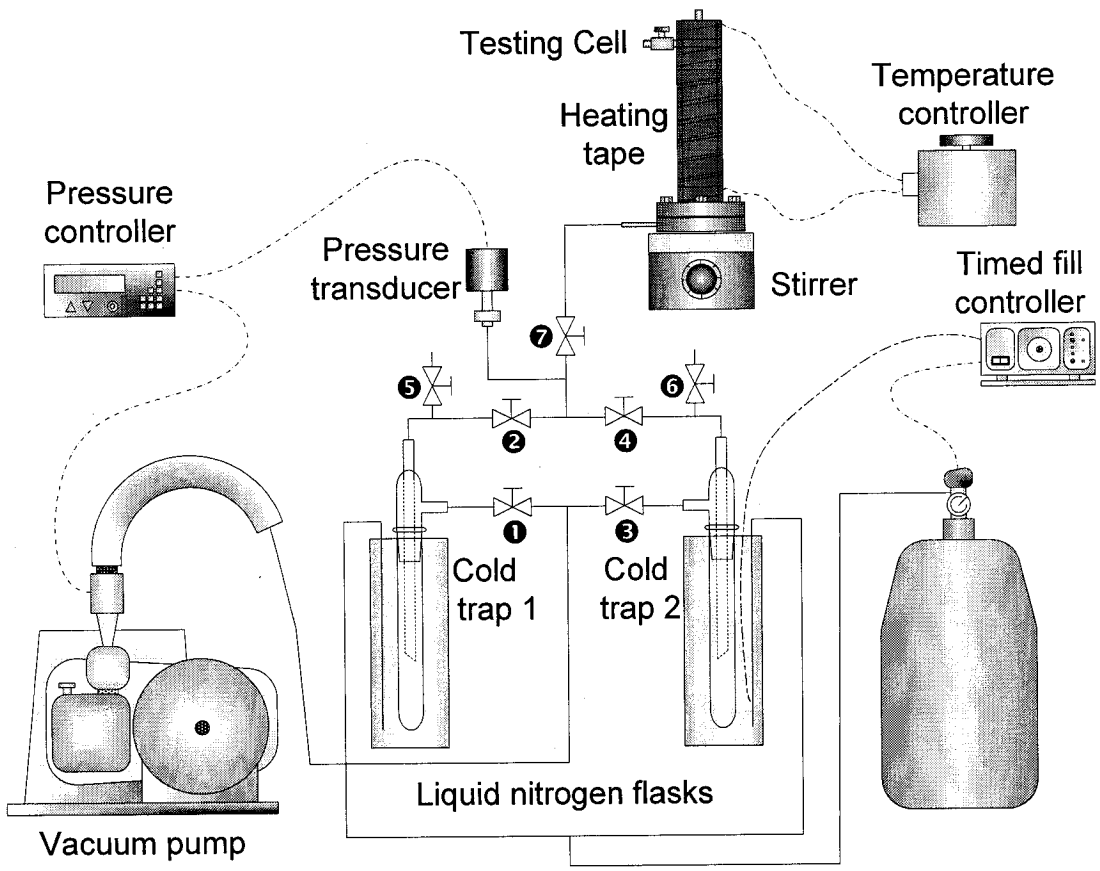

Figure 3.13 Schematic layout of the vacuum membrane distillation system

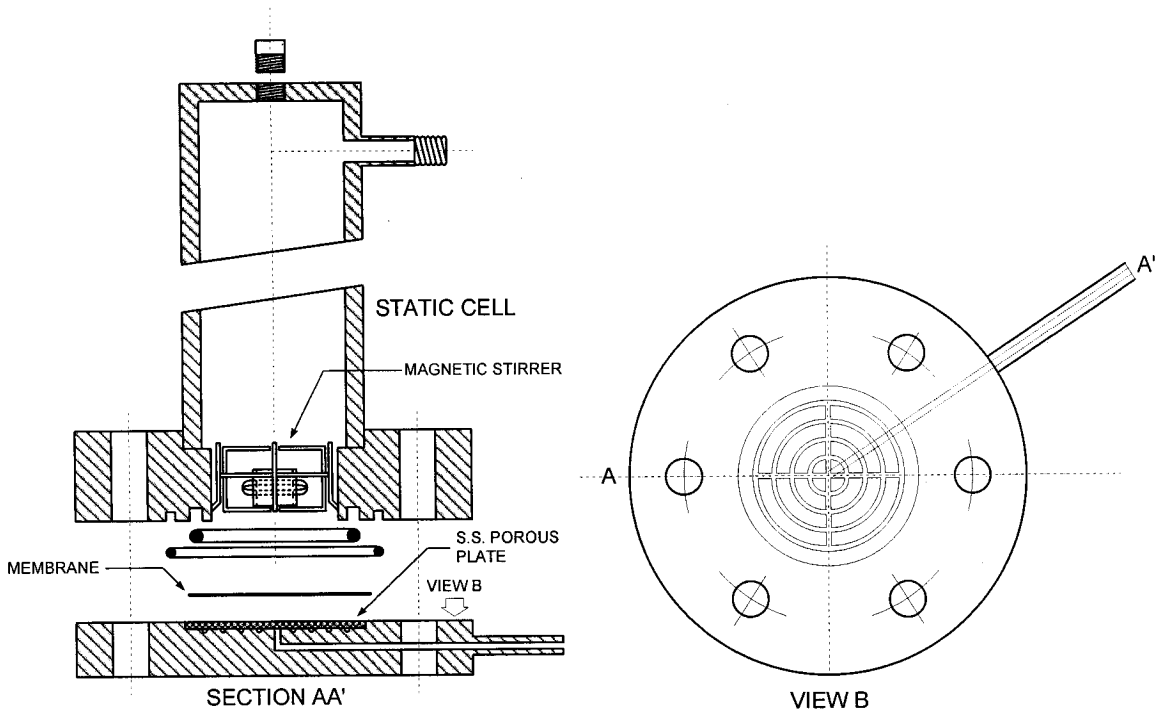

Figure 3.14 Lab scale static testing cell for vacuum membrane distillation (Sourirajan and Matsuura, 1985)

4. Results and Discussion (Part 1): Study on the Effects of Blending tSMM in PES Membranes

The tSMM1, which was synthesized as mentioned in Section 3.2, was used in this study to prepare many different membranes with different tSMM1 concentrations in the membrane casting solutions and different membrane preparation conditions, especially different evaporation times. The time period from the time after the solution casting on a glass plate to the time when the cast solution film together with the glass plate was immersed into gelation water bath was called the 'evaporation time' due to the solvent evaporation occurring during this period. Investigations were made on the effects of tSMM blending in PES membranes on 1) the pore size and pore size distribution, 2) mechanical strength, 3) tSMM surface migration. For this purpose the following experiments were performed.

1) PES membranes with and without tSMM blending were subjected to a bubble-point and gas permeation test and a pure water permeation test. Then, the pore size and pore size distribution were determined based on the method described in Section 3.5. The pure water permeation (PWP) rate was then calculated based on the pore size and the number of pores obtained from the bubble-point and gas permeation test and the results were compared with the real experimental PWP data.

2) PES membranes with and without tSMM blending were subjected to a mechanical strength test according to the method described in Section 3.6. Comparison of PES membranes with and without SMM blending was made in terms of the maximum tensile strength and %elongation.

3) Contact angle measurement and XPS analysis were conducted for PES membranes with and without tSMM blending. Contact angle measurement gives an idea of tSMM's surface migration. From XPS analysis, one can analyze the contents of SMM in the surface region quantitatively.

4.1 Effect of tSMM on the Pore Size and Pore Size Distribution

To study the effect of tSMM on the pore size and pore size distribution, the pure water permeation and bubble-point & gas permeation test were performed and the results were analyzed by the method described in Section 3.5. The dry membranes used in this study were the ones prepared in Section 3.3.1 and their preparation conditions are summarized in Table 4.1. The tSMM1 synthesis according to the method described in Section 3.2.1 was used in this study. The contact angles of the membranes were also included in Table 4.1. The surface contact angle seems unchanged by addition of tSMM1 to the PES membrane, when the evaporation time is zero.

Water flow rates were measured at different pressures for both B1 and B2 membranes. The flux could be calculated from the flow rate. Since the effective diameter of the membrane was 3.1 cm, the flux [m h^{-1}] is 4.77 times the flow rate [mL s^{-1}]. The pure water flux [m h^{-1}] vs. transmembrane pressure [kPa] is plotted in Figure 4.1. For both the B1 and B2 membrane, the water flux increased as the transmembrane pressure increased along a linear regression line from the origin. It should be noted that the water permeation flux of B2 (with tSMM blending) is lower than B1 (without tSMM blending). The reason may be either the pore size and pore size distribution changed or hydrophobicity changed by blending tSMM. The data on the contact angle, shown in Table 4.1, preclude the second possibility. Hence, the change in water flux should be due to the change in the pore size and pore size distribution.

Table 4.1 Preparation conditions of the membranes used for water permeation, bubble-point & gas permeation test

Membrane Code	Casting solution composition (by weight)	Evap. Time [min]	Gel. Temp. [°C]	Contact Angle [°]
B1	PES:PVP:NMP = 10:10:80	0	4	66.7 ± 2.7
B2	PES:PVP:tSMM1:NMP = 10:10:1.5:78.5	0	4	67.1 ± 3.1

From the linear regression line, the constant, a' in Equation 3.1 was calculated for both B1 and B2 membrane:

For the PES membrane without tSMM1, B1,

$$J_w = 0.0593\Delta P \tag{4.1}$$

and for the PES membrane with tSMM1, B2,

$$J_w = 0.0304\Delta P \tag{4.2}$$

where the unit of J_w is [m hr^{-1}] and that of ΔP is [kPa].

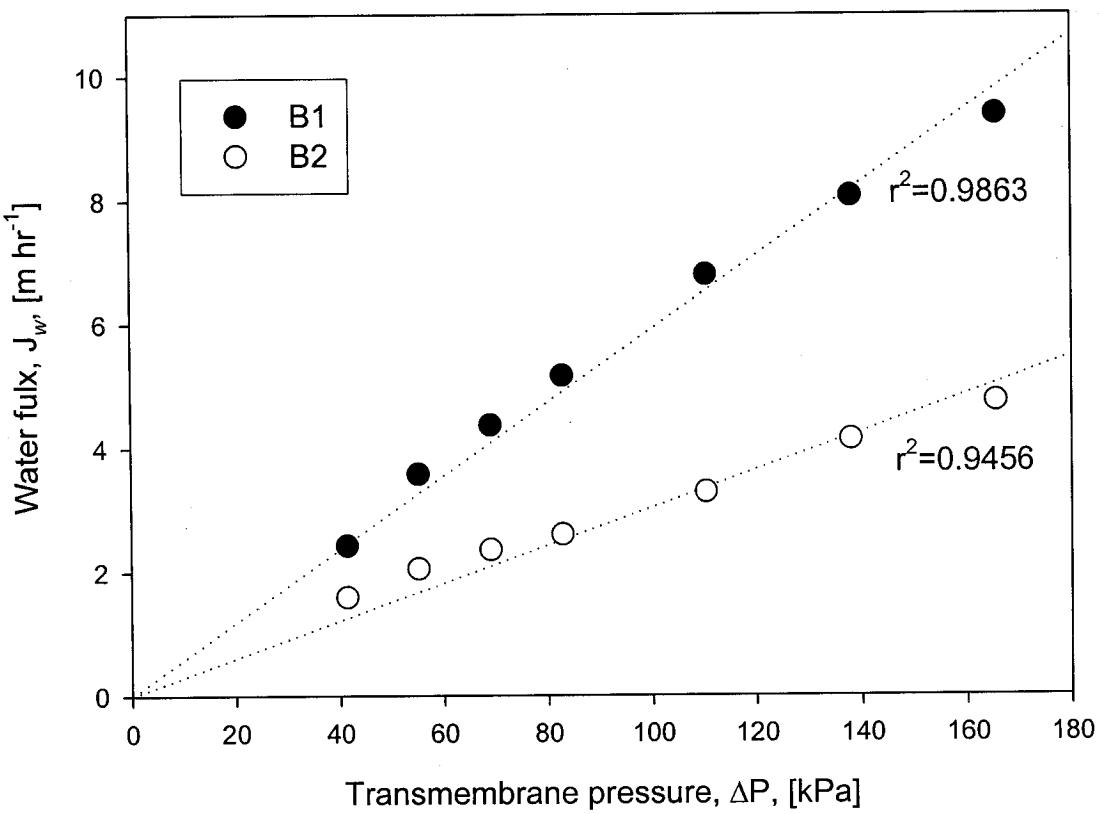

Figure 4.1 Plots for water permeation experiments: ● B1, ○B2, ---- linear regressions for PES and tSMM blended PES membrane

Bubble-point and gas permeation tests were then conducted to study the effect of tSMM1 blending on the pore size and the pore size distribution of the PES membranes, as described in Section 3.5. Air flux was measured at progressively increasing transmembrane pressure differences from the point "**a**" on Figure 4.2 to the point "**b**". The air flux was also measured by decreasing the pressure from "**b**" to "**c**". At the maximum pressure, all the pores of the membranes are supposed to be open for the air flow, and therefore when the pressure is decreased from the point "**b**" to "**c**", the air flux will be on the same line as that of the dry membrane (see also Figure 2.9). As shown in Figure 4.2, for both membranes, B1 and B2, the trend was the same as that described in Figure 2.9. A rightward shift of the curve was observed by adding tSMM (membrane B2), particularly when the transmembrane pressure difference was gradually increased.

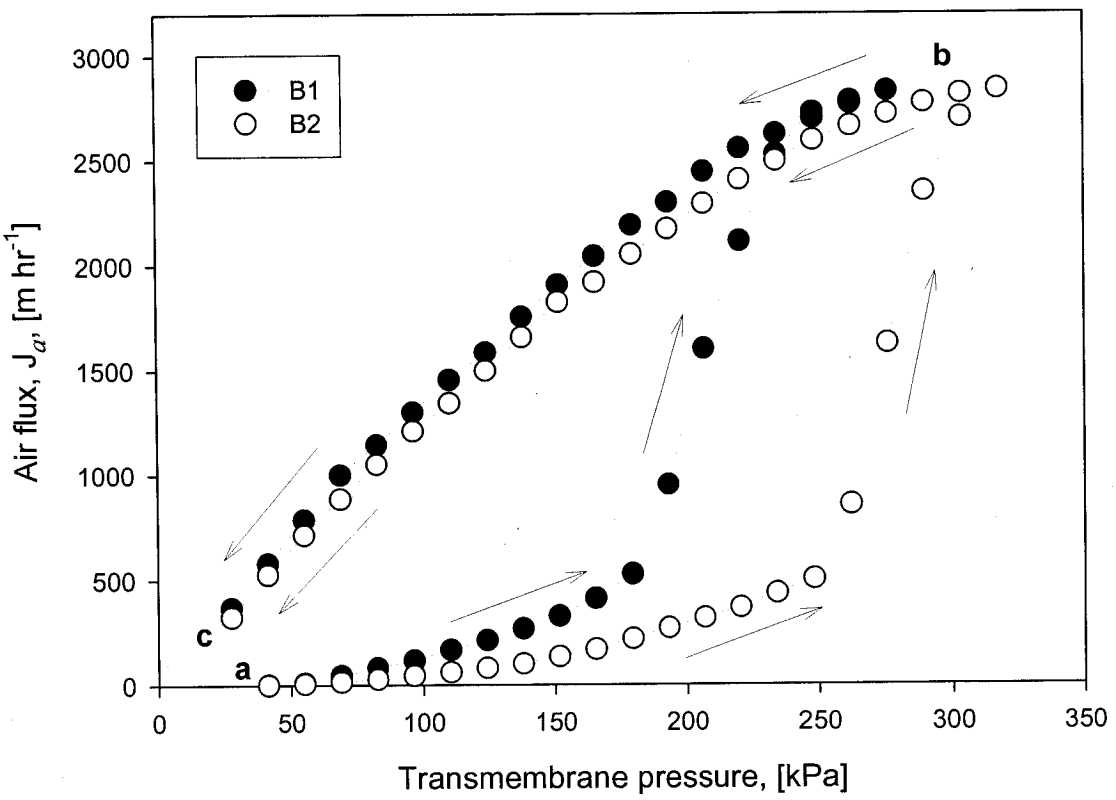

Figure 4.2 Experimental data of Bubble-point & gas permeation test

Using the data acquired during the pressure increase (**a** → **b**), air flux versus pore radius was calculated according to the method described in Section 2.5.1. Figure 4.3 shows the results of such calculation, in which the air flux, ΔJ_a is the air flux which passes through the pores with a radius, r. According to the figure, the air passed the membrane mostly through the pores with the sizes between 0.62 and 0.84 μm for B1 and those between 0.48 and 0.62 μm for B2. This means that most pores in B1 and B2 membrane belong to the pore size ranges given above, and therefore the mean pore size of the membrane, B1, must be larger than that of B2.

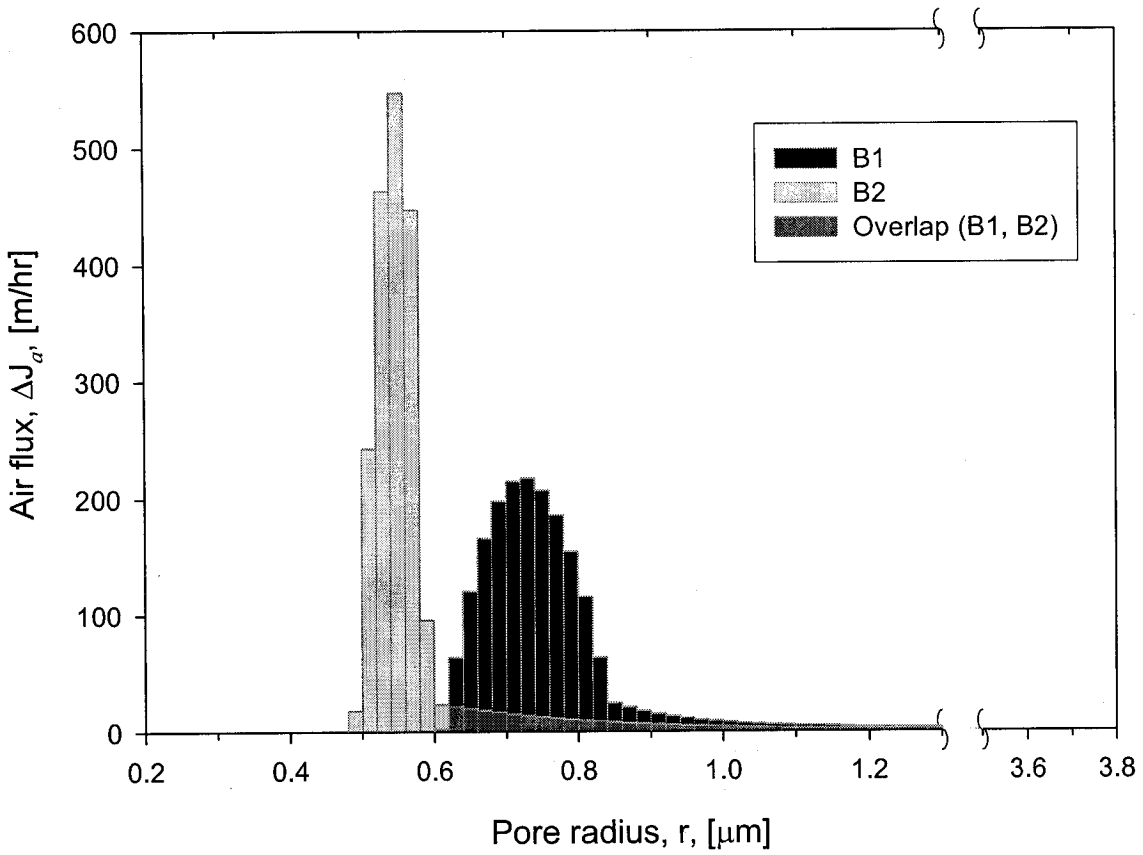

Figure 4.3 Plot for pore size versus flow rate

Then, the pore density, the numbers of pores per unit area, for each membrane was calculated using a transport model, based on the method described in Section 2.5.1. The Poiseuille flow was assumed to be the only pore flow mechanism in the analysis, since according to Shao et al. (2004), the contribution of the Knudsen flow was less than 5 %, when the pore sizes were from 0.01 to 100 μm and water was used as a pore-filling liquid in their bubble-point test. The assumption of the Poiseuille flow is hence justifiable.

Slight rearrangement of Equation 2.5 yielded the following equation, by which the pore density was calculated using the data shown in Figure 4.3,

$$n_i = \Delta J_{a,i} \cdot \frac{8\eta\psi}{\pi r_i^4} \cdot \frac{\delta_p}{\Delta P_i} \tag{4.3}$$

where n_i [m^{-2}] is the density of pores of radius r_i [m], ψ is a tortuosity factor, η [kg m^{-1} s^{-1}] is the air viscosity and δ_p [m] is the pore length. Parallel cylindrical pores were assumed, and therefore tortuosity factor was taken as unity. The experiments were performed at 21°C and $\eta = 1.84 \times 10^{-5}$ kg m^{-1} s^{-1}. The pore length was considered to be equal to the skin layer thickness, which was taken as 0.2×10^{-6} m, a value well within the range of the skin layer thickness mentioned by other researchers (Riley et al., 1964; Micheals et al., 1971; Strathmann et al., 1975; Kakuta et al., 1980; Fane et al., 1981) for ultra/microfiltration membranes made of various materials.

The results are shown in Figure 4.4. From the figure, it is observed that most of the pores are in a range between 0.62 and 0.84 μm for the membrane B1 and most of the pores are in the range between 0.48 and 0.62 μm for the membrane B2. Therefore, it could be concluded that the pore size of the membrane was reduced and also the pore size distribution narrowed by adding tSMM1 into the PES membrane.

Pure water permeation flux was then calculated based on the distribution of pore densities in Figure 4.4 by taking into account that the flow of water followed the Hagen-Poiseuille dependence, as:

$$a_p = \frac{\pi \sum_{i=1}^{n} n_i r_i^4}{8\eta_w \delta_p} \tag{4.4}$$

where a_p [m hr^{-1} kPa^{-1}] is water permeability of the membrane and $\eta_w = 0.979 \times 10^{-3}$ kg m^{-1} s^{-1}, the water viscosity at 21°C. The results are presented in Figure 4.5 along with the experimental data from Figure 4.1. In both experimental results and theoretical calculation the water permeation flux is less for B2 than B1 membrane, as expected. However, the calculated water fluxes were much higher than the experimental values. The difference might have been caused by the following assumptions;

(1) The tortuosity factor was assumed to be unity.

(2) Only Poisuille flow model was considered for gas transport mechanism.

(3) The pore length was assumed to be 0.2 μm.

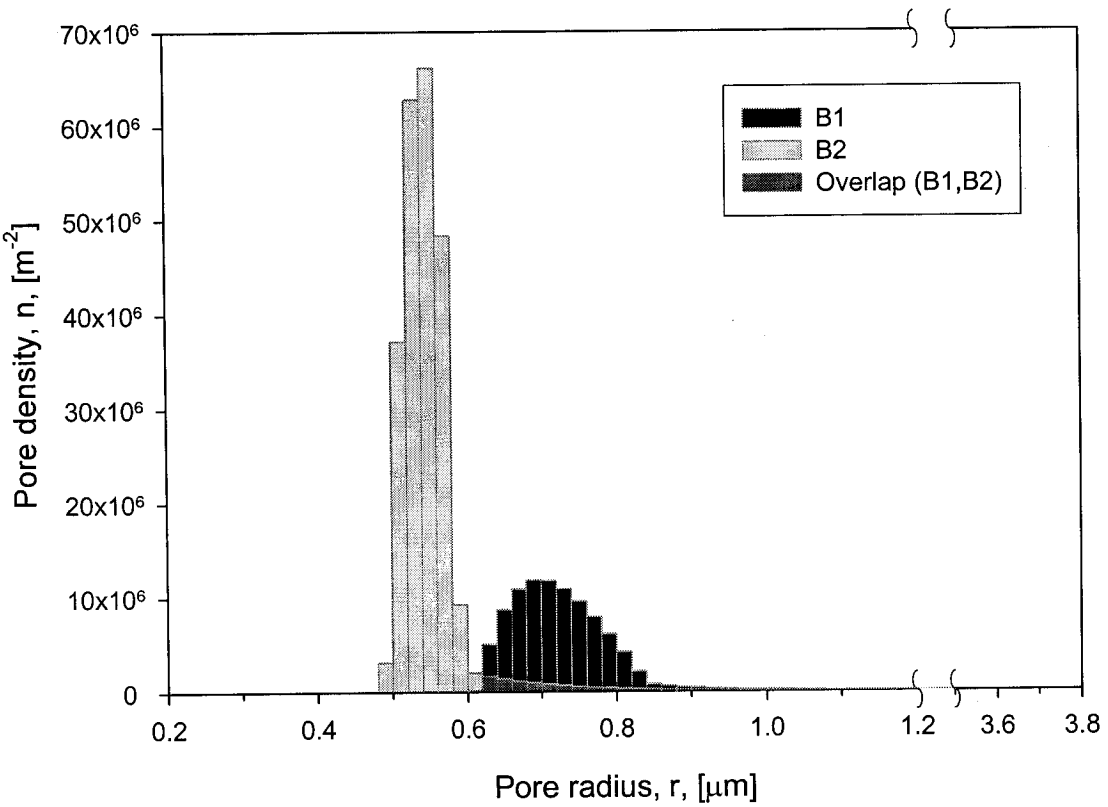

Figure 4.4 Plot for pore size versus number of pores

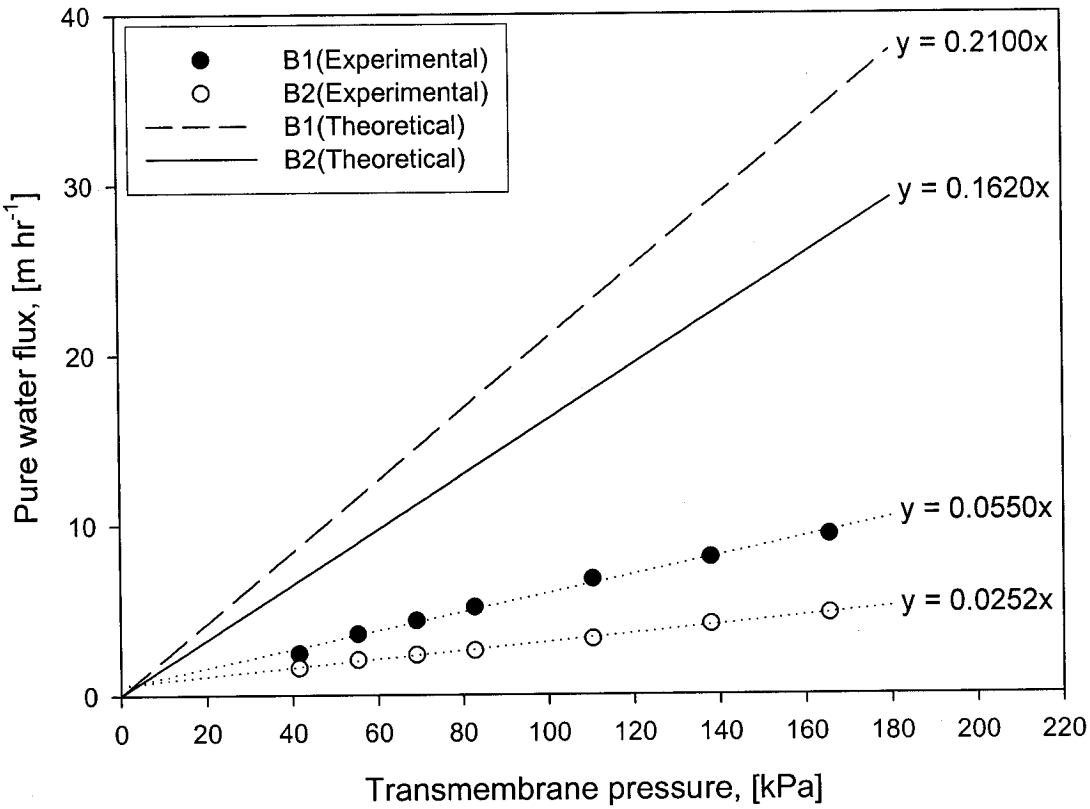

Figure 4.5 Plots for the theoretical water flow rates using Poiseulle flow model

4.2 Effect of tSMM on the Mechanical Properties

Comparison of the mechanical properties of PES membranes, with and without blending tSMM1, was made by measuring maximum tensile strength and % elongation using Instron instrument. The membranes used in these experiments are listed in Table 4.2. B1 and B2 membrane are the same as those in Section 4.1 and they are porous as shown in Section 4.1 by water permeation, bubble-point and gas permeation tests. The membranes H1 and H2, prepared with a long evaporation period at a high temperature are dense and homogeneous.

The effect of tSMM1 on the mechanical properties of the PES membrane is thought to be enhanced by the H membranes.

The instrument was connected to a computer which was programmed to calculate the maximum tensile strength and % elongation from the tensile strength versus time curve. Firstly, the 'B series' membranes were tested with 2 mm/min head speed, and then the 'H series' membranes were tested with 2 and 5 mm/min head speed. The results are given in Table 4.3. In the case of porous membranes (B1 and B2), no noticeable changes occurred either in the % elongation or in the maximum tensile strength by the addition of tSMM. On the other hand, in the case of dense and homogeneous membranes (H1 and H2) the maximum tensile strength decreased slightly and the % elongation increased about twofold by the addition of tSMM. Comparing the B series and H series membranes, the % elongation of the homogeneous membrane (H1) was slightly lower that that of the porous membrane (B1). When tSMM was blended, the % elongation of H2 was higher than that of B2. The maximum tensile strengths of the H series membranes were much higher than the B series membranes, both in the absence and presence of tSMM. According to the Table 4.3, it was also found that both % elongation and tensile strength data increased slightly by an increase in the head speed.

Table 4.2 Preparation conditions of the membranes used for the mechanical property study

Membrane Code	Casting solution composition (by weight)	Evap. Temp. [°C]	Evap. Time [min]	Gelation Media (Temp., Time)
B1	PES:PVP:NMP = 10:10:80	RT	0	Water (@4°C, 1 h)
B2	PES:PVP:tSMM1:NMP = 10:10:1.5:78.5	RT	0	Water (@4°C, 1 h)
H1	PES:PVP:NMP = 10:10:80	110	8	Vacuum (@RT, 48 h)
H2	PES:PVP:tSMM1:NMP = 10:10:1.5:78.5	110	8	Vacuum (@RT, 48 h)

As mentioned, the % elongation change by adding tSMM did not occur for the porous membrane (between B1 and B2) but it did occur for the homogeneous membranes (H1 and H2). Maybe this is because there was no time for surface migration of tSMM and hence the concentration of tSMM at the membrane surface, when the evaporation time was zero. (Migration is believed to occur during the solvent evaporation.) For a longer evaporation period, tSMM had enough time to migrate to the surface where tSMM molecules aggregated. Dispersion of tSMM aggregates may have led to the increase of the % elongation. This mechanical strength change might have happened because the tSMM was synthesized based on polyurethane chemistry. Ratner and Paynter (1984) reported that the unique chemical structure of polyurethanes yielded elastomers with excellent mechanical properties (tensile strength and flex fatigue), abrasion resistance, biodegradation resistance and ease of handling (fabrication). Typical data plots are shown in Figure 4.6 for each membrane that is listed in Table 4.3.

Table 4.3 Mean values of mechanical properties

Membrane Code	Head speed [mm/min]	% Elongation	Maximum tensile strength [MPa]
B1	2	6.7 ± 0.7	1.84 ± 0.14
B2	2	6.5 ± 0.6	1.82 ± 0.07
H1	2	6.1 ± 1.1	51.57 ± 2.10
H2	2	11.4 ± 2.1	48.02 ± 2.66
H1	5	6.5 ± 2.6	55.75 ± 2.48
H2	5	14.0 ± 2.3	51.16 ± 3.79

(a) Crosshead speed: 2 mm/min

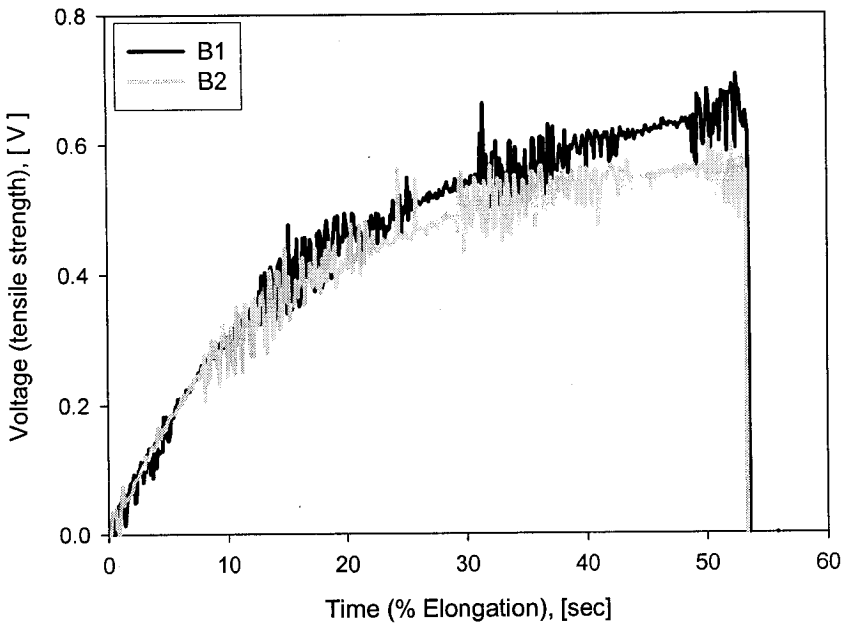

(b) Crosshead speed: 2 mm/min

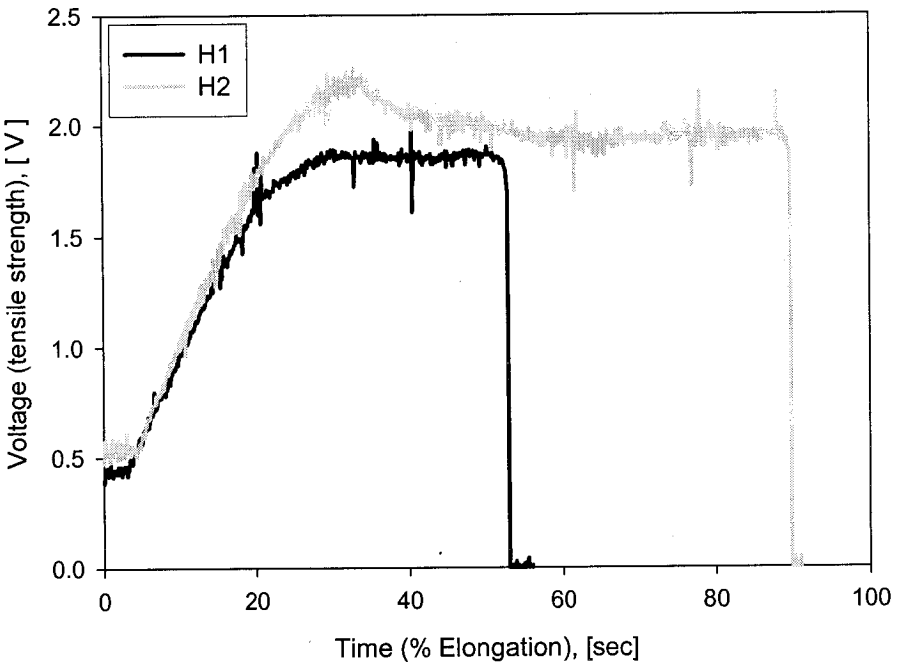

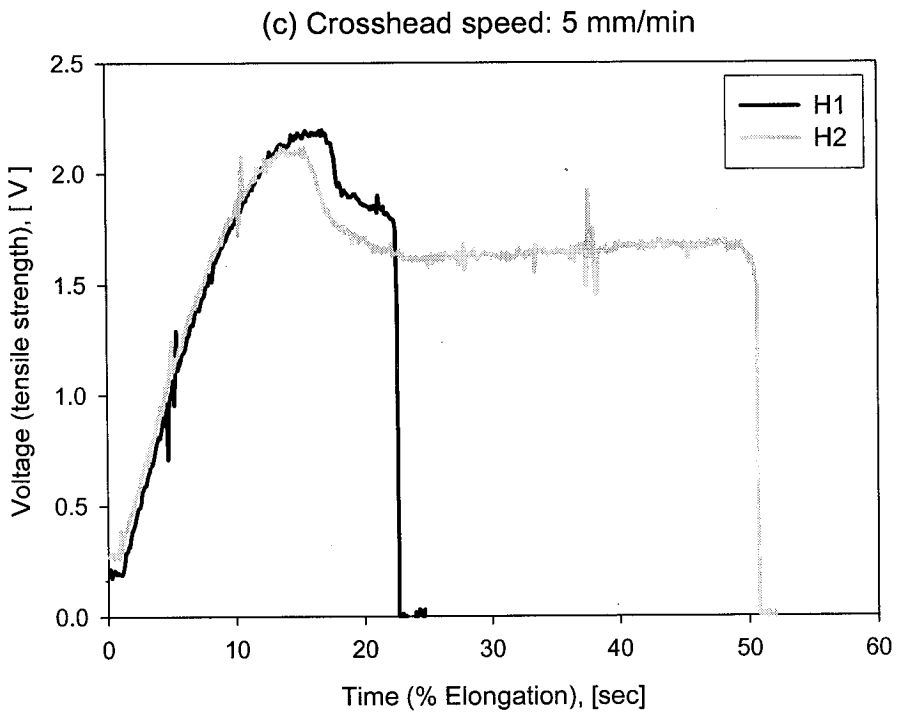

Figure 4.6 Results of mechanical strength test by INSTRON for PES and tSMM blended PES membranes at moving head speed 2 or 5 mm/min

4.3 Contact Angle Measurement for Study on the tSMM Movement

The membranes which were subjected to contact angle measurements are listed in Table 4.4. As mentioned in Section 3.7, the contact angles measured in this study were all advancing contact angles. The contact angles for C1(0) and C2(0), prepared with zero, evaporation time were measured and the results were 66.5±1.8° and 66.8±2.4°, respectively. This confirmed the contact angles of membranes B1 and B2 in Table 4.1. It was therefore concluded that the presence of tSMM did not affect the contact angle, when evaporation time was zero. This indicated that a certain period was necessary for the migration of tSMM toward the membrane surface to occur.

Table 4.4 Preparation conditions of the membranes used for the contact angle measurements

Membrane Code	Casting solution composition (by weight)	Evap. Temp. [°C]	Evap. Time [min]	Cast thickness [mm]
C1(0)	PES:NMP = 20:80	RT	0	0.12
C1(3)	PES:NMP = 20:80	110	3	0.12
C1(5)	PES:NMP = 20:80	110	5	0.12
C1(7)	PES:NMP = 20:80	110	7	0.12
C2(0)	PES:tSMM1:NMP = 20:1.5:78.5	RT	0	0.12
C2(3)	PES:tSMM1:NMP = 20:1.5:78.5	110	3	0.12
C2(5)	PES:tSMM1:NMP = 20:1.5:78.5	110	5	0.12
C2(7)	PES:tSMM1:NMP = 20:1.5:78.5	110	7	0.12
C3(3)	PES:tSMM1:NMP = 20:1.5:78.5	110	3	0.18
C3(5)	PES:tSMM1:NMP = 20:1.5:78.5	110	5	0.18
C3(7)	PES:tSMM1:NMP = 20:1.5:78.5	110	7	0.18
C4(3)	PES:tSMM1:NMP = 20:1.5:78.5	110	3	0.24
C4(5)	PES:tSMM1:NMP = 20:1.5:78.5	110	5	0.24
C4(7)	PES:tSMM1:NMP = 20:1.5:78.5	110	7	0.24
C2(∞)	PES:tSMM1:NMP = 20:1.5:78.5	110	2,000	0.12

The PES membranes without tSMM were prepared with evaporation periods of 3, 5 and 7 min (C1 series). The cast thickness was maintained at 0.12 mm. These membranes were then subjected to the contact angle measurement. The average contact angle did not change with a change in evaporation period as shown in Figure 4.7. This indicates that solvent evaporation has no effect on the contact angle of the PES membranes. Finally, 9 PES membranes with tSMM blending of 3 different cast thicknesses (0.12, 0.18 and 0.24 mm) and of 3 different evaporation periods (3, 5 and 7 min) (C2 ~ C4 series) were prepared and the contact angles were measured. The results are also given in Figure 4.7.

The figure shows that the contact angle increased with an increase in evaporation period

and also depended on the film thickness. The contact angle increased as the film thickness became smaller. In particular, the contact angle increased from 80° to 106° when the film thickness was 0.12 mm. The increase in contact angle with evaporation time clearly indicates the migration of tSMM towards the surface of the film, while the solvent is being evaporated, rendering the surface more hydrophobic. C2(∞), the homogeneous membrane that was expected to have the largest content of tSMM in the surface, had the highest contact angle of 108±1.2°.

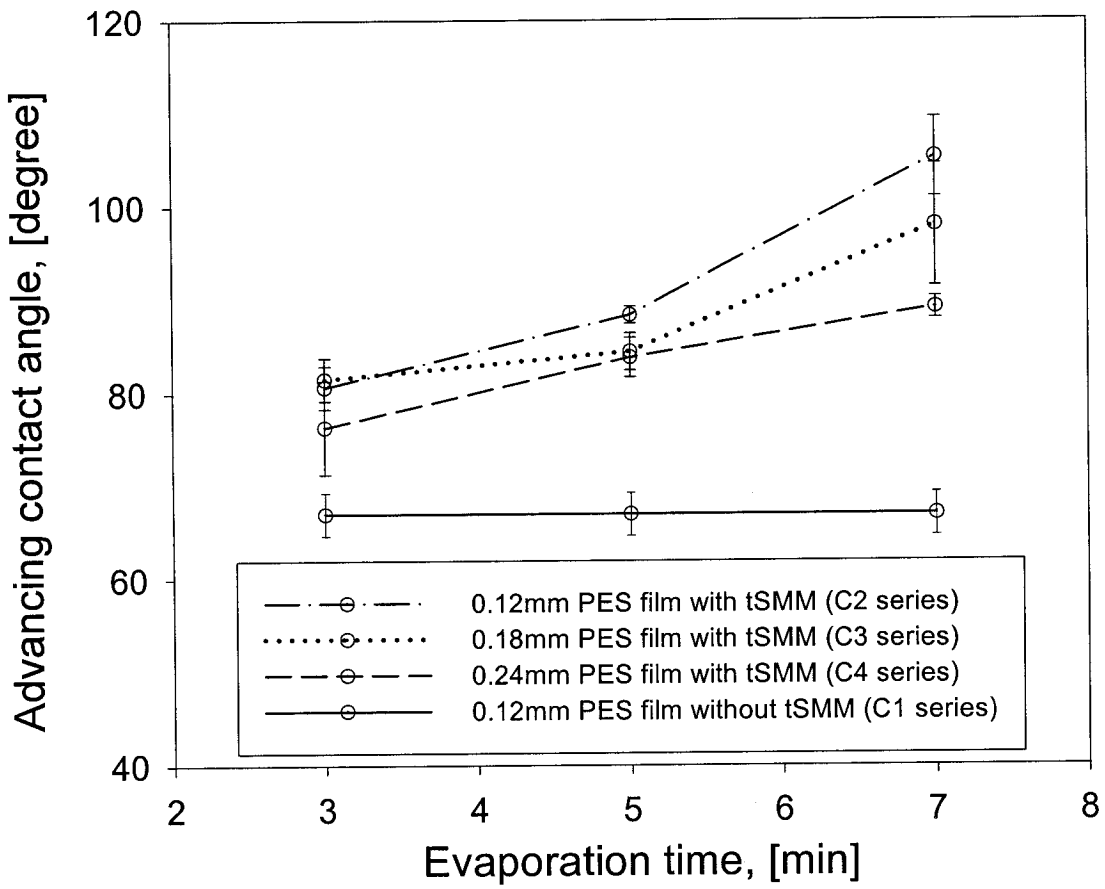

Figure 4.7 Contact angel measurement data for PES and SMM blended PES membranes

4.4 XPS for Study on the tSMM Movement

Six membranes in Table 4.4 (C2 and C4 series) with two different cast film thickness (0.12 and 0.24 mm) and three different evaporation periods (3, 5 and 7 min) were prepared for this study. Two areas were chosen from each membrane and subjected to XPS analysis at two take-off angles, i.e. 0° and 60°, which correspond to the X-ray sampling depths of 6.3 and 3.15 nm, respectively. All samples contained carbon, oxygen, fluorine, nitrogen and sulfur, except for some membranes in which no sulfur was detected. It should be noted XPS does not detect hydrogen. The results of XPS analysis are summarized in Table 4.5 and 4.6. In both tables, it is noticed that fluorine contents at the sampling depth of 3.15 nm are higher than those at 6.3 nm. This means that tSMM, which contains fluorine, is more concentrated near the membrane surface. C2(0) and C2(∞) with a cast film thickness of 0.12 mm and evaporation periods of 0 and 2000 min, respectively, were also prepared and subjected to XPS analysis at 60° of take-off angle. Since the atomic composition of the membrane surface was better represented by the data at the sampling depth of 3.15 nm, those data were chosen in Figure 4.8 to show the effect of the cast film thickness and evaporation period on the atomic per cent of fluorine. In Tables 4.5, 4.6 and 4.7, XPS data are summarized. The tables also show the calculated atomic compositions for pure PES and pure tSMM compositions excluding hydrogen, as hydrogen did not appear in the XPS data. The evaluation method (for pure PES and tSMM) is given in Appendix E.

It should be noted that the fluorine content at 2000 min of evaporation time in Figure 4.8 corresponds to the saturation of the surface by tSMM, after a long period of solvent evaporation. The figure clearly shows that the fluorine content increased with an increase in evaporation period, approaching to an equilibrium concentration. During the first seven minutes, the fluorine content was increased by 23.9 atomic %, while during the periods from seven to 2,000 min, it was increased by only 8.1 atomic %. Two important parameters emerged from these experiments, one is the maximum equilibrium concentration (in this case, 35.9 atomic %) and the other is the minimum evaporation time that is required to

reach the equilibrium concentration (in this case, according to the data trend, seems to be few minutes after 7 minutes evaporation time). From the calculated composition of tSMM and the measured surface composition of C2(∞) in Table 4.7, when compared to the atomic compositions of pure PES and tSMM, suggests the following two steps in the process of the surface coverage with tSMM. Firstly, no sulfur was detected at the surface of C2(∞), indicating complete displacement of PES from the surface by tSMM. Secondly, the measured fluorine content in the surface of C2(∞) (35.9 atomic %) was much higher than the calculated fluorine content in pure tSMM (16.4 atomic %), indicating conformational reorientation of tSMM molecules at the surface; i.e. the fluorine end groups in the tSMM molecule (Figure 3.2) was oriented perpendicular to the polymer solution/air interface, leading to the higher fluorine content at the surface than the fluorine content in pure tSMM.

It also shows that surface fluorine content was higher when the cast film was thinner. This means that tSMM migrated more to the membrane surface with an increase in evaporation period and decrease in cast film thickness. Hence, the results from XPS experiments agreed with those from contact angle measurements.

Table 4.5 Atomic percent* measured by XPS analysis of tSMM blended membranes (I)

(cast film thickness, 0.12 mm)

Membrane	C2(3)	C2(5)	C2(7)	C2(3)	C2(5)	C2(7)
(Evaporation time)	(3 min)	(5 min)	(7 min)	(3 min)	(5 min)	(7 min)
Sampling depth	3.15 nm			6.3 nm		
Atoms (core level)	Content [atomic %]			Content [atomic %]		
Carbon (C1s)	73.0	68.8	57.4	72.8	70.9	63.7
Oxygen (O1s)	16.0	15.8	11.1	16.3	16.8	12.9
Fluorine (F1s)	5.3	9.8	27.8	4.6	6.2	19.2
Nitrogen (N1s)	1.8	2.3	3.7	2.0	2.0	4.2
Sulfur (S2p)	3.8	3.3	0.0	4.4	4.1	0.0

*Error range is ± 5 ~ 10%

†Theoretical pure PES composition, atomic % without hydrogen: C (75.0), O (18.7), S (6.3)

‡Theoretical pure tSMM composition, atomic % without hydrogen: C (64.8), O (15.0), N (3.8), F (16.4)

Table 4.6 Atomic percent* measured by XPS analysis of tSMM blended membranes (II)

(cast film thickness; 0.24 mm)

Membrane (Evaporation time)	C4(3) (3 min)	C4(5) (5 min)	C4(7) (7 min)	C4(3) (3 min)	C4(5) (5 min)	C4(7) (7 min)
Sampling depth	3.15 nm			6.3 nm		
Atoms (core level)	Content [atomic %]			Content [atomic %]		
Carbon (C1s)	71.3	72.4	67.0	72.4	71.3	70.1
Oxygen (O1s)	16.8	16.9	14.4	17.0	17.0	15.9
Fluorine (F1s)	5.9	8.1	13.8	4.3	5.6	8.6
Nitrogen (N1s)	2.0	-	4.1	1.8	2.7	4.0
Sulfur (S2p)	4.0	2.6	0.8	4.5	2.8	1.4

*Error range is ± 5 ~ 10%

†Theoretical pure PES composition, atomic % without hydrogen: C (75.0), O (18.7), S (6.3)

‡Theoretical pure tSMM composition, atomic % without hydrogen: C (64.8), O (15.0), N (3.8), F (16.4)

Table 4.7 Atomic percent* measured by XPS analysis of tSMM blended membranes (III)

(cast film thickness, 0.12 mm)

Membrane (Evaporation time)	C2(0) (0 min)	C2(∞) (2,000 min)
Sampling depth	3.15 nm	
Atoms (core level)	Content [atomic %]	
Carbon (C1s)	63.9	53.3
Oxygen (O1s)	19.0	7.2
Fluorine (F1s)	3.9	35.9
Nitrogen (N1s)	4.6	3.6
Sulfur (S2p)	3.2	0.0

*Error range is ± 5 ~ 10%

†Theoretical pure PES composition, atomic % without hydrogen: C (75.0), O (18.7), S (6.3)

‡Theoretical pure tSMM composition, atomic % without hydrogen: C (64.8), O (15.0), N (3.8), F (16.4)

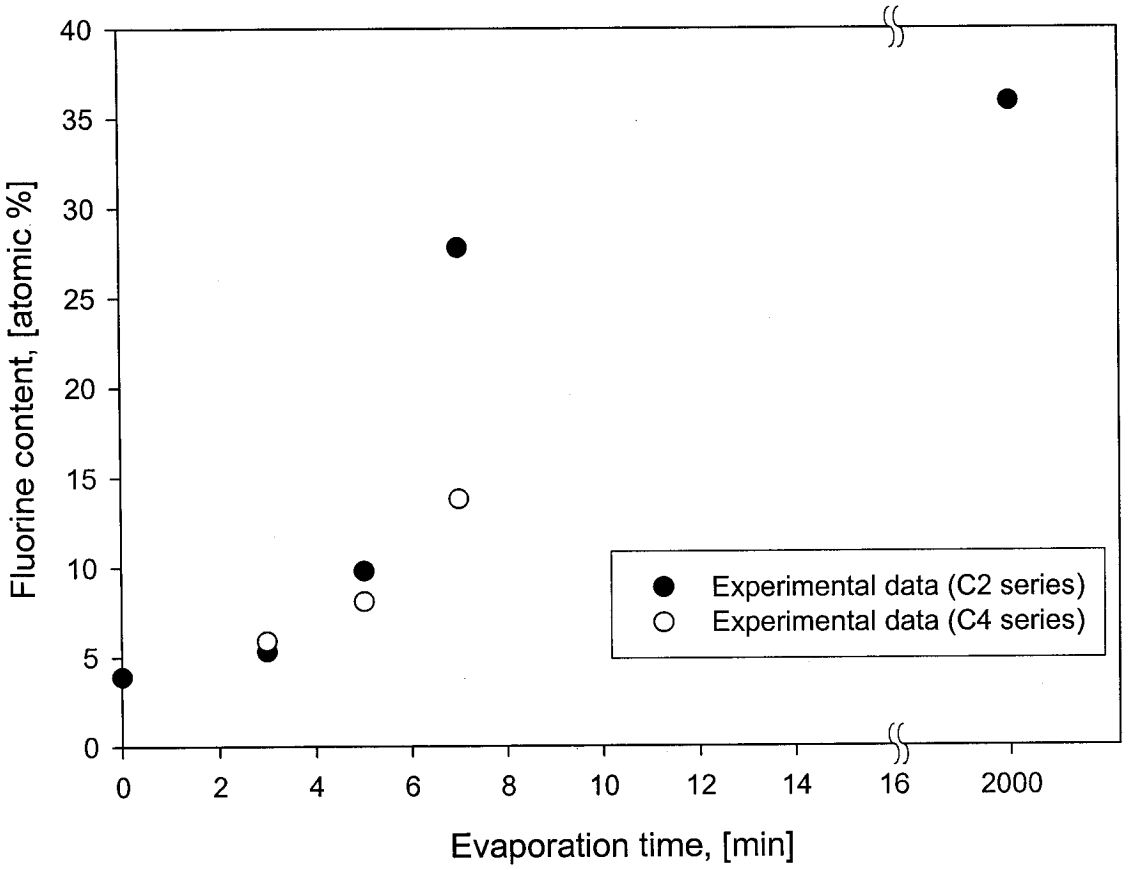

Figure 4.8 XPS fluorine content versus evaporation time

4.5 Summary of Chapter 4 (Part 1)

1. The pore size of the membrane was reduced and also the pore size distribution narrowed by adding tSMM1 into the PES membrane, when there was no evaporation time during the membrane preparation.
2. The maximum tensile strength decreased slightly and the % elongation increased about twofold by the addition of tSMM1 into the PES membrane when the membranes were dense and homogeneous, while no significant differences in the mechanical properties were

observed when the membranes were porous.

3. As evidenced by contact angle measurement and XPS analysis, 1) no surface migration of tSMM1 was detected when membranes were prepared with zero evaporation period; 2) the surface migration of tSMM1 increased with an increase in evaporation time; 3) more surface migration of tSMM1 was detected for a thinner membrane; and 4) the tSMM1 was preferentially oriented with fluorocarbon end groups at the outermost surface of the membrane.

5. Results and Discussion (Part 2): Study on the Kinetic of Surface Migration of tSMM in PES Membrane Preparation

The purpose of this chapter is to establish the kinetics of SMM migration by deriving model equations based on experimental data which is shown in Chapter 4. There have been a large number of studies on the tSMM and on the tSMM migration. However, there has been no study on the kinetics of SMM migration to the surface. The contents in this chapter were published in 'Macromolecules (v.35, 3017-3021, 2002)'.

5.1 Theoretical Study

According to the experimental results in Chapter 4, it was observed that the migration of tSMM to the surface of membrane occurred when the cast solution on a glass plate was kept in an oven at a predetermined temperature during the membrane preparation and the migration stopped when the cast solution with the glass plate was put into water gelation bath or when the cast solution was completely dried in the oven. The time period that the cast solution with glass plate was kept in the oven was called the 'evaporation time' or 'evaporation period' in this study because during that time the solution evaporation must take place. A schematic diagram of tSMM migration is shown in Figure 5.1.

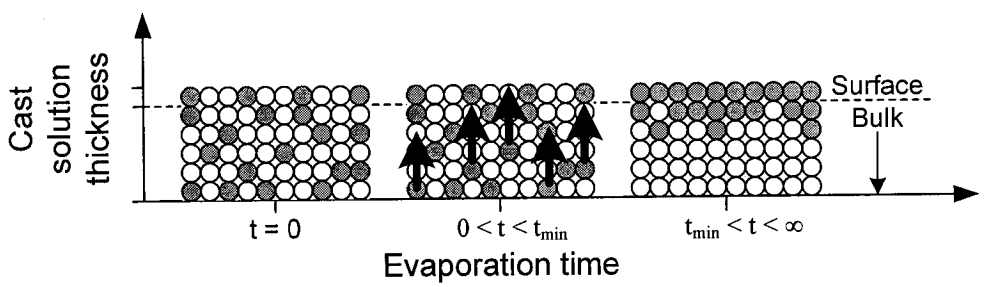

Figure 5.1 Schematic diagram illustrating tSMM migration: ●, tSMM molecule; ○, base polymer; t_{min} , the minimum evaporation time to reach the equilibrium concentration at the surface of a membrane

A kinetic model for tSMM migration that is occurring in the polymer solution film while it is placed in the oven was established under the following assumptions. It should be noted that solvent evaporation took place together with the tSMM migration.

1. There is a bulk layer of thickness L, from which tSMM migrates.

2. There is a surface layer of thickness δ, into which tSMM migrates.

3. There is a plane of boundary between the bulk layer and the surface layer through which tSMM migrates.

4. The polymer densities in both bulk and surface layers are constant.

5. Both L and δ decrease with time as solvent evaporates. However, $L\varepsilon$ and $\delta\varepsilon$, where ε is the volume fraction of polymer (PES + tSMM) in the solution, does not change since polymer does not evaporate and ε increases making $L\varepsilon$ and $\delta\varepsilon$ constant.

6. Mass transfer through the plane of boundary is accelerated with time because the distance tSMM passes through to migrate into the surface layer is shortened as more solvent evaporates. The mass transfer coefficient is arbitrarily given by

$$k = k^{\circ}t^{2} \tag{5.1}$$

where k° and k are the mass transfer coefficients at the beginning and time = t, respectively. Even though k is over zero at t = 0 and any term is added in the equation to consider its effect, the final result would be almost the same as the one obtained by using Equation 5.1.

7. The driving force for the tSMM migration is (the surface tSMM concentration in equilibrium with the bulk tSMM concentration – the surface tSMM concentration). The migration stops when the above concentration difference becomes zero.

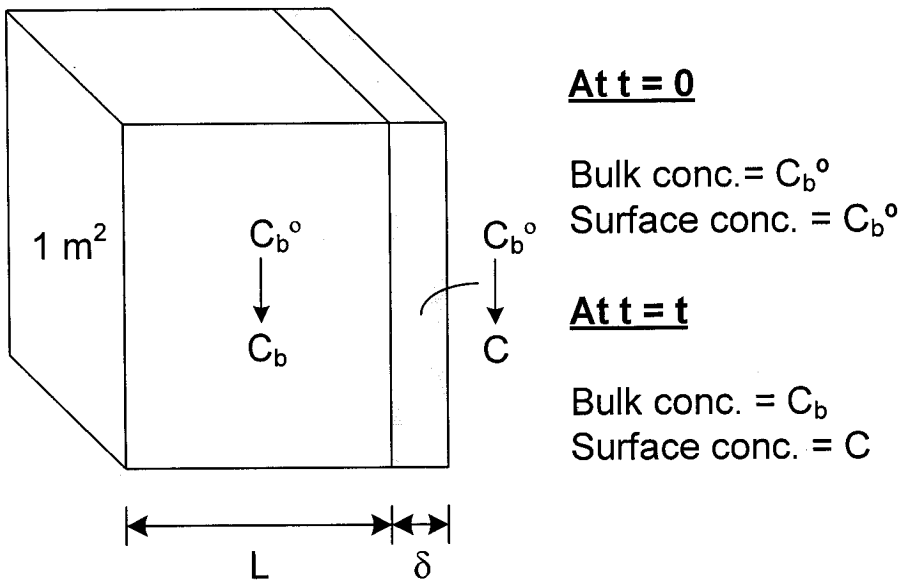

Figure 5.2 Schematic representation of the bulk and surface layer

The bulk and surface layer and the tSMM c oncentration in each layer are schematically shown in Figure 5.2. It should be noted that C in Figure 5.2 is defined as tSMM concentration in polymer phase (without including solvent) and is called tSMM concentration hereafter.

Considering that the tSMM concentration is initially (at t = 0) $C_b°$, both in the bulk and the surface layer, and $C_b°$ is lowered to C_b at the bulk layer while $C_b°$ is increased to C at the surface layer at t > 0, the mass balance for the polymer over unit area of boundary plain yields,

$$L\varepsilon C_b + \delta\varepsilon C = (L\varepsilon + \delta\varepsilon)C_b° \tag{5.2}$$

or

$$C_b + (\delta / L)C = (1 + (\delta / L))C_b° \tag{5.3}$$

where δ/L is assumed unchange.

Suppose the surface tSMM concentration, C, is related to the tSMM concentration in the bulk layer, C_b, by the following equation, when they are in equilibrium

$$C^* = \alpha C_b \tag{5.4}$$

where C^* is equilibrium surface concentration and α is the proportionality constant.

Then, the driving force for the tSMM migration can be given as

$$C^* - C = \alpha C_b - C \tag{5.5}$$

Mass transfer through unit area of the boundary plain allows the accumulation of SMM in the surface layer, which is given by

$$d(\delta\varepsilon C)/dt = k(C^* - C) \tag{5.6}$$

Combining Equations (5.1), (5.3), (5.5) and (5.6) and rearranging, we obtain

$$dC/\left[\left\{\left(\alpha(\delta/L)+\alpha\right)/\left(\alpha(\delta/L)+1\right)\right\}C_b^\circ - C\right] = \left(\alpha(\delta/L)+1\right)\left(k^\circ/\delta\varepsilon\right)t^2 dt \tag{5.7}$$

Integration of equation (5.7) with a boundary condition $C = C_b^\circ$ at $t = 0$ yields

$$(C^\infty - C)/(C^\infty - C_b^\circ) = \exp(-\beta t^3) \tag{5.8}$$

where C at time $= \infty$ is

$$C^\infty = \left\{\left(\alpha(\delta/L)+\alpha\right)/\left(\alpha(\delta/L)+1\right)\right\}C_b^\circ \tag{5.9}$$

and

$$\beta = k^{\circ}\left(\alpha\left(\delta / L\right)+1\right)/3\delta\varepsilon \tag{5.10}$$

Since fluorine content in the membrane is proportionate to the SMM concentration in SMM/PES mixtures (without solvent), C in equations (5.8) and (5.9) can be replaced by fluorine content, C_f.

Then,

$$(C_f^{\infty} - C_f)/(C_f^{\infty} - C_{f,b}{}^{\circ}) = \exp(-\beta t^3) \tag{5.11}$$

where C_f is the fluorine content at the surface, $C_{f,b}{}^{\circ}$ is C_f at time $t = 0$ and also the fluorine content in the bulk at $t = 0$, C_f^{∞} is C_f when $t = \infty$ and given by

$$C_f^{\infty} = \left\{\left(\alpha\left(\delta / L\right)+\alpha\right)/\left(\alpha\left(\delta / L\right)+1\right)\right\} C_{f,b}{}^{\circ} \tag{5.12}$$

Equation (5.10) will remain the same.

5.2 Experimental Verification of the Kinetic Model

In Section 4.4, XPS analyses with two different membrane thicknesses (the cast film thickness of 0.12 and 0.24 mm respectively) and two different X-ray sampling depths of 3.15 and 6.3 nm were performed.

The experimental data for the cast film thickness of 0.12 mm and the X-ray sampling depth of 3.15 nm (C2 series membranes in Table 4.4) was simulated by Equation 5.11 by setting $C_{f,b}{}^{\circ}$ and C_f^{∞} equal to 3.9 and 35.9 fluorine atomic %, respectively, which were the experimental values in Table 4.7. The data for the cast film thickness of 0.24 mm and the X-ray sampling depth of 3.15 nm (C4 series membranes in Table 4.4) was also simulated by

the same equation. The $C_{f,b}^{o}$ and C_f^{∞} were set to the same values for C2 series membranes because the casting solution compositions were the same and at the infinity evaporation time the concentration of tSMM must be the same. The parameter, β, for each case of cast film thickness was obtained by linear regression analysis based on the data at different evaporation times (0 ~ 7 min) and Equation 5.11. The lines on Figure 5.3 indicate the theoretical values calculated by Equation 5.11 and the resulted β parameters. The experimental fluorine contents were plotted along with the simulated theoretical lines. It should be noted that the value $(C_f - C_{f,b}^{o})/(C_f^{\infty} - C_{f,b}^{o})\times 100$ changes from 0 to 100%. The time required for this value to reach 1% is called initial time lag (t_{lag}) and the time required to reach 99% is called the minimum evaporation time (t_{min}). In both membrane series, the simulation lines represent the experimental values satisfactorily. In particular, the initial lag time and the tendency for fluorine content to level off at the final stage of evaporation period are well represented by the theoretical line.

During the calculation for modeling, decrease in the parameter β by increasing the cast solution film thickness was observed and it was suspected that there must be a relationship between the cast solution thickness and the parameter, β. In this study, we had only two β points as shown in Figure 5.4. Two different regression methods, based on linear and exponential decay, were applied to those data points, regression results being also provided in the figure. Between the two cases considered the exponential decay seems more feasible, because in the case of linear regression β becomes negative when a cast solution thickness is over 0.29 mm. This means that the surface fluorine content will become decreasing with time according to equation 5.11, which is opposite to the tSMM surface migration. More experimental data with different cast solution thicknesses are required to establish a more precise relationship between the cast solution thickness and the parameter, β. The regressions were performed by the scientific computer software, 'SigmaPlot v.9.0 (Systat Software, Inc.)'. The initial lag time and the minimum evaporation time for each case are listed in Table 5.1.

Table 5.1 Initial lag time and minimum evaporation time of C2 and C4 series membranes

Membrane Code	Initial lag time (t_{lag}) [min]	Minimum evaporation time (t_{min}) [min]
C2	1.2	11
C4	2.1	16.5

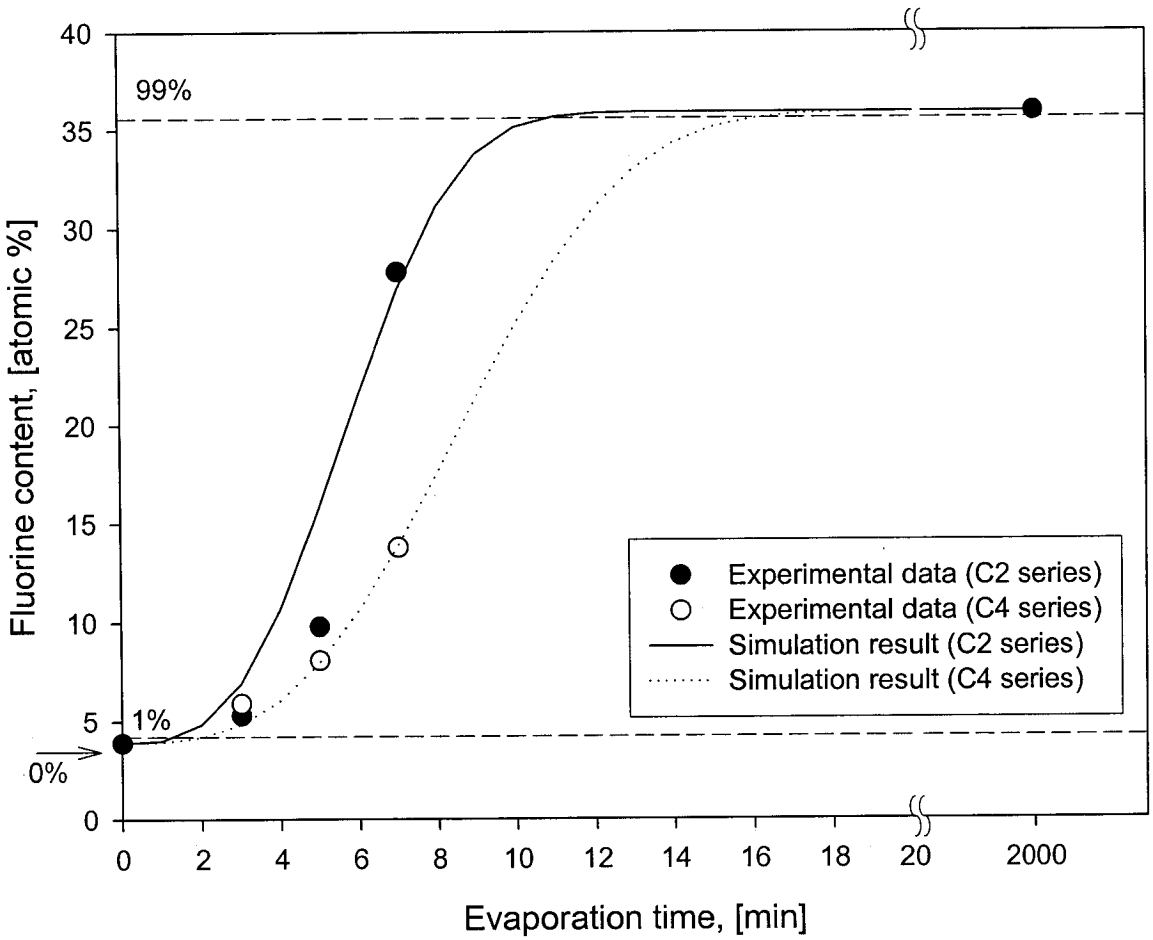

Figure 5.3 Comparison of experimental XPS values with the results from theoretical calculations

As shown in Figure 5.3 and Table 5.1, as the cast solution film thickness increases, both the initial lag time and the minimum evaporation time increase, resulting in a rightward shift of the simulation line. The experimental data support this predicted trend.

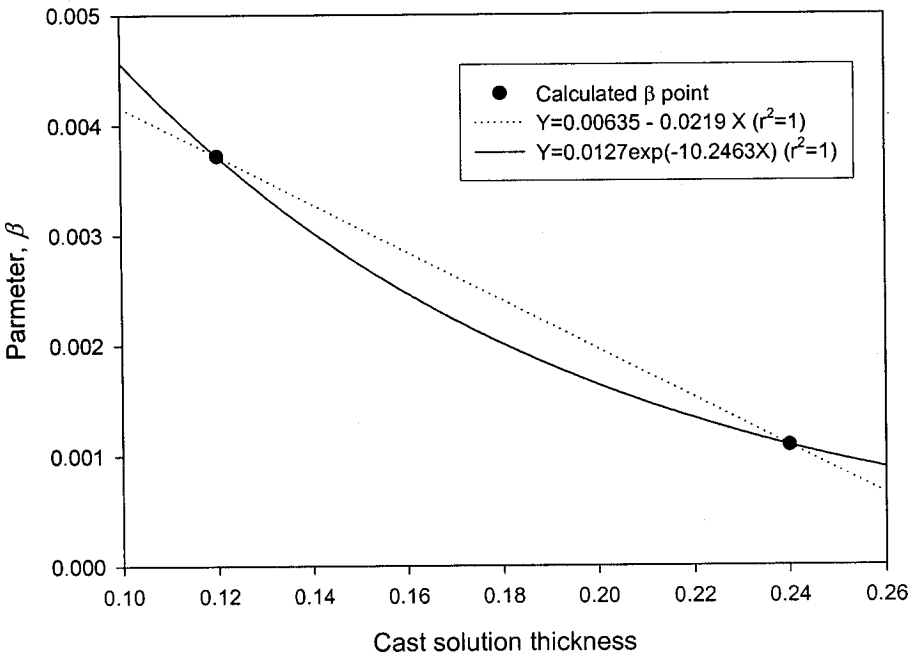

Figure 5.4 Relationship between β and the cast solution thickness for C2 and C4 series membranes

Despite satisfactory agreement between the model calculation and the experiment, it should be admitted that the model seems to be an over-simplification. In particular, it is a serious drawback that the model cannot predict any tSMM concentration profile in the X-ray depth direction that was observed experimentally. It should be also pointed out that the fluorine content obtained by XPS experiments do not necessarily a gree with the fluorine content calculated on the basis of tSMM/PES molar ratio. For example, the fluorine content that corresponds to the initial weight ratio of tSMM/PES = 7/93 should be equal to 1.32 atomic %, while the initial bulk fluorine content is 3.9 atomic %. The maximum fluorine content achieved was 35.9 atomic %, as stated earlier, which is far greater than the theoretical fluorine content of 19.16 atomic % for pure SMM. The ratio of the final surface

concentration to the initial bulk concentration is 19.16/1.32 = 14.5 according to the theory while it is 35.9/3.9 = 9.2 by experiment. The method of calculation for the fluorine content (atomic %) in the tSMM incorporated PES membrane was provided in Appendix F.

5.3 Summary of Chapter 5 (Part 2)

A model proposed for the kinetics of tSMM1 surface migration could represent the experimental data on the surface florine content provided by the XPS experiments satisfactorily. About 12 and 18 min were required to complete the tSMM1 surface migration for the casting solution films of C2 and C4 series membranes, respectively, under the experimental conditions adopted in this study.

6. Results and Discussion (Part 3): Potential of tSMM Blended PES Membranes for Membrane Distillation Purpose

In Chapter 4 the effects of blending tSMM on the pore size and the pore size distribution, the mechanical strength, the contact angle and the surface atomic composition of polyethersulfone (PES) membrane were discussed. In this chapter, the focus is on the effect of tSMM blending on the PES membrane performance in membrane distillation. More specifically, the effects of membrane preparation conditions on the pure water permeation flux (PWP) and liquid entry pressure of water (LEP_w) were investigated.

6.1 Effect of tSMM1 on Pure Water Permeation of PES Membrane

The membranes prepared in Section 3.3.4 and used for this study are listed in Table 6.1. Both O1 (PES) and O2 (PES with tSMM1) membranes were subjected to pure water permeation experiments, the results of which are depicted in Figure 6.1. The PWP experiments were made according to the method described in Section 3.5. The effective diameter of the membrane was 3.4 cm. The water permeation rate started to increase from the origin for the membrane, O1, while the membrane, O2, sustained water above the membrane surface until transmembrane pressure difference became 110 kPa, which was defined as the LEP_w of the membrane. This is because of the higher hydrophobicity of the surface of the O2 membrane. Conventional hydrophilic and hydrophobic membranes would exhibit the trends that are similar to O1 and O2, respectively, on PWP tests. These data also resemble those which are shown in Figure 4.2. The presence of tSMM in the tSMM blended membrane changes the surface characteristic to hydrophobic from hydrophilic.

Table 6.1 Preparation conditions of the membranes used for water permeation

Membrane Code	Casting solution composition (by weight)	Evap. Temp. [°C]	Evap. Time [min]	Gel. Temp. [°C]
O1	PES:NMP = 12:88	110	2	4
O2	PES:tSMM1:NMP = 12:2:86	110	2	4

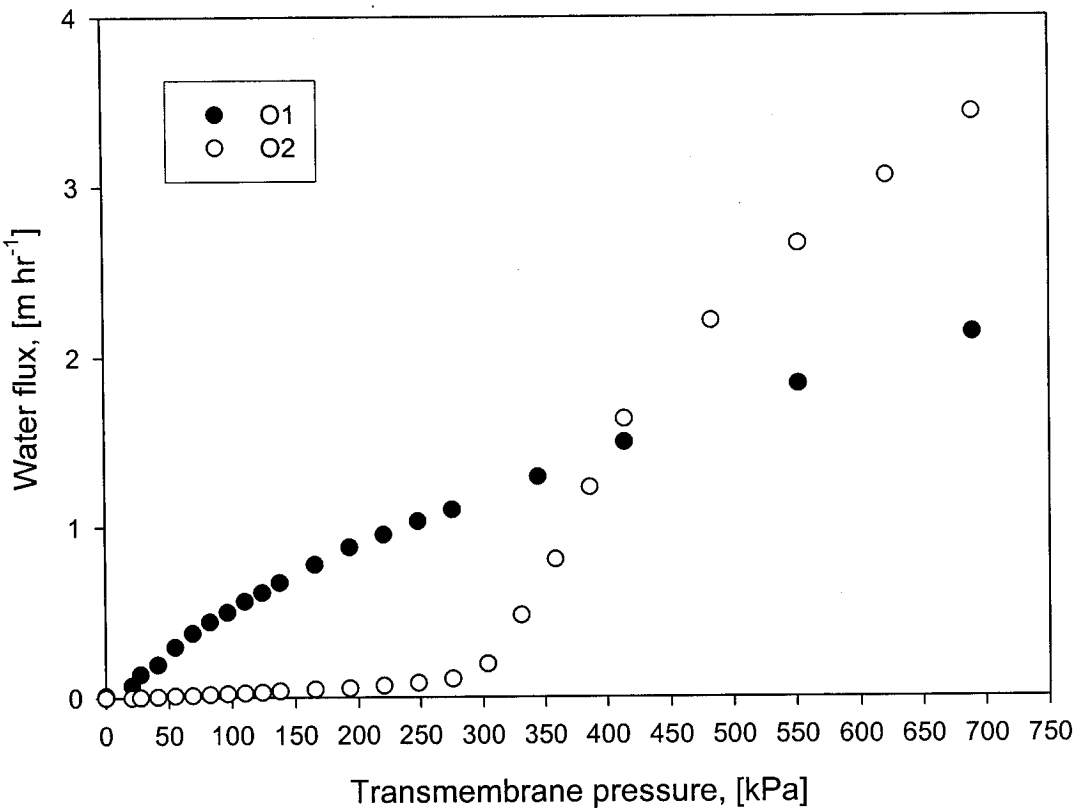

Figure 6.1 Pure water permeation flux versus transmembrane pressure

6.2 tSMM2 Synthesis and Characterization

Because of quantity limitation of tSMM1 supplied from University of Toronto, tSMM was synthesized in University of Ottawa as mentioned in section 3.2 and named tSMM2. The synthesized tSMM2 was characterized by GPC using polystyrene standard and elemental analysis. The results were summarized in Table 6.2, where GPC and elemental analysis data for tSMM1 (Mandeep, 2001) are also shown. As shown in the table, both number average molecular weight (M_n) and weight average molecular weight (M_w) of tSMM2 were less than those of tSMM1. Fluorine content of tSMM2 was also about half of tSMM1 in the reference.

Table 6.2 Molecular weights obtained from GPC results and fluorine content from elemental analysis for two samples of tSMM

Type of SMM	M_n	M_w	Polydispersity*	Fluorine content (wt%)
tSMM1	20,000	25,000	1.30	13.4
tSMM2	14,600	22,600	1.55	6.85

* Polydispersity = M_w/M_n

6.3 Effect of tSMM2 Blending on the Properties of PES Membranes

The tSMM2 blended PES membranes were tested by contact angle measurement and XPS for the tSMM migration study. The conditions of the membrane preparation are listed in Table 6.3.

Table 6.3 Preparation conditions of the membranes used for water permeation

Membrane Code	Casting solution composition (by weight)	Evap. Temp. [°C]	Evap. Time [min]	Cast solution thickness [mm]
P1(0)	PES:tSMM2:NMP = 12:2:86	RT	0	0.20
P1(5)	PES:tSMM2:NMP = 12:2:86	110	5	0.20
P1(10)	PES:tSMM2:NMP = 12:2:86	110	10	0.20
P1(15)	PES:tSMM2:NMP = 12:2:86	110	15	0.20
P1(20)	PES:tSMM2:NMP = 12:2:86	110	20	0.20
P1(25)	PES:tSMM2:NMP = 12:2:86	110	25	0.20
P2(0)	PES:tSMM2:NMP = 12:2:86	RT	0	0.25
P2(5)	PES:tSMM2:NMP = 12:2:86	110	5	0.25
P2(10)	PES:tSMM2:NMP = 12:2:86	110	10	0.25
P2(15)	PES:tSMM2:NMP = 12:2:86	110	15	0.25
P2(20)	PES:tSMM2:NMP = 12:2:86	110	20	0.25
P2(25)	PES:tSMM2:NMP = 12:2:86	110	25	0.25
P3(0)	PES:tSMM2:NMP = 12:2:86	RT	0	0.30
P3(5)	PES:tSMM2:NMP = 12:2:86	110	5	0.30
P3(10)	PES:tSMM2:NMP = 12:2:86	110	10	0.30
P3(15)	PES:tSMM2:NMP = 12:2:86	110	15	0.30
P3(20)	PES:tSMM2:NMP = 12:2:86	110	20	0.30
P3(25)	PES:tSMM2:NMP = 12:2:86	110	25	0.30
P1(∞)	PES:tSMM2:NMP = 12:2:86	110	2,000	0.20

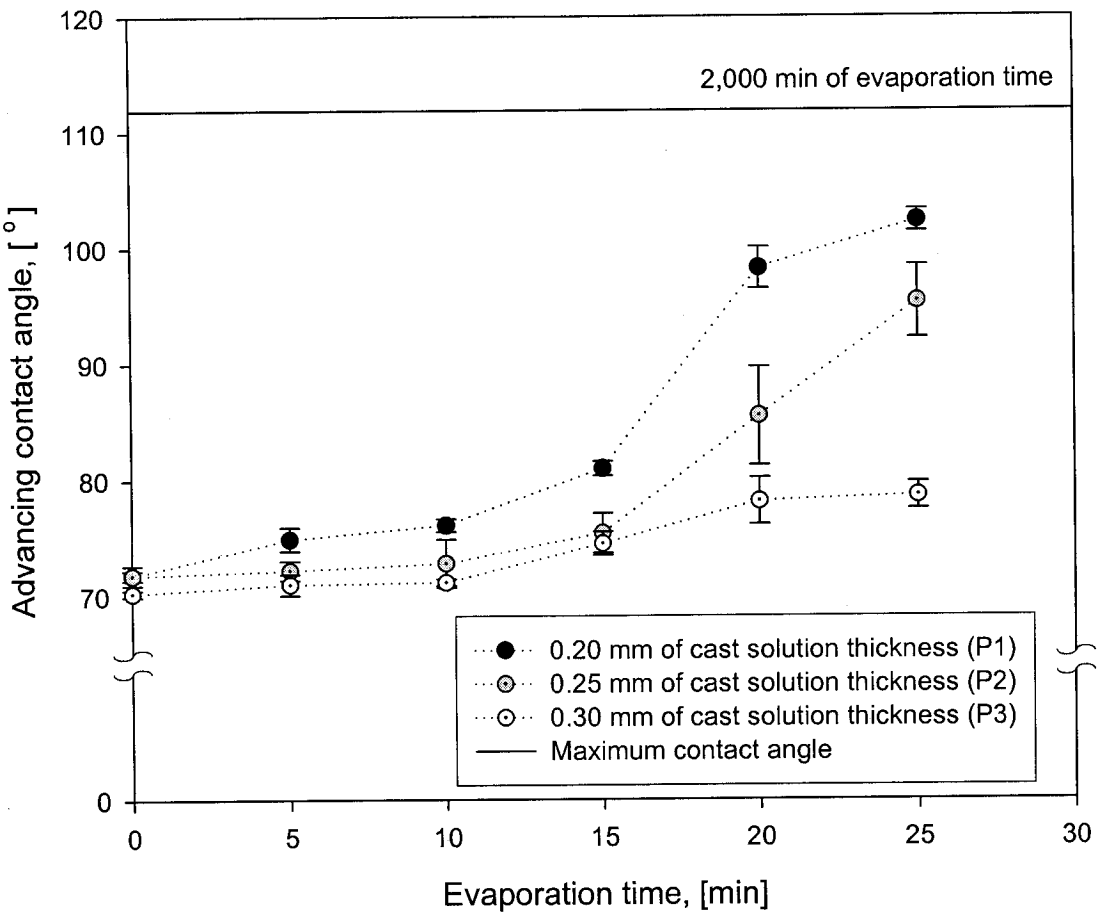

Figure 6.2 Contact angle as functions of evaporation time and casting film thickness

Figure 6.2 shows the results of contact angle measurements for each membrane given in Table 6.3. Increase in the contact angle by increasing the evaporation time was observed similar to tSMM1. For a given evaporation time the contact angle increased as the cast solution thickness was decreased. The fluorine contents in tSMM2 blended PES membranes determined by the XPS analysis are also shown in Figure 6.3. The data are in accordance with the contact angle data shown in Figure 6.2; i.e. more tSMM molecules migrate to the membrane surface with an increase in the evaporation time and tSMM molecules migrate faster when the membrane is thinner.

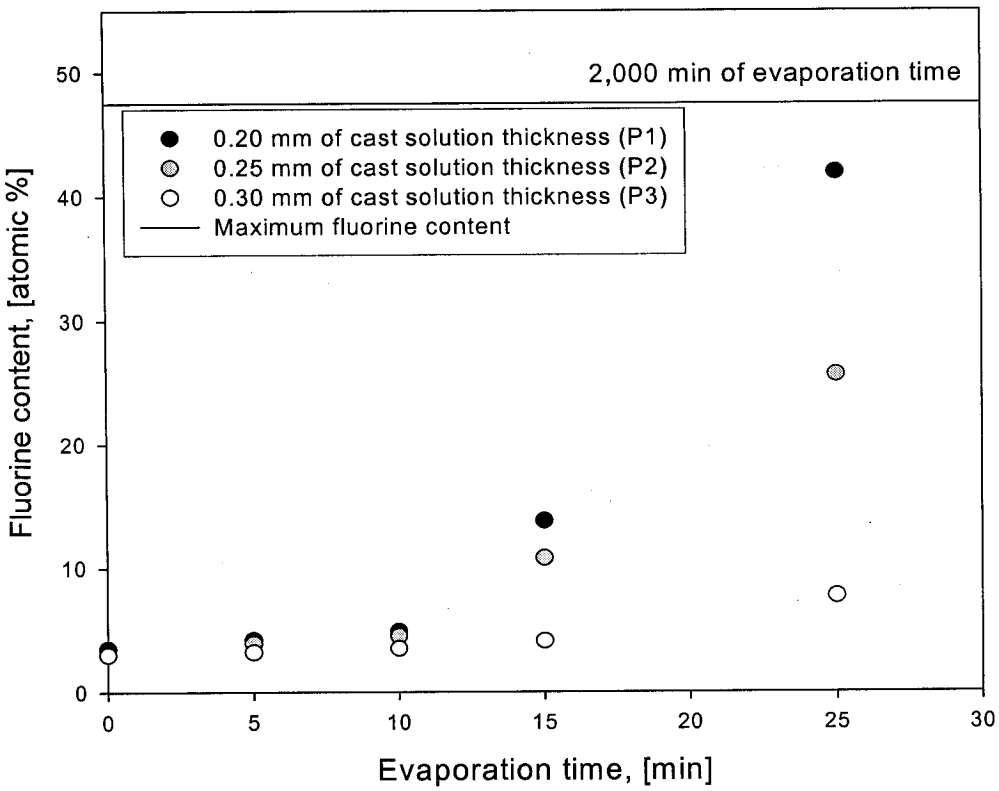

Figure 6.3 Fluorine content as functions of evaporation time and casting film thickness

6.4 Study on the tSMM2 migration using the Kinetic model in Chapter 5

Based on the fluorine content data in Figure 6.3 and the Equation 5.11, the parameter β was obtained for each cast film thickness by nonlinear regression analysis. β vs. thickness was then plotted and an exponential decay regression was attempted, as it was done in Chapter 5. The solid line in Figure 6.4 represents the regression line so obtained. Then, using the β values on the simulation line, fluorine contents were back-calculated by Equation 5.11 for each cast solution thickness as a function of evaporation time. In Figure 6.5, the experimental and the back-calculated fluorine contents are compared. The agreement of calculated and experimental data is excellent. Therefore, it was proved that if the relationship between the β and the cast solution thickness is provided for any tSMM blended membrane system, the tSMM migration can be precisely determined by the kinetic model derived in Chapter 5.

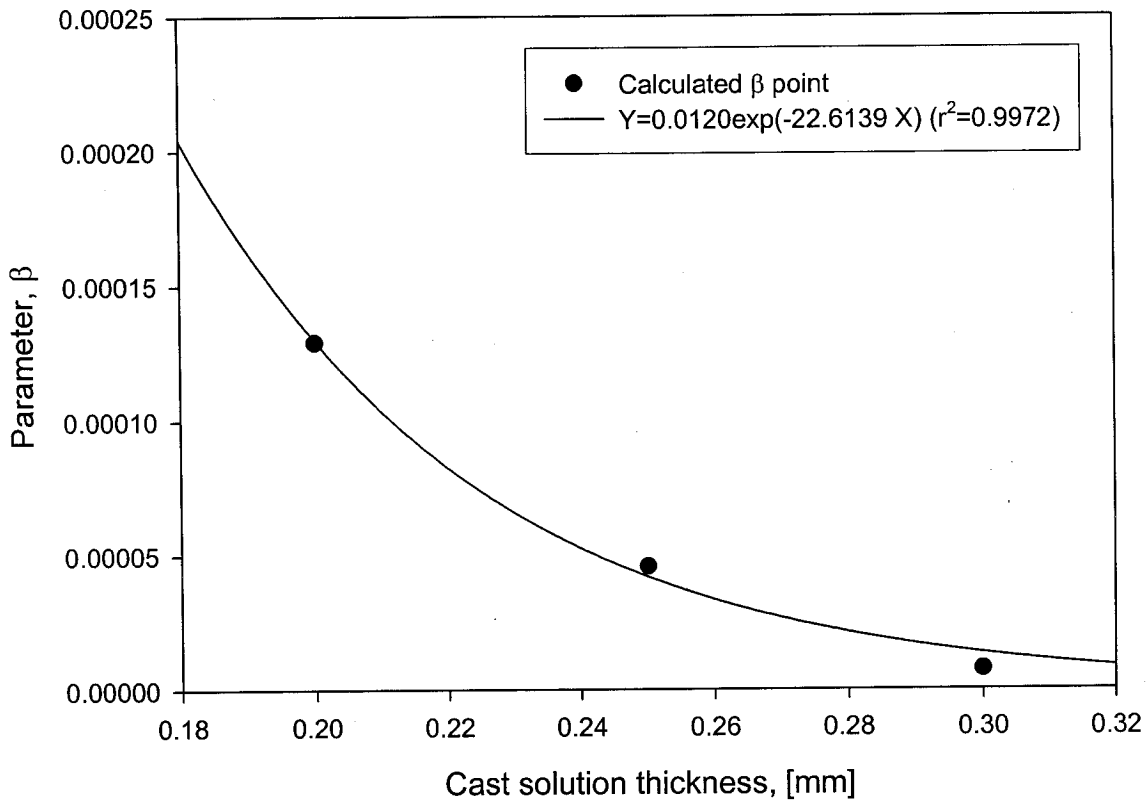

Figure 6.4 Relationship between β and the cast solution thickness in 'P series' membranes

Based on data in Figure 6.5, the initial lag time and the minimum evaporation time which were defined in Section 5.2 for each membrane series were determined and the results listed in Table 6.4.

Table 6.4 Initial lag time and minimum evaporation time of P1, P2 and P3 series membranes

Membrane Code	Initial lag time (t_{lag}) [min]	Minimum evaporation time (t_{min}) [min]
P1	4.3	36
P2	6.1	52
P3	9.0	77

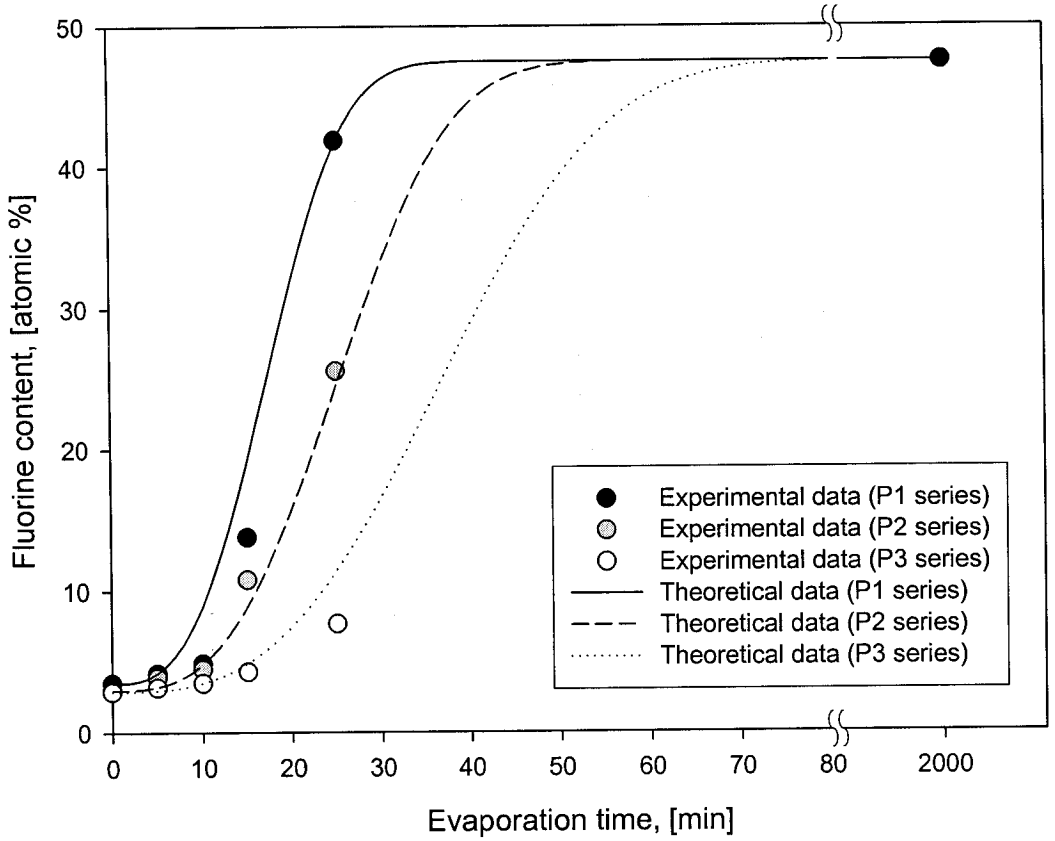

Figure 6.5 Comparison of experimental XPS values with the results from theoretical calculations (P series)

6.5 Study on the Potential of PES Membranes with tSMM2 for MD Process

Liquid Entry Pressure of water (LEP_w), which is the pressure that must be applied onto pure water before it penetrates into dried membrane pores, was measured. This pressure depends on the pore size and the hydrophobicity of the membrane. The results are shown in Figure 6.6. LEP_w increased with an increase in evaporation time. In particularly, a high LEP_w value of 552 kPa (80 psi) was reached, indicating that membranes for membrane distillation can be produced from PES membrane by blending tSMM2.

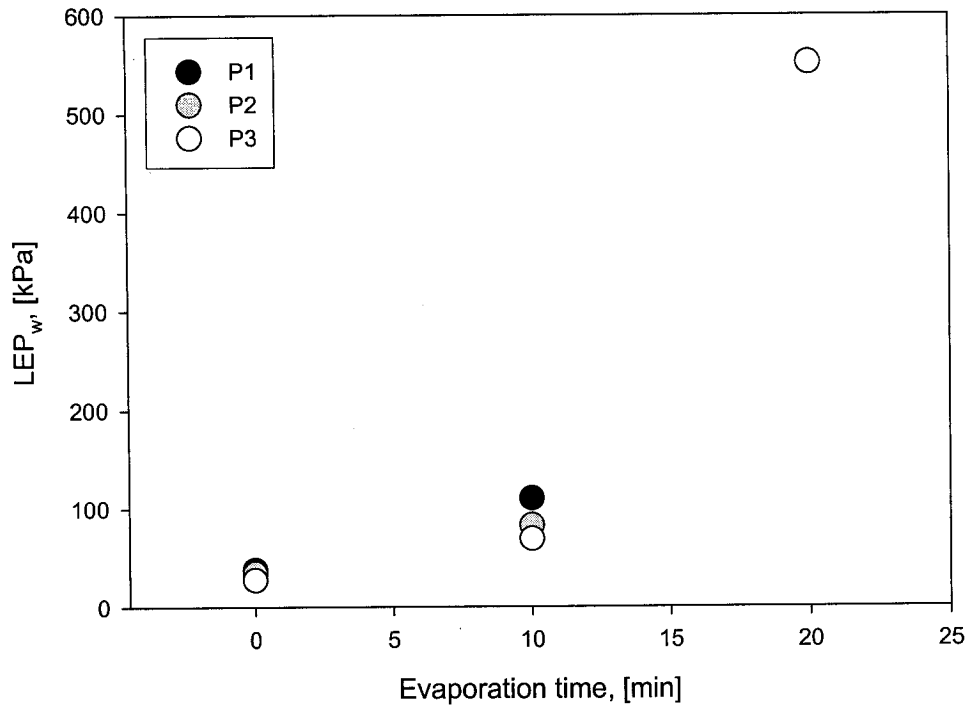

Figure 6.6 Water Entry Pressure as functions of evaporation time and casting film thickness

6.6 Summary of Chapter 6 (Part 3)

1. As evidenced by contact angle and XPS analysis with tSMM2 blended PES membranes, Conclusion 3 of Chapter 4 was confirmed, although less fluorine content was detected by the elemental analysis in tSMM2 than in tSMM1.
2. The kinetic model was applied to the data from XPS experiments for tSMM2 blended PES membranes. It was found that the relationship between the parameter β and the cast solution film thickness could be well described by an exponential decay regression.
3. Liquid entry pressure (LEP_w) increased with an increase in evaporation time, which indicated that membranes for membrane distillation (MD) could be produced from PES membrane by blending tSMM.

7. Results and Discussion (Part 4): Synthesis of nSMM and Effects of nSMM on the Properties of PES Membranes

From the previous experiments, it was found that relatively long evaporation periods (>10 min) and a high temperature (110°C) were required for the surface migration of tSMM (traditional SMM) in the casting solution of PES. In general, if a long evaporation period is applied during the preparation of a membrane, the pore size will decrease and the surface hydrophobicity of the membrane will increase. Hence, the requirement of a long evaporation period for SMM surface migration will be in conflict with the preparation of hydrophobic ultra/microfiltration membranes (with surfaces of high hydrophobicity and large size pores), which are desired in this work. Therefore, the development of a new SMM was attempted to lower the migration period and the temperature at which migration occurs. A new SMM, designated as nSMM, was designed, synthesized and tested. A set of nSMM blended PES membranes were also prepared under different conditions and tested.

The nSMM was developed based on the chemical structure similar to tSMM. However, to increase the migration speed, PDMS component was incorporated in its chemical structure instead of PPO in tSMM (Figure 3.3). The nSMM was designed to have even lower surface energy and therefore to be more hydrophobic than tSMM.

Throughout this study, the nSMM was synthesized twice. Using the first batch of nSMM (nSMM1), some preliminary experiments were carried out to characterize nSMM and to know the effects of nSMM blending on PES membrane performance. Based on the results, further detailed experiments were carried out with the second batch of nSMM (nSMM2) to know if nSMM blended PES membranes have a potential to be used for membrane distillation. Moreover, some experiments were conducted to know the effect of nSMM blending on PES membrane performance in ultrafiltration. Some membranes suitable for membranes distillation, especially for vacuum membrane distillation (VMD), were obtained.

7.1 Molecular Weight Distribution of nSMM

Two batches of nSMM prepared under identical condition were characterized by GPC using polystyrene standard. The results are summarized in Table 7.1, in which GPC data for tSMM obtained in the earlier work (see Table 6.2) are shown as well. Both number and weight average molecular weight of the two nSMM batches were larger than those of the tSMM. Although the number average molecular weights of the nSMMs from the different batches are similar, the weight average molecular weight of the second batch is almost twice as large as that of the first sample, resulting in a twice as large polydispersity. The synthesis of nSMM is not yet fully under control and more careful preparation procedure will be needed in the future.

7.2 Elemental Analysis of nSMM

As shown in Figure 3.3, nSMM contains carbon (C), oxygen (O), hydrogen (H), nitrogen (N), fluorine (F) and silicon (Si). The experimental and theoretical data for weight percentages are listed in Table 7.2. The experimental data were achieved by elemental analysis for nSMM2 and the theoretical data were calculated based on the molecular weight of MDI, PDMS and Zonyl BA-L. More specifically, m, y and q in Figure 3.3 were set as 6, 9 and 2, respectively. Experimental and the theoretical values agreed reasonably well for each atom except for carbon and fluorine.

Table 7.1 Molecular weights obtained from GPC for two samples of nSMM

Type of SMM	M_n	M_w	Polydispersity*
tSMM1	20,000	25,000	1.30
tSMM2	14,600	22,600	1.55
nSMM1 (batch #1)	15,000	31,500	1.98
nSMM2 (batch #2)	16,000	62,100	3.8

* Polydispersity = M_w/M_n

Table 7.2 Experimental and theoretical weight percentages in nSMM2

Content	Experimental (wt%)	Theoretical (wt%)
Carbon (C)	44.33	32.07
Oxygen (O)	17.76	16.63
Hydrogen (H)	6.72	6.98
Nitrogen (N)	4.82	5.20
Fluorine (F)	10.10	18.34
Silicon (Si)	16.27	20.78

7.3 Contact Angle Measurements for nSMM1 blended PES membranes

An nSMM1 film was prepared and its contact angle was measured before contact angle measurements for nSMM1 blended PES membranes. The contact angle of nSMM1 was featured by its very high advancing contact angle of 125°. Since the contact angle of PES is about 67° (see Table 4.1), the contact angles of blended PES membranes are expected to be between the above two values. In fact, the measured contact angles were higher than that of PES and lower than that of nSMM1 without exception. However, the contact angle changed depending on the condition of membrane preparation.

The nSMM1 blended PES membranes were tested by contact angle measurement for the nSMM migration study. The conditions of the membrane preparation are listed in Table 7.3. As shown in the Table, the effects of nSMM1 on the contact angle of PES membranes were studied by changing PES concentration, evaporation time, and evaporation temperature. As mentioned in Section 3.7, the contact angles measured in this study were all advancing contact angles.

Table 7.3 Preparation conditions of the membranes used for contact angle measurements

Membrane code	Casting solution composition (by weight)	Evap. Temp. [°C]	Evap. Time [min]	Cast solution thickness [mm]
N1	PES:nSMM1:NMP = 15:1.5:83.5	RT	0	0.25
N2	PES:nSMM1:NMP = 18:1.5:80.5	RT	0	0.25
N3	PES:nSMM1:NMP = 21:1.5:77.5	RT	0	0.25
N4	PES:nSMM1:NMP = 18:1.5:80.5	RT	4	0.25
N5	PES:nSMM1:NMP = 18:1.5:80.5	RT	8	0.25
N6	PES:nSMM1:NMP = 18:1.5:80.5	RT	12	0.25
N7	PES:nSMM1:NMP = 15:0.9:84.1	RT	0	0.25
N8	PES:nSMM1:NMP = 15:0.9:84.1	110	4	0.25
N9	PES:nSMM1:NMP = 15:0.9:84.1	110	8	0.25
N10	PES:nSMM1:NMP = 15:0.9:84.1	110	12	0.25

Figure 7.1 shows the effect of PES concentration in the film casting solution, while maintaining the nSMM1 concentration at 1.5 wt%, on the contact angle (N1-N3). The polymer solution film was immersed into water immediately after casting. Hence, it was considered that the evaporation period was zero. Interestingly, the contact angles were considerably above that of PES film in all cases. In other words, the contact angle immediately responded to the presence of nSMM1. This was natural since some nSMM molecules were present at the membrane surface from the very beginning and there seemed to be an immediate conformational rearrangement - facing of the fluorine end groups to the air-surface interface - even before the nSMM1 migration took place. The reason for the immediate response of nSMM1, which did not occur for tSMM, could also be found in higher hydrophobicity of nSMM1, less miscibility between PES and nSMM and their synergetic affects to nSMM's migration speed. The casting solution prepared with nSMM was milky while the solution with tSMM was transparent. Therefore, the phase separation in the casting solution could have affected the migration process of nSMM. Even though the evaporation period was designated as zero, there was few seconds of time interval between casting and immersion. It could then be suspected that during this time period some migration already occurred. Detailed explanation for the conformational rearrangement will be given below. The contact angle decreased however as the PES concentration in the polymer dope increased.

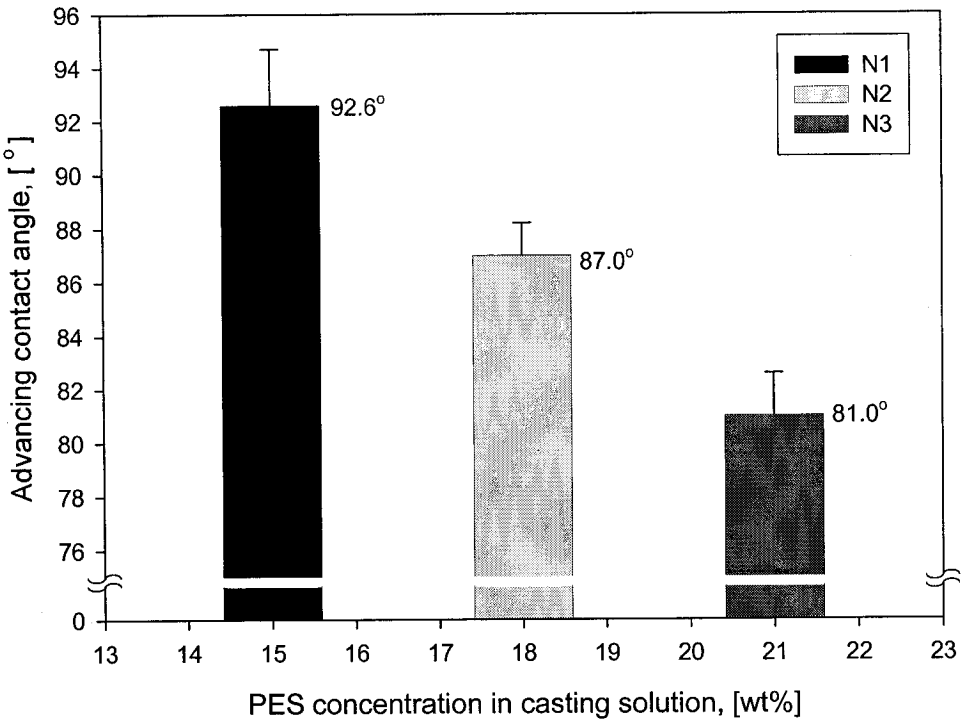

Figure 7.1 PES concentration versus contact angle at evaporation time of zero

Figure 7.2 shows the effect of evaporation time on the contact angle (N2, N4-N6). The dope composition was PES/nSMM1/NMP (18/1.5/80.5). The polymer solution film cast on a glass plate was kept at room temperature before immersion into water. Figure 7.2 shows that the contact angle increased as the evaporation time increased. This indicates that a certain amount of time is required to develop the nSMM's capacity to increase the contact angle fully, when the cast film is kept at room temperature.

It should be noted that, unlike tSMM, surface migration of nSMM1 took place at room temperature. The difference between tSMM and nSMM came from their molecular structures as discussed later.

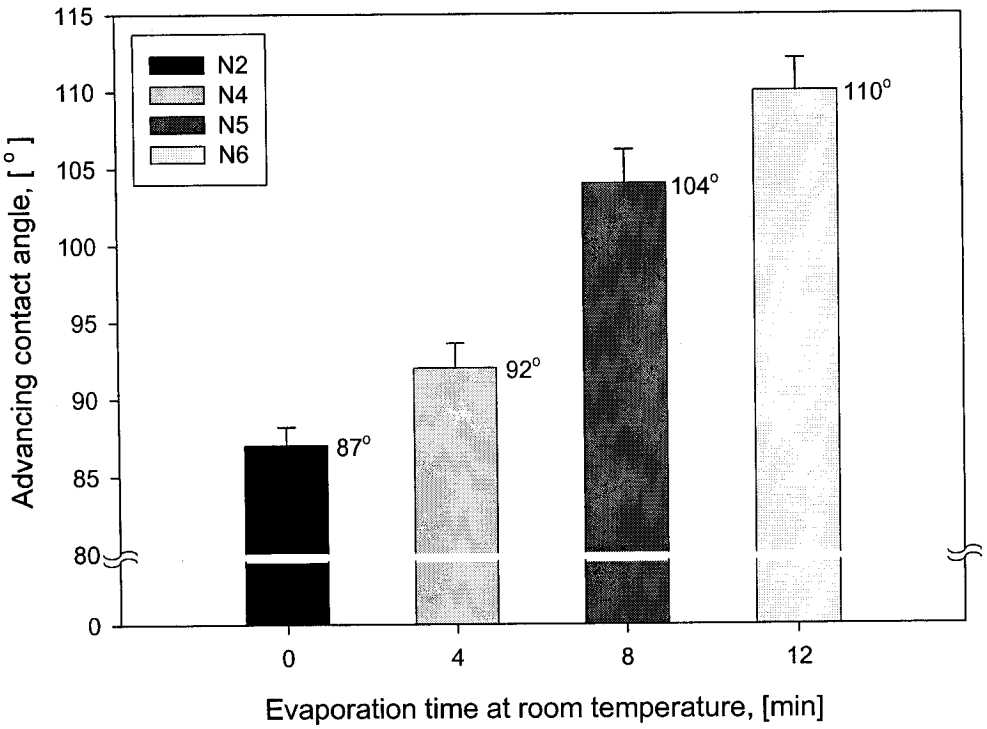

Figure 7.2 Contact angle versus evaporation time at room temperature

Figure 7.3 also shows the effect of evaporation time on the contact angle at 110°C evaporation temperature (N7-N10). The polymer dope composition was PES/nSMM1/NMP (15/0.9/84.1). The polymer solution was kept in the oven at 110°C before it was immersed into water. The membrane surface showed a high contact angle even after a short evaporation period and then gradually decreased as the evaporation time increased. All these data can be interpreted in the following way. Looking into the structure of nSMM, the macromolecule consists of a hard segment originating from methylene bis-p-phenyl diisocyanate (MDI), a soft segment originating from α,ω-aminopropyl (polydimethyl siloxane) (PDMS) and two fluorohydrocarbon chains in both ends of the prepolymer originating from Zonyl BA-L. MDI and PDMS form a polyurethane-urea (PUU) chain (Part A in Figure 3.3) that is end-capped by two fluorhydrocarbon chains (Part B in Figure 3.3). It should be noted that the soft segment of the earlier tSMM was polypropylene oxide,

which was replaced by a more hydrophobic α,ω-aminopropyl (polydimethyl siloxane) in nSMM. Hence, the polyurethane-urea chain (Part A) is also hydrophobic. It is difficult to assess the hydrophobicity of Part A alone, but it may be represented by the contact angle of PDMS, which is 110° (Owens and Wendt, 1969). It is also known that the contact angle of MDI-PDMS polyurethane-urea polymer with 1,4-butanediol (BD), the structure of which is similar to nSMM, is 93° (Park, 2002). Part B is fluorohydrocan chain and is also very hydrophobic. It would be reasonable to represent Part B's contact angle by that of polytetrafuoroethylene (Teflon), which is 116°. Briefly both Part A and Part B are hydrophobic but Part B is more hydrophobic than Part A. In the earlier tSMM, Part B was exposed to air at the air/polymer solution interface and part A was buried in the solution since Part A was hydrophilic. In the new nSMM both Part A and Part B are hydrophobic and allowed to be exposed to air. But Part B is more hydrophobic than Part A and, as a result, tends to be more readily exposed to air than part A.

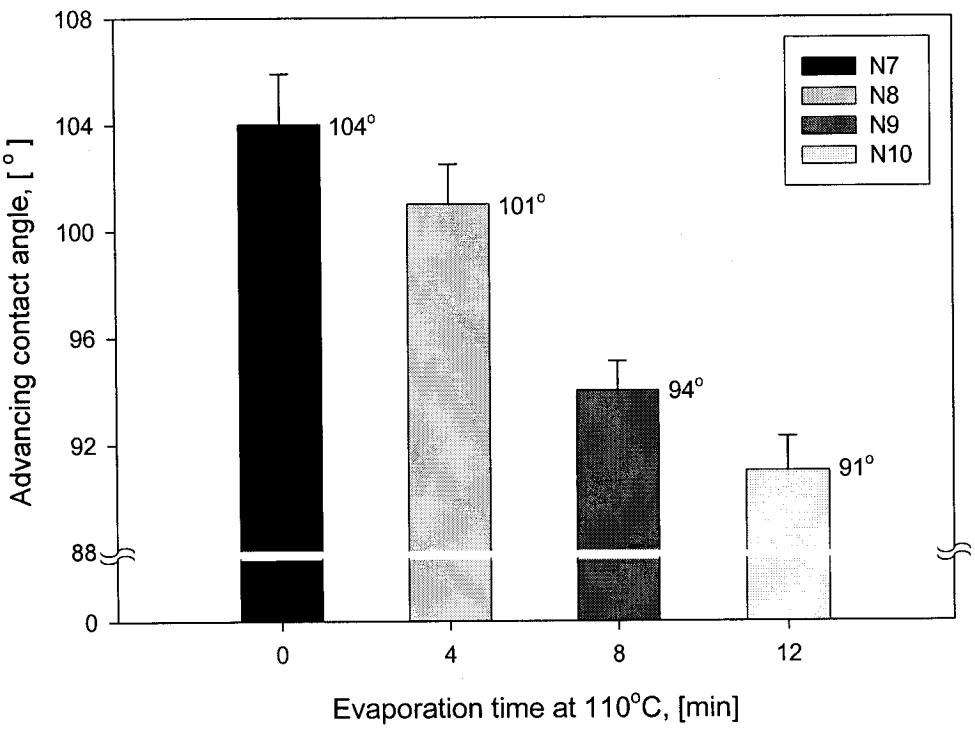

Figure 7.3 Contact angle vs. evaporation time at 110°C

It is postulated that there are two steps for the surface coverage with nSMM. The first is nSMM migration to the surface and the second is conformational rearrangement of nSMM at the surface, by which Part B of nSMM is oriented perpendicular to the polymer solution/air interface, leading to exposure of Part B to the air. Both are kinetic processes that require certain time periods for completion. Both processes occur simultaneously. It seems reasonable to assume that the surface migration is slower than the conformational rearrangement.

The hydrophobicity of Part A and Part B, the times required for the completion of surface migration and conformational re-arrangement all have to be taken into account to understand the experimental results from the contact angle measurement.

At room temperature, nSMM migration to the surface is very slow, therefore the increase in contact angle with evaporation time as observed in Figure 7.2 is a result of the gradual conformational rearrangement through which Part B of nSMMs is oriented perpendicular to the interface. It should be noted that a certain amount of nSMM is present at the surface even before migration starts to occur. The more the fluorohydrocarbon is oriented perpendicularly, the higher becomes the contact angle. The conformational re-arrangement of nSMM is also viscosity dependent and slows down as the viscosity of the solution increases. Hence, the contact angle becomes smaller as the PES concentration in the polymer solution increases (Figure 7.1).

When the temperature is 110°C, the conformational change occurs during a short time period. Hence, we could observe a high contact angle after a very short evaporation period. This is then followed by nSMM migration. When the concentration of nSMM increases at the air/polymer solution interface, not only Part B but also Part A of nSMMs will be exposed to the air. As the migration progresses, the contact angle gradually decreases, since the hydrophobicity of Part A is lower than that of Part B. This is observed in Figure 7.3

7.4 XPS Tests for nSMM1 Blended PES Membranes

The above interpretation given for the results of the contact angle measurement is further supported by the XPS results. Figures 7.4 and 7.6 show the change in atomic composition at the membrane surface. During the XPS tests the take-off angle was kept at 0°, corresponding to the X-ray sampling depth of 6.3 nm. The membranes used in Figure 7.4 were N2, N4-N6 and the membranes used in Figure 7.6 were N7-N10 in Table 7.3; the solution films for N2, N4-N6 were not placed in the oven after casting, while those for N7-N10 were. Figures 7.4 and 7.6 both show that fluorine atom (Fl) was present at the surface after a very short evaporation period (few seconds) and increased further with an increase in evaporation period. However, compared to the results in Figure 7.4, the change was very little in Figure 7.6. The concentrations of silicon (Si), on the other hand, changed differently with evaporation time. In the case of Figure 7.4, the change in the silicon concentration was far less than the change in the fluorine concentration. Considering that the fluorine content represents the presence of Part B while the silicone content represents the presence of Part A of the nSMM at the surface, the above results indicate that conformational change by which the Part A is exposed to the air dominates the process. Sulfur, which could come only from PES, was not detected, indicating that the surface was fully covered with nSMM. On the other hand, in Figure 7.6 the concentration of silicon was small in the beginning, but increased significantly with evaporation time and almost doubled at the evaporation time of 12 min. The change in fluorine concentration was not as much as that of silicone. These results are understandable by assuming that the presence of fluorine at the surface was due to the conformational change of nSMM that occurred in the very initial stage, which was followed by slower surface migration. As the surface migration of nSMM progresses, more of the Part A of the macromolecule comes to the surface and hence the silicon concentration increases. In Figure 7.6 sulfur was detected and its concentration decreased with evaporation time. This is due to the increase of both fluorine and silicon concentrations at the surface. Increase in the fluorine content by increasing the evaporation time for N2, N4-N6 was also observed clearly in Figure 7.5.

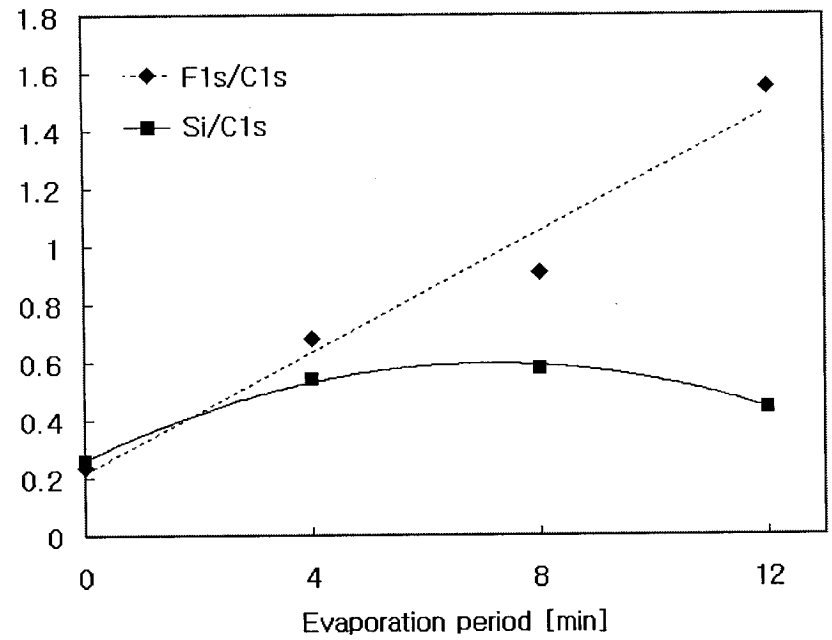

Figure 7.4 Effect of evaporation time on the surface atomic compositions of F_{1s} and Si_{2p} (N2, N4, N5 and N6)

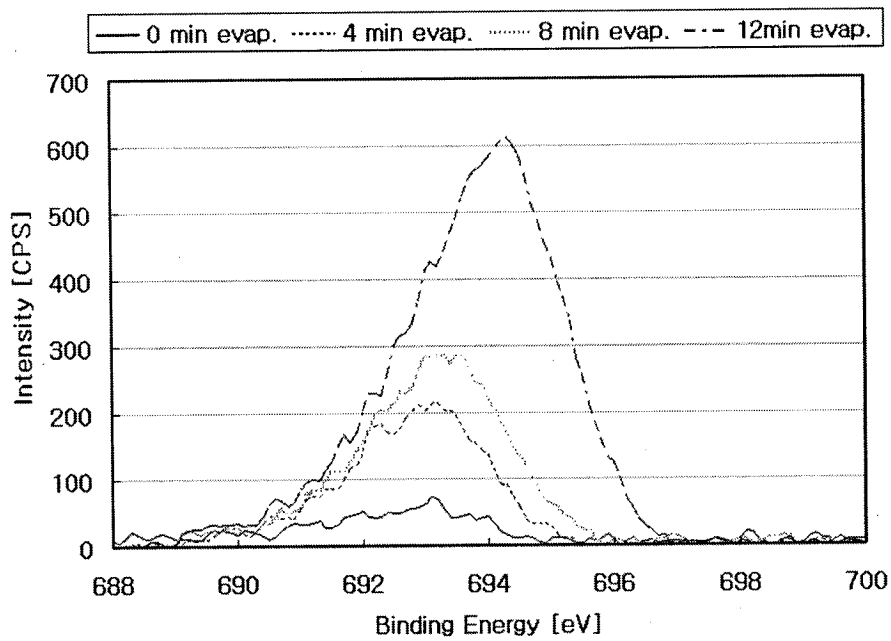

Figure 7.5 Fitted F_{1s} XPS spectra for the membranes shown in Figure 7.4 with different evaporation time (N2, N4, N5 and N6)

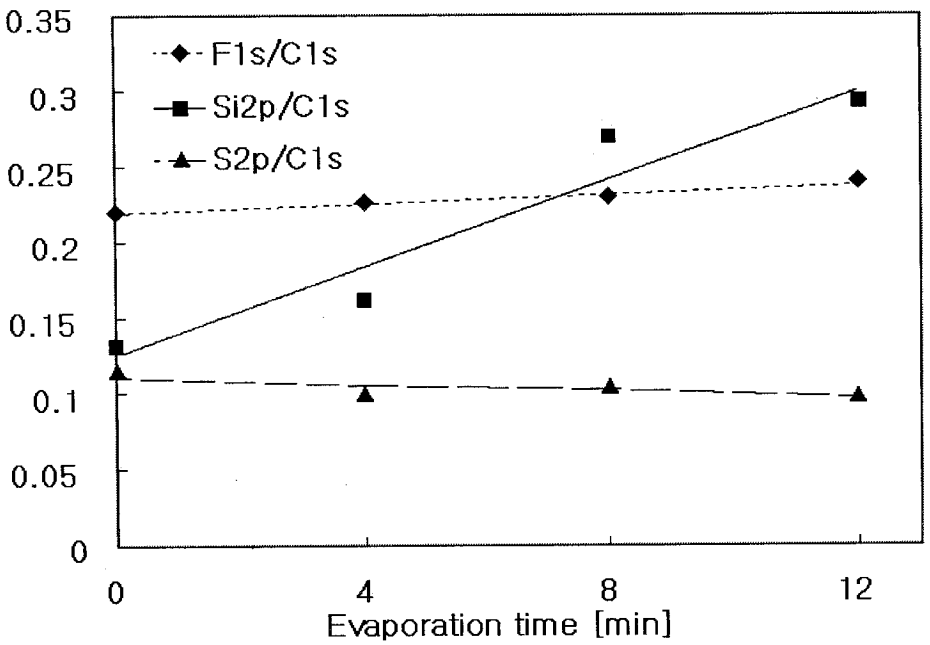

Figure 7.6 Effect of evaporation time on the surface atomic compositions of F, Si, and S (N7, N8, N9 and N10)

Membrane N1 was chosen for analysis of the top side and the bottom side surface by XPS. Remember that a contact angle of 92.6° was obtained for the N1 membrane (see Figure 7.1). Figure 7.7 and Figure 7.8 show the XPS spectra for the top side and bottom side surface, respectively. From both figures, differences between the top and the bottom side can be clearly seen. First, in the top surface region, silicone (Si2p and Si2s) was detected, while sulfur (S2p, S2s) was absent. On the other hand, at the bottom surface, the opposite was observed. As for nitrogen (N1s) and fluorine (F1s), they were detected on both surfaces, but the intensities at the top surface were more than at the bottom surface. These observations indicate that the nSMM1 migration occurred more toward the top surface.

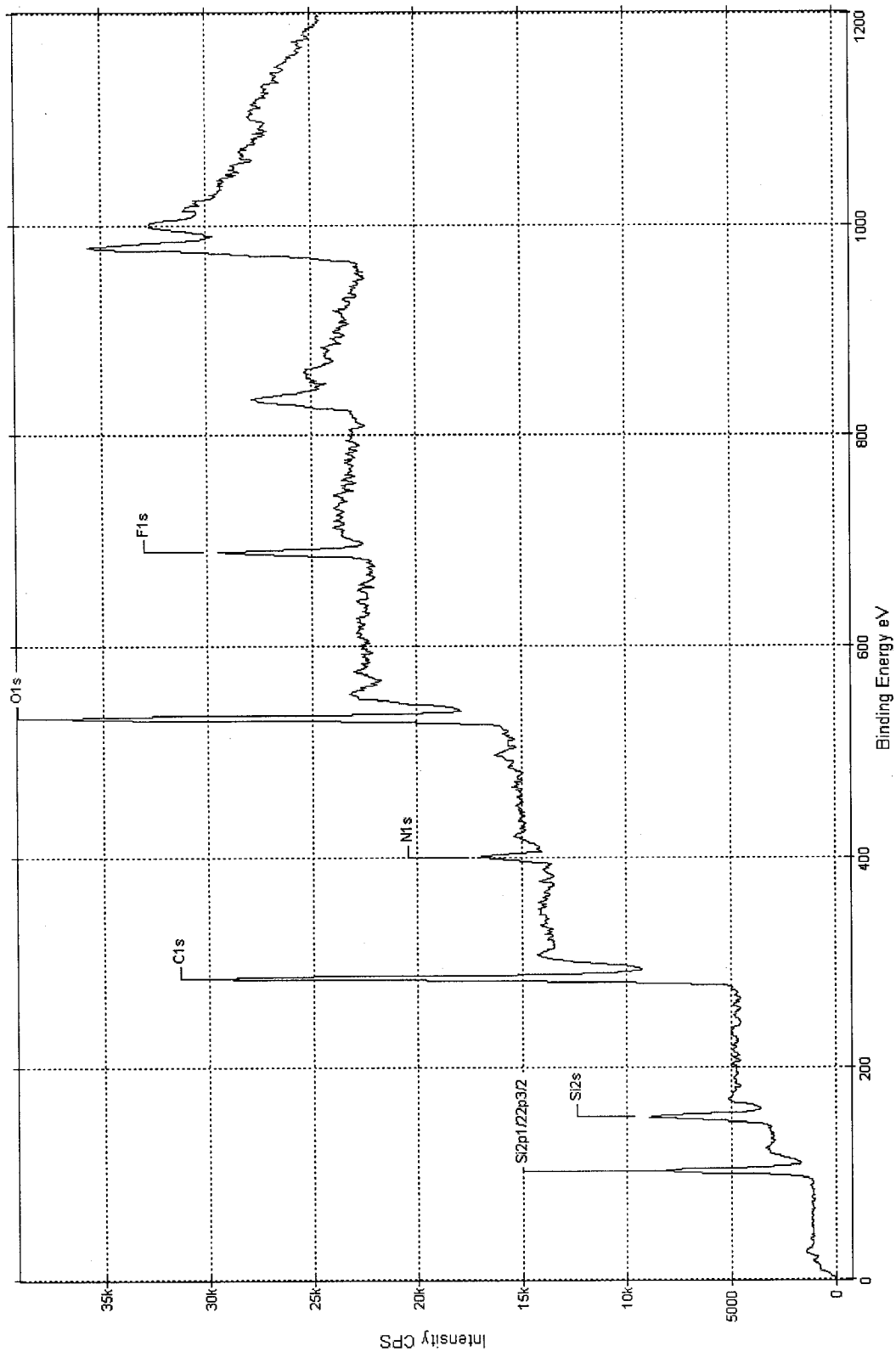

Figure 7.7 Intensity vs. Binding Energy for top surface side of nSMM1 blended PES membrane (N1)

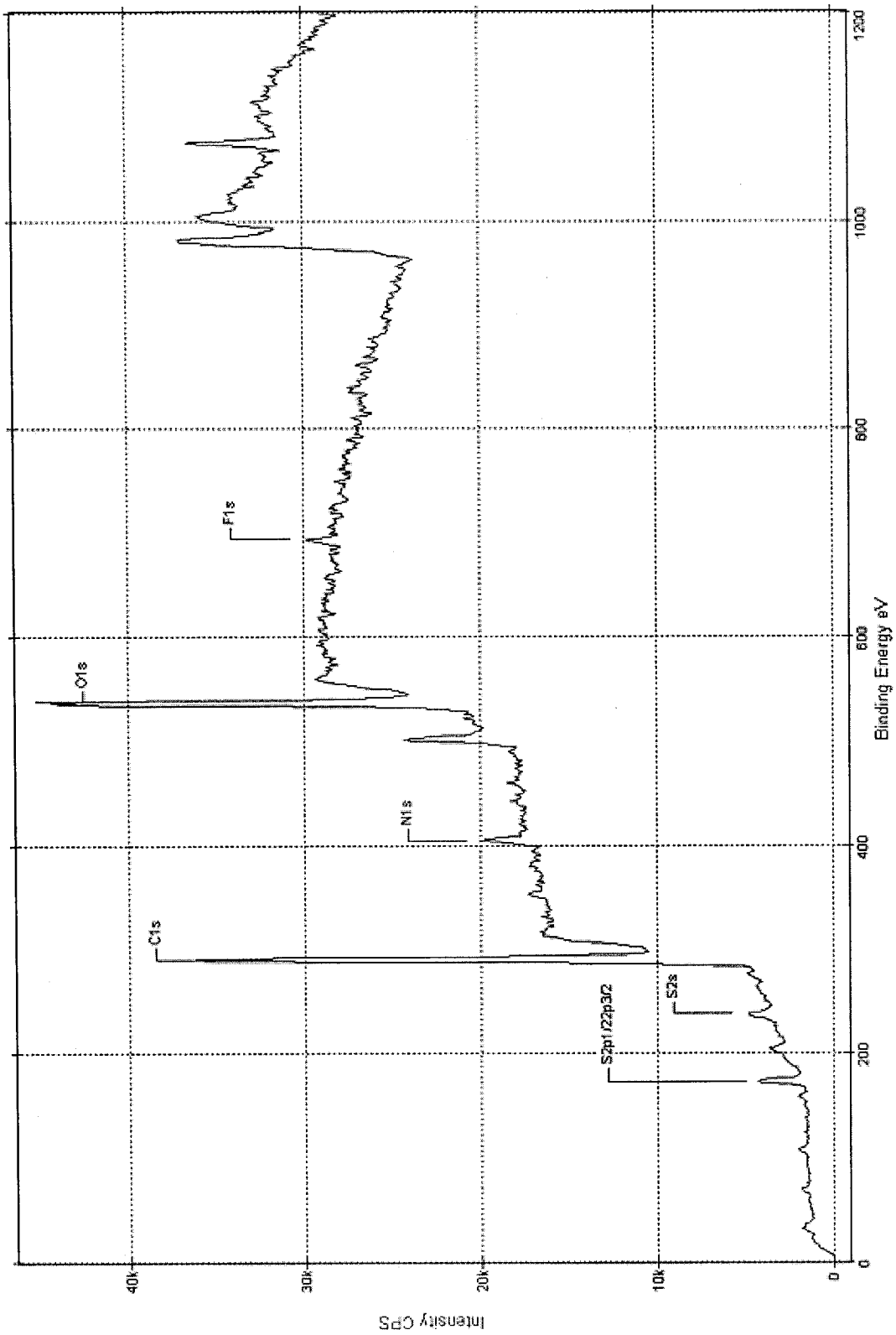

Figure 7.8 Intensity vs. Binding Energy for bottom side of nSMM1 blended PES membrane (N1)

7.5 Contact Angle Measurements for nSMM2 Blended PES Membranes

Contact angles were measured also for membranes prepared by blending the nSMM2 sample. The membranes used in this study are listed in Table 7.4. As shown in Table 7.4, in preparation of these membranes PES concentrations were changed from 15 to 18 wt%, while nSMM2 concentration was maintained at 1.5 wt%, the balance being NMP solvent. The membranes were kept at room temperature for a predetermined period for the migration of nSMM2. The results are summarized in Table 7.5. The data were considerably different from those for nSMM1 sample reported in Figures 7.1 and 7.2 but the trend was similar; i.e. advancing contact angle decreased with an increase in PES concentration (A1, A2 and A3) and increased with an increase in evaporation time (A4 and A2). The only exception is PES concentration of 15 wt% that showed a lower advancing contact angle than those for 17 and 18 wt% (see Table 7.5). This exception and the differences between nSMM1 and nSMM2 samples in their contact angle values are probably due to the higher polydispersity of the nSMM2 sample.

Table 7.4 Preparation conditions of the membranes used for contact angle measurements

Membrane code	Casting solution composition (by weight)	Evap. Temp. [°C]	Evap. Time [min]	Cast solution thickness [mm]
A1	PES:nSMM2:NMP = 15:1.5:83.5	RT	4	0.25
A2	PES:nSMM2:NMP = 17:1.5:81.5	RT	4	0.25
A3	PES:nSMM2:NMP = 18:1.5:80.5	RT	4	0.25
A4	PES:nSMM2:NMP = 17:1.5:81.5	RT	0	0.25

Table 7.5 Effect of polymer concentration and evaporation time on advancing contact angle

Memdbrane	A1	A2	A3	A4
PES concentration, [wt%]	15	17	18	17
Evaporation time, [min]	4	4	4	0
Adv. contact angle (degree)	94	100	97	90

7.6 Morphology of nSMM1 Blended PES Membranes Using FE-SEM

Typical cross sectional pictures for nSMM1 blended PES membranes are given in Figure 7.9. These pictures were taken for the membranes prepared from polymer dopes whose compositions were PES/nSMM1/NMP: (a) 15/1.5/83.5 (N1), (b) 18/1.5/80.5 (N2), and (c) 21/1.5/77.5 (N3) by weight. In all cases, a top skin layer supported by a finger-like porous sublayer was observed. No distinctive surface layer resulting from the nSMM migration to the surface of membrane was observed. Similar pictures were taken for other nSMM1 blended membranes.

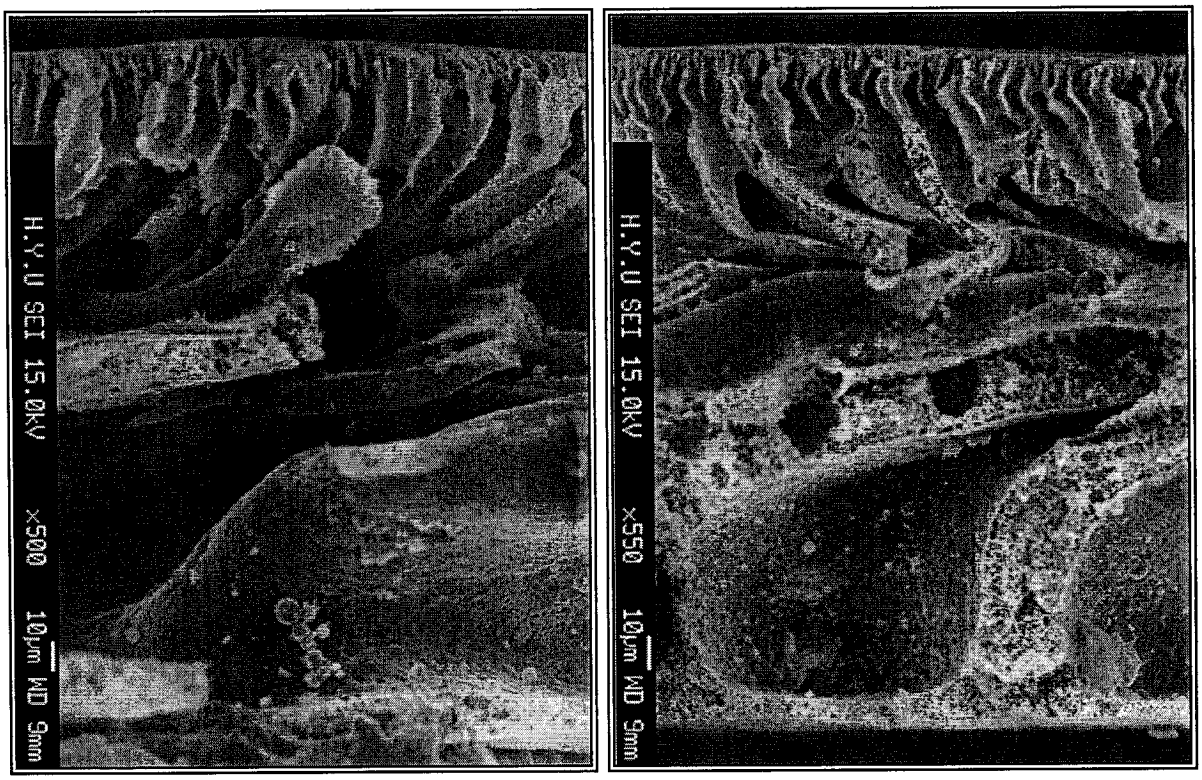

(a) (b)

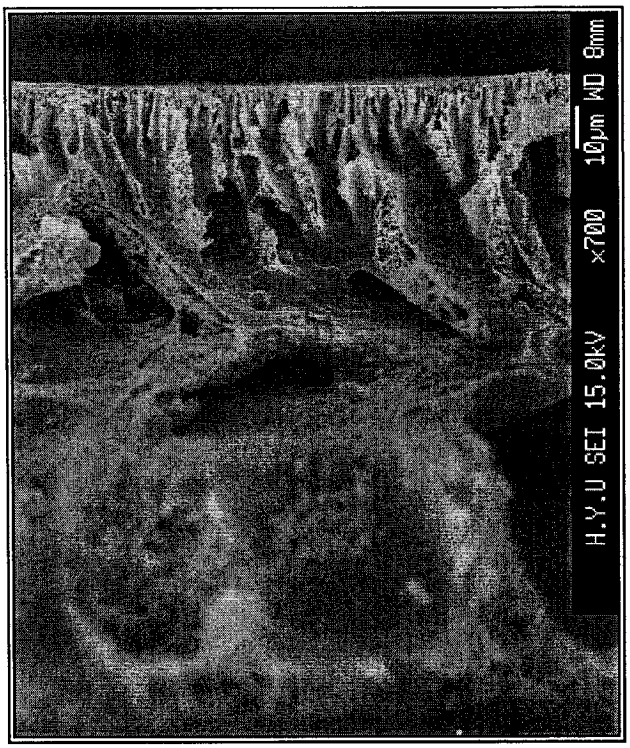

(c)

Figure 7.9 SEM pictures for PES membranes (1.5 wt% of nSMM1 in casting solution and 0 minute evaporation time) with different PES concentration in casting solution: (a) 15 wt% (N1), (b) 18 wt% (N2), (c) 21 wt% (N3)

7.7 Pure Water Permeation Analysis for nSMM2 Blended PES Membranes

Typical water flow rate versus pressure data are shown in Figure 7.10 for a membrane made from a dope whose composition is PES/nSMM2/NMP (17/1.5/81.5 by weight) (A2). The evaporation time was 4 min at room temperature. Similar data were obtained for other membranes. From Figure 7.10 a liquid entry pressure of water (LEP_w) is found to be 207.0 kPa (30 psi). LEP_w for other membranes are summarized in Table 7.6. Comparing Tables 7.3 and 7.4 and Tables 7.5 and 7.6, the parallel relationship between the advancing contact angle and LEP_w data is obvious; i.e. LEP_w increases as contact angle increases. LEP_w data are an important factor to decide if a membrane is potentially useful for the purpose of membrane distillation. However, higher LEP_w of a membrane does not always mean that

the membrane is more suitable for membrane distillation process. In particular, a large number of non-wettable pores are required for membrane distillation processes to achieve a high membrane flux.

Table 7.6 Effect of polymer concentration and evaporation time on LEP_w

Memdbrane	A1	A2	A3	A4
PES concentration, [wt%]	15	17	18	17
Evaporation time, [min]	4	4	4	0
LEP_w (kPa)	27.6	207.0	110.4	13.8

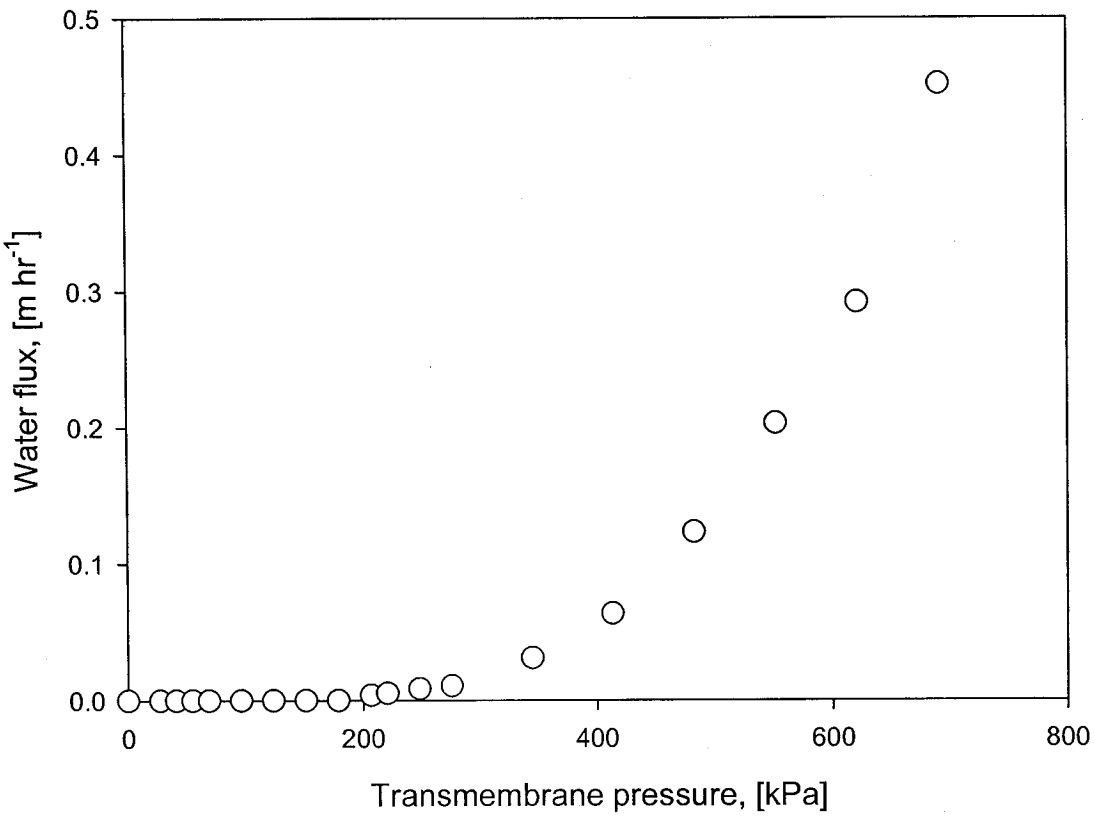

Figure 7.10 Pure water permeation flux versus pressure for A2 membrane

7.8 Ultrafiltration Tests for nSMM2 Blended PES Membranes

According to the experimental results given in the earlier part of this chapter, it was found that the newly developed nSMM was more suitable than tSMM to be used in SMM blended membranes for the purpose of membrane distillation, since high surface hydrophobicity could be achieved under relatively mild conditions such as lower evaporation temperature and shorter evaporation period with nSMM. As defined earlier in Chapter 3, the evaporation temperature is the temperature of an environment at which solvent evaporation took place from the casting dope. Even when the solvent evaporation was only marginal when the environment was kept at room temperature, it was called evaporation temperature. Similarly, the evaporation period is defined as a period between the time of film casting on a glass plate and the time of immersing the cast film together with the glass plate into gelation media, water, as stated in the experimental section (Chapter 3). It is supposed that solvent evaporation took place during this period, however little it might be.

Given the fact that the performance of membranes for membrane distillation is governed by the hydrophobicity and the pore structure at the membrane surface, the membrane pore size and its distribution are considered as one of the most important information in membrane characterization. Hence, the pore size and the pore size distribution of nSMM blended PES membranes were determined by the ultrafiltration method. The second batch of nSMM, i.e. nSMM2 was used throughout this study. The experimental method and the theory involved in the analysis of the ultrafiltration data are given in the earlier part of the thesis. Eleven membranes were prepared under different conditions as shown in Table 7.7. The membranes used in this study were kept in water until they were subjected to ultrafiltration experiments.

Table 7.7 Membrane preparation conditions for ultrafiltration experiments

Membrane	Casting solution composition (by weight)	Evap. Temp. [°C]	Evap. Time [min]	Gel. Temp. [°C]
U1	PES:PVP:NMP = 15:7:78	RT	0	4
U2	PES:PVP:NMP = 17:7:76	RT	0	4
U3	PES:nSMM2:PVP:NMP = 15:1.5:7:76.5	RT	0	4
U4	PES:nSMM2:PVP:NMP = 17:1.5:7:74.5	RT	0	4
U5	PES:nSMM2:PVP:NMP = 15:1.5:7:76.5	RT	4	4
U6	PES:NMP = 15:85	RT	4	4
U7	PES:nSMM2:NMP = 15:1.5:83.5	RT	4	4
U8	PES:nSMM2:NMP = 17:1.5:81.5	RT	4	4
U9	PES:NMP = 17:83	RT	4	4
U10	PES:nSMM2:NMP = 15:1.5:83.5	RT	4	18
U11	PES:nSMM2:NMP = 15:1.5:83.5	RT	4	40

In the table, compositions of the casting dopes, evaporation temperature, evaporation period and gelation media temperature are listed.

According to the method described earlier, pore sizes and their distributions of the membranes were calculated from the ultrafiltration data with polyethylene glycol (PEG) and polyethylene oxide (PEO) solutions of various molecular weights. PEG and PEO did not affect significantly the pore structure as the permeation flux of the membrane with these solutes, when present in the feed, was very close to the pure water permeation flux. The percent separation of the PEG/PEO solutes on the ordinate vs. their Stokes diameters on the abscissa of a log-normal probability plot is depicted in Figure 7.11. Based on these plots, a straight line relationship could be established for each membrane with a reasonably high correlation factor ($\geq$0.9 in most cases) by applying linear regression analysis.

The values of the geometric mean pore size (μ_p) and the geometric standard deviation (σ_p) around the mean were determined from Figure 7.11, as described in the theoretical section, and the results summarized in Table 7.8.

Table 7.8 Geometric mean pore size (μ_p) and geometric standard deviation (σ_p) for various membranes calculated from separation data

Membrane	Mean Pore Size, μ_P [nm]	Geometric Std. Dev., σ_p
U1	4.96	2.94
U2	2.44	3.10
U3	6.20	3.44
U4	6.44	2.80
U5	65.00	9.31
U6	11.50	1.86
U7	41.40	2.77
U8	57.50	11.55
U9	8.40	2.11
U10	43.30	2.93
U11	61.50	3.51

From the above table, the following important relationships between the membrane preparation conditions and the mean pore sizes can be established:

Comparing U1:U3 membrane pairs as well as U2:U4 membrane pairs, the mean pore size increases by blending nSMM to PES membranes. Note that the evaporation period of these membranes is zero. At 4 min evaporation period, comparison is made for the membrane pairs U6:U7 and U9:U8. Again, blending of nSMM resulted in an increase in the mean pore sizes. Comparing zero evaporation period and 4 min evaporation period (U3:U7 and U4:U8 membrane pairs), it seems that 4 min evaporation period resulted in larger mean pore sizes when nSMM is blended. However, it can not be concluded at this stage that this is an effect of evaporation period since in U3 and U4 membranes PVP was present in the casting dope, while it was absent in U7 and U8 membranes. When U3 membrane is compared with U5 membrane, the effect of evaporation period becomes more obvious. Both membranes were

cast from the same casting dope containing PVP. Only the evaporation period was changed from 0 of U3 to 4 min of U5. The pore size increased from 6.2 to 65 nm from U3 to U5. Hence, it can be firmly concluded that pore size increases with an increase in evaporation period, particularly when nSMM is blended. Together with the data in Figure 7.2, it can also be concluded that the mean pore size increases as the surface hydrophobicity increases. This is probably due to weaker tendency for water molecules to be dispersed in a polymer of high hydrophobicity, resulting in larger clusters of water molecules.

The decrease in the pore size by adding PVP in the membrane casting solution without nSMM was observed by comparing U1 and U6. Although U6 had 4 min evaporation time and U1 had 0 min evaporation time, the mean pore size of U1 was smaller than that of U6. This indicates that as PVP added, the pore size increased. However, when PVP was added into the membrane casting solution with nSMM, the increase in the pore size occurred by addition of PVP as observed from U5 and U6. Therefore, the effect of PVP seems to be changed by whether nSMM is included in the membrane casting solution or not.

Based on the comparison of U7, U10 and U11, an increase in the temperature of gelation media increases the mean pore size. Similar effects were reported by Spricigo et al. (2002) and Alsari et al. (2001) for PES membranes.

It should be emphasized at this point that the nSMM blended membranes with 4 min evaporation time (e.g. U5, U7, U8, U10 and U11) possess much larger mean size pores compared to other membranes.

Probability density function curves were also generated from Equation 2.11 by using the values of mean pore size and geometrical standard deviation given in Table 7.8 and results shown in Figure 7.12. Much larger mean pore sizes of U5, U7, U8, U10 and U11 membranes than other membranes are obvious from this figure.

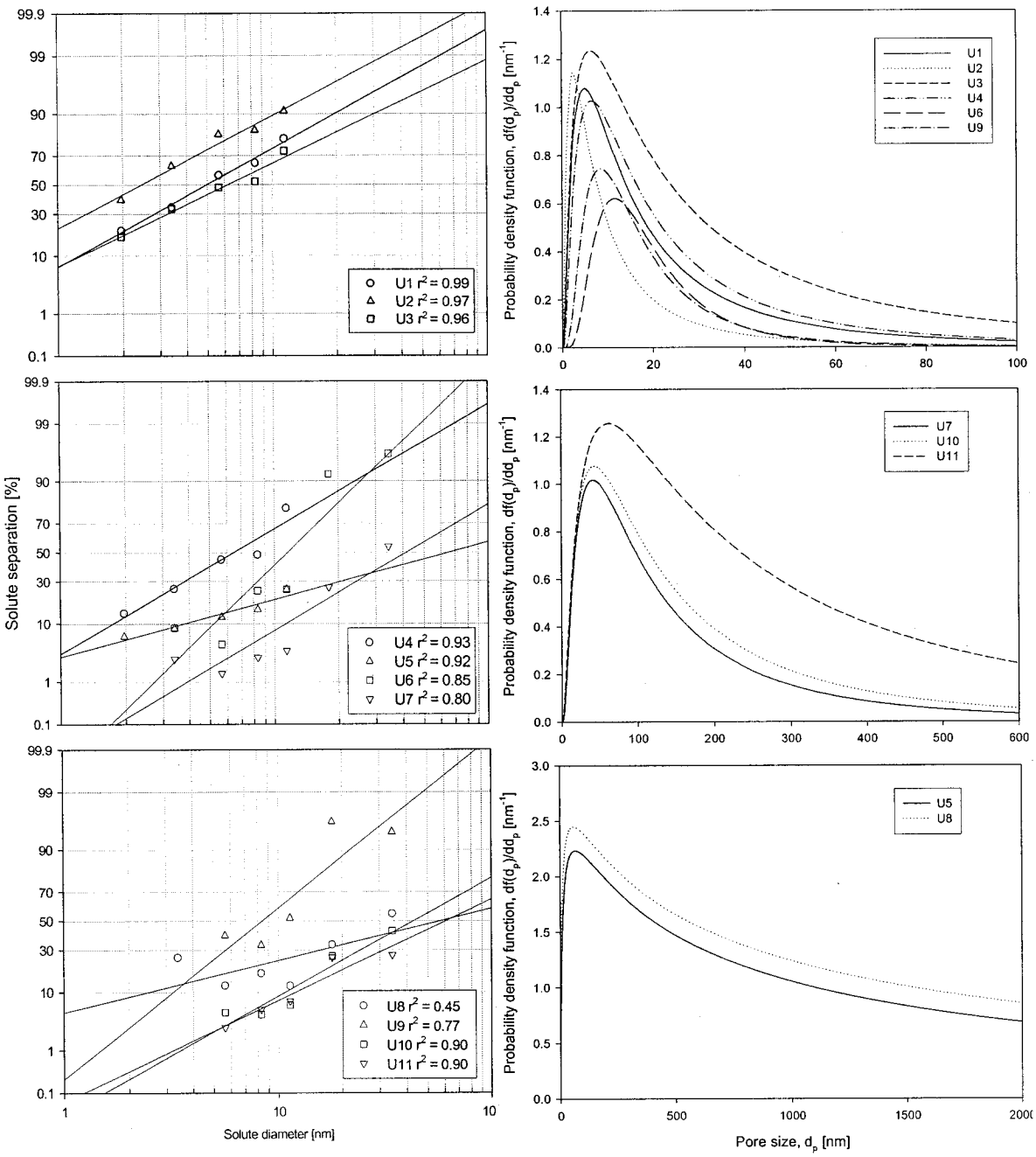

Figure 7.11 Solute separation curves (solute diameter versus their separation) plotted on log-normal probability papers

Figure 7.12 Probability density function curves

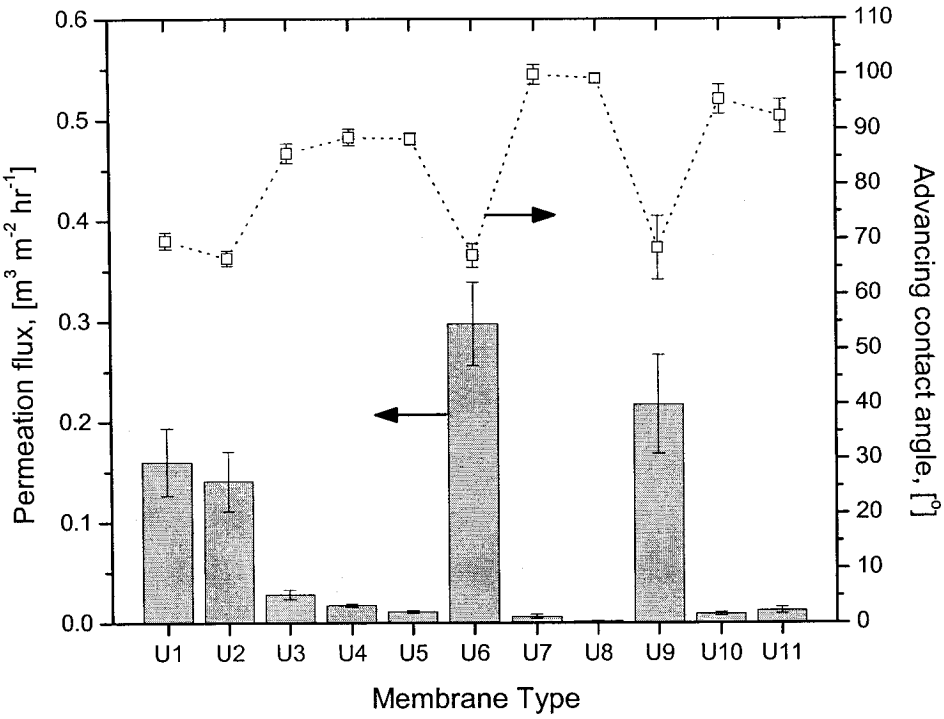

Figure 7.13 Comparison of pure water permeation flux and contact angle of all U series membranes

The pure water permeation data are shown in Figure 7.13. Interestingly, U5, U7, U8, U10 and U11 membranes that were identified as membranes of very large mean pore sizes showed very low flow rates without exception. The reason for these unexpected results can be given by superimposing the contact angle data on the same graph. U1, U2, U6 and U9 membranes of high permeation rates correspond to contact angles lower than 70° without exception. Remember all of these membranes do not contain nSMM. These results seem to be quite natural, since nSMM blended membranes have highly hydrophobic surfaces and water must pass through only a small number of pores that have large pore sizes. Hence, pure water permeation flux will decrease.

It is also interesting to note that contact angle data can be classified into three groups. The first one corresponds to the membranes that do not contain any nSMM (U1, U2, U6 and

U9). Their contact angles are between 65° and 70° as already observed for PES in the previous chapters. The second one corresponds to the membranes that contain SMM but do not contain PVP (U7, U8, U10 and U11). Their contact angles are between 90° and 105°. The third group corresponds to the membranes that contain both nSMM and PVP and their contact angles are between those of the first and second group.

Further to elucidate the effects of hydrophobicity (contact angle) and mean pore size on the pure water permeation flux, contact angle, mean pore size and pure water permeation flux data are given in Figure 7.14 for those membranes which contain nSMM. In the figure, U3 and U4 membranes that also contain PVP show higher pure water permeation fluxes than any other membranes due to their lower contact angles (higher surface hydrophilicity) even though their mean pore sizes are small. Comparison of the data for U7, U10 and U11 membranes are even more interesting. It should be recalled that these membranes were prepared under exactly the same conditions except for the temperature of the gelation media (water) that was increased from U7 (4°C) to U10 (18°C) and further to U11 (40°C). It is obvious from the figure that the pure water permeation flux increases from U7 to U11 progressively, while at the same time the mean pore size increases and the contact angle decreases (hydrophilicity increases). Thus, the effects of the mean pore size and the contact angle are as expected. Increase in the mean pore size with an increase in gelation bath temperature (or decrease in the mean pore size with a decrease in gelation bath temperature) agrees with the results reported by Alsali et al. (2001). According to Alsari et al., a decrease in the gelation bath temperature caused a decrease in the rate of solvent/nonsolvent exchange, which further resulted in a delay in polymer precipitation. This allowed an increase in polymer concentration at the membrane surface, leading to the formation of smaller pores. Increase in surface hydrophilicity with increasing gelation bath temperature also coincides with the data of Hester and Mayes (2002). Using *hydrophilic* SMM, they demonstrated that surface localization of their hydrophilic SMM during coagulation in the gelation media (pure water) occurred by the diffusion of the two polymer components, i.e. SMM and the host polymer into which the SMM was blended, prior to

gelation. They mentioned that by increasing the mobility of the polymers, e.g. by raising the gelation bath temperature, higher SMM surface concentrations could be achieved. Since their SMM was hydrophilic, the hydrophilicity of the membrane surface increased at higher gelation bath temperature. In contrast to Hester and Mayers' work, '*hydrophobic* SMM' was used in this study.

Similar to their case, an increase in the gelation bath temperature caused the increase in the mobility of the two polymer components, i.e. PES and nSMM in this study. nSMM that has once been accumulated at the membrane surface by its migration toward the surface might have moved back into the PES bulk when the surface was brought into contact with hydrophilic water. This SMM relocalization occurred more readily at higher gelation bath temperature because of the higher mobility of polymers. Hence, the surface hydrophobicity decreased with an increase in gelation bath temperature.

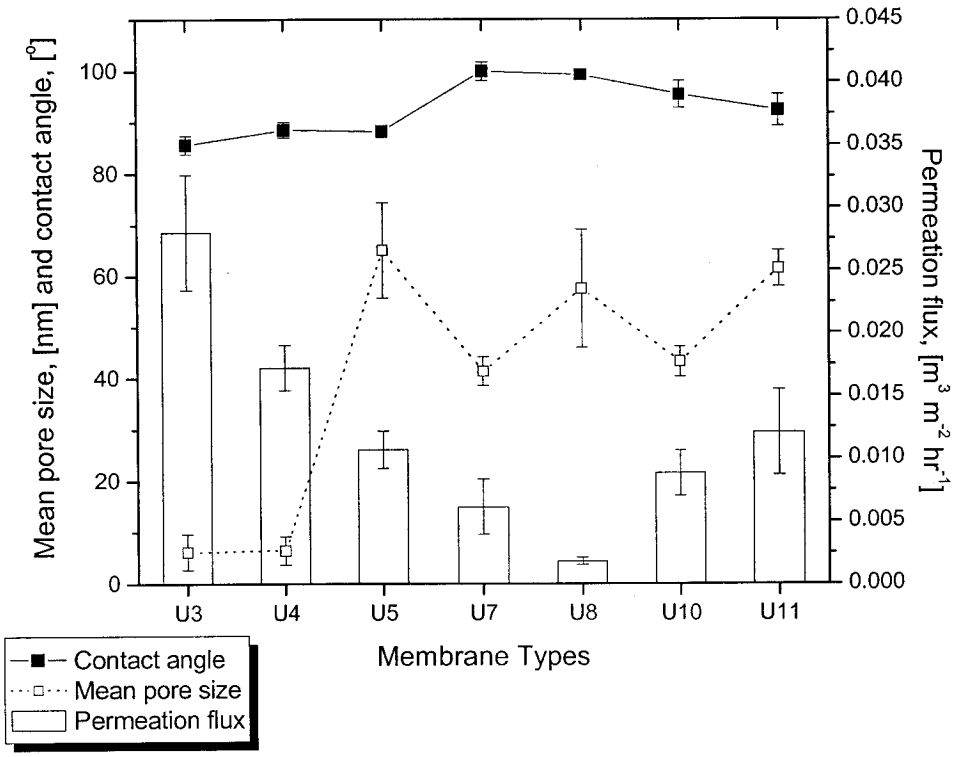

Figure 7.14 Comparison of PWP flux, contact angle and mean pore size for membranes with nSMM

7.9 Summary of Chapter 7 (Part 4)

1. A new type of Surface modifying macromolecules (nSMM1 and nSMM2) that consist of MDI (hard component), PDMS (soft component) and fluorohydrocarbon chains (chain extender) were successfully designed and synthesized. It was found that the nSMM effectively increased the surface hydrophobicity of polyethersulfone membranes when blended.
2. Because of the higher hydrophobicity of nSMM compared with tSMM synthesized earlier, high surface hydrophobicity could be achieved under milder membrane preparation conditions such as lower evaporation temperature and shorter evaporation period.
3. The hydrophobicity of nSMM blended PES membranes changed depending on the conditions of membrane preparation.
4. The changes can be interpreted by postulating; there are two parts (Part A and Part B) in nSMM. Both Part A and Part B are hydrophobic but Part B is more hydrophobic. There are two steps in nSMM surface coverage, conformational rearrangement of nSMM and surface migration. By the conformational change Part B of the nSMM is exposed to the air. As surface migration of nSMM progresses, more Part A is air-exposed while Part B exposure is maintained.
5. The above view of nSMM surface coverage is supported by Fl and Si concentrations on the membrane surface measured by XPS.
6. The liquid entry pressure of water (LEP_w) increased as the advancing contact angle increased.
7. The mean pore size increased with an increase in evaporation time of the casting solution blended with nSMM. The mean pore size increased as the surface hydrohpobicity increased.
8. The nSMM blended membranes with relatively large mean pore sizes showed very low pure water permeation rates. This is because nSMM blended membranes have highly hydrophobic surfaces and water must pass thorugh ony a small number of pores that have large pore sizes.

9. When PVP was added to the PES membrane casting solution containing nSMM, the mean pore sizes decreased but, at the same time, the contact angle decreased. As a result, the pure water permeation flux increased.

10. nSMM relocalization in the gelation media occurred more readily at higher gelation bath temperature because of the higher mobility of polymers. Hence, the surface hydrophobicity decreased with an increase in gelation bath temperature.

8. Results and Discussion (Part 5): Vacuum Membrane Distillation (VMD) Using nSMM Blended PES Membranes

From ultrafiltration experiments together with contact angel measurements, the results of which are given in Section 7, it was concluded that U7, U8 membranes in Table 7.7 had the highest potential for Vacuum Membrane Distillation (VMD) from the point of view of their high contact angles (over 100°) and their relatively large mean pore sizes (over 40 nm) compared to other membranes.

In this chapter, membranes are prepared from four casting solutions of different compositions and characterized by several different techniques, such as SEM, contact angle measurement and PWP tests. The purpose of these tests is to obtain membrane characterization parameters that are related to VMD processes. Finally, VMD experiments are conducted and the results compared with theoretical prediction based on a mathematical model (Bandini et al., 1997).

The membranes used in this study are listed in Table 8.1. All membranes which were subjected to the further tests were dried after preparation. It should be recalled that all the membranes which were used for ultrafiltration experiments (U series) in Chapter 7 were kept in distilled water until they were used.

Casting solution compositions, and other conditions of membrane preparation for V1 and V2 membranes were the same as to those of U8 and U7 membranes, respectively (see Section 7.8). A small amount of water was added to the casting solutions for V3 and V4 membranes, from which two effects were expected on the final form of PES membranes. (1) As a non-solvent, pure water in the casting solution could enlarge the pore size and/or increase the number of pores. (2) Since water is hydrophilic, nSMM will be driven to the surface due to the repulsive force working between water and nSMM. Thus, nSMM surface migration will be facilitated.

Table 8.1 Preparation conditions of the membranes used for VMD processes

Membrane	Casting solution composition (by weight)	Evap. Temp. [°C]	Evap. Time [min]	Gel. Temp. [°C]
V1	PES:SMM:NMP = 17:1.5:81.5 (= U8)	RT	4	4
V2	PES:SMM:NMP = 15:1.5:83.5 (= U7)	RT	4	4
V3	PES:SMM:H2O:NMP = 17:1.5:2:79.5	RT	4	4
V4	PES:SMM:H2O:NMP = 15:1.5:2:81.5	RT	4	4

8.1 Surface Observation of nSMM2 Blended PES Membranes

When the cast film is immersed together with the glass plate in to the gelation bath, water at 4°C, coagulation of the film starts to occur. After one hour of gelation period coagulation can be assumed to be completed. It is interesting to note that the top surface layer of the membranes could be easily scraped off at this stage. This suggests that segregation of extremely hydrophobic nSMM occurred from the host PES polymer at the membrane surface. After keeping the membranes in water overnight and drying them, the surface layer could no longer be peeled off. When the dried membranes were re-immersed to and kept in water for one week, the surface layer could not be peeled off. This means that the adhesion between the nSMM layer and PES porous sublayer seems strong enough for practical applications once the membranes are dried.

To confirm the surface segregation of nSMM layer, observation of the membrane surface was made by an optical microscope (Olympus Microscope Model BH20UMA, with 100 times magnification). A microscopic picture of the V1 membrane was taken from the top of the surface. Before taking the picture a small piece of the top skin was partially removed. The picture is presented in Figure 8.1. The Figure shows clearly that there are two distinct portions: the A (grey) where the top surface layer remains and B (white) where the top surface layer was removed and the bulk layer is exposed. The top surface layer, most likely, is composed of nSMM and the bulk layer PES.

Contact angles of the surfaces of the top layer as well as the bulk layer were measured. The contact angle of the top layer (Figure 8.1(a)) was 109.42±0.38° and that of the bulk surface was 73.83±2.86°. Since the reported contact angles of nSMM film and PES film are 125° and 67°, respectively, the above contact angle data confirm that nSMM indeed dominates at the top surface layer and PES in the bulk layer.

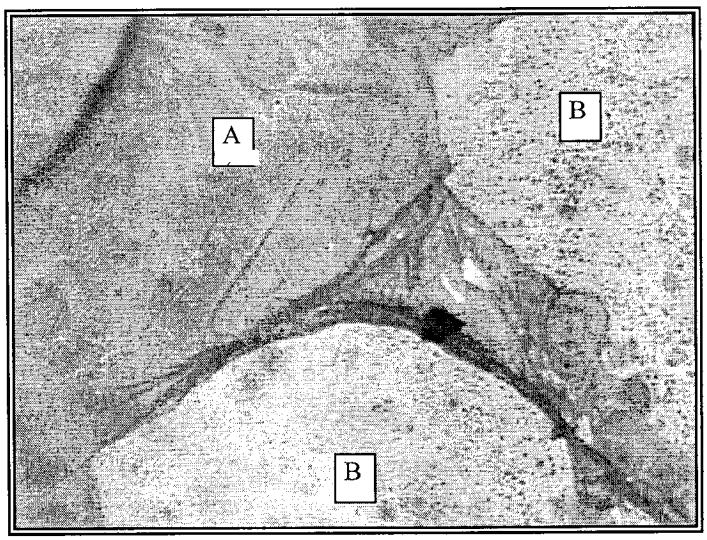

Figure 8.1 A microscopic picture (×100) of V1 membrane taken by Olympus electrical microscopy showing (a) the top surface layer, A and (b) the surface of the bulk layer, B

8.2 Morphological Study Using SEM

The SEM cross-sectional pictures are given in Figure 8.2 to 8.5 for the four 'V series' membranes. In accordance to Figure 8.1, two distinct layers are found. The structure of the membrane that consists of a skin layer and a porous sublayer is very similar to that of a membrane prepared by dip-coating. In Appendix G, the cross-section of the membrane from which the surface layer was removed is presented. Looking into Figures 8.2 to 8.5, membranes with 17 wt% PES in their casting solutions, V1 and V3 have 'finger like' pores from the top side to the bottom side, while membranes with 15 wt% PES in their solutions, V2 and V4 have 'finger like' pores from top side to some point in the middle and macro-pores are formed below that point. According to the Figures 8.2 to 8.5, the total thicknesses

of the membranes and the thicknesses of their surface layers were measured and the results listed in Table 8.2.

As shown in Table 8.2, by increasing the PES concentration in the casting solution, the total thickness of the membrane increases, while by adding water into the casting solution, the surface layer thickness decreases.

Table 8.2 Thicknesses of membranes and surface layers for 'V series' membranes

Membrane	Membrane thickness [μm]	Surface layer thickness [μm]
V1	113.0 ± 0.7	1.05 ± 0.08
V2	93.1 ± 0.5	0.73 ± 0.08
V3	125.2 ± 3.7	0.53 ± 0.09
V4	106.6 ± 4.0	0.63 ± 0.05

8.3 Contact Angle Measurements

The contact angles of the membranes in Table 8.1 were also measured and the results presented in Table 8.3. For every membrane the surface was found to be very hydrophobic. Comparing V1/V3 and V2/V4 membrane pairs, it can be concluded that the addition of water increases the contact angle, even though the change is only marginal. This confirms that the nSMM migration to the surface took place indeed faster when water was present in the casting solution.

Table 8.3 Contact angles for 'V series' membranes

Membrane	Contact angle [degree]	Membrane	Contact angle [degree]
V1	109.42 ± 0.38	V3	112.67 ± 1.66
V2	116.92 ± 2.91	V4	119.33 ± 1.72

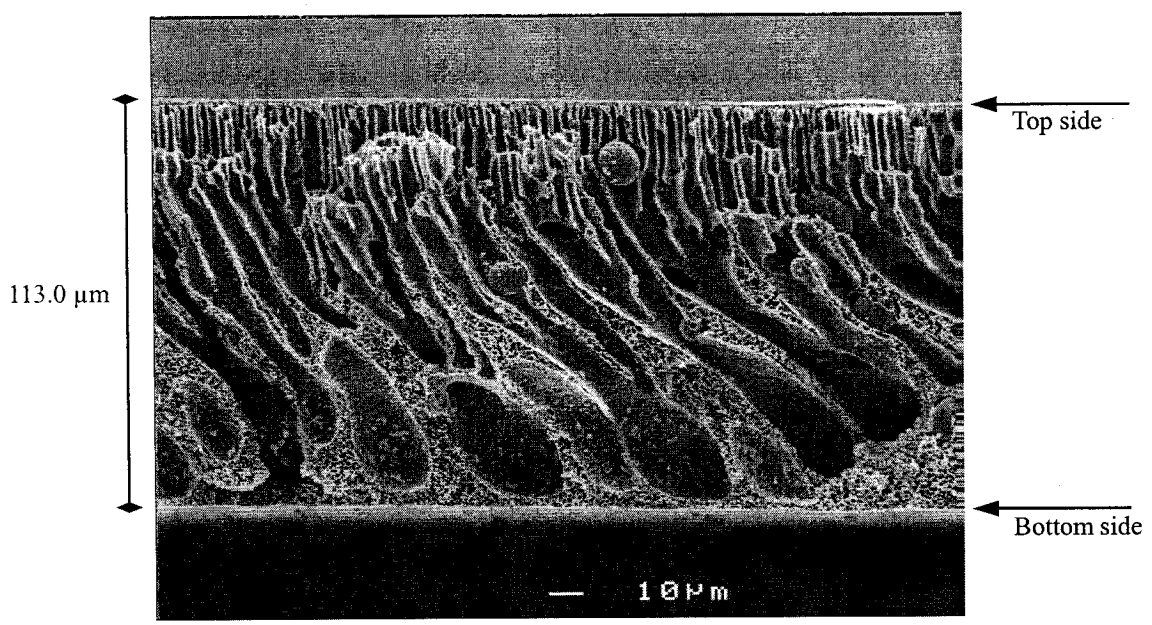

(a) Membrane profile (× 500)

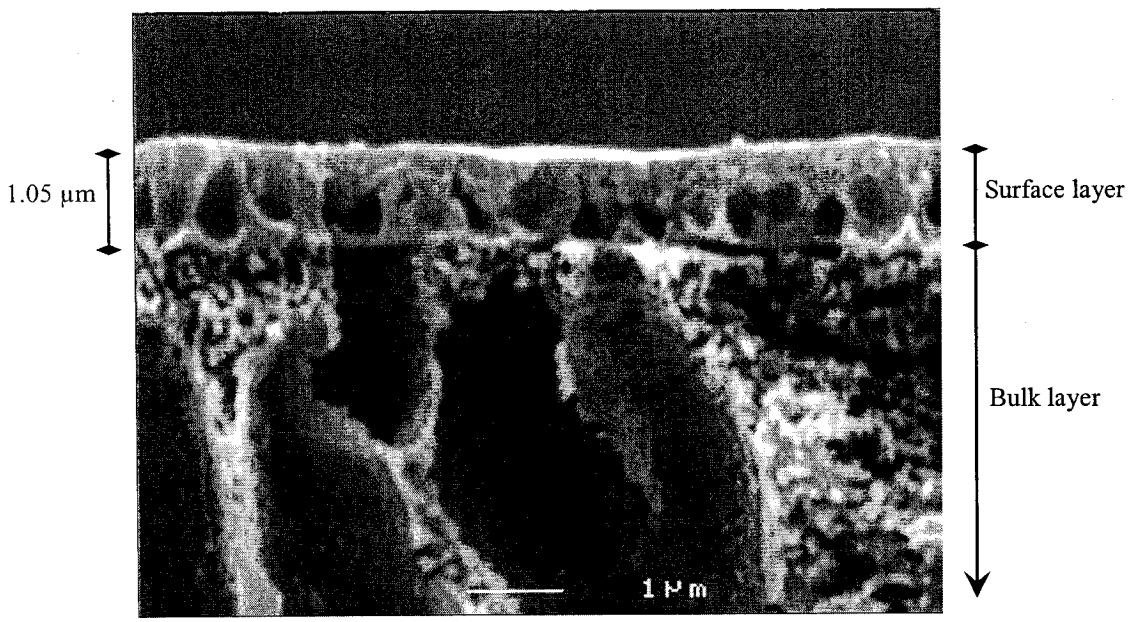

(b) Magnified top surface part (× 1500)

Figure 8.2 SEM pictures of V1 membrane for (a) membrane profile and (b) magnified top surface part

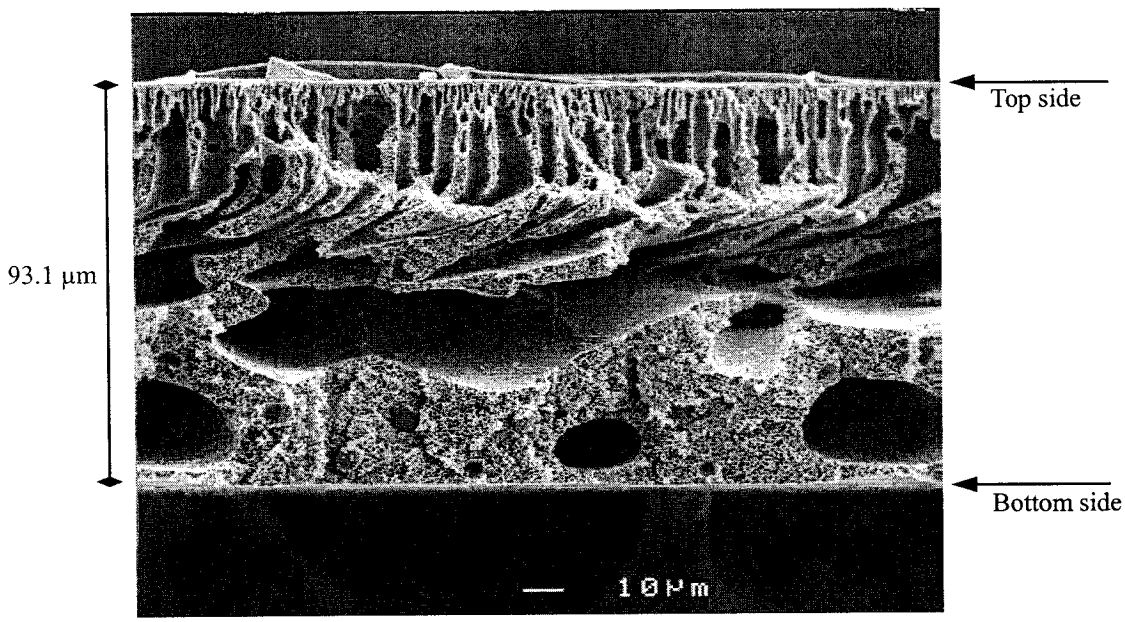

(a) Membrane profile (× 600)

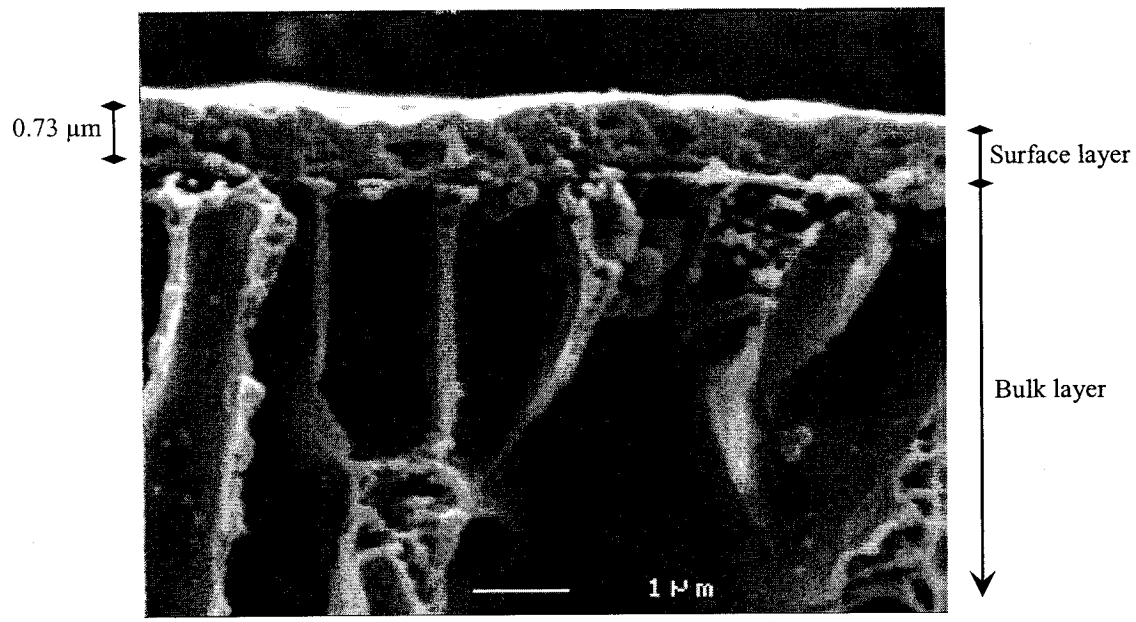

(b) Magnified top surface part (× 1500)

Figure 8.3 SEM pictures of V2 membrane for (a) membrane profile and (b) magnified top surface part

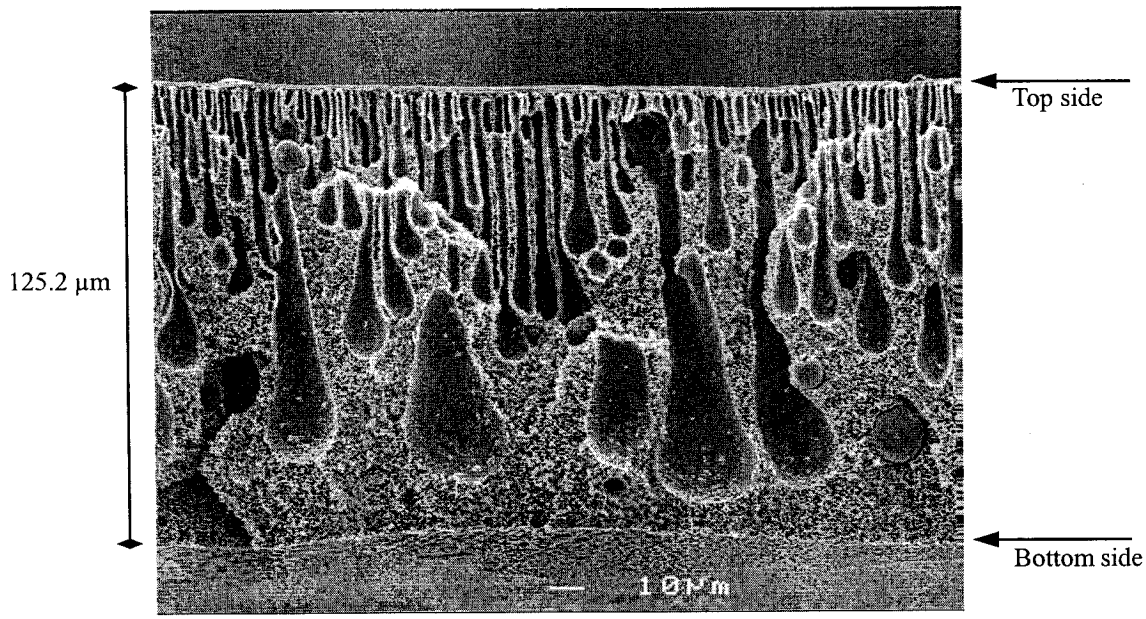

(a) Membrane profile (× 500)

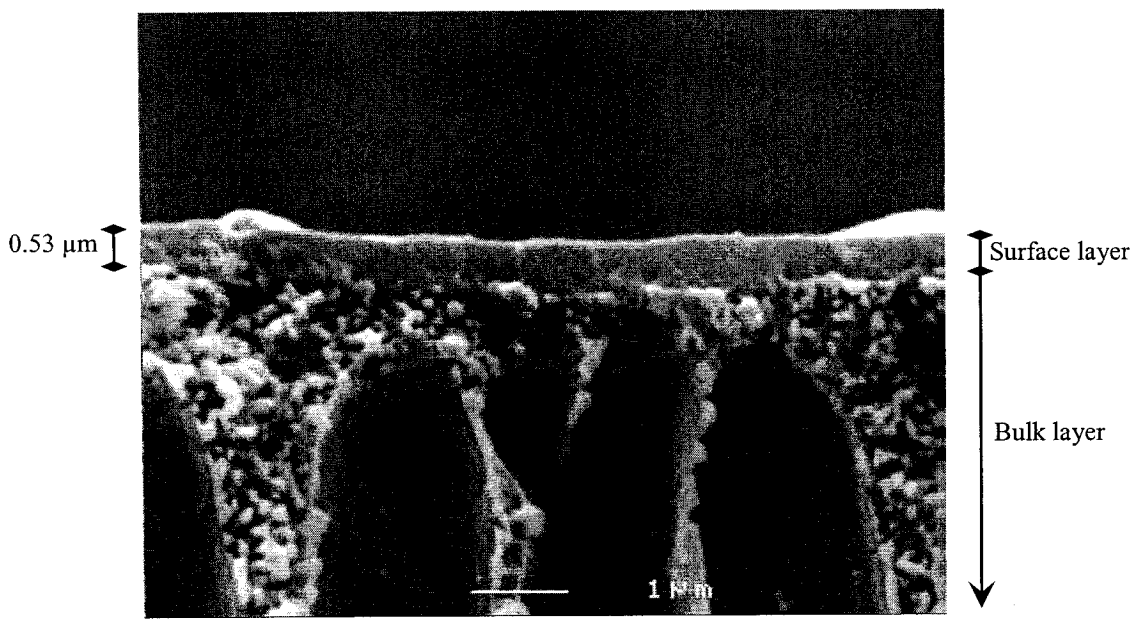

(b) Magnified top surface part (× 1500)

Figure 8.4 SEM pictures of V3 membrane for (a) membrane profile and (b) magnified top surface part

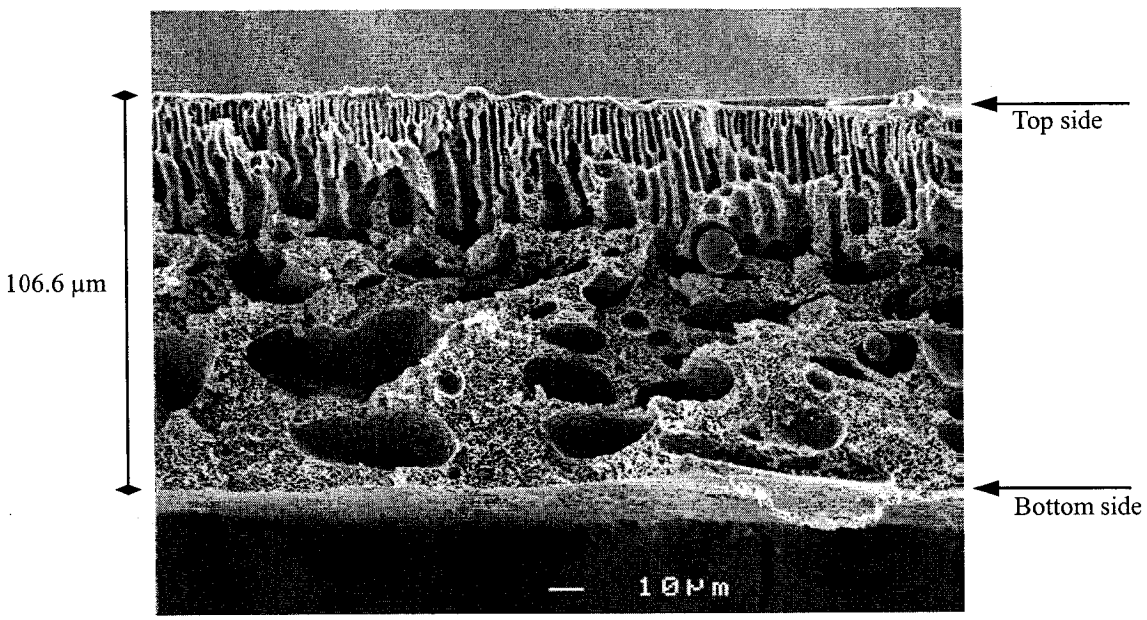

(a) Membrane profile (× 500)

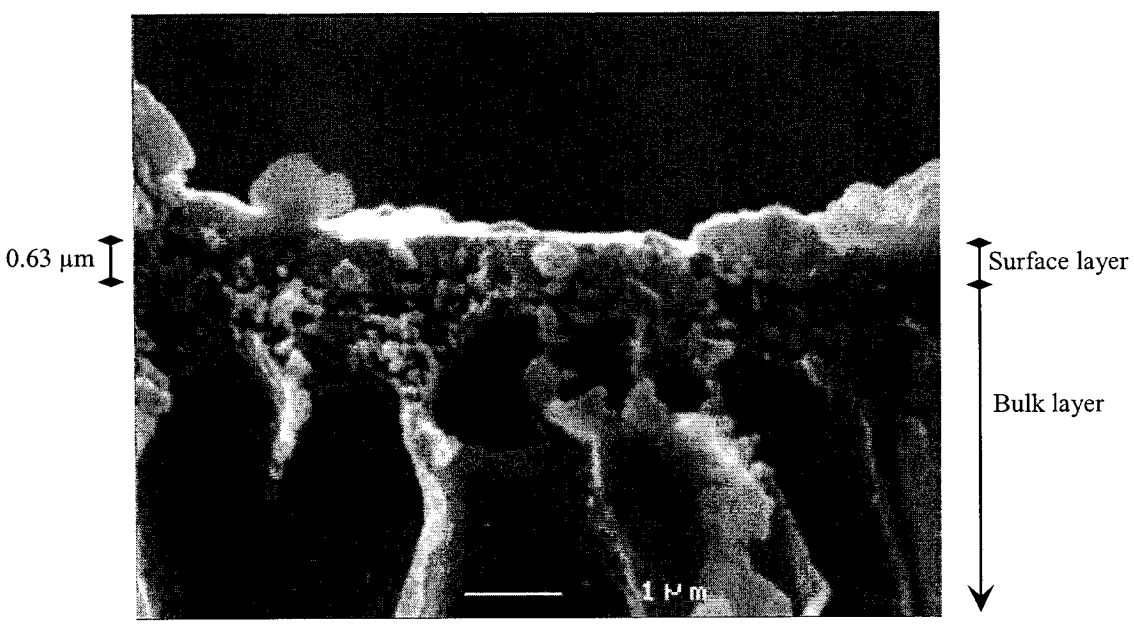

(b) Magnified top surface part (× 1500)

Figure 8.5 SEM pictures of V4 membrane for (a) membrane profile and (b) magnified top surface part

8.4 Pure Water Permeation Analysis

Pure water permeation tests were also conducted using a static membrane cell (Figure 3.4(a)) for all 'V series' membranes. Typical pure water permeation data (water flux vs. pressure) for each membrane are given in Figure 8.6. For all membranes the water flow rate increases progressively with an increase of pressure applied on water and each curve shows a sigmoidal shape. Accordingly, the data for each membrane are divided into the following three regions. In the first region, the water flux remains zero despite an increase in pressure to a certain point, which is hereafter called Liquid entry pressure of water (LEP_w). In this region, entry of water is prevented for all pores due to the high hydrophobicity of the membrane, hence no water flux. Upon achieving LEP_w, the largest pore is opened. In the second region, the water flux increases exponentially with an increase in pressure, corresponding to opening of progressively smaller pores. By the end of this region all the pores have been opened. In the third region, the flux increases linearly with pressure, since no more pores will be opened. It should be reminded that the water flux vs. pressure curve is very similar to air flux vs. pressure curve shown earlier when the bubble point method was discussed (see Section 2.5.1). Based on the experimental data given in Figure 8.6, LEP_w values were obtained and summarized in Table 8.4. Comparing Table 8.3 with Table 8.4, it is found that LEP_w decreases as the contact angle increases, i.e. the membrane with the highest contact angle (the strongest hydrophobicity) had the lowest LEP_w and vice versa. This trend seems rather surprising, since the largest LEP_w is expected for the membrane of the strongest hydrophobicity. It should be recalled, however, that we observed an increase in the pore size with an increase in hydrophobicity as a result of nSMM accumulation on the membrane surface, when we studied the effect of evaporation period on the contact angle as well as the pore size of nSMM blended PES membranes in Section 7.8. Moreover, the effect of the pore size was found stronger than that of the contact angle on the ultrafiltration flux. It is therefore safely concluded that the pore size became larger as the contact angle increased also for the "V series" membranes under investigation.

Table 8.4 Liquid entry pressure of water (LEP_w) for 'V series' membranes

Membrane	LEP_w [kPa]	Membrane	LEP_w [kPa]
V1	510.2 ± 28.0	V3	313.0 ± 29.1
V2	259.2 ± 57.8	V4	108.9 ± 68.3

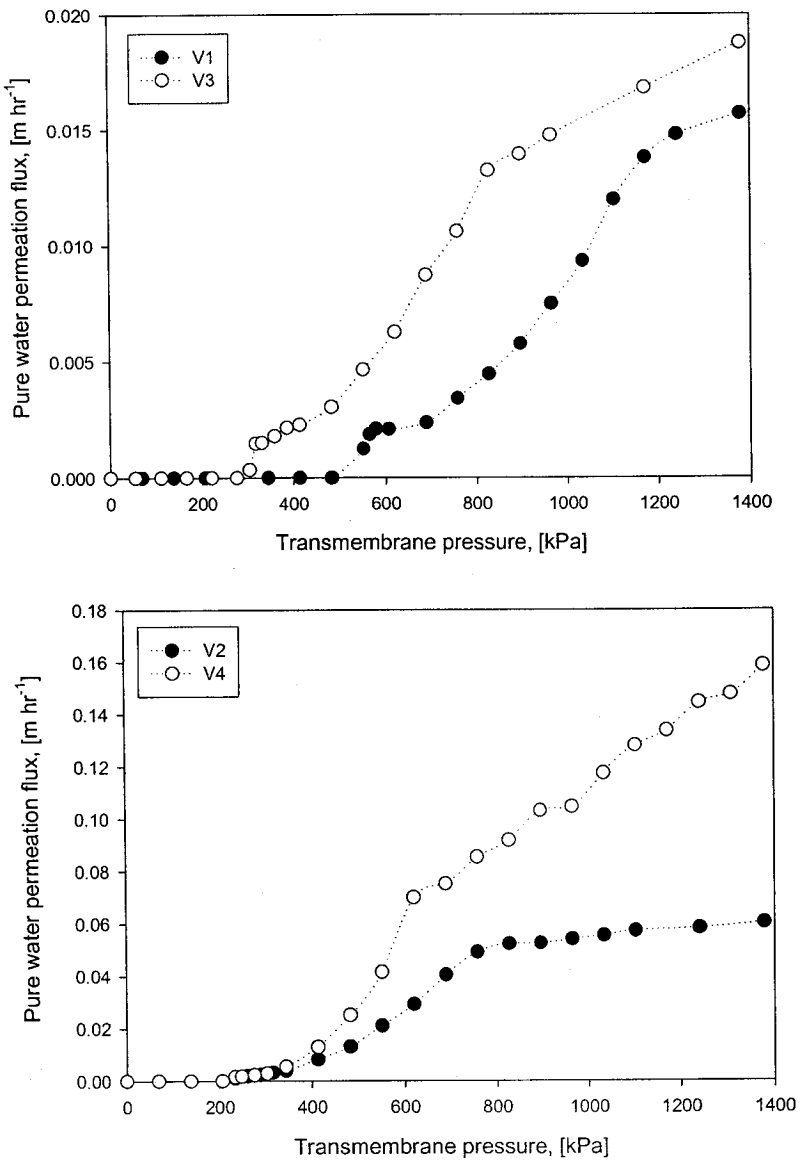

Figure 8.6 Pure water permeation flux versus pressure for 'V series'

8.5 Vacuum Membrane Distillation with Pure Water

Among the four 'V series' membranes characterized in the previous section, V3 and V4 were subjected to vacuum membrane distillation (VMD) experiments. The reason for choosing V3 and V4 is found in their higher contact angles as well as their lower liquid entry pressure of water (LEP_w), which indicates that V3 and V4 membranes are more hydrophobic and more porous than the other membranes of the "V series". Pure water was used as a feed stream in this experiment. The temperature of the feed was 26°C and the downstream pressure was changed from about 0.4 to 5.3 kPa (3 to 40 torr). VMD experiments were performed with those membranes to investigate the influence of the downstream pressure on water flux.

The results are presented in Figure 8.7. Water flux for the V4 membrane was higher than V3 membrane since the pore size of the V4 is larger than V3. As the down stream pressure decreased, water flux increased showing an inverted S-shape trend for both membranes, V3 and V4. At the pressures higher than the water vapor pressure, $P°_W$ (3.36 kPa at 26°C), the flux of water vapor was very low; however at the pressures lower than the $P°_W$, the flux of water vapor was much higher. These results agreed to the plot shown in Section 2.4.3. Comparing to the results of pervaporation tests with tSMM1 blended PES membranes by J. G. Minnery (2000), the pure water flow rate from VMD is about twofold higher.

Theoretically speaking, the water flux should be zero when the permeate side pressure is above the saturation vapor pressure of water, since there is no driving force for vapor to permeate through the membrane pore. The water permeation flux observed above the saturation vapor pressure is therefore difficult to understand. It could however be attributed to the increase in saturation vapor pressure at a curved water/air interface.

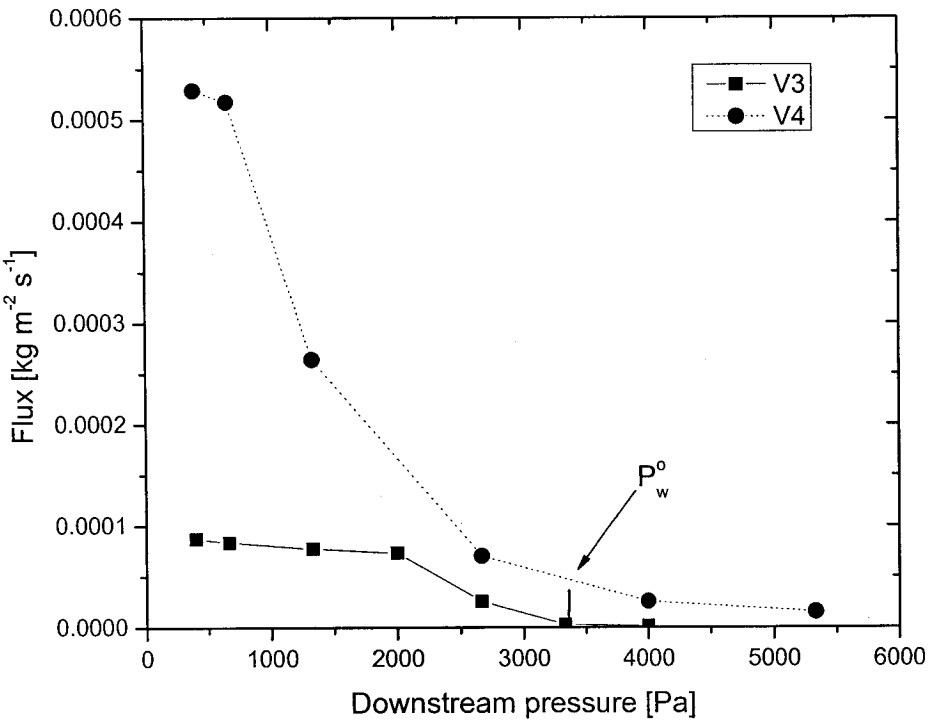

Figure 8.7 VMD experiments with single component feed (pure water)

8.6 Vacuum Membrane Distillation with Water-Ethanol Mixture

VMD experiments were conducted with a water-ethanol mixture using a V3 membrane. The pressure range studied was between 0 and 2000 Pa, since in this pressure range relatively high fluxes could be achieved. The concentration of ethanol in the feed mixture was ca. 1000 ppm, the temperature of the feed was 26°C and a maximum stirring rate was 54 revolutions/s (rps). Measured total trans-membrane fluxes and ethanol concentrations in the permeate are presented in Figure 8.8 together with the flux of pure water from the previous experiment (Figure 8.7). In Figure 8.8, it is observed that (1) as the down stream pressure increases, the trans-membrane flux decreases and, correspondingly, the ethanol concentration in the permeate increases and (2) the flux for the VMD experiment with the

water-ethanol mixture was higher than pure water feed. Both trends in flux and ethanol concentration in the permeate agree with those in the literature (Bandini et al., 1997; Lawson and Lloyd, 1996). It is important to notice the appreciable effect of the downstream pressure on the ethanol concentration in the permeate; higher pressure may lead to a high ethanol content in the permeate such as up to about 1900 ppm. This might have been resulted from a significant reduction of the driving force for water flux as the pressure increased, whereas the driving force for ethanol underwent only a small decrease. It is also reasonable to attain the higher flux of water-ethanol mixture than that of pure water due to the higher vapor pressure of water-ethanol mixture than that of pure water. Therefore, there could be an optimum downstream pressure from the economic point of view, which will give an optimum flux and ethanol concentration in the permeate.

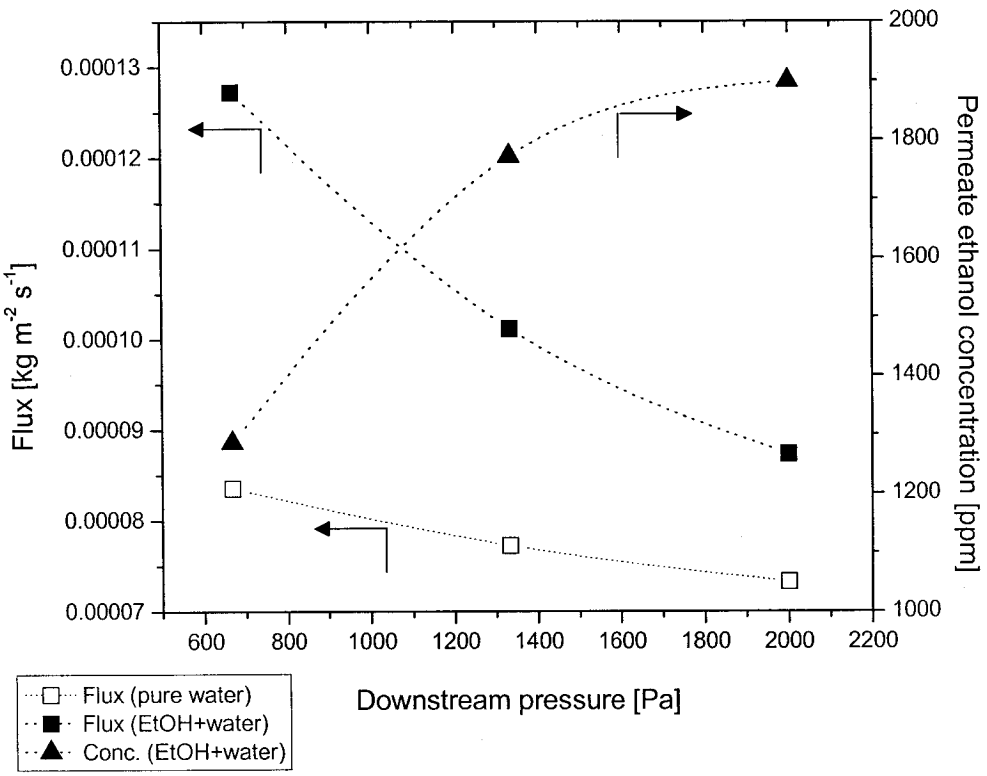

Figure 8.8 VMD results of V3 with binary mixture feed (ethanol+water)

Similar study using VMD of 5 wt% ethanol-water mixture was done by Bandini et al. (1992) with a PTFE membrane (TF200) under 3333 Pa (25 torr) at 35°C. According to their results, the highest flux and separation factor achieved are 0.0055 kg m^{-2} s^{-1} and 7.0, respectively, while the corresponding values in Fig. 8.8. are 0.0009 kg m^{-2} s^{-1} and 2.1 under 2000 Pa, respectively. This seems to be understandable in terms of lower ethanol concentration, feed temperature and permeate pressure, adopted in this work. Therefore the nSMM blended PES membrane must have a high potential as an alternatives for commercial hydrophobic VMD membranes.

8.7 Modeling and Evaluation of VMD Performance

Based on the modeling described in Section 2.5.3, calculation of ethanol concentration in the permeate was attempted and the results compared with the experimental data shown in Figure 8.8. The detailed calculations and discussion follow in the rest of this Section. All equations were presented and the symbols defined in the Section 2.5.3. The sequence of the calculation is as follows.

1) The temperature at the liquid-membrane interface, T_I, is assumed.
2) The experimental data for the permeate flux and the ethanol concentration in the permeate that correspond to the permeate side pressure of 1999.84 Pa are chosen to calculate heat and mass transfer coefficients (h and k_L in Equations 2.28 and 2.29 respectively).
3) Then, using the measured flux data and the calculated h and k_L, the ethanol concentrations are calculated for the other permeate side pressures of 1333.22 and 666.32 Pa.
4) Calculated ethanol concentrations are compared with the experimental values to find T_I that gives the best fit between calculated and experimental values.

The conditions of VMD experiments and the corresponding results are summarized in Table 8.5.

Table 8.5 VMD experiment condition and results

P_2[a]	T_b[b]	N_t[c]	C_b[d]	C_p[e]
Pa	[°C]	[kg m^{-2} s^{-1}×10^{-5}]	[ppm]	[ppm]
1999.84	26	8.7326	919.55	1898.96
1333.22	26	10.1135	948.73	1771.88
666.32	26	12.7229	854.19	1286.16

[a] P_2 is the pressure at the permeate side [b] T_b is the temperature of the feed [c] N_t is the total mass flux
[d] C_b is the feed bulk concentration in terms of TOC [e] C_p is the permeate concentration in terms of TOC

8.7.1 Air permeation tests for membrane permeability

Membrane permeability to the species i, $K_m\sqrt{M_i}$ was already defined in Equation 2.23,

$$N_i = K_m\sqrt{M_i}\Delta P_i \tag{2.23}$$

where N_i is the mass flux, ΔP_i the partial pressure difference across the membrane, and M_i the molar mass, respectively. Subscript i is the ith component (VOC). A simple air permeation experiment was performed to evaluate the K_m value for the membrane V3 according to the method described in the Section 2.4.3. In this experiment the temperature was maintained at 21°C and the transmembrane pressure was changed by changing the downstream side (permeate side) pressure from 6.9 to 48.3 kPa (1 to 7 psi) while the upstream side pressure was kept at an atmospheric pressure. In Figure 8.9 air flux is given vs. pressure difference across the membrane. The linear behavior observed indicates that viscous flow in the pores is negligible with respect to Knudsen diffusion. According to Equation 2.23, K_m could be calculated from the slope to be 3.26 × 10^{-9} (s $kgmol^{1/2}$ m^{-1} $kg^{-1/2}$). As reported by Bandini et al. (1997), only 2% change in K_m coefficient occurs due to temperature changes from 20°C to 35°C. The value measured in air at 21°C can be therefore used with confidence in the elaboration of all the data obtained.

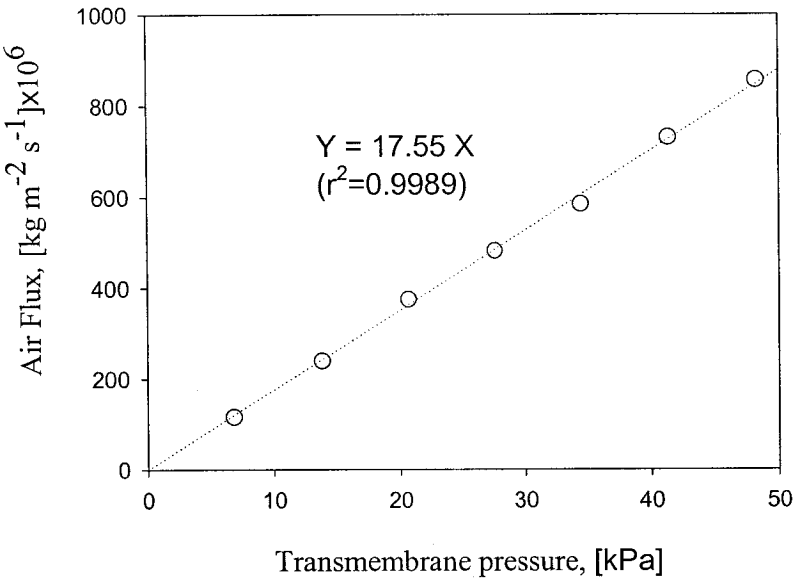

Figure 8.9 Air permeation test of the membrane, V3 at 21°C

8.7.2 Heat and Mass Transfer Coefficients Calculation

According to the calculation sequence given earlier, a set of temperatures at the liquid-membrane interface (T_I) was assumed, which were 20, 21, 22, 23 and 24°C. Using T_I and experimentally obtained data in Table 8.5 (P_2 = 1999.84 Pa), heat transfer coefficient in the liquid phase, h ($W \cdot m^{-2} \cdot K^{-1}$) was calculated by Equation 2.28.

$$\sum_i J_i \Delta H_i = h(T_b - T_I) \tag{2.28}$$

where ΔH is the molar latent heat of vaporization (J mol^{-1}), T_b the bulk liquid temperature (26°C), and the i represents each component (ethanol and water) involved in this study. The values of ΔH for ethanol and water at 18°C were obtained from Perry's Chemical Engineers' Handbook (1984), which is presented in Appendix H. Then, the values of ΔH at different temperatures were calculated by a widely used equation, which was proposed by Watson (Smith and Van Ness, 1987):

$$\frac{\Delta H_2}{\Delta H_1} = \left(\frac{1 - T_{r2}}{1 - T_{r1}} \right)^{0.38} \tag{8.1}$$

where T_r is the reduced temperature, which is defined as:

$$T_r = \frac{T}{T_c} \tag{8.2}$$

where T_c is the critical temperature and T_c values for water and ethanol are listed in the table in Appendix G. The heat transfer coefficient, h, was obtained for all assumed T_I values.

The mass-transfer coefficient in the liquid phase, k_L was, then, calculated using Equation 2.29:

$$\frac{J_t}{k_L c_L} = \ln \frac{x_{i,I} - J_i / J_t}{x_{i,b} - J_i / J_t} \tag{2.29}$$

In this equation, J_t comes from the total mass flux at 1999.84 Pa, which value is given in Figure 8.5. Remember J_t is no longer mass flux but molar flux. J_i, the individual molar flux can be calculated from the total mass flux and the permeate composition also given in Table 8.5 corresponding to 1999.84 Pa. c_L is the total molar concentration of the feed solution. Since the ethanol concentration is small the water molar concentration at 26 °C can be used. $x_{i,b}$ is the mole fraction of individual component in the feed and can be obtained from the feed composition given in Table 8.5. To obtain k_L from Equation 2.29, we need $x_{i,I}$ from the Liquid-Vapor Phase equilibrium data for either ethanol or water. However, in this study, the equation is applied for ethanol, since the system is more sensitive to the change of ethanol concentration.

In order to obtain $x_{i,I}$, an assumption is made that the evaporation of the ethanol-water mixture takes place at the liquid-membrane interface. Hence, the temperature T_I will be used for the equilibrium calculation.

First, using the individual flux (in this case ethanol) and the total flux, P_I and $Y_{i,I}$ are calculated from the following two Equations (2.25) and (2.26),

$$J_i = \frac{K_m}{\sqrt{M_i}}(P_I Y_{i,I} - P_2 Y_{i,2}) \tag{2.25}$$

$$J_t = \frac{K_m}{\sqrt{M}}(P_I - P_2) \tag{2.26}$$

All other quantities are known in the above equations.

The liquid-vapor equilibrium Equation 2.30 is then used to calculate $x_{i,I}$:

$$P_i = \gamma_i \; x_i \; P_i^{\circ} \tag{2.30}$$

where P_i° is the saturation vapor pressure of ethanol, which can be obtained by Antoine equation at T_I and the activity coefficient of ethanol, γ_i, is yielded by NRTL model (Equation 2.31). The parameter values used for NRTL model are reported in Table 8.6 (Izquierdo-Gil, 2004).

The results of the calculation for heat and mass transfer coefficients are presented in Table 8.7. According to Table 8.7, as the temperature drops at the interface, the temperature difference, $T_b - T_I$, increases, heat transfer coefficient, h increases and mass transfer coefficient, k_L decreases.

Table 8.6 NRTL model equation and the parameters values used (Izquierdo-Gil, 2004)

NRTL equations $$\ln\gamma_i = x_k^2\left[\tau_{ki}\left(\frac{G_{ki}}{x_i + x_k G_{ki}}\right)^2 + \frac{\tau_{ik}G_{ik}}{(x_k + x_i G_{ik})^2}\right] \tag{2.31}$$

NRTL parameters $\tau_{ik} = a_{ik} + b_{ik}/T$, $G_{ik} = \exp(-\phi\tau_{ik})$

i component = ethanol, k component = water

a_{ik}	a_{ki}	b_{ik} (K)	b_{ki} (K)	ϕ
0.49854	1.01535	-456.00	536.269	0.24

Table 8.7 Results of heat and mass transfer coefficient calculations in VMD at 1999.84 kg/m·s^2

	Case #1	Case #2	Case #3	Case #4	Case #5
$T_b - T_I$ [K]	2	3	4	5	6
h [W/m^2·K]	34.816	41.745	52.153	69.500	104.192
k_L [m/s]	0.007810	0.002921	0.001880	0.001425	0.001171

8.7.3 Evaluation of theoretical ethanol concentration in the permeate

Using the heat transfer coefficient and mass transfer coefficient so obtained, the ethanol concentrations in the permeate were calculated for the permeate pressures, 1333.22 and 666.32 Pa, respectively, and compared with the experimental data. The comparison is shown in Figure 8.10. Generally, the calculated values from the cases #1 to #3 seem to be better fitted to the experimental data than any other cases. T_I is therefore most likely between 22 to 24°C. It should be noted that the temperature in the liquid bulk used was 26°C.

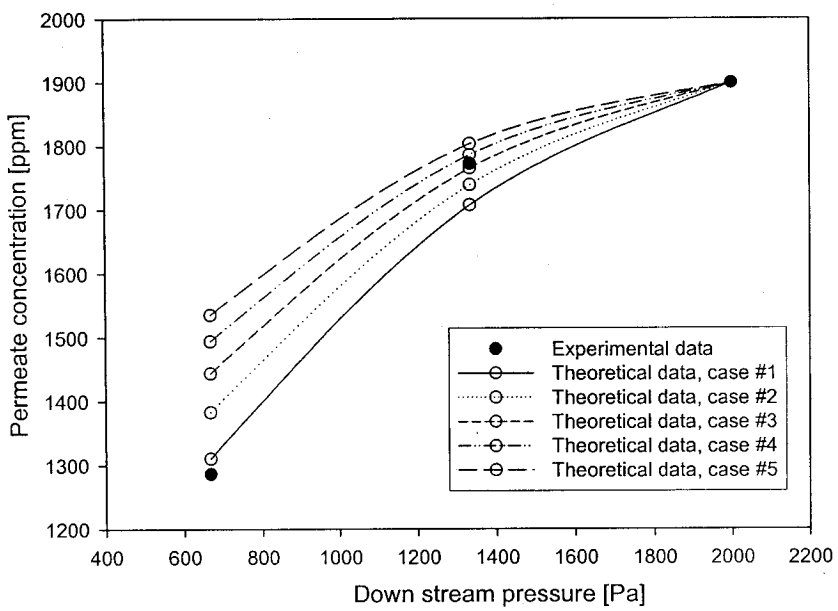

Figure 8.10 Result of VMD model calculation with experimental data

8.8 Summary of Chapter 8 (Part 5)

1. A distinctive surface layer was observed in nSMM blended PES membranes as evidenced by optical microscopic and SEM pictures.
2. nSMM blended PES membranes were successfully prepared to be highly hydrophobic and to be porous for the purpose of vacuum membrane distillation process to separate ethanol from water.
3. A mathematical model for VMD was developed considering both concentration and temperature polarization. The model could predict the ethanol concentration in the permeate reasonably well.

9. Conclusions

1. Versatility of a novel method to prepare membranes for membrane distillation was tested successfully. The new approach is based on membrane surface modification by blending surface modifying macromolecules (SMMs) to the host polyether sulfone polymer.

2. Migration of SMMs to the membrane surface requires a certain amount of time. This was evidnced by no observable difference in membrane properties, such as surface contact angle and mechanical strength, between the PES membrane and the tSMM1 blended PES membrane when no time was given for the SMM to migrate during solvent evaporation. However, a slight decrease in the pore size was noticed when tSMM1 was blended.

3. The surface migration of tSMM1 increased with an increase in solvent evaporation period. This was confirmed by an increase in contact angle and an increase in surface fluorine content as the solvent evaporation period was increased. Per cent elongation of the tSMM1 blended PES membrane also increased about twofould when the membrane experienced a long evaporatyion period.

4. As for the surface migration of tSMM1, a proposed kinetic model was found to represent the experimental XPS data satisfactorily. Based on the model, the minimum required time for the completion of tSMM1 surface migration was calculated and reported.

5. Liquid entry pressure (LEP_w) increased with an increase in evaporation time, which indicated that membranes for membrane distillation (MD) could be produced from PES membrane by blending tSMM2.

6. A new type of surface modifying macromolecules (nSMM1 and nSMM2) that consisted of MDI, PDMS and fluorohydrocarbon chains were designed and synthesized successfully. Because of the higher hydrophobicity of nSMM compared with tSMM synthesized earlier,

high hydrophobicity could be achieved at the membrane surface under milder membrane preparation conditions, such as lower evaporation temperature and shorter evaporation period, when nSMM was blended into PES membrane.

7. The surface hydrophobicity of nSMM blended PES membranes was affected both by the temperature and the period of solvent evaporation. This is due to a unique feature of the nSMM structure. The liquid entry pressure of water (LEP_w) increased as the surface hydrophobicity increased by blending nSMM..

8. Blending nSMM not only increased the surface hydrophobicity but also increased the mean pore size of the membrane. Hence, nSMM blended membranes should are the most appropriate for membrane distillation. This was confirmed by VMD experiements for the separation of an alcohol/water mixture.

9. A proposed VMD model, in which both concentration and temperature polarization were considered, could predict the concentration pf ethanol in the permeate.

10. A distinctive surface layer of nSMM was formed in nSMM blended PES membranes, as observed by optical microscope and SEM analysis. This offers a novel method of surface coating.

10. Recommendations

The following recommendations are made concerning possible future extensions for the research.

1. The relationship between the parameter, β in the kinetic model equation and the cast solution thickness can be established by more extensive experiments with XPS. Energy Dispersive X-ray (EDX) with SEM Analysis will give the information on the fluorine content along the cross section and this will help to understand more on the SMM migration kinetics.

2. nSMM synthesis is not yet fully under control and more reserches on the nSMM synthesis with more careful preparation procedure will be needed in the future for building up a more information on nSMM.

3. To prepare a more suitable membrane for the purpose of membrane distillation, further study on the effect of nSMM on the properties of PES membrane should be performed and also polymers other than PES should be used as the host polymers for membrane preparation.

4. VMD results were presented for only one system (ethanol-water) at one concentration, temperature, stirring speed, for 3 different permeate pressures and for only one membrane in this thesis. Further extended studies are required.

5. VMD was the only process for which nSMM blended membranes were applied in this study. Investigations should be extended to other MD processes (e.g. DCMD, AGMD and SGMD).

11. References

Affrossman, S., P. Bertrand, M. Harshorne, T. Kiff, D. Leonard, R. A. Pethrick and R. W. Richards, "Surface Segregation in Blends of Polystyrene and Perfluorohexane Double End Capped Polystyrene Studied by Static SIMS, ISS, and XPS", Macromolecules, 29, 5432-5437, 1996.

Alsari, A. M., K.C. Khulbe and T. Matsuura, "The Effect of Sodium Dodecyl Sulfate Solutions as Gelation Media on the Formation of PES Membranes", J. Membr. Sci., 279–293, 2001.

Amy, G. L., R. M. Narbaitz and W. J. Cooper, "Removing VOCs from Groundwater Containing Humic Substances by Means of Coupled Air Stripping Adsorption", J. Amer. Water Works Assoc., 79, 49-54, 1987.

Andrade, J.D., "Surface and Interfacial Aspects of Biomaterial Polymers", Plenum Press, New York, N.Y., 105-195, 1985.

Bagger-Jørgensen, R., A. S. Meyre, C. Varming and G. Jonsson, "Recovery of Volatile Aroma Compounds from Black Current Juice by Vacuum Membrane Distillation", 64, 23-31, 2004.

Banat, F. A. and J. Simandl, "Revmoval of Benzene Traces from Contaminated Water by Vacuum Membrane Distillation", Chem. Eng. Sci., 51, 1257-1265, 1996.

Bandini, S., C. Gostoli and G. C. Sarti, "Separation Efficiency in Vacuum Membrane Distillation", J. Membr. Sci., 73, 217-229, 1992.

Bandini, S., A. Saavedra and G. C. Sarti, "Vacuum Membrane Distillation: Expeirments and Modeling", AIChE Journal, 43, 398-408, 1997.

Bandini, S. and G. C. Sarti, "Heat and Mass Transport Resistances in Vacuum Membrane Distillation Per Drop", AIChE Journal, 45, 1422-1433, 1999.

Bandini, S. and G. C. Sarti, "Concentration of Must through Vacuum Membrane Distillation", 149, 253-259, 2002.

Bessières, A., M. Meireles, R. Coratger, J. Beauvillain and V. Sanchez, "Investigations of Surface Properties of Polymeric Membranes by Near Field Microscopy", J. Membr. Sci., 109, 271-284, 1996.

Bhatia, Q.S., D.H. Pan and J.T. Koberstein, "Preferential Surface Adsorption in Miscible Blends of Polystyrene and Poly(vinyl methyl ether)", Macromolecules, 21, 2166-2175, 1988.

Bhowmick, M., "A Novel Closed Loop Air Stripping Process", Ph, D. Theses, Dept. of Civil and Mineral Engineering, University of Minnesota, Minneapolis, MN, 1992.

Bloemen, H. J. Th. and J. Burn, "Chemistry and Ananlysis of Volatile Oragnic Compounds in the Envioronment", Blackie Academic & Professional, New York, NY, 1993.

Brewer, J., "Literature Reviews and Research Scooping Study on the Treatment of Volatile Organic Carbon Compounds in the Off-gas from Contaminated Groundwater and Soil Remedial Technologies", National Groundwater and Soil Remediation Program, Environment Canada, Ottawa, 1991.

Briggs, D., "Surface Analysis of Polymers by XPS and Static SIMS", Cambridge University Press, Cambridge, U.K., 1998.

Budkowski, A., U. Steiner and J. Klein, "The effects of Confinement and Surface Interactions on Coexistence in a Binary Polymer Mixture", J. Chem. Phys., 97(7), 5229-5238, 1992.

Cabassud, C. and D. Wirth, "Membrane Distillation for Water Desalination: How to Choose an Appropriate Membrane?", Desalination, 157,307-314, 2003.

Capannelli, G., F. Vigo and S. Munari, "Ultrafiltration Membranes-Characterization Method", J. Membr. Sci., 15, 289-313, 1983.

Cartwright, P., "Pollution Prevention Drives Membrane Technologies", Chem. Eng., Sep., 84-87, 1994.

Chang, J. P., M. L. Green, V. M. Donnelly, R. L. Opila, J. Eng, Jr., J. Sapjeta, P. J. Silverman, B. Weir, H. C. Lu, T. Gustafsson and E. Garfunkel, "Profiling Nitrogen in Ultrathin Silicon Oxynitrides with Angle-Resolved X-ray Photoelectron Spectroscopy", J. Appl. Phys., 87, 4449-4455, 2000.

Chen, J. and J. A. Gardella Jr., "Solvent Effects on the Surface Compostion of Poly(dimethylsiloxane)-co-Polystyrene/Polystyrene Blends", Macromolecules, 31, 9328-9336, 1998.

Chen, W. and T. J. McCarthy, "Adsorption/Migration of a Perfluorohexylated Fullerence from the Bulk to the Polymer/Air Interface", Macromolecules, 32, 2342-2347, 1999.

Cheng, D. Y. and S. J. Wiersma, "Composite Membrane for a Membrane Distillation System", United States Patent, 4316772, 1982.

Clark, M. B. Jr., C. A. Burkhardt and J. A. Gardella Jr., "Surface Studies of Polymer Blends. 4. An ESCA, IR, and DSC Study of the Effect of Homopolymer Molecular Weight on Crystallinity and Miscibility of Poly(ϵ-caprolactone)/Poly(vinyl chloride) Homopolymer Blends", Macromolecules, 24, 799-805, 1991.

Couffin, N., C. Cabassud and V. Lahoussine-Turcaud, "A New Process to Remove Halogenated VOCs for Drinking Water Production: Vacuum Membrane Distillation",

Desalination, 117, 233-245, 1998.

Datta, R., S. Dechapanichkul, J. S. Kim, L. Y. Fang and H. Uehara, "A Generalized Model for the Transport of Gases in Porous, Non-porous, and Leaky Membranes. I. Application to Single Gases", J. Membr. Sci., 75, 245-263, 1992.

Deslandes, Y., G. Pleizier, D. Alexander and P. Santerre, "XPS and SIMS Characterization of Segmented Polyether Polyurethanes Containing Two Different Soft Segments", Polymer, 39, 2361-2366, 1998.

Dullien, F. A. L., "Porous Media-Fluid Transport and Pore Structure", Academic Press, London, 1979.

Fane, A. G., C. J. D. Fell and A. G. Waters, "The Relationship between Membrane Surface Pore Characteristics and Flux for Ultrafiltration Membranes", J. Membr. Sci., 9, 245-262, 1981.

Fanelsa, A., R. Schellenberg, F. U. Hillebrecht and E. Kisker, "Emission Direction Dependence of the Magnetic Linear Dichroism in Valence Band and Core Level Photoemission From Co/Cu(001)", Solid State Communications, 96, 291-296, 1995.

Fang, Y., "Separation of Liquid Mixtures by Membrane", Ph. D. thesis, Department of Chemical Engineering, University of Ottawa, Ottawa, 1997.

Fang, Y., V.A. Pham, T. Matsuura, J.P. Santerre, and R.M. Narbaitz "Effect of Surface-Modifying Macromolecules and Solvent Evaporation Time on the Performance of Polyethersulfone Membranes for the Separation of Chloroform/Water Mixtures by Pervaporation", J. Appl. Polym. Sci., 54, 1937-1943, 1994.

Garbassi, F., M. Morra, and E. Occhiello, "Polymer Surfaces: Form Physics to Technology", John Wiley & Sons, New York, NY, 1996.

Geoghegan, M., T. Nicolai, J. Penfold and R. A. L. Jones, "Kinetics of Surface Segregation and the Approach to Wetting in an Isotopic Polymer Blend", Macromolecules, 30, 4220-4227, 1997.

Hamza, A., V.A. Pham, T. Matsuura, and J.P. Santerre, "Development of Membranes with Low Surface Energy to Reduce the Fouling of Ultrafiltration Applications", J. Membr. Sci., 131, 217-227, 1997.

Hariharan, A., S. K. Kumar and T. P. Russell, "Reversal the Isotopic Effect in the Surface Behavior of Binary Polymer Blends", J. Chem. Phys., 98(5), 4163-4173, 1993a.

Hariharan, A., S. K. Kumar, M. H. Rafailovich, J. Soklov, X. Zheng, D. Duong, S. A. Schwarz and T. P. Russell, "The Effect of Finite Film Thickness on the Surface Segregation in Symmetric Binary Polymer Mixtures", J. Chem. Phys., 99(1), 656-663. 1993b.

Hernandez, A., J. I. Calvo, P. Pradanos and F. Tejerina, "Pore Size Distibutions in Microporous Membranes. A Critical Analysis of the Bubble Point Extended Method", J. Membr. Sci., 112, 1-12, 1996

Hester, J. F. and A. M. Mayes, "Design and Performance of Foul-resistant poly(vinylidene fluoride) membranes prepared in a single-step by surface segregation", J. Membr. Sci., 202, 119-136, 2002.

Ho, J.Y., "The Effects of Surface Modifying Macromolecules on the Blood Compatibility of Polyethersulfone Membranes Intended for Biomedical Applications", M.A.Sc. Thesis, Department of Chemical Engineering and Applied Chemistry, University of Toronto, Toronto, Canada, 1997.

Ho, J.Y., T. Matsuura, and J.P. Santerre, "The Effect of Fluorinated Surface Modifying Macromolecules on the Surface Morphology of Polyethersulfone Membranes", J. Biomater. Sci. Polymer Ed., Vol. 11, Nº. 10, 1085-1104, 2000.

Hsieh, F. U., T. Matsuura and S. Sourirajan, "Reverse Osmosis Separations of Polyethylene Glycols in Dilute Aqueous Solutions Using Porous Cellulose Acetate Membranes, J. Appl. Polym. Sci., 23, 561-573, 1979.

Hoffmann, E., D. M. Pfenning, E. Philippsen, P. Schwahn, M. Sieber, R. When, D. Woermann and G. Wiedner, "Evaporation of Alcohol/Water Mixtures through Hydrophobic Porous Membranes", J. Membr. Sci., 34, 199-206, 1987.

Hunter, P and S. T. Oyama, "Control of Volatile Oragnic Compound Emissions-Conventional and Emerging Technologies", John Wiley & Sons, Inc., 2000.

Iyengar, D. R., S. M. Perutz, C. Dai, C. K. Ober and E. J. Kramer, "Surface Segregation Studies of Fluorine-Containing Diblock Copolymers", Macromolecules, 29, 1229-1234, 1996.

Izquierdo-Gil, M. A. and G. Jonsson, "Factors Affecting Flux and Ethanol Separation Performance in Vacuum Membrane Distillation (VMD)", J. Membr. Sci., 214, 113-130, 2003.

Izquierdo-Gil, M. A., J. Abildskov and G. Jonsson, "The use of VMD Data/Model to Test Different Thermodynamic Models for Vapour-Liquid Equilibrium", J. Membr. Sci., 239, 227-241, 2004.

Jones, R. A. L., E. J. Kramer, M. H. Rafailovich, J. Sokolov, and S. A. Schwarz, "Surface Enrichment in an Isotopic Polymer Blend", Phys. Rev. Lett., 62, 280-283, 1989.

Kakuta, A., M. Kuramoto, M. Ohno, H. Kushida, A. Tanioka and K. Ishikawa, "Freeze-Dried Cellulose Acetate Membrane Fine Structure Observation", J. Polym. Sci., Polym. Chem. Ed. 18, 3229-3243, 1980.

Kesting, R. E.,"Synthetic Polymeric Membranes", John Wiley & Sons, New York, NY, 1985.

Kajiyama, T., K. Tanaka and A. Takahara, "Surface Segregation of the Higher Surface Free Energy Component in Symmetric Polymer Blend Films", Macromolecules, 31, 3746-4749, 1998.

Khayet, M., D. E. Suk, R. M. Narbaitz, J. P. Santerre and T. Matsuura, "Study on Surface Modification by Surface-Modifying Macromolecules and its Applications in Membrane-Separation Process", J. Appl. Polym. Sci., 89 (11), 2902-2916, 2003.

Khayet, M., K. C. Khulbe and T. Matsuura, "Characterization of Membranes for Membrane Distillation by Atomic Force Microscopy and Estimation of their Water Vapor Transfer Coefficients in Vacuum Membrane Distillation Process", J. Membr. Sci., 238, 199-211, 2004.

Khayet, M. and T. Matsuura, "Surface Modification of Membranes for the Separation of Volatile Organic Compounds form Water by Pervaporation", Desalination, 148, 31-37, 2002.

Khayet, M. and T. Matsuura, "Pervaporation and Vacuum Membrane Distillation Processes: Modeling and Experiments", AIChE Journal, 50, 1697-1712, 2004.

Kosuko, M., M. E. Mullins, K. Ramandathan, and T. N. Rogers, "Catalytic Oxidation of Groundwater Stripping Emissions", Environmental Progress, 7, 136-142, 1988.

Larbot, A., L. Gazagnes, S. Krajewski, M. Bukowska and K. Wojciech, "Water Desalination using Ceramic Membrane Distillation" Desalination, 168, 367-372, 2004.

Lawson, K. W., M. S. Hall and D. R. Lloyd, "Compaction of Microporous Membranes used in Membrane Distillation. I. Effect on Gas Permeability", J. Membr. Sci., 101, 99-108,

1995.

Lawson, K. W. and D. R. Lloyd, "Membrane Distillation. I. Module Design and Performance Evaluation using Vacuum Membrane Distillation", J. Membr. Sci. 120, 111-121, 1996.

Lawson, K. W. and D. R. Lloyd, "Review Membrane Distillation", J. Membr. Sci., 124, 1-25, 1997.

Lee, H. and L. A. Archer, "Functionalizing Polymer Surfaces by Field-Induced Migration of Copolymer Additives. I. Role of Surface Energy Gradients", Macromolecules, 34, 4572-4579, 2001.

Lee, W. K., I. Losito, Jr. J. A. Gardella and Jr. W. L Hicks, "Synthesis and Surface Properties of Fluorocarbon End-Capped Biodegradable Polyesters", Macromolecules, 34, 3000-3006, 2001.

Levenston, B. H., "Background Information for an Environment Code of Practice for Dry Cleaning Facilities", Environment Canada, Ottawa, 1991.

Li, J., Z. Xu, Z. Liu, W. Yuan, H. Xiang, S. Wang and Y. Xu, "Microporous Polypropylene and Polyethylene Hollow Fiber Membranes. Part 3. Experimental Studies on Membrane Distillation for Desalination", Desalination, 155153-156, 2003.

Mahmud, H., J. Minnery, Y. Fang, V. A. Pham, R. M. Narbaitz, J. P. Santerre and T. Matsuura, "Evaluation of Membranes Containing Surface Modifying Macromoleucles: determination of the chloroform separation from aqueous mixtures via pervaporation", J. Appl. Polym. Sci. 79, 183-189, 2001.

Mandeep, "Characterization and Plasma Protein Binding Studies of Surface Modified Polyethersulfone", M.A.Sc. thesis, Department of Chemical Engineering and Applied

Chemistry, University of Toronto, Toronto, ON, 2001.

Martinez, L., F. J. Florido-Diaz, A. Hernandez and P. Pradanos, "Characterisation of three Hydrophobic Porous Membranes used in Membrane Distillation Modelling and Evaluation of their Water Vapour Permeabilities", J. Membr. Sci., 203, 15-27, 2002.

Matsuura, T., J. P. Santerre, and R. Narbaitz, "Fluoropolymeric Membranes for Environmental Contaminant Removal", Proposal for Strategic Grant, submitted to Natural Sciences and Engineering Research Council of Canada, Ottawa, 1992.

Matsuura, T., "Synthetic Membranes and Membrane Separation Processes", CRC Press, Boca Raton, FL, 1993.

McGregor, F. R., P. J. Piscaer and E. M. Aieta, "Economics of Treating Waste Gases from an Air Stripping Tower Using Photochemical Generated Ozone", Ozone Sci. Eng., 10, 339-352, 1988.

Meireles, M, A. Bessieres, I. Rogissart, P. Aimar and V. Sanchez, "An Appropriate Molecular Size Parameter for Porous Membranes Calibration", 103, 105-115, 1995.

Mengual, J. I., M. Khayet and M. P. Godino, "Heat and Mass Transfer in Vacuum Membrane Distillation", Int. J. Heat Mass Transf., 47, 865-875, 2004

Michaels, A. S.,"Analysis and Prediction of Sieving Curves for Ultrafiltration Membranes: A Universal Correlation?", Sep. Sci. Technol. 15, 1305-1322, 1980.

Michaels, A. S., L. Nelsen and M. C. Porter, "Ultrafiltration in; M. Bier (Ed), Membrane Process in Industry and Biomedicine", Plenum Press, New York, 197, 1971.

Minnery, J.G., "The Effect of Surface Modifying Macromolecules on Pervaporation Membranes and the Effect of Pervaporation Conditions on the Morphology of Modified

Membranes", M.A.Sc. Thesis, Department of Chemical Engineering, University of Ottawa, Ottawa, Canada, 2000.

Mosqueda-Jimenez, D. B., R. M. Narbaitz, T. Matsuura, G. Chowdhury, G. Pleizier and J. P. Santerre, "Influence of Processing Conditions on the Properties of Ultrafiltration Membranes", J. Membr. Sci., 231, 209-224, 2004a

Mosqueda-Jimenez, D. B., R. M. Narbaitz and T. Matsuura, "Manufacturing Conditions of Surface-Modified Membranes: Effects on Ultrafiltration Performance", Sep. Purif. Technol., 37, 51-67, 2004b

Mulder, M., "Basic Principles of Membrane Technology", Kluwer Academic Publisher, Boston, MA, 117-119, 1996.

Mukhopadhyay, N., E. C. Moretti, "Current and Potential Future Industrial Practices for Reducing and Controlling Volatile Organic Compounds, Center for Waste Reduction Technologies", American Institute of Chemical Engineers, New York, 1993

Nabi, G., "Light-Scattering Studies of Aqueous Solutions of Poly(ethylene oxide), Pakistan J. Sci., 20, 136-140, 1968.

Norton, L. J., E. J. Kramer, F. S. Bates, M. D. Gehlsen, R. A. L. Jones, A. Karim, G. P. Felcher and R. Kleb, "Neutron Reflectometry Study of Surface Segregation in an Isotopic Poly(ethylenepropylene) Blend: Deviation from Mean-Field Theory", Macromolecules, *28*(25), 8621-8628, 1995.

Okada, T., and T. Matsuura, "Predictability of Transport Equations for Pervaporation on the Basis of Pore-flow Mechanism", J. Membr. Sci., 70, 163-175, 1992.

O'Malley, J.J., H.R. Thomas and G.M. Lee, "Surface Studies on Multicomponent Polymer Systems by X-ray Photoelectron Spectroscopy. Polystyrene/Poly(Ethylene Oxide) Triblock

Copolymer", Macromolecules, 12, 996-1001, 1979.

Owens D.K. and R.C. Wendt, "Estimation of the Surface Free Energy of Polymers", J. Appl. Polym. Sci., 13, 1741-1747, 1969.

Pan, D.H.-K. and W.M. Prest Jr., "Surfaces of Polymer Blends: X-ray Photoelectron Spectroscopy Studies of Polystyrene/poly(vinyl methyl ether) Blends", J. Appl. Phys., 58, 2861-2870, 1985.

Park, H. B., Personal Communication, 2002.

Peng, M., L. M. Vane and S. X. Liu, "Recent advances in VOCs Removal from Water by Pervaporation", J. Hazard. Mat., B98, 69-90, 2003.

Perry, R. H. and D. W. Green, "Perry's Chemical Engineers' Handbook", 6th Ed., McGraw-Hill, 3-127, 1984

Pham V. A., "Surface Modifying Macromolecules for Enhancement of Polyethersulfone Pervaporation Membrane Performance", M.A.Sc. thesis, Department of Chemical Engineering, University of Ottawa, Ottawa, 1995.

Pham, V.A., J.P. Santerre, T. Matsuura, and R.M. Narbaitz, "Application of Surface Modifying Macromolecules in Polyethersulfone Membranes: Influence on PES Surface Chemistry and Physical Properties", J. Appl. Polym. Sci., 73, 1363-1378, 1999.

Pinnau, I., and B.D. Freeman, "Membrane Formation and Modification", ACS Symposium Series 744, American Chemical Society, Washigton, DC, 2000.

Porter, M. C., "Concentration Polarization with Membrane Ultrafiltration", I&EC Product Res. and Dev., 11, 234, 1972.

Ratner, B. D. and R. W. Paynter, "Polyurethan surfaces: The Importance of Molecular weight distribution, Bulk chemistry and casting conditions", in "polyurethanes in Biomedical Engineering", H. Planck, G. Egbers and I. Syré, Eds., Elsevier Science Publishers, Amsterdam, 41-68, 1984.

Reichelt, G, "Bubble Point Measurements on Large Areas of Microporous Membranes", J. Membr. Sci., 60, 253-259, 1991.

Riley, R., J. O. Gardner and U. Merten, "Cellulose Acetate Membranes: Electron Microscopy of Structure", Science 143, 801-803, 1964.

Sarti, G. C, C. Gostoli and S. Bandini, " Extraction of Organic Compounds from Aqueous Streams by Vacuum Membrane Distillation", J. Membr. Sci., 80, 21-33, 1993.

Schmidt ,J. J., J. A. Gardella Jr. and L. Salvati Jr., Surface Studies of Polymer Blends. 2. An ESCA and IR Study of Poly(methyl methacrylate)/Poly(vinyl chloride) Homopolymer Blends, Macromolecules, 22, 4489-4495, 1989.

Schofield, R. W., A. G. Fane and C. J. D. Fell, "Heat and Mass Transfer in Membrane Distillation", J. Membr. Sci., 33, 299-313, 1987.

Schofield, R. W., A. G. Fane and C. J. D. Fell, "Gas and Vapour Transport through Microporous Membranes. I. Knudsen-Poiseuille Transition", J. Membr. Sci., 53, 159-171-1990.

Shao, P., Y. M. Huang, X. Feng and W. Anderson, "Gas-Liquid Displacement Method for Estimating Membrane Pore-Size Distributions", AIChE Journal, 50, 557-565, 2004.

Shen, T.T. and G. H. Sewell, "Control of VOC Emissions from Waste Management

Facilities", J. Environ. Eng., ASCE, 114, 1392, 1988.

Singh, S., K. C. Khulbe, T. Matsuura and P. Ramamurthy, "Membrane Characterization by Solute Transport and Atomic Force Microscopy", J. Membr. Sci., 142, 111-127, 1998.

Smith, J. M. and H. C. Van Ness, "Introduction to Chemical Engineering Thermodynamics", McGraw-Hill, 4th Ed., Singapore, 116, 1987.

Smolders, C. A. and A. C. M. Franken, "Terminology for membrane distillation", Desalination, 72, 249-262, 1989.

Sourirajan, S. and T. Matsuura, "Transport through Reverse Osmosis, Part I, II", in "Reverse Osmosis/Ultrafiltration Process Principles", National Research Council Canada, Ottawa, ON, 79-357, 1985.

Spricigo, C.B., J.C.C. Petrus, R.A.F. Machado, L.A.V. Sarmento and A. Bolzan, "Preparation and Characterization of Polyethersulfone Membranes for Use in Supercritical Medium", J. Membr. Sci., 205, 273–278, 2002.

Strathmann, H., "Synthetic Membranes and Their Preparation", in "Handbook of Industrial Membrane Technology", M. C. Porter, ed., Noyes Publications, Park Ridge, NJ, 1990.

Strathmann, H., K. Kock, P. Amar and R. W. Baker, "The Formation Mechanism of Asymmetric Membranes", Desalination 16, 179-203, 1975.

Strauch, P., "VOC Recovery with Membrane Technology", Membrane Technology, v.1995, n.68, 1995

Suk, D.E., G. Pleizier, Y. Deslandes and T. Matsuura, "Effects of Surface Modifying Macromolecule (SMM) on the Properties of Polyethersulfone Membranes", Desalination, 149, 303-307, 2002a.

Suk, D.E., G. Chowdhury, T. Matsuura, R. M. Narbaitz, P. Santerre, G. Pleizier and Y. Deslandes, "Study on the Kinetics of Surface Migration of Surface Modifying Macromolecules in Membrane Preparation", *Macromolecules,* 35, 3017-3021, 2002b.

Theocaris, P. S. and V. Kefalas, "Dynamic Mechanical Properties of Polystyrene-Polyurethane Blends", J. Appl. Polym. Sci., 42, 3059-3063, 1991.

Thomas, H.R. and J.J. O'Malley, "Surface Studies on Multicomponent Polymer Systems by X-ray Photoelectron Spectroscopy. Polystyrene/Poly(ethylene oxide) Diblock Copolymer", Macromolecules, 12, 323-329, 1979.

Urtiaga, A. M., G. Ruiz and I. Ortiz, "Kinetic Analysis of the Vacuum Membrane Distillation of Chloroform from Aqueous Solutions", J. Membr. Sci., 165, 99-110, 2000.

Urtiaga, A. M., E. D. Gorri, G. Ruiz and I. Ortiz, "Parallelism and Differences of Pervaporation and Vacuum Membrane Distillation in the Removal of VOCs from Aqueous Streams", Sep. Purif. Technol., 22, 327-337, 2001.

USEPA, Fact Sheet, Drinking Water Regulations Under the Safe Drinking Water Act., USEPA, Office of Drinking Water, Washington D. C., 1990.

Villaluenga, J. P. G., P. Godino, M. Khayet, B. Seoane and J. I. Mengual, "Pervaporation of Alcohols and Methyl tert-Butyl Ether through a Dense Poly(2,6-dimethyl-1,4-phenylene oxide) Membrane", Ind. Eng. Chem. Res., 43, 2548-2555, 2004.

Youm, K. H. and W. S. Kim, "Prediction of Intrinsic Pore Properties of Ultrafiltration Membrane by Solute Rejection Curves: Effect of Operating Conditions on Pore Properties", J. Chem. Eng. Japan, 24, 1-7, 1981.

Ward, R.S., K.A. White, and C.B. Hu, "Use of Surface Modifying Additives in the Development of a New Biomedical Polyurethaneurea", in "Polyurethanes in Biomedical Engineering", Planck H., G. Egbers, I. Syre, Eds., Elsevier, Amsterdam, the Netherlands, 1984.

Wijmans, J. G. and R. W. Baker, "The Solution-Diffusion Model: a Review", J. Membr. Sci., 107, 1-21, 1995.

Wu, Y., Y. Kong, X. Lin, W. Liu and J. Xu, "Surface-Modified Hydrophilic Membranes in Membrane Distillation", J. Membr. Sci., 72, 189-196, 1992.

Zander, A. K., M. J. Semmens and R. M. Narbaitz, "Removing VOCs by Membrane Stripping", J. AWWA, 81, 76-81, 1989.

Zhang, D., D. H. Gracias, R. Ward, M. Gauckler, Y. Tian, Y. R. Shen and G. A. Somorjai, "Surface Studies of Polymer Blends by Sum Frequency Vibrational Spectroscopy, Atomic Force Microscopy, and Contact Angle Goniometry", J. Phys. Chem. B, 102, 6225-6230, 1998.

Zhang, L., G. Chowdhury, C. Feng, T. Matsuura, R. Narbaitz, "Effect of Surface-Modifying Macromolecules and Membrane Morpholgy on Fouling of Polyethersulfone Ultrafiltration Membranes", J. Appl. Polym. Sci., 88, 3132-3138, 2003.

Zhao, X., W. Zhao, J. Sokolov, M. H. Rafailovich, S. A. Schwarz, B. J. Wilkens, R. A. L. Jones and E. J. Kramer, "Determination of the Concentration Profile at the Surface of d-PS/h-PS Blends Using High-Resolution Ion Scattering Techniques", Macromolecules, 24, 5991-5996, 1991.

Appendix A Chemical Structures of the Materials

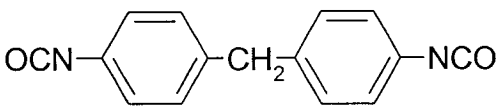

methylene bis-*p*-phenyl diisocyanate (MDI)

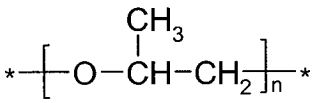

polypropylene diol (PPO)

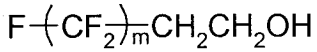

Zonyl BA-L™ (BAL)

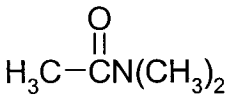

N,N-diethylacetamide (DMAc)

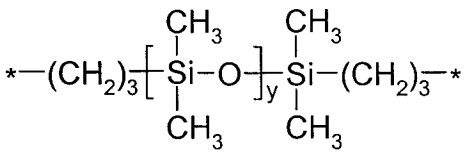

α, ω-Aminopropyl poly(dimethyl siloxane) (PDMS)

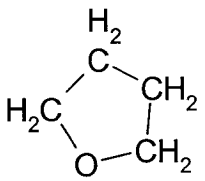

Tetrahydrofurane (THF)

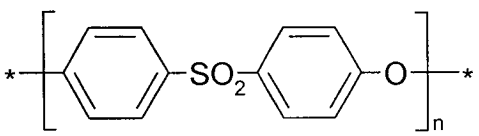

Polyethersulfone (PES)

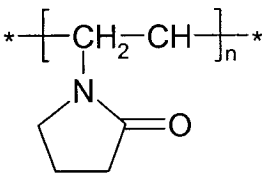

Polyvinyl pyrrolidone (PVP)

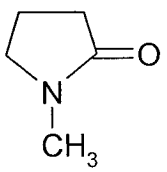

N-methyl pyrrolidone (NMP)

Appendix B Distillation and Degassing Apparatuses

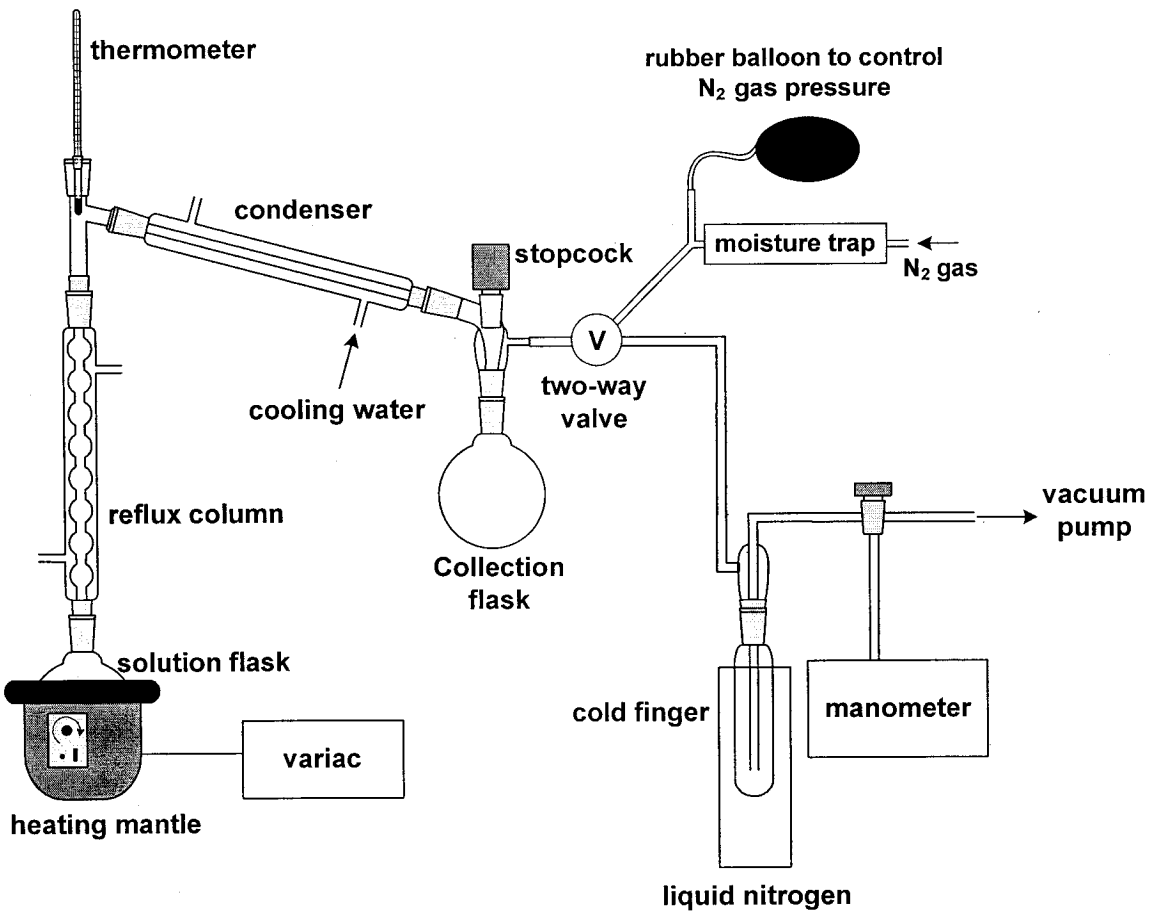

Appendix C tSMM1 synthesis apparatus

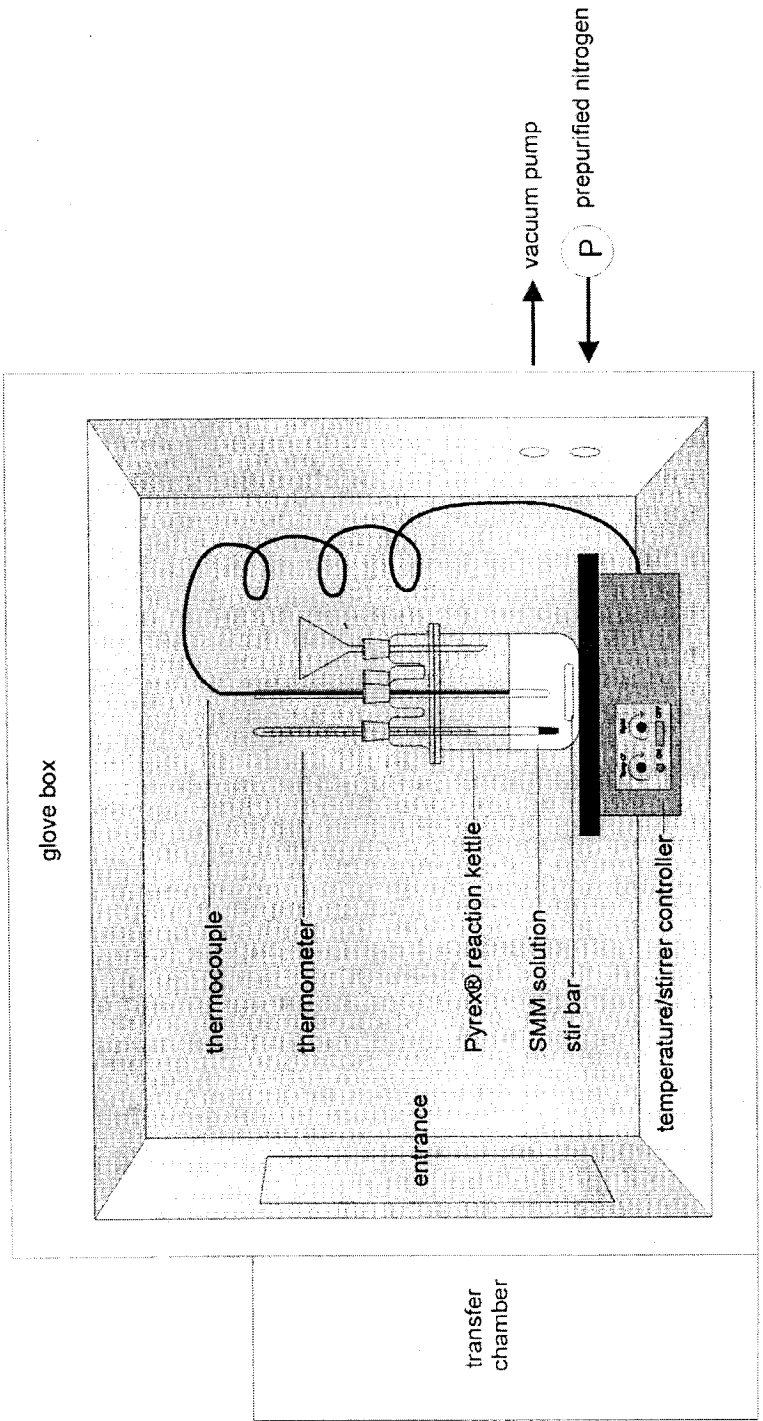

Appendix D tSMM2 and nSMM synthesis apparatus

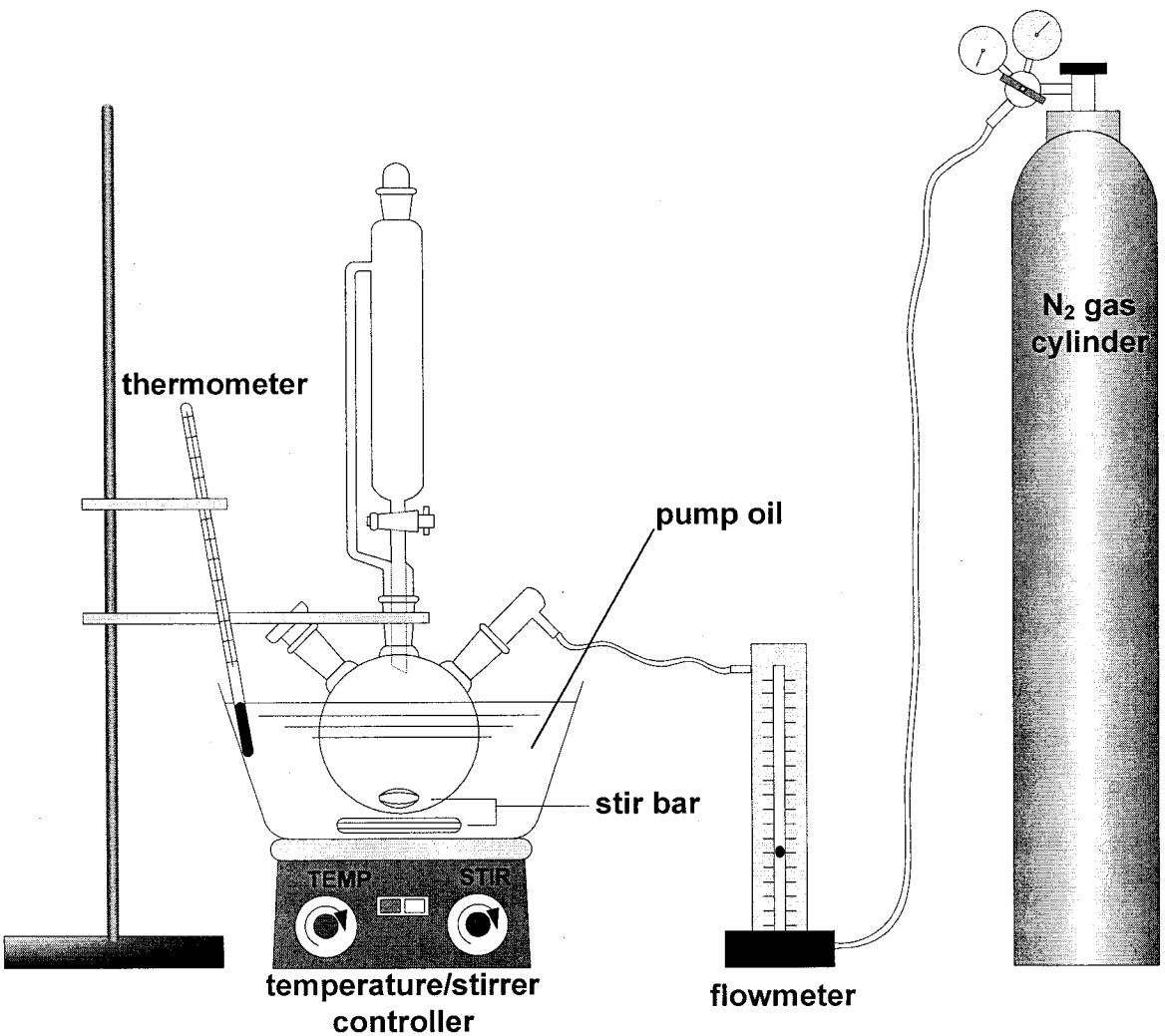

Appendix E Compositions of the pure tSMM and the pure PES

In Figure 3.2, the chemical structure of tSMM is presented and in the structure, m, n, and q values can be calculated from the molecular weight and the molar ratio of the reagent of the reagents which were used in the tSMM synthesis. The molecular weights of polypropylene diol (PPO) and Zonyl BA-L^{TM} (BAL) are given in Chapter 3.1.1 and their chemical structures are provided in Appendix A. Using that information, n and m were calculated by:

425(PPO) = 16(O) + 2×1(H) + n × [3×12(C) + 16(O) + 6×1(H)]

433(BAL) = 19(F) + [12(C) + 2×19(F)] × m + 12(C) + 5×1(H) + 16(O)

Therefore, n = 7.02 and m = 7.58 were achieved and from the molar ratio of the reagents for tSMM synthesis, q = 2 was withdrawn. Therefore the molecular weight of tSMM could be estimated as 2468.32.

To calculate the elemental weights in pure tSMM:

$$\text{F wt\%} = \frac{2\times[19(F)+2m\times19(F)]}{2486.32} = 24.7$$

$$\text{N wt\%} = \frac{2\times14(N)\times q+214(N)}{2486.32} = 3.4$$

$$\text{C wt\%} = \frac{[m\times12(C)+2\times12(C)]\times2+[15\times12(C)+3\times12(C)\times n]\times q+15\times12(C)}{2486.32} = 51.3$$

$$\text{O wt\%} = \frac{4\times16(O)+[3\times16(O)+16(O)\times n]\times q}{2486.32} = 15.5$$

$$\text{H wt\%} = \frac{[4\times1(H)]\times2+[12\times1(H)+6\times1(H)\times n]\times q+12\times1(H)}{2486.32} = 5.1$$

where F, N, C, O, H represent the fluorine, nitrogen, oxygen and hydrogen elements, respectively. The fluorine wt% is converted to atomic % by

$$\textbf{\textit{F atomic \%}} = \frac{\frac{F(wt\%)}{19(F)}}{\frac{F(wt\%)}{19(F)} + \frac{N(wt\%)}{14(N)} + \frac{C(wt\%)}{12(C)} + \frac{O(wt\%)}{16(O)}} \times 100$$

where the term, $\frac{H(wt\%)}{1(H)}$, is discarded to make the result comparable to the XPS data. It should be noted XPS does not detect hydrogen.

Substituting the elemental atomic weights into the above equation, then, fluorine is converted into atomic % by:

$$\text{F atomic \%} = \frac{\frac{24.7(wt\%)}{19(F)}}{\frac{24.7(wt\%)}{19(F)} + \frac{3.4(wt\%)}{14(N)} + \frac{51.3(wt\%)}{12(C)} + \frac{15.5(wt\%)}{16(O)}} \times 100 = 19.16$$

That is to say, 24.7 wt% of fluorine is equivalent to 19.16 atomic % of fluorine.

Similarly, we have:

C atomic % = 62.99

N atomic % = 3.58

O atomic % = 14.27

Polyethersulfone (PES) has the repeating unit with chemical formula [-$C_{12}H_8O_3S$-]

Weight of the repeating unit $= 12\times12(C) + 8\times1(H) + 3\times16(O) + 1\times32.1(S) = 232.1$

To calculated the elemental weights in the pure PES:

C wt% $= 12\times12(C)/232.1 = 62.04$

H wt% $= 8\times1(H)/232.1 = 3.45$

O wt% $= 3 \times 16(O) / 232.1 = 20.68$

S wt% $= 1 \times 32.1(S) / 232.1 = 13.83$

where S represent the sulfur element. The elemental weights in wt% is converted to those in atomic % by the same method used for tSMM and the results are:

C atomic % = 75.00

O atomic % = 18.75

S atomic % = 6.25

Appendix F Estimation of fluorine content in the dry membrane

Suppose the membrane casting solution was made of following components (wt%):

polyethersulfone (PES):	20 %
tSMM:	1.5 %
N-methyl pyrrolidone (NMP):	78.5 %

When the above solution was cast into a membrane and gelled in the water, NMP as a solvent was supposed to leach out completely. Then, the dry membrane was considered to be made of PES and SMM. Therefore, the weight ratio of (the amount of tSMM/the amount of PES) in the membrane must be 7/93.

The elemental weights in the pure tSMM and PES were calculated in Appendix E. Therefore,

To calculate the elemental weights in 7 wt% of tSMM in the membrane:

F wt% = F wt% in pure tSMM × 0.07 = 24.7 × 0.07 = 1.73

N wt% = N wt% in pure tSMM × 0.07 = 3.4 × 0.07 = 0.24

C wt% = C wt% in pure tSMM × 0.07 = 51.3 × 0.07 = 5.39

O wt% = O wt% in pure tSMM × 0.07 = 15.5 × 0.07 = 1.09

H wt% = H wt% in pure tSMM × 0.07 = 5.1 × 0.07 = 0.36

To calculate the elemental weights in 93 wt% of PES in the membrane:

C wt% = C wt% in pure PES × 0.93 = 62.04 × 0.93 = 57.70

H wt% = H wt% in pure PES × 0.93 = 3.45 × 0.93 = 3.21

O wt% = O wt% in pure PES × 0.93 = 20.68 × 0.93 = 19.23

S wt% = S wt% in pure PES × 0.93 = 13.83 × 0.93 = 12.86

Therefore, to calculate the elemental weights in the membrane:

Total C wt% = 57.70 + 3.59 = 61.29

Total O wt% = 19.23 + 1.09 = 20.32

Total F wt% = 1.73

Total N wt% = 0.24

Total S wt% = 12.86

Total H wt% = 3.57

Using the procedure in Appendix E, fluorine wt% is converted to fluorine atomic % by:

$$\text{F atomic\%} = \frac{\frac{1.73(wt\%)}{19(F)}}{\frac{61.29(wt\%)}{12(C)} + \frac{20.32(wt\%)}{16(O)} + \frac{1.73(wt\%)}{19(F)} + \frac{0.24(wt\%)}{14(N)} + \frac{12.86(wt\%)}{32.1(S)}} \times 100$$

$$= 1.32$$

Appendix G SEM picture of V1's bottom layer

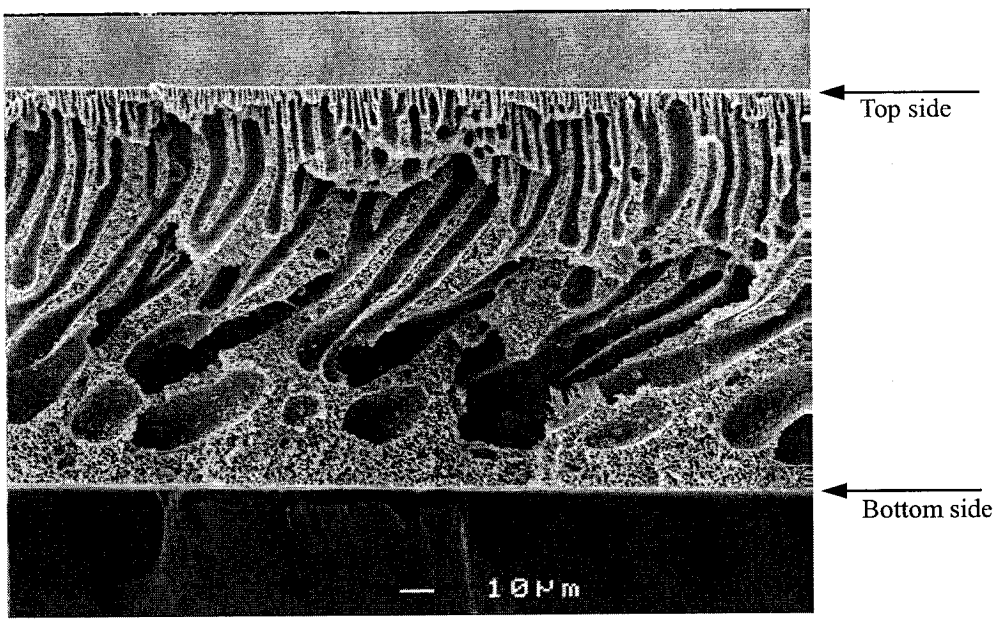

(a) Membrane profile (× 500)

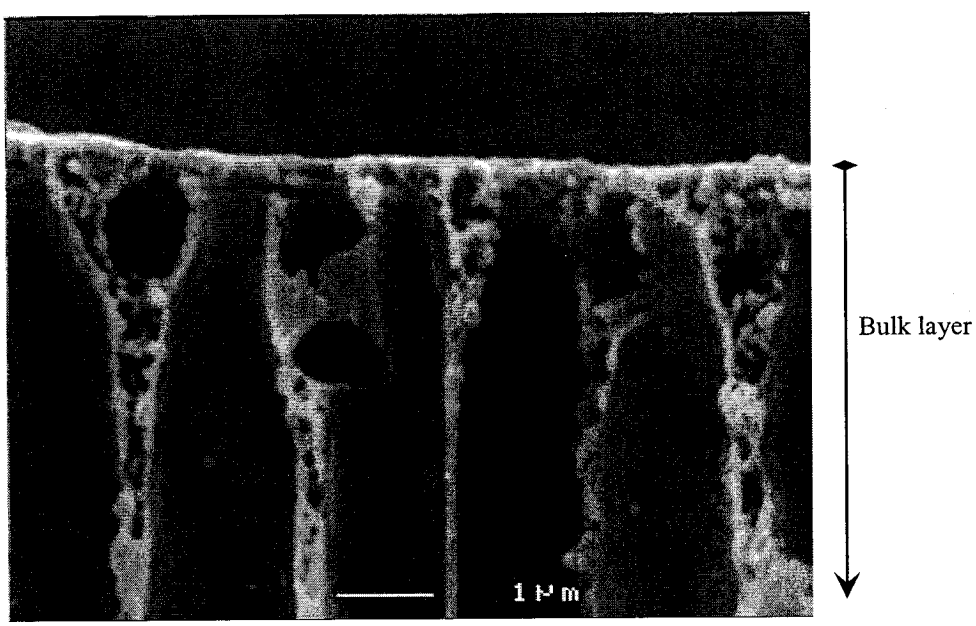

(b) Magnified top surface part (× 1500)

Appendix H Latent heat of vaporization

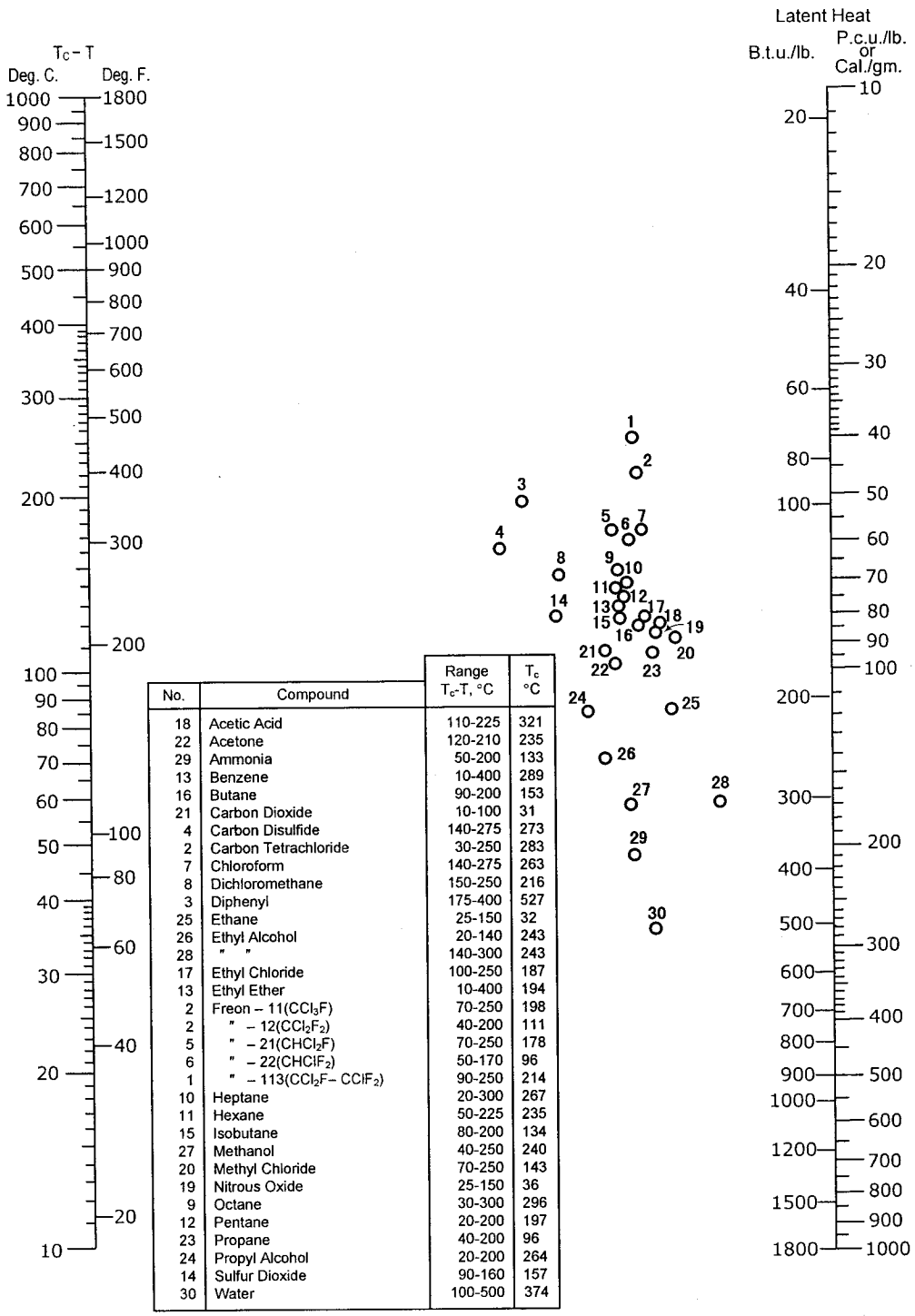

No.	Compound	Range T_c-T, °C	T_c °C
18	Acetic Acid	110-225	321
22	Acetone	120-210	235
29	Ammonia	50-200	133
13	Benzene	10-400	289
16	Butane	90-200	153
21	Carbon Dioxide	10-100	31
4	Carbon Disulfide	140-275	273
2	Carbon Tetrachloride	30-250	283
7	Chloroform	140-275	263
8	Dichloromethane	150-250	216
3	Diphenyl	175-400	527
25	Ethane	25-150	32
26	Ethyl Alcohol	20-140	243
28	" "	140-300	243
17	Ethyl Chloride	100-250	187
13	Ethyl Ether	10-400	194
2	Freon – 11(CCl_3F)	70-250	198
2	" – 12(CCl_2F_2)	40-200	111
5	" – 21($CHCl_2F$)	70-250	178
6	" – 22($CHClF_2$)	50-170	96
1	" – 113($CCl_2F-CClF_2$)	90-250	214
10	Heptane	20-300	267
11	Hexane	50-225	235
15	Isobutane	80-200	134
27	Methanol	40-250	240
20	Methyl Chloride	70-250	143
19	Nitrous Oxide	25-150	36
9	Octane	30-300	296
12	Pentane	20-200	197
23	Propane	40-200	96
24	Propyl Alcohol	20-200	264
14	Sulfur Dioxide	90-160	157
30	Water	100-500	374